# Estimating stem profile using canopy metrics: a forest inventory application for airborne remote sensing

by

Robert Musk
B.For.Sci. (University of Melbourne)
Grad. Dip. Env.Stud.(Hons) (University of Tasmania)

A thesis submitted in fulfilment of the requirements for the degree of Doctor of Philosophy (Ph.D.)

School of Geography and Environmental Studies,
University of Tasmania, Sandy Bay, Australia
May 2006

# Declaration

This thesis contains no material which has been accepted for a degree or diploma by the University or any other institution, except by way of background information and duly acknowledged in the thesis, and to the best of my knowledge and belief no material previously published or written by another person except where due acknowledgement is made in the text of the thesis, nor does the thesis contain any material that infringes copyright.

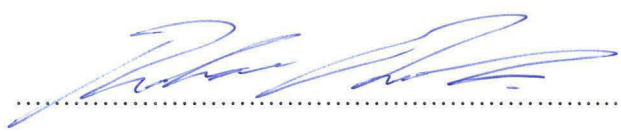

.....

Robert Musk

# Authority of Access

This thesis may be made available for loan and limited copying in accordance with the *Copyright Act 1968.*

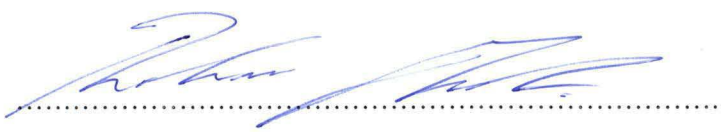

Robert Musk

# Acknowledgements

I would like to thank my supervisors for their guidance, enthusiasm and forbearance throughout my candidature. In particular, Dr Jon Osborn has been a constant source of ideas throughout the writing of this thesis. I have enjoyed our time working together immensely. Dr Richard Coleman is an excellent tutor in the dark arts of mixed effects modelling who was always willing to give his time to provide constructive advice on my work. Dr Cris Brack's practical forestry knowledge, his obvious love of new ideas and keen interest in developing new approaches to old problems are always inspiring.

Norske Skog at Boyer in Tasmania enabled my candidature in a range of ways. They provided a financial top-up to my scholarship. They provided me with access to their estate and to their inventory databases. They also provided me with access to staff who assisted me with field work. I am particularly grateful to Sandra Hetherington and Jody Bruce for their managerial support; and to Nigel Youd and Tony Wells for their enthusiasm, dedication and humour during the fieldwork. They are a lot of fun to work with.

I am also grateful to Michelle and my family and friends, for their love and support throughout.

# Abstract

The precision of plot based inventories is limited by the spatial variability of forest metrics. This thesis develops an inventory method for the assessment of radiata pine (*Pinus radiata* D. Don) plantations that exhibit high spatial variability. The method utilises forest canopy metrics that may be acquired using airborne remote sensing technologies in the estimation of individual tree stem profile properties.

A review of the growth behaviour of radiata pine isolates the period prior to significant silvicultural interventions as the optimum sampling age. A review of recent developments in remote sensing technologies isolates tree location and height as the best potential sampling covariates. Tree height, location and stem profile data in two age cohorts are drawn from a single radiata pine estate in south-eastern Tasmania, Australia. Local density indices are derived using tree height and location data and their utility for predicting breast height diameter is evaluated. Segmented and variable-form stem profile models employing individual tree height and local density are then derived using mixed and generalized least-squares modelling methodologies in order to facilitate estimation of merchantable timber volume.

It is shown that neighbour tree location, distance and height with respect to a subject tree, are all significant breast height diameter predictors. Their influence is attributed to the asymmetric and one-sided nature of the interactions between trees during stand development. The stem profile models are shown to provide merchantable volume estimates with acceptable bias, with simple segmented models preferred for their parsimony. Mixed modelling methods are shown to best describe the variance-covariance structure of the stem profile data, with some attendant advantages in model predictive behaviour. The evaluation shows that remote sensing products may be used for plantation inventory in many radiata pine stands.

# Table of Contents

# List of Figures

## Chapter 2



## Chapter 3



## Chapter 4



## Chapter 5

## Chapter 6



## Chapter 7

# List of Tables

## Chapter 5



## Chapter 6

## Chapter 7

# Glossary

| | | |
|---|---|---|
| DBH or $D$ | Stem diameter at 1.3 metres | |
| $D_u$ | Stem diameter under bark at 1.3 metres | (cm) |
| $D_o$ | Stem diameter over bark at 1.3 metres | (cm) |
| $d$ | Stem diameter under bark at height $h$ | (cm) |
| $G$ | Basal area at 1.3 metres | ($m^2Ha^{-1}$) |
| $H$ | Total tree height | (m) |
| $h$ | Height above ground on uphill side at diameter $d$ | (m) |
| $z = \frac{h}{H}$ | Relative height | |
| $V$ | Volume | ($m^3$) |
| $t$ | Age | (years) |
| $M$ | Mean dominant height | (m) |
| | (Mean height of the 100 largest diameter trees $Ha^{-1}$) | |
| $N$ | Stocking | ($Ha^{-1}$) |
| $\alpha_i$ and $\beta_i$ | Model parameters | |
| $k = \frac{\pi}{40000}$ | Basal area to diameter conversion factor | |

Further symbols are defined as required throughout the text.

*Chapter 1*

# Introduction

## 1.1 Research objective and aims

Plot based sampling techniques are employed in timber inventory to produce the information required for effective management of timber resources (Husch et al. 2003, pg. 290-293). Resource variation within management units can limit inventory precision and in these circumstances, manual assessment of tree- or stand-level metrics from aerial photographs may be used to augment ground-based assessment (Hall et al. 1989; Biggs 1990). Recently developed remote sensing technologies may also be used in metric assessment where the automation of data analysis is reducing the subjectivity of interpretation and increasing the spatial coverage per unit cost, so increasing the potential sampling rate of measurement over manual methods (Anderson et al. 2001; Hyyppä et al. 2001). High resolution, airborne laser scanner and photographic imaging systems may be used to survey a range of forest attributes, including the location of individual trees (Pinz 1998; Pollock 1999; Walsworth and King 1999), the delineation of individual tree crowns (Gougeon 1995; Gougeon and Leckie 1999; Culvenor 2000), and the measurement of individual tree height (Morsdorf et al. 2004), canopy height (Nelson et al. 1988; Nilsson 1996; Wijanarto 2001) and canopy depth (Lefsky et al. 1999; Zimble et al. 2003).

While recent advances in remote sensing technologies have been rapid, changes to the timber market are also occurring with increasing speed. In adapting to changing market demand, management interest in timber resources is increasingly focused not on quantifying total wood volumes, but on quantifying the availability of specific timber products (Pelz 1993). The identification of specific timber products allows managers to more accurately price their resource. It also allows

them to strategically target market opportunities and manage the timber supply more effectively. This has positive flow-on effects throughout the timber processing chain (Goulding et al. 2000). Within Australia, the interest in quantifying specific timber products is magnified by both the increasing shift in timber production from native forests to higher cost, higher yielding plantations (Parsons et al. 2004) and the coincident increasing proportional sawlog production from these plantations (Ferguson et al. 2002). These recent developments suggest that new approaches to utilising remotely sensed data in timber inventory warrant investigation.

The objective of this thesis is to develop methods to estimate merchantable timber volumes in even-aged stands of radiata pine (*Pinus radiata* (D. Don)), a common timber plantation species, that can effectively utilise tree-level, remotely sensed data products. While many published studies have developed allometric equations to relate tree-level remotely sensed data to breast height diameter or total stem volume (Biggs 1990), converting these estimated stem metrics to timber product information requires additional models. In other areas of forest mensuration, stem profile models have largely replaced the partial volume and volume ratio equations that are used to generate timber product estimates from other tree metrics. Mensurationists prefer stem profile models because they may be used to estimate diameter within specified components of the stem, and by integration, estimate volume to specified log diameter or length constraints, all without recourse to new data or analyses (Bruce and Max 1990). This flexibility makes stem profile models an ideal inventory tool for identifying specific timber products. However, direct stem profile modelling has not previously been attempted using remotely sensed data. The present study addresses this gap.

The feasibility of using remotely sensed data to directly model stem profile is supported by the observation that *within*-tree differences in stem profile are largely a function of relative height (Larson 1963; Kozak et al. 1969), and the contention that *between*-tree stem profile differences will be a function of tree metrics that have been used to predict stem metrics in previous remote sensing work. In order to fulfil the objective, specific aims of the thesis are to:

1) Identify potential remotely sensed data products suited to stem profile prediction and optimal age of data capture through a review of recent remote sensing developments and growth processes in radiata pine timber plantations.

2) Develop and evaluate indexes both to capture the information content in potential remotely sensed data products and to efficiently summarise these potential products to a form amenable to further modelling.

3) Develop and evaluate stem profile prediction models utilising the developed indexes and tree height measurements.

## 1.2 Research contribution

The resolution of the thesis aims forms the basis of a significant contribution to the field of forest inventory. It provides an important link between forest inventory and emerging remote sensing technologies. The development of these methods and models will facilitate future work to compare financial and temporal acquisition costs of remote sensing survey and ground based sampling in light of measurement and sampling errors.

## 1.3 Thesis outline

The thesis is presented in eight chapters.

This chapter has introduced the objective and aims of the thesis. Recent developments in remote sensing technologies promise spatially extensive tree-level forest surveys. Coincident changes in both timber management objectives and the resources under management have led to increased demands for timber product estimation. These demands warrant the investigation of new forest inventory methods. The modeling of tree-level data which may sensed remotely to provide timber volume estimates is proposed as the research objective.

Chapter 2 reviews the use of remote sensing technologies in radiata pine inventory and the potential for the application of more recently developed systems. It identifies tree-level metrics that are candidates for routine extraction from airborne remotely sensed data. This chapter then reviews the growth habit of radiata pine and explores how between-tree interactions influence the growth of the stand and the growth of individual trees. Of the latter, both the gross growth trajectory differences that occur between trees, and the ways in which within-stem photosynthate allocation affects the size and shape of tree stems are reviewed. Methods to characterise these phenomena are introduced. Methods suited to use in the context of remote sensing inventory and appropriate age cohorts are identified.

Chapter 3 describes the radiata pine estate in south eastern Tasmania, Australia that was chosen as the study area. The chapter describes the biophysical characteristics of the estate, the history of its establishment, its silvicultural management, and the effects of these factors upon stand and tree metrics. The age structure and high variability in stand condition make the estate an ideal candidate for remote sensing based inventory.

Chapter 4 describes the data collection method. The sampling strategy is explained and field data collection and pre-processing methods are described. The distributional characteristics of the sampled data are also described.

Chapter 5 presents a local tree density study. A number of local tree density indexes are adapted for use with remotely sensed data. These indexes are then used to predict the breast height diameter of subject trees, and subsequently, to infer the nature and extent of between-tree interactions in each dataset. It is argued that the use of local tree density indexes provides a biologically interpretable method to summarise potentially remotely sensed data products to a form amenable to further modelling of alternative tree metrics such as stem profile. Implications for forest inventory in spatially variable radiata pine plantations are discussed.

Chapters 6 and 7 describe a stem profile modelling study. In chapter 6, previously published segmented polynomial, and variable-exponent stem profile models are adapted for use with total height and local density data and applied using two methods appropriate to the nested and heterogenous data structure. A new model is developed to overcome some of the modelling difficulties which are encountered.

In Chapter 7, comparisons between the models and fitting methods are drawn by evaluating their utility in estimating diameter at given heights, volume within specified height constraints, merchantable height within specified diameter constraints and total volume within specified size class constraints. Potential inventory applications of the models are identified.

Chapter 8 presents the conclusions of the thesis, summarising the results of the thesis against the stated aims.

*Chapter 2*

# Review

## 2.1 Overview

In this chapter, fields of research pertinent to the objective of the thesis are reviewed and the research rationale is further developed.

Previous remote sensing based inventory research in radiata pine (*Pinus radiata* (D. Don)) is reviewed. These studies, and many others, have employed tree metrics such as total height and crown area to predict breast height diameter and total volume (Hall et al. 1989; Biggs 1990). Local density indexes, which characterise between-tree interaction, have also been used in some previous work. Some more recently published remote sensing research is then reviewed. Both the development of new sensor systems and the digitisation of remotely sensed data have allowed data analysis to become increasingly automated, improving repeatability and reducing costs per unit area. It is suggested that tree height and location survey are likely to more precise and accurate than surveys of crown dimension in radiata pine. It is proposed that these metrics may be used to characterise the extent of between-tree interactions.

A simple study using a growth model parameterised for Tasmanian radiata pine and inventory plot data from the study site are used to show that the component of basal area which is grown between the onset of between-tree interactions and subsequent thinning is likely to be a substantial component of the total by thinning age, suggesting methods to characterise it may well improve stem size prediction in stands at the first, and possibly second thinning. Further reviews of the nature of between tree interactions show that these interactions are thought to largely occur between proximate neighbouring trees and also above ground, suggesting that tree locations and heights may well be suitable for their

characterisation. Previously developed methods to characterise interactions are then described. Those that are suited to reformulation using tree height and location are indicated.

Stem development theories and methods to describe stem shape are then presented. Several development theories find support in empirical studies; however no single theory has yet been adequate to describe stem shape with the precision required for timber inventory. Instead, empirical models are used. The development of profile modelling is described briefly. That development has seen models published of increasing complexity with increasing management demands. It has also seen improvements to parameter estimation methods in light of the correlated and heterogenous profile data common to such studies that complicate inference and hypothesis testing. Model forms and fitting methods which may be suited to use in remote sensing based inventory are indicated.

## 2.2 Inventory by airborne remote sensing

### 2.2.1 An historical overview

Remote sensing is a general term which 'describes the action of obtaining information about an object with a sensor which is physically separated from the object' (Harrison and Jupp 1989). Historically, remote sensing activities in forest inventory have been dominated by the use of aircraft mounted cameras that capture imagery on chemical film. Broadly, the uses of remote sensing in forest inventory are twofold. Measurements from remotely sensed data can be used to predict the dimensions of tree or stand metrics such as breast height diameter or stand volume. Alternatively, the classification of areal regions of relatively homogeneous remotely sensed data into uniform continuous units can be used to map forest features: features such as structural strata, species composition, and age. The scale at which the data are captured reflects the purpose to which it is applied. Medium to small-scale imagery (eg. 1:25 000) is usually applied to mapping tasks, and the photo-plot measurement of stand level variables such as top height, canopy closure and stocking. Large-scale imagery (eg. 1:5 000 scale) is usually applied to the photo-plot measurement of individual trees. Photo interpretation and photo-plot measurement is still undertaken manually by Tasmanian plantation management agencies (Thompson 2000; Rush 2002).

Research in using airborne remote sensing in Australian forest inventory began in the years immediately post WWII. Cromer and Aitkin (1948) estimated stand volumes of norfolk island pine (*Araucaria heterophylla*). Later workers mapped native forest types (Carron and Hall 1954; Lawrence and Walker 1954). Concurrent research was published in the early 1970's on the application of aerial photography to radiata pine inventory in New Zealand (Avery 1971; Avery and Canning 1973; Avery and Canning 1974; Myers 1974) and Australia (Spencer 1972; Thompson 1976; Spencer 1979). This body of work in radiata pine focussed on predicting tree stocking to assess establishment success early in the rotation and tree-level stem metric prediction at later ages prior to the significant reduction in height increment in intensively managed thinned stands.

Spencer (1972) argued that double phase sampling in radiata pine forests using photo-sample plots, followed by ground truthing, was financially advantageous when compared to traditional single phase ground based inventory schemes. In his review of aerial photography applications to forest inventory, he argued that medium- to small-scale imagery was unsuited to plantation assessment because the errors associated with stand-level estimates of stand volume were too large for the results to be of use in the characteristically small, relatively homogeneous radiata pine forests. He argued that instead, measurements of total height and crown width of individual trees should be used to estimate tree stem metrics. He then developed regression equations to relate photo sample plot measured height and crown width to stem diameter at breast height and merchantable volume. Avery and Canning (1973, 1974) approached the problem in a similar manner and reported similar findings in their work in similar radiata pine forests. For example, they used linear regression to predict ground measured overbark breast height diameter using photo measured crown diameter and reported an $R^2$ of 0.84. They also fitted models which included photo measured tree height as an additional predictor and reported an $R^2$ of 0.89. These studies drew data from repeatedly and recently thinned 12-year-old stands, where stocking ranged between 200 and 540 stems per hectare. It is important to note that, with such low stockings, crown edges were evidently easy enough to measure in both photo and ground plots.

Trees increase in height during growth in order to elevate reproductive and dispersal organs, shade out competitors and increase exposure to light; so facilitating greater rates of photosynthesis (Rich et al. 1986; Aarssen 1995; O'Brien et al. 1995). The latter outcome of height growth leads to greater stem growth and ensures that tree stem and height metrics relate in a positive manner, with the

strength of the relationship being greatest during the rotation phase in which rapid height growth occurs. Positive correlations also exist between tree stem and crown metrics, both because the tree needs to grow stem wood to keep its crown aloft and because the extent of crown exposure has a large bearing on the photosynthetic capacity of the tree and therefore, realised stem growth potential (Larson 1963). Crown metrics such as diameter or surface area are therefore widely used in remote sensing based inventories (Biggs 1990). Earlier researchers also considered stem metric prediction models which, in addition to both tree height and crown metrics, included local density indexes as further covariates.

Local density indexes may be defined by relating subject and neighbour tree metrics. The correlation between local density and stem metrics is induced by the interactions between neighbouring trees that control the allocation of limited growth resources, both between trees and within them. Local density indexes thus characterise divergent realised stem growth trajectories, realised trajectories that may not be accounted for in other tree metrics. Sayn-Wittgenstein and Aldred (1967) investigated the use of local density in a large-scale photo forest inventory of three species in the forests of the North American Pacific Northwest. They defined local density in two ways. First, local density was defined as the number of trees within a total height dependent radius about the subject; and secondly, as the proportion of the subject tree crown shaded by the crowns of its neighbours. They found that neither index offered any great improvement over those models that already included total height and crown diameter. These findings mirrored those of earlier researchers who considered the additional independent variables: stand density (Bonnor 1964), crown class and number of trees within a fixed radius (Lyons 1964). Consequently, later large-scale photo inventory research ignored local density and focussed instead on capturing crown and height metrics (Hall et al. 1989; Biggs 1990).

### 2.2.2 Recent developments

Many automated methods to extract tree or stand metrics from airborne remote sensing data are already operational and research in this area is ongoing (1998).

#### *2.2.2.1 Individual tree location*

There are a wide range of approaches to automatically delineating the location of trees and/or the size of their crowns in high-resolution spatial imagery (e.g. Gougeon 1995; Pinz 1998; Bolduc et al. 1999; Lefsky et al. 1999; Pollock 1999; Rudemo 1999; Walsworth and King 1999). One of the first published was the 'valley following' approach (Gougeon 1995). The algorithm that Gougeon developed exploits the fact that the areas between trees crowns are characterised by a lower radiometric response since, being lower than the proximate crown apexes, are subject to more shadowing. He termed these areas 'valleys'. First, the imagery is masked to remove areas of non-vegetation and extreme shadow. A moving window of stipulated size is then applied to locate the pixels about which all immediate neighbouring pixels have larger radiometric values. The algorithm then assesses the neighbouring pixels about each of these defined local minima. Neighbours, which are darker than either perpendicularly adjacent pixel, are coded as 'valley' pixels. This 'valley' pixel recognition phase is iterated until no further recoding occurs. A rule-based program is then applied to locate and complete partially delineated crowns. Because the algorithm uses shadow to locate crowns, it works best in stands comprised of well defined tree crowns, using imagery captured at high solar zenith angles so that inter-crown shadow is accentuated (Gougeon, 1995). Its use is practically limited to stands that are at least moderately dense, since image shadow is assumed to mark crown edges (Gougeon and Leckie 1999).

Gougeon's 'valley following' algorithm was modified to count individual tree stems in radiata pine stands in a New Zealand study (Andrew et al. 1999). Researchers investigated a range of pre-processing options, including image thresholding techniques and moving window sizes, and compared results obtained using imagery captured at several different solar zenith angles. They reported error variances as low as 0.035 about a standardised mean of 1.00. In a later report, Goulding et al. (2000) compared this approach to the counting of individual trees in radiata pine stands to both geo-statistical and multi-stage satellite image analysis approaches and concluded that stocking estimates are best achieved using Gougeon's approach.

While several alternative tree delineation methods exist, two further approaches have been deemed most suited to stands with regularly spaced trees and dense canopies of uniform height and illumination (Walsworth and King 1999), such as are found in younger radiata pine stands. The high pass filter method involves the use of a moving window to identify pixels with maximum radiometric values which

in a stand height model. The accuracy of any one point in the derived model is too low to extract the heights of individual trees (Wijanarto 2001). Approaches to the extraction of individual tree height from the more geometrically accurate airborne laser scanner data have also been published, eg. (Hyyppä et al. 2001; Persson et al. 2002; Popescu et al. 2002; Morsdorf et al. 2004). The fusion of spatially continuous radiometric data with geometrically accurate laser scanner data also offers much promise for the derivation of individual tree information (Leckie 1990). While techniques to fuse the data sources have thus far been only moderately successful (St-Onge and Vega 2003; Morsdorf et al. 2004), work in this area is also likely to continue (Leckie et al. 2003).

### 2.2.3 Summary of airborne remote sensing developments

While spatially extensive stocking and canopy height estimates are of immediate utility to forest managers, as Spencer (1972) noted, tree-level data are likely to be more useful for subsequent timber metric estimation in radiata pine since the potential precision of tree-level timber estimation is higher than that of stand-level estimation. Fortuitously, the new technologies largely promise tree-level resolution.

Prior to reaching 20 to 25 years of age, radiata pine height growth is relatively rapid and tree crowns are characteristically conical in shape. In terms of tree height, this phase is most suited to remote sensing based estimation because a relatively strong relationship is present between tree height and other stem metrics. The relationships are not so obvious with respect to other canopy metrics. radiata pine stands in Tasmania typically close canopy by age 8, are thinned at about 15 years after planting, and again at 20 years after planting (Neilsen 1990; Rush 2003). Where undisturbed by thinning, neighbouring tree crowns typically interlock in post-canopy closure stands. Mechanised thinning is normally used, so trees are removed from out rows and bays, generating varied between-tree spacings. Some trees retain all immediate neighbours, while others lose some or most immediate neighbours; thus some trees retain interlocking crowns with their neighbours while others do not[2]. Crown delineation algorithms are still effective at

[2] This is in contrast to the radiata pine stands that were previously studied in remote sensing inventory research which were subject to intensive pruning and manual thinning. Researchers in these stands make no mention of difficulties in identifying crown extent, either in imagery or in the field (Spencer 1972, Avery and Canning 1973 and 1974). Particularly in unthinned stands, but also featuring in thinned stands, the trees used in this study carried crowns which interlocked with neighbours to such an extent that branch ownership was obscured, precluding accurate ground based measurements of crown diameter.

identifying individual trees under these conditions (Andrew et al. 1999; Morsdorf et al. 2004). However, the accuracy of the measurement of individual tree crown extent is likely to be dependent on the extent of the interlocking region and this may be varied and unreliably assessed. In contrast, the accuracy of locating individual trees using most automated data analysis methods relies more on the spatial resolution and solar illumination properties of the data, rather than the nature of tree spacing and crown interaction (Andrew et al. 1999).

Those early researchers who evaluated local density indexes derived using tree location and height information (Bonnor 1964; Lyons 1964; Sayn-Wittgenstein and Aldred 1967) did so where reliably assessed crown metrics were also available, which made local density measures largely superfluous (Hall et al. 1989; Biggs 1990). In such a situation, the existence of a non-spurious local density correlation with a stem metric is predicated upon the existence of spatial correlation that is not accounted for in other tree metrics. The utility of local density has not been tested in the absence of reliably assessed crown metrics. The following discussion explores the growth processes in radiata pine within stands, between trees, and within trees. This discussion illuminates the potential role of local density information in describing stem size and profile.

## 2.3 Growth interactions in radiata pine

### 2.3.1 Stand-level growth

Silvicultural activities in radiata pine stands are designed to ensure that stand growth is allocated amongst individual trees in a way that maximises the net value of the merchantable timber volume. This is achieved by manipulating the extent of between-tree interactions throughout the rotation. Stands are typically planted at high stockings and subsequently thinned at regular intervals; the first of which occurs at some point after canopy closure. Thinning reduces the interactions between retained trees, particularly competitive interactions, so that high stem volume production can be maintained on the trees with the best form and least defect. Thinning is scheduled to occur after canopy closure in order to limit the greater stem taper, larger knot formation and other stem defects that are characteristic of open grown trees (Neilsen 1990). These activities all ensure that some component of tree growth occurs under circumstances in which trees interact. The influence of between-tree interactions on stand basal area growth and how this

varies with stand condition up to thinning age can be explored using existing inventory data and a stand growth model.

The data used in the following discussion were captured in the age 10 inventory in the Uxbridge Moogara radiata pine estate. This estate is situated in south eastern Tasmania[3]. The data consist of basal area, mean dominant height and stocking estimates derived from measurements in plots located by systematic stratified design. They are well suited to this discussion because they are derived from a single estate which, while comprised of stands of highly varying quality, was planted over a relatively short period. There are limited differences in the planted genetic material, experienced climatic conditions, and establishment and inventory methods, so limiting the number and degree of influence of nuisance covariates. Data from 137 plots were available for use in the following analysis. These data are also described further in Chapter 3.2.3.

A basal area growth model can be used to predict when stocking begins to influence stand basal area growth. It may also be used to predict the sum total basal area grown between the point in time at which interactions begin and the point in time at which they are interrupted by thinning activities.

Candy (1989b) modelled Tasmanian radiata pine basal area using a Gompertz-like growth model which, in projection form, is given by:

$$G_{t_k} = G_{t_{k-j}} \times e^{e^{\alpha+\beta+\log(t_{k-j})}} - e^{e^{\alpha+\beta+\log(t_k)}} \qquad (2.1)$$

Where:

$G_k$ is projected basal area at age $t_k$;

$G_{t_{k-1}}$ is basal area at age $t_{k-j}$. This is typically age at inventory, i.e. $t_{k-j}$=10 years.

$\alpha$ and $\beta$ are model parameters.

Large variability in stand condition is reflected in the inventory data. Candy (1999) also derived second stage models to localise predictions for each plot. These models use basal area, stocking and mean dominant height at inventory age as covariates and are described further in Appendix I.

[3] A detailed description and map locating the Uxbridge Moogara radiata pine estate appears in Chapter 3.2.

In the absence of thinning or other manipulations of stand basal area, equation 2.1 predicts the trajectory of stand basal area growth from establishment to maturity to be of sigmoid form. The point of inflection between the concave and convex components isolates the point of growth deceleration. It is generally accepted that the onset of deceleration is due to the reduction in the availability of the resources required for stand growth, and this can be attributed to the competing resource uptake between neighbouring trees within the stand (e.g. Donald 1963; Assman 1970; Harper 1977; Brand and Magnussen 1988; Keddy 1989; Radtke and Burkhart 1999; Radtke et al. 2003). The point in time at which growth inflects can be determined by calculating the second partial derivative of basal area with respect to age. This is given by:

$$\frac{dG_{t_k}^{\ 2}}{d^2t} = G_{t_{k-1}} \frac{\beta}{t_k^{\ 2}} e^{\alpha+\beta\log(t_k)+e^{\alpha+\beta\log(t_{k-1})}-e^{\alpha+\beta\log(t_k)}} \left(1-\beta\left(1-e^{\alpha+\beta\log(t_k)}\right)\right) \qquad (2.2)$$

A plot of basal area increment (equation 2.1) and the second partial derivative of basal area with respect to age (equation 2.2), localised for the median stand metrics from the Uxbridge Moogara inventory dataset, is presented in Figure 2.1. The increase in the second derivative from the time origin in Figure 2.1 corresponds to the acceleration in basal area growth from zero to a predicted maximum at a decimal age of 4.5. From this point, the magnitude of the acceleration decreases again, reaching zero at a predicted decimal age of 11.5, after which deceleration occurs. 40% of the basal area increment prior to 15.5 decimal years[4] is predicted to have grown under decelerating conditions where between-tree interactions are believed to influence increment.

It is useful to consider these relationships at the plot level to gain a greater understanding both of the extent of variability in stand condition which is present in the estate, and of how stand condition impacts on the timing and development of the between-tree interactions that influence stand basal area growth. Figure 2.2 presents scatter plots of stocking and mean dominant height, at measurement age (t=10) and projected through to thinning age (t=15.5). Point colours represent the percentage of basal area at the specified age which is predicted to have accumulated after the inflection age. The predicted percentage of post-inflection increment and the predicted inflection age are determined using equation 2.2, localised for the stand metrics recorded for each plot.

[4] 15.5 decimal years is the time after planting at which thinning operations are nominally scheduled to occur Rush, M. (2003). First thinning age in the Norske Skog estate is 15 to 16 years.

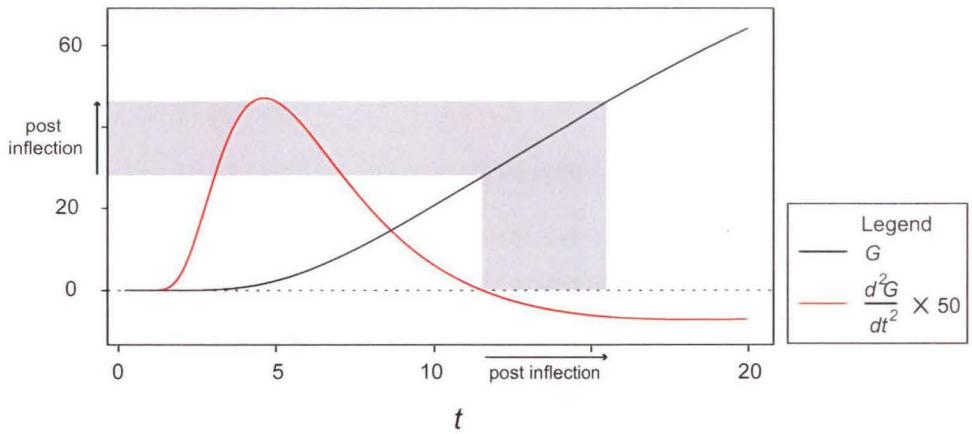


Figure 2.1 Median Basal Area and the second derivative of basal area with respect to time versus time since planting for radiata pine in the Uxbridge Moogara estate

The plots that are predicted to have inflected by the age of measurement are restricted to those which display the larger inventory metric values. Of the total 137 plots, 43 are predicted to have inflected by the age of measurement and 31 do not inflect by thinning age. The quantity of the predicted basal area grown after inflection varies widely between the plots, ranging up to 67% of the total. The plots that are predicted to inflect prior to thinning age are restricted to those with stockings at thinning age in excess of approximately 750 stems $Ha^{-1}$. The relationship between mean dominant height and post-inflection increment is weak.

While the total predicted post-inflection basal area increment for many plots is a significantly large component of the total, viewing the basal area increment curve in Figure 2.1, it is also evident that predicted stand-level changes in slope are rather minor about the inflection point. This indicates that the predicted stand-level changes in basal area growth after inflection, and therefore differences in realised stand basal area at thinning age, are also likely to be rather small. At a tree level, changes in basal area growth and subsequent realised basal area at thinning age may be more significant for a number of reasons. Despite the nominally even spaced grid planting, varying realised between tree distances attributable to establishment mortality, together with varying growth rates among trees attributable to localised environmental conditions and genotypic differences are likely to cause variation in the timing of the onset and extent of interactions between trees. The nature of the interactions may result in unequal resource allocation and subsequent divergent stem growth trajectories, so the observed decrease in stand basal area increment may be spread unevenly among individuals. Finally, trees may also optimise growth to account for interactions and so allocate resources within the stem in different ways. The nature of resource allocation in

the presence of between tree interactions, firstly between-, and secondly within-trees, will now be discussed further.

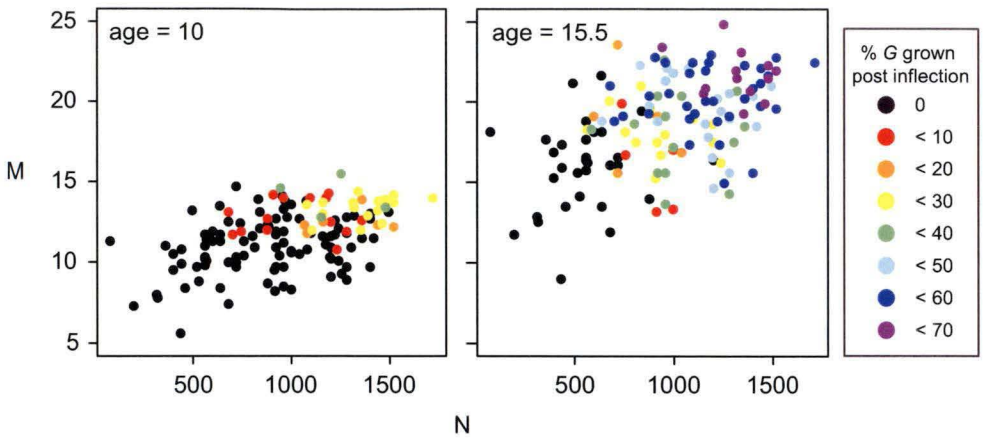


Figure 2.2 Scatter plots of mean dominant height versus stocking as measured at age 10 and as predicted at age 15.5 for the Uxbridge Moogara inventory data. Point colours represent the percentage class of basal area increment at the specified age which is grown post inflection as predicted using a two-stage Gompertz model fitted for Tasmanian radiata pine (Candy 1989b; Candy 1999).

### 2.3.2 Between-tree growth interactions

Researchers who have investigated the allocation of limited resources between trees refer to the process as competition. The vast majority of competition studies have occurred in the context of modelling the growth of individual trees (Simard and Sachs 2004), although some have inferred growth patterns using static data (e.g. Newton and Jolliffe 1998; Wright et al. 1998; Drever and Lertzman 2001). Many of the evaluation techniques which have been used in this field have application in tree-level remote sensing based inventory.

#### *2.3.2.1 Modes of competition*

Competition between trees can be considered to occur along a continuum between complete symmetry and asymmetry. Symmetric competition refers to the equal sharing of a limiting resource proportional to the size of the competing individuals, whereas asymmetric competition refers to any resource sharing which deviates from this size constrained equality (Begon 1984; Weiner 1990; Schwinning and Weiner 1998). Symmetric competition is thought to largely occur below ground, where proximate roots belonging to interacting neighbouring trees may both generate zones of depletion which impact upon one another's subsequent resource uptake. Since the uptake of water and nutrients is passive, the quantity consumed by each individual is believed to be directly proportional to the size of its root mass (Weiner 1985; Weiner and Thomas 1986; Casper and Jackson 1997; Schwinning and Weiner 1998). Asymmetric competition is thought to largely occur above ground as competition for light. Since light is a directionally supplied resource, any two leaves covering the same area of ground must receive disproportionate quantities dependent upon their respective positions. In other words, larger individuals generally shade out smaller neighbours, while those same smaller neighbours cannot reciprocate shading to the same degree (Gifford and Evans 1981; Perry 1985; Weiner 1985; Weiner and Thomas 1986; Schwinning and Weiner 1998), although this may be mediated somewhat by crown structure (Vanclay 1994) and overall plant density (Schwinning 1996).

A further theoretical distinction can be drawn between two-sided and one-sided modes of competition (Cannell et al. 1984; Weiner 1985; Weiner and Thomas 1986; Brand and Magnussen 1988; Newton and Jolliffe 1998; Simard and Sachs 2004). Two-sided competition refers to situations where smaller trees can affect the resource uptake of their larger neighbours. Competition then is said to occur upward from below. One-sided competition refers to situations where larger trees affect the resource uptake of their smaller neighbours without reciprocation; this is competition downward from above. The mechanisms thought to drive two and one-sided competition are the same as those driving symmetric and asymmetric competition, respectively. The degree of asymmetry refers to the degree of inequality of resource sharing, while the degree of sidedness refers to the magnitude of upward or downward competition (Brand and Magnussen 1988). Methods to evaluate sidedness in competition studies are a recent development (Newton and Jolliffe 1998; Simard and Sachs 2004).

Species-specific growth strategies may influence the mode of competition. The rapid height growth that is a common feature in species which form even-aged monocultures is viewed as a resource pre-emption strategy (Newton and Jolliffe 1998; Newton and Jolliffe 1998; Berntson and Wayne 2000) as it maximises each individual's opportunity to access available light to the long term detriment of its neighbours. Resource pre-emption growth strategies therefore typically occur under asymmetric, one-sided competitive conditions. In contrast, species which grow in height slowly and produce spreading crowns early are believed to more commonly employ a resource depletion strategy (Newton and Jolliffe 1998; Newton and Jolliffe 1998; Berntson and Wayne 2000) in which neighbouring individuals compete for below-ground resources. Resource depletion typically occurs under symmetric, two-sided competitive conditions.

#### *2.3.2.2 Competition effects on tree size distributions*

The development of a log-normal distribution in plant size (or positive skewness) has been widely observed in even-aged, mono-specific plant populations (Ford 1975; Diggle 1976; Gifford and Evans 1981), including even-aged tree plantations (Bliss and Reinker 1964; Gates 1978; Gates and Westcott 1982; Gates et al. 1983; Bi 1989) and forests (West 1981; Newton and Jolliffe 1998). From an initial, nominally Normal density of plant sizes, positive skewness in plant size develops as larger plants grow faster than their neighbours. While factors other than competition can also be related to the temporal change in the size distribution of trees within a stand, including variability in the initial size distribution, micro site characteristics and individual physiological vigour (Ross and Harper 1972), most early researchers inferred that this phenomenon was caused by competition because greater positive skewness was observed in populations with closer initial spacings (Harper 1967).

Several researchers used distribution-modifying functions to analyse growth in even-aged plant monocultures with a view to exploring the effects of symmetric and asymmetric competition in the development of size distributions (Westoby 1982; Hara 1984; Hara 1984; Westoby 1984; Brand and Magnussen 1988; West et al. 1989). The technique entails defining a size distribution of a plant population through time using a forward-diffusion equation, the three coefficients of which are defined in second-stage models. The three second-stage models are functions at each time interval of, respectively, the mean growth rate of individuals within each size class (termed 'drift'), the variance in growth rate of individuals within each

size class (termed 'diffusion'), and finally, the probability of death for individuals within each size class (termed 'mortality'). By examining the magnitude of the contribution of each second-stage model, it is possible to infer the dominant mode of competition present. The magnitude of the drift term reflects the expressed degree of symmetric competition, while the magnitude of the diffusion term reflects the expressed degree of asymmetric competition.

West et al. (1989) used distribution-modifying functions to study growth responses to between-tree spacing in radiata pine plantations at Mt Burr in South Australia. Applying Hara's (1984a; 1984b) method to tree DBH data from 18 unthinned plots planted at grid spacings varying from 1.8 to 3.3 m, the results showed the largest contribution to be from diffusion in every plot between the first measurement age of 9 years up to 45 years, supporting the assertion that asymmetric competition is the dominant process by which limited resources are allocated in these plantations. The observed minor drift contribution observed in their study corroborates visual inspection of the fitted basal area growth model presented in Figure 2.1 in which predicted changes to the median basal area increment with the onset of competition appear very minor.

Negative skewness earlier in stand development has been observed in radiata pine. Using the same dataset, Gates et al. (1983) studied stand-level phenomena and found that DBH distribution skewness became negative from the time of planting, then increased, becoming positive from an average age between 10 and 35 years at tree spacings of 1.8 and 3.3 metres respectively. These researchers argued that the larger trees were more likely to begin competing first during the establishment of competitive relations, slowing their growth rates sooner relative to the smaller trees. They attributed skewness reversal to the development of asymmetric competition with full site occupancy.

In yet another study using this dataset, West and Borough (1983) reported on the relationship between tree DBH and DBH growth rate. This study showed that the relationship is linear at early ages, but develops into a segmented system with time, in which trees of DBH less than approximately 20 centimetres largely stop growing, while those over 20 centimetres in size tend to continue growing with the same linear relationship to DBH. The growth of some individuals comprised a transition zone between the two growth states. They observed during field inspection at the end of the experiment that the non-growing trees together comprised a secondary tree canopy that was 'largely overtopped' by the canopy of

are then coded as tree crown apexes (Pinz 1998; Walsworth and King 1999). The size of the window affects the number of local maxima identified so the optimum window size is that which encompasses individual tree crowns only. The 'template matching' approach (Pollock 1999) is slightly more sophisticated and involves the construction of a model of the theorised radiometric response of individual tree crowns of differing shape and size. The radiometric model is used as a template that is matched to imagery in a moving window and regions of pixels that are suitably similar to the template are then recoded as tree crowns. The approach works best in areas with trees of similar shapes and sizes since this limits the range of pixel configurations that need to be defined (Larsen 1998).

Many algorithms designed for use with optical image data may also be modified for use in the analysis of the geometric models of forest canopy produced from the processing of airborne laser scanner data (Lefsky et al. 1999; Popescu et al. 2002). Airborne laser scanner systems employ an aircraft mounted, scanning pulsed laser device to measure the three dimensional coordinates of an array of points over the ground below. The first return, intermediate returns, and the last return for each pulse can be discriminated in order to separate underlying points in the terrain from points in the overlying forest, and further interpolation of the filtered ALS data produces models of canopy height. As the density of the point array increases, the distance between interpolation points decreases, with an attendant improvement in the accuracy of the derived canopy model (St-Onge and Vega 2003). The density of the point array is limited by the laser instrument design and configuration, and the flying height and speed of the aircraft. With the release of each new laser instrument design the pulse rate has increased[1] and a continued improvement in the accuracy of canopy models is expected (Evans et al. 2001; Leckie et al. 2003).

#### *2.2.2.2 Individual tree and stand height*

Several methods to derive moving average stand height from remote sensing data have been published (e.g. Nelson et al. 1988; Nilsson 1996; Wijanarto 2001). Stereo pairs of aerial photography can be used to derive models of canopy geometry. Where a terrain model is available, its subtraction from the canopy model results

[1] For example, the first released Optech airborne laser scanner instrument (Optech ALTM 1020) generated 5000 laser strike measurements per second. The latest released instrument (Optech ALTM 3100) generates 100 000 per second. This is the maximum possible pulse rate using the current technology since the pulses are indistinguishable at greater rates (Pers. Comm· Jonas, D. 2004)

the growing trees. They noted that no plots in their study contained non-growing trees prior to age 15.

#### *2.3.2.3 Summary of between-tree interactions*

The Mt Burr studies described by West and Borough (1983), Gates et al. (1983), and West et al. (1989), showed that DBH growth in radiata pine was dominated by asymmetric competition by age 9. Early negative skew in the diameter distribution gave way to positive skew with time as the component of tree diameter grown under asymmetric competitive conditions increased. Post-interaction DBH growth tended toward a linear relationship with DBH for all but a small component of the stand that tended to stop growing altogether. This led to the development of a two-tiered canopy by the end of the experiment at age 45.

The asymmetric competition which dominates between-tree interactions in radiata pine causes the growth trajectories of competing individuals to diverge[5], suggesting that methods to characterise its outcomes at the tree level will improve remote sensing based inventory. Because asymmetric competition occurs above ground, between immediate neighbours, and is driven by access to light, tree height and location data should be useful tree metrics with which to characterise the competitive status of an individual at a given moment in time as they should adequately describe the light environment experienced by each individual tree.

The Mt Burr studies show that the nature of competition within radiata pine changes through time. A snapshot of asymmetric competitive status will not; therefore, necessarily describe past growth well, so opportunities to characterise interaction are limited. Prior to significant interactions early in stand development, the growth of individual trees is independent of neighbour effects; thus characterisation of competitive status at this time is likely to be poor. Characterisation of the asymmetric competitive status after thinning is also likely to be poor, given the removal of some the individuals that previously contributed to growth trajectory divergence. From a more practical perspective, the full benefits of profile modelling are realised at later ages when increasing quantities of harvested volume are comprised of sawlog for which diameter and length constraints are more substantial. This reasoning suggests this research should focus on stands at ages immediately prior to first thinning at the optimum age for

[5] This is the 'diffusion' phenomenon defined in the distribution modifying functional studies described in Chapter 2.3.2.2.

characterising competitive status and immediately prior to second thinning at a more favourable age for stem profile modelling.

### 2.3.3 Evaluating between-tree interactions

Competition indexes have been developed to quantify the response of individual trees to between-tree interactions (Weigelt and Jolliffe 2003). These indexes are mathematical expressions of the influence of the size and, in many cases, the location of, or distance to, neighbouring trees with respect to the subject. A distinction can be drawn between the distance independent indexes that relate the size of the subject tree in some way to the stand average, and the distance dependent indexes that also include some measure of neighbour dimension, and spatial location or distance from the subject (Whyte and Woolons 1992). While distance independent indexes attempt to describe the general environmental influences and competitive effects experienced by an individual within a stand, distance dependent indexes incorporate the influence of individual interacting neighbours (Tome and Burkhart 1989).

While one might assume that incorporating the spatial location of trees would improve the performance of an index for the prediction of tree growth, the results of numerous studies demonstrate that this assumption does not necessarily hold. Lorimer (1983) found that including inter-tree distance added no accuracy to the prediction of tree diameter growth in even-aged hardwoods in Wisconsin, USA. Hatch et al. (1975), and Martin and Ek (1984), found inter-tree distances to be of little value in modelling diameter and basal area growth respectively in red pine (*Pinus resinosa*). Daniels et al. (1986) modelled basal area growth in loblolly pine (*Pinus* taeda) and found little difference in performance between a distance dependent competition index and crown ratio. Several researchers have attributed these results to the efficiency of diameter as an expression of tree growth, noting that competition indexes often have a lower correlation with growth than does diameter (e.g. Martin and Ek 1984; Biging and Dobbertin 1995). Lederman and Stage (2001) argue that the nature of competition should be considered as well. They noted that asymmetric competition is more likely to occur over a smaller area and be best characterised using a distance dependent index; whereas a distance independent index, incorporating stand averages measured over larger distances, would best characterise the more diffuse symmetric competition.

The majority of indexes have been derived for use in modelling the diameter growth of individual trees[6]. The same metric is most often also used in index formulation, presumably because of the convenience of its assessment and the strength of its relationship with total biomass. The latter would suggest tree height is a less suitable competition metric; however the situation is less clear if the nature of competition is considered. Intuitively, the neighbour metric which causes reduced growth in a subject will best characterise competitive status. When competition for light resources is the dominant process the optimum metric is one which characterises the influence of neighbouring trees on the quantity of light acquired by the subject. Hatch et al. (1975) used this rational in formulating an index which used exposed crown surface area rather than tree diameter to assess changes in diameter increment and demonstrated some minor improvements in doing so.

In reformulating the index by replacing the predicted metric (usually diameter) with the metric responsible for the competitive influence (height and location) one further complication arises. While the degree of symmetry is represented formally in many index formulations, the use of an alternate metric in index formulation to that which is predicted in the modelling exercise also means that the symmetry of the competitive relationship is conflated with the allometry of the metric relationship. With these factors in mind, the competition indexes are now described and those which are amenable to reformulation using tree height are indicated.

#### *2.3.3.1 Distance dependent competition indexes*

The distance dependent indexes can be separated into four groups:

- the area potentially available indexes, (e.g. Brown 1965; Moore et al. 1973; Pelz 1978; Nance et al. 1988);
- the area overlap indexes, (e.g. Opie 1968; Gerrard 1969; Bella 1971; Tome and Burkhart 1989);
- the point density indexes, (e.g. Spurr 1962; Pukkala and Kolstrom 1987); and
- the distance weighted size indexes, (e.g. Weiner 1984; Silander and Pacala 1985) and distance weighted size ratio indexes, (e.g. Hamilton 1969; Hegyi

[6] Many modellers have investigated individual tree basal area growth. This metric is derived from transformed diameter measurements.

1974; Lorimer 1983; Martin and Ek 1984; Daniels et al. 1986; Tome and Burkhart 1989).

*2.3.3.1.1 Area Potentially Available index*

Area Potentially Available (APA) index (Brown 1965) values are calculated as the planar area of the polygon defined about the subject tree by perpendicular bisectors positioned between the subject and each of its neighbours. The intersections of the perpendicular bisectors form the corner points of the APA polygon. This concept is adapted from that of the Voronoi diagram in which an area is divided into a continuous tessellation of non-overlapping polygons. APA polygons for a hypothetical stand are illustrated in Figure 2.3.

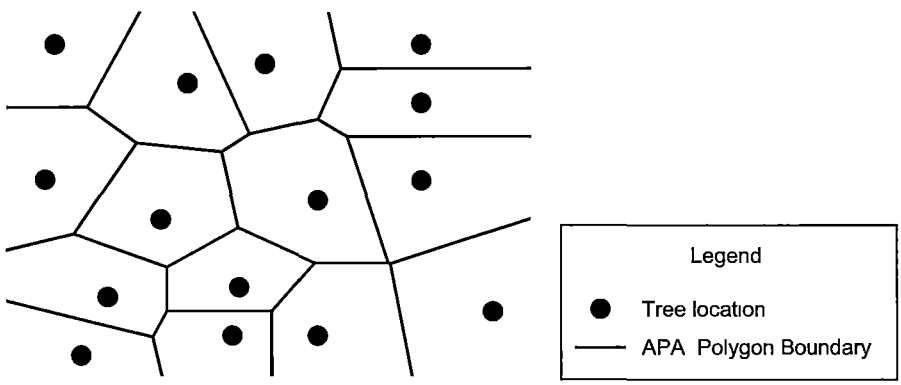


Figure 2.3 Area Potentially Available (APA) polygons defined by perpendicular bisectors for a hypothetical stand.

While Brown (1965) set the locations of the perpendicular bisectors equidistant between competitors, later authors modified these locations according to some measure of relative tree size (Moore et al. 1973; Pelz 1978). For example, Moore et al. (1973) modified the extent of each APA polygon by adjusting the location of each bisector proportional to the relative diameters of the competitors between which each bisector lay.

Their modification was calculated as:

$$a_j = A_j \frac{D}{\left(D + D_j\right)}. \tag{2.3}$$

Where:

$a_j$ is the distance from the subject tree to the perpendicular bisector between the subject tree and the *jth* neighbour tree;

$A_j$ is the distance from the subject tree to the *jth* neighbour tree;

$D$ is the breast height diameter of the subject tree;

$D_j$ is the breast height diameter of the *jth* neighbour tree.

Moore et al. (1973) study investigated stem increment in terms of diameter and basal area. For the latter they defined $a_j$ proportional to $D^2$:

$$a_j = A_j \frac{D^2}{\left(D^2 + D_j^2\right)}. \tag{2.4}$$

Tome and Burkhart (1989) incorporated asymmetry in a formal way by adding a power term to the bisector location function:

$$a_j = A_j \frac{D^k}{\left(D^k + D_j^k\right)}. \tag{2.5}$$

Where:

$k$ is a weighting factor defining the degree of competitive asymmetry.

An asymmetric formulation ($k$=2) has been found to be a better predictor of diameter growth than that formulation containing the linear diameter term (Tome and Burkhart 1989; Fox 2000).

Nance et al. (1988) constrained the extent of the polygons in order to avoid the derivation of large irregular polygons in situations where spatial arrangement of trees became overly irregular. They did this by constraining the area over which each polygon may extend to that defined by a circle with its centre over the

subject tree. They defined the circle area by partitioning the total plot area to each individual within the plot according to their relative diameter:

$$pa_i = \sqrt{\frac{pa\left(D \Big/ \sum_{j=1} D_j\right)}{\pi}}. \tag{2.6}$$

Where:

$pa_i$ is the area of the constrained circle about the subject tree;

$pa$ is the total plot area.

The APA index is a candidate for formulation using tree height and location data.

*2.3.3.1.2 Point Density index*

Spurr (1962) proposed the Point Density index to describe competition at a particular point in the stand. He developed two variants, one that includes the subject tree and one that does not, and selected competitors using a fixed angle gauge sweep centred at the subject tree.

Those variants are defined respectively by:

$$PDI = \frac{2500\left[\sum_{j=1}^{n_i}(j+0.5)\left(D_j \Big/ A_{ij}\right)^2\right]}{n}. \tag{2.7}$$

And:

$$PDE = \frac{2500\left[\sum_{j=1}^{n_i}(j-0.5)\left(D_j \Big/ A_{ij}\right)^2\right]}{n}. \tag{2.8}$$

Where:

$A_{ij}$ is the distance in metres between the subject tree and the *jth* neighbour tree.

The use of the fixed angle gauge in competitor selection precludes the reformulation of the Point Density indexes using tree height data.

*2.3.3.1.3 Distance Weighted Size Ratio index*

The Distance Weighted Size Ratio (DWSR) index (Hamilton 1969; Hegyi 1974) values are the sum of the size ratios between the subject and its neighbour divided by the distance between them. The use of the size ratio makes the index independent of local stand basal area.

The Distance Weighted Size Ratio (DWSR) index is given by:

$$DWSR = \sum_{j=1}^{n} \left[ R_j A_{ij}^{-1} \right]. \tag{2.9}$$

Where:

$R_j$ is the influence of the *jth* neighbour tree given by:

$$R_j = \left( \frac{D_j}{D} \right). \tag{2.10}$$

The DWSR index is also a candidate for formulation using tree height and location data.

*2.3.3.1.4 Distance Weighted Size index*

The Distance Weighted Size (DWS) index is equivalent to the DWSR index except the tree size component enters the index as a metric rather than a ratio of subject to neighbour tree size. Unlike the DWSR index, this formulation relates the index to local stand basal area. Weiner (1984) presents a typical formulation wherein the index takes the form:

$$DWS_w = \sum_{j=1}^{n} \left[ D_j A_{ij}^{-2} \right]. \tag{2.11}$$

The DWS index is unsuitable for reformulation using tree height because no height analogue to basal area exists.

*2.3.3.1.5 Area Overlap index*

Area Overlap (AO) index values are calculated as the ratio between the zone of influence of a tree and the area of the overlap between the zone of influence of the subject tree and its neighbours. The zone of influence is defined as the area over

which each tree can potentially consume resources. The area of overlap is defined as that component of the zone of influence in which the subject tree competes with its neighbours for resources (Opie 1968; Gerrard 1969). Thus the index is a measure of the degree to which the growing space of an individual is overlapped by its neighbours.

The zone of influence is assumed circular. The definition for the circle area has been defined as linearly proportional to tree diameter (Opie 1968; Gerrard 1969; Alemdag 1978), equal to the crown projection area (Biging and Dobbertin 1992), or equal to the size of the crown of a tree with the same dimension that is grown in an environment where competition is absent (Bella 1971; Monserud and Ek 1974; Alemdag 1978).

Zones of influence and areas of overlap for a hypothetical stand are illustrated in Figure 2.4.

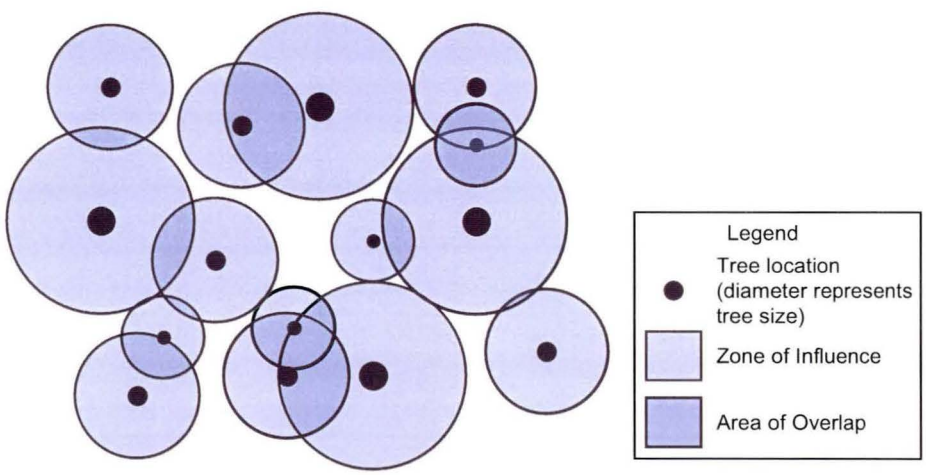


Figure 2.4 Zones of influence and area of overlap for a hypothetical stand.

The Area Overlap index typically takes the form (Tome and Burkhart 1989):

$$AO = \sum_{j=1}^{n} R_{k_j} \left( \frac{ao_j}{ZI} \right) \tag{2.12}$$

Where:

$AO$ is the area of overlap index value for the subject tree calculated using $n$ neighbours $j$;

$ZI$ is the zone of influence of the subject tree;

$ao_j$ is the area of the zone of influence of the subject tree which is overlapped by the zone of influence of its *jth* neighbour;

$R_{k_j}$ is the weighted influence of the *jth* neighbour tree given by:

$$R_{k_j} = \left(\frac{D_j}{D}\right)^k . \tag{2.13}$$

Where:

$k$ is the weighting factor defining the degree of competitive asymmetry. Typical $k$ values tested range between 1 and 3.

The AO index is also a candidate for reformulation using tree height and location data. However its location dependent character makes it similar to the APA index.

#### *2.3.3.2 Distance independent indexes*

Distance independent indexes use either a raw stand metric, or relate the size of the subject tree to that of some stand metric.

Stage (1973) proposed an index that is the sum of plot basal area of trees larger than the subject. It is equivalent to:

$$SBL = \sum_{j=1}^{m} D_j^2 . \tag{2.14}$$

Where:

$m$ is the number of $j$ neighbouring trees larger than the subject.

Daniels et al. (1986) proposed their index as the ratio of the subject trees basal area to that the mean plot basal area. It is equivalent to:

$$RBA = \frac{D^2}{\sum_{j=1}^{n}\left(D_j^2\, n^{-1}\right)} . \tag{2.15}$$

Again, neither distance independent index is suitable for reformulation using tree height because no height analogue to basal area exists.

#### *2.3.3.3 Summary of between-tree interaction evaluation*

Competition indexes may be used to evaluate the competitive environment about a subject tree. The area over which competition is assessed effects index utility and improves asymptotically as it is increased. The distance independent indexes relate the size of the subject tree to the stand average, while distance dependent indexes incorporate tree locations or inter-tree distances. The nature of competition is likely to influence the utility of these index types, with asymmetric competition best characterised using distance dependent indexes, while symmetric competition is best characterised using distance *in*dependent indexes. The use of tree height in index formulation is not without precedent. It has been argued the tree height is a useful metric because it characterises the light environment, an important growth regulator in young radiata pine stands. Apart from the difficulty of measurement when compared with breast height diameter in ground based studies, there are two further disadvantages to its use. It is generally not as well related to biomass and the allometric relations between height and diameter conflate with the between-tree competitive relations. A number of indexes have been proposed. Several are suitable for reformulation using tree height so that they may be calculated from remotely sensed data and these have been indicated.

### 2.3.4 Stem profile development and evaluation

#### *2.3.4.1 Stem shape and profile descriptions*

The Mt Burr studies investigated breast height diameter increment and neglected possible changes in biomass allocation within the trees that may have led to changes in stem shape. Moreover, differences in stem shape between trees may be influenced by between tree interactions other than competition. Before exploring the effects of between tree interactions on the deposition of stem wood during growth and subsequent affects on stem shape, some definitions and descriptions are required.

Tree stem shape is often defined as the change in the diameter of the stem along its length. More specifically, Gray (1956) defined *form* as the characteristic shape of a solid as determined by the power index applied to diameter in the diameter-height curve of such a solid, and *taper* as the rate of narrowing in diameter in relationship to the increase in height of a solid of a given form. Most authors make

no such distinction and refer to taper and form synonymously as the change in diameter with distance along the stem (Larson 1963; Bi and Turner 1994). In this thesis, Gray's definitions will be used unless otherwise noted. Stem profile will refer to taper and form.

The profile of the tree stem is irregular and complex (Larson 1963), nevertheless stem profiles may be described by assuming they conform to mathematically tractable functions. Solids of revolution offer a useful model for stem description to facilitate discussion.

If a curve of the general form:

$$Y = K\sqrt{X^r}\ ; \tag{2.16}$$

is rotated about the $X$ axis, a solid of revolution is produced (Husch et al. 2003). Varying the value of the exponent $r$ adjusts the curvature of the function and so produces solids with different profiles. When $r = 2$, the solid of revolution is a cone, when $r = 1$, a paraboloid, and when $r = 3$, a neiloid. Solids of revolution produced by increasing values of $r$ are presented in Figure 2.5.

Solids of revolution can be used to represent the irregularity and complexity of profile within a single tree stem (Ormerod 1973; Newberry and Burkhart 1986; Newnham 1988). Truncated solids of revolution may be joined end on end to define a whole stem where an appropriate value for $r$ is chosen for each frustum and $K$ is defined appropriately to scale the diameter and height data. While any degree of complexity could be described by this method, a stack of three solids gives a simple description of the average mature forest grown conifer tree. The shape that tree stems tend to resemble within the crown approaches that of a cone. Below the crown, but above the butt swell, the shape often resembles the frustum of a parabola, and within the butt swelling, the frustum of a neiloid. The two points of inflection between the three stem segments are smooth (Larson 1963). The idealised tree stem comprised of these three solids of revolution is illustrated in Figure 2.6.

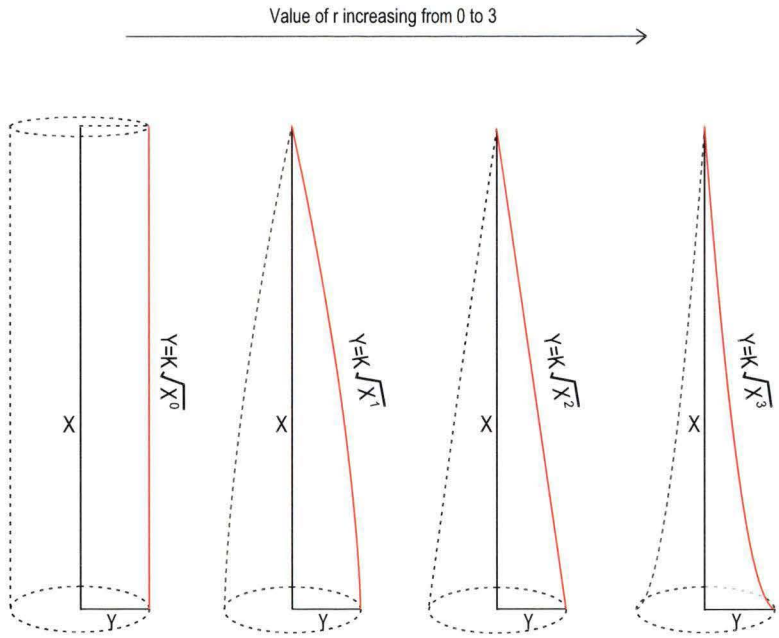


Figure 2.5 Solids of revolution descriptive of tree form (after Husch, Beers, and Kershaw 2003, pg 120)

### *2.3.4.2 Stem profile development theories*

Realised stem size and profile results from the pattern of wood deposition through time. In terms of increment differences along the stem during a single growing season, wood deposition increases from the stem tip downward, reaching a maximum at some point between the height of maximum foliage area and the base of the live crown while the minimum growth occurs somewhere between this point and ground level (Larson 1963; Barker 1980). In forest trees, the base of the crown typically rises as tree growth proceeds through multiple growing seasons; thus the region on the stem of maximum growth rises also; and so too do the points of inflection. Because live crown size and length have a large impact on wood deposition, in allometric terms much of the variation in stem profile between trees can be related to variation in the size of the live crown and it's distribution along the stem (Larson 1963).

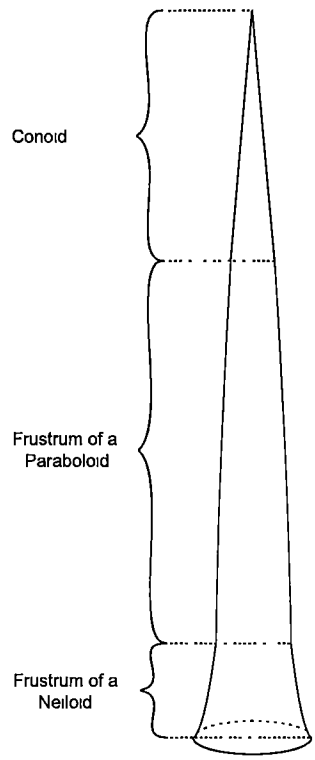


Figure 2.6 Geometric forms assumed by portions of a tree stem (Adapted from Husch, Beers and Kershaw 2003, pg.121)

The shape of the live crown influences stem profile directly through its impact on the quantities of photosynthate available for stem growth and their distribution, and also through its indirect influences on the physical forces exerted on the stem (Larson 1965; Osawa 1993). When two trees of the same total height but different crown length are compared, the tree with the longer crown exhibits a greater rate of taper below the crown and a larger breast height diameter (Gray 1956; Muhairwe 1994). The isolation of crown influences upon stem formation is difficult because they do not operate independently (Osawa 1993; Rennolls 1994; Henry and Aarssen 1999; Thornley 1999; Dean et al. 2002). Nevertheless, numerous investigators have attempted to attribute stem growth and/or subsequent profile characteristics to one or more development theories. Nutritional, hormonal, biomechanical and water conductive theories have all been proposed to explain the growth process (Larson 1963; Valinger 1992). These theories highlight the role of between tree interactions in stem profile development, principally through their effects on crown development.

#### *2.3.4.2.1 Nutritional theory*

Nutritional theories of growth view the tree as an integrated system of sources and sinks. The sources (foliage and fine roots) supply photosynthate, water, and other

nutrients to growing sinks (the cambial and apical meristematic tissues) (Lanner 1976). Nutritional theories have been used to justify the relative unresponsiveness of height growth to between tree interactions when compared to that of stem diameter. Total height growth largely results from the annual growth of the apical shoot. In most conifers, the potential length of extension of the apical shoot is limited by the number of stem units developed in the bud from the preceding growth season (Lanner 1976). In contrast, total diameter growth does not rely preceding cambial development and so is not limited to a set number of cell divisions. Meristematic tissues are also thought to compete for assimilates, with success being dependent upon the timing of growth (Lanner 1985) and the proximity of the meristem to the assimilate source (Kramer and Kozlowski 1979; Wareing 1982). Apical meristematic growth is rarely limited by competition within the tree from the cambial meristem because it occurs early in the growing season when assimilates are in abundance, and because it is proximate to the foliage, which is the principle assimilate supply. Being the weaker competitor, the cambial meristem is therefore reliant on assimilates which are excess to apical requirements (Jackson et al. 1976; Lanner 1976). Thus diameter growth is more variable than height growth and more readily influenced by resource limitation.

#### *2.3.4.2.2 Hormonal theory*

Hormonal theories stipulate a role for plant hormones, both in the direct regulation of stem wood deposition, and also in the indirect regulation of stem wood deposition through their impact on the morphological development of the crown. The external application of the growth hormone ethylene has been shown to increase shoot extension and radial increment in several tree species (Brown and Leopold 1973) including radiata pine (Barker 1979). The removal of actively growing apical tissues in individual branches reduces wood deposition along the branch and downward into the main stem. Studies in the supply of the growth hormone auxin, which is produced in these tissues, indicate a regulatory role for this hormone in this circumstance (Larson 1962). Later research has focussed on the role of a group of chromoprotein hormones, termed phytochromes. Phytochrome production is regulated by the ratio of intercepted red to near-infrared (R:IR) radiation. Phytochrome production is increased in the reduced R:IR light ratio environments that occur due to crowding and this causes increased shoot elongation and reduced branching. Higher production of phytochromes in response to neighbour presence has also been observed irrespective of shading, indicating that neighbours can be detected even before shading occurs (Ballaré et

al. 1987; Ballaré et al. 1990). Over time the modifications to growth caused by increased phytochrome production lead to the development of deeper and narrower crowns, which, in turn, produce stems with longer conical segments and reduced taper (Smith and Whitelam 1997).

#### *2.3.4.2.3 Water conductive theory*

The pipe theory of stem development is the principal water conductive theory that has been used to describe the process of wood deposition (Valentine 1985; Makela and Hari 1986; Osawa et al. 1991). The theory posits that stem cross-sectional area within the crown needs to increase linearly with an increasing total foliage amount above it because an invariant amount of conducting tissue is required to supply the foliage tissue with the water needed for tissue function and mechanical support. Below the live crown, the growth in diameter along the stem length is assumed invariant and required to supply newly grown crown tissue. This accumulation occurs over the top of a fixed amount of disused stem, itself deposited for earlier grown crown foliage (Shinozaki et al. 1964; Shinozaki et al. 1964). In assessing the validity of the theory, Chiba et al. (1988) and Osawa et al. (1991) confirmed that the relationship between foliage mass and sapwood area growth is linear at both the crown base and at breast height. Kershaw and Maguire (2000) suggested the theory was incomplete as they found non-linearities in the relationship at different points along the length of the stem. More recently, the pipe theory has been used to describe the development of stem profile in process models (Rennolls 1994; Makela 2002). These models can predict, at least figuratively, the conical form of stem profile within the corn and the paraboloidal form below, although not the neiloid form present in the stem base because the butt swell is not accounted for. Deleuze and Houllier (2002) modelled stem profile development by empirically adjusting a process model to generate stem profile which could account for butt swell. It is unfortunate that the quantitative predictive utility of process models is poor due to the large number of inputs required (Osawa 1993; Hopkins and Leipold 1996; Thornley 1999).

#### *2.3.4.2.4 Biomechanical theory*

Biomechanical theories suggest changes to the pattern of wood deposition within the stem occur in response to physical forces acting upon the stem (McMahon and Kronauer 1976; Wilson and Archer 1979). The 'constant stress' and 'elastic similarity' theories (McMahon and Kronauer 1976) are the two most studied. The

primary assumption in both of these theories is that the greater mechanical strength of the stem results from modifications to stem diameter while wood strength properties remain relatively invariant.

The constant stress theory assumes that the tree regulates growth to ensure that the lateral pressure caused by wind operating upon the crown exerts a constant bending stress along the stem (McMahon and Kronauer 1976; O'Brien et al. 1995). Assuming that the stem is a material of uniform resistance, Dean and Long (1986a) derived a regression model from the flexure formula for cantilever beams that predicted stem diameter at a given height as a function of the bending moment at that height, i.e.:

$$d = \alpha M^{\beta} . \tag{2.17}$$

Where:

$\alpha$ and $\beta$ are model parameters;

$M$ is the bending moment at the given height which, assuming constant wind pressure, is a product of leaf area above the given height and leverage exerted at the given height, i.e.:

$$M = A \times l . \tag{2.18}$$

Where:

A is total leaf area above the given height;

$l$ is exerted leverage at the given height.

The constant stress model may also be formulated in terms of breast height diameter and total height (O'Brien et al. 1995; Henry and Aarssen 1999), in which case:

$$D = \alpha H^{\beta} \tag{2.19}$$

Where:

$\alpha$ and $\beta$ are model parameters, of which the exponent term is hypothesised to equal one third to one half depending upon the degree to which the stem is rigidly anchored in the ground (Gray 1956; Newnham 1965), i.e. $0.333 \leq \beta \leq 0.5$

The elastic similarity theory assumes that the tree instead regulates growth to ensure that the stem can resist buckling under it own weight. Assuming also that the stem is a vertically orientated tapering column of uniform resistance, this requires stem deflection from the vertical to remain constant relative to height (McMahon 1973; King and Loucks 1978; Rich 1986; Rich et al. 1986; O'Brien et al. 1995). Under such conditions the exponent term in equation (2.19) is hypothesised to equal two thirds, i.e. $\beta = 0.666$

The production of ethylene has been shown to increase within the tree in response to increases in bending stresses (Leopold et al. 1972), evidence that bending stress stimulates the production of this growth hormone. Results from numerous studies provide further indirect support for a biomechanical basis to stem profile development. Over a 15 year period, Jacobs (1954) compared radiata pine trees which were prevented from swaying using guy ropes during growth with those that were not. He found that trees subject to wind sway grew more in diameter and less in height, and that diameter growth shifted lower in the stem when compared to un-guyed trees. Similar findings are reported in other species (Larson 1965; Holbrook and Putz 1989; Valinger 1992). In Valinger's work (1992), the occurrences of changes in stem profile with guying were largely restricted to the region below the live crown. Others have manually shaken or applied lateral weights to seedlings growing under greenhouse conditions to simulate wind pressure and generally report similar findings, with a re-allocation of growth to diameter at the expense of height and/or a concurrent shift in diameter growth to lower in the stem (Holbrook and Putz 1989; Osawa 1993; Downes et al. 1994; Osler et al. 1996).

Numerous studies have considered static height and diameter data drawn from forest populations and have generally found that the fitted exponent term values for equation (2.19) conform well to the constant stress theory in particular (Boyd 1950; Newnham 1965; Quirk and Freese 1976; Long et al. 1981; Dean and Long 1986a; Morgan and Cannell 1994; Dean et al. 2002), although others report at least some support for the alternative (King and Loucks 1978; O'Brien et al. 1995). The stipulated exponent term values in equation (2.19) under the different theories are very close together and so isolating a statistically significant value to support one over another is very difficult (Niklas 1994; Henry and Aarssen 1999). Model II regression[7] is a more valid method to use where natural variation and

[7] Also termed reduced major axis regression.

measurement error occurs in both diameter and height (Sokal and Rohlf 1995), yet most researchers have published Model I regression parameters and the lack of methodological consistency in published research makes valid comparisons impossible (Henry and Aarssen 1999). At a broader level, Henry and Aarssen (1999) have also noted the difficulties faced by researchers attempting to separate out the conflated effects of age, competition and biomechanical stresses on stem development and argued that no studies have employed appropriate methods to achieve this aim. In their most basic form, the biomechanical theory describes stem profile above the neiloid, within the crown free bole. Several more precise formulations take into account crown leaf area and also describe stem profile within the crown (Dean and Long 1986a; West et al. 1989; Morgan and Cannell 1994; Fourcaud et al. 2003; Fourcaud and Lac 2003). All are insufficient to explain the formation of the neiloid in the base of the tree (Morgan and Cannell 1994).

#### *2.3.4.3 Summary of stem profile development theories*

Between-tree interactions influence the pattern of wood deposition within the stem, and thus influence stem profile. Stem growth is regulated by assimilate availability and hormone concentrations. Hormone production is directly influenced by both the local wind and light environment (Morgan and Cannell 1994; Smith and Whitelam 1997; Dean et al. 2002). The light environment in particular influences the development of crown shape (Holbrook and Putz 1989; Smith and Whitelam 1997). Because assimilates are preferentially deposited near the assimilate source, crown shape also influences stem wood deposition. Thus the influences of neighbouring trees are both direct, through their influence on hormone production, and also indirect, through the incremental changes which they bring upon the morphology of the crown. Because the influences upon stem formation are multiple, no single unifying theory has been successful in describing all the complexity of profile that arises; moreover, numerous inputs would be required to do so. This also highlights why mensurationists have generally avoided stem development theories in building stem profile models.

### 2.3.5 Evaluating stem profile

Tree stem shape is highly variable, both within and between trees, and so is difficult to describe mathematically (Kozak and Smith 1993). Increasingly complex models have been published as the resource information requirements of forest management agencies have increased (Newnham 1988; Bruce and Max 1990).

The accuracy of any profile model is largely dependent upon its ability to realistically depict stem profile. The complexity and variability of profile is a common cause of prediction bias, both within and between trees. While bias in diameter prediction within a tree may be minimal overall, often large biases occur in the area of butt sweep and/or the stem tip. Similarly, a minimal overall bias in diameter prediction for an average size tree may not extend to very small or very large trees. Realism may be achieved by ensuring that the model: is constrained so that diameter is forced to decrease monotonically from the tip to the base of the stem (Grosenbaugh 1966); tracks average stem profile, which often requires the model to include two inflection points, the lower of which is near breast height diameter (McTague and Bailey 1987), and; takes into account differences between trees attributable to competition and density (Kozak and Smith 1993).

There are several, more practical, issues regarding model fitting and use. Kozak and Smith (1993) stated that profile models should be reliant on easily measurable independent variables and also that the parameter estimates be readily obtainable using standard statistical techniques such as ordinary least squares. The ready availability of open source statistical software has reduced the importance of this model feature. They also stated that it is advantageous for a model to be algebraically, as opposed to numerically, integrable, and also invertible in order to allow rapid calculation of the model outputs because profile models are recursively called upon within log bucking routines. Reductions in computing cost have also reduced the importance of this model feature. To ensure reasonable volume estimates, models are often constrained in a number of ways. They may be constrained to pass through a measured diameter (e.g. at breast height), diameter may be constrained to equal zero at total height, and more generally, diameter may be constrained to equal non negative values along the stem length (McTague and Bailey 1987). Stem profile models may also be formulated in such a way as to suit the estimation of particular stem characteristics at the expense of others. Some researchers position the ability of the model to generate unbiased volume estimates above the generation of unbiased diameter measurements. Demaerschalk (1971; 1972) was the first researcher to publish a method to ensure that integration of the profile model over total tree height yields volume estimates that are equal to those of stem volume models derived using the same data. Models that exhibit this feature are termed 'compatible'. While enforcing compatibility typically introduces some bias to diameter estimation, it is sometimes preferred in practical application (Gordon 1983; Ormerod 1986; Candy 1989a).

For a profile model to be of use it must be accurate enough to meet its specified purpose. Some researchers have stated that a profile model should be at least as accurate in predicting *total* volume as does a volume model derived using the same data (Bruce and Max 1990; Flewelling and Raynes 1993), and this benchmark has been used to assess model performance in past work (Biging 1984). Most researchers conduct model assessments by testing the ability of a model to accurately estimate both diameter along the stem and stem volumes within specified diameter or height constraints (Kozak and Smith 1993). These latter model outputs can be used to generate *merchantable* stem volume estimates and allow the model to be used both to optimise log cutting patterns and also to calculate proportions of log stack volume belonging to specified timber utilisation categories (Goulding and Murray 1976). The ability to estimate the latter has also been used to assess model performance (Gál and Bella 1995).

Various approaches have been taken in modelling stem profile. One approach entails diameter determination at set heights and the use of an interpolation method to estimate stem profile between them (Kilkki et al. 1978; Lappi 1986; Flewelling and Raynes 1993; Ojansuu 1993). These complicated 'diameter determination' models are derived through the joint estimation of a number of diameters at a number of pre-specified heights and so require diameter data collected at pre specified heights. This approach was not considered in this thesis. Most research has focussed on the use of stem data drawn from measurements along the tree stem that are located to facilitate realistic stem description and so may vary to accommodate stem damage and other defects. In their reviews, some researchers have chosen to classify past efforts using such data according to whether the modelling approach used is empirical or geometric (Broad and Wake 1995; Fang and Bailey 1999; Zhang et al. 2002).

In an empirical approach, stem diameter is modelled as some function of breast height diameter, total height, and relative height; or some transformation of these variables. Function choice is driven by the search to minimise model bias and error. It is often hard to explain the significance of the resultant parameters because no assumptions are made about true stem shape, other than those implied by variable selection (Fang and Bailey 1999). While empirical models may be relatively easy to fit using commonly available regression techniques, over-parameterisation problems such as multicollinearity often result where large numbers of variables are fitted (Kozak 1997), and variable selection can be highly data driven (Bi 2000; Eerikäinen 2001). Over-parameterisation can also complicate

the comparison of stem profiles using models (Lee et al. 2003). Models derived using empirical approaches find ready application in timber inventory since log scaling rules employ diameter estimates to calculate log volume, and so when those rules are changed, individual log volumes are easily calculated. Empirically derived models are not always easy to integrate to facilitate volume calculation and are not always compatible.

In contrast, geometric approaches to stem profile modelling take the shape or volume of solids of revolution as the starting point, either modelling the outline of a solid of revolution directly, or modelling the volume of a solid of revolution and then differentiating this model to estimate diameters along the stem (Demaerschalk 1973; Reed and Green 1984). The parameters of geometric models are easier to interpret because they describe shape inherently and compatible estimates of volume are easily obtained (Fang et al. 2000) although often at the expense of profile realism (Zhang et al. 2002). Alternatively, one can classify past modelling attempts according to final overall model structure since many models contain elements of both approaches.

#### *2.3.5.1 Whole bole modelling approaches*

Metzger (1894) assumed the constant stress model of stem formation and assumed therefore that the relationship between diameter and the height at which it is measured is that of a cubic paraboloid. This geometric model is given by:

$$H - h = \beta d^3 \tag{2.20}$$

In this model [eqn. (2.20)], the estimated parameter describes taper while form is assumed invariant between trees. A graphical analysis of actual data led Gray (1956) to assume that the shape of the stem below the live crown was better described by a quadratic paraboloid. This geometric model is given by:

$$H - h = \beta d^2 \tag{2.21}$$

Behre's (1923) two-parameter hyperbola model is an example of a simple whole model that instead was derived empirically. It allows more flexibility in shape, however the parameters are not so easily interpreted.

Behre's model is given by:

$$\frac{d}{D} = \frac{z}{\beta_0 + \beta_1 z}. \tag{2.22}$$

A further difference lies in the use of relative size dimensions in model formulation. The use of relative height helps to reduce estimation bias in the upper part of the stem. The use of relative diameter helps to standardise predictions across tree size classes.

These simple whole bole models [eqns. (2.20), (2.21) and (2.22)] have formed the basis of many later approaches. For example, Gray's (1956) quadratic paraboloid stem profile model may be rewritten as:

$$d = \beta (H - h)^{1/2} \tag{2.23}$$

While Gray assumed that form is constant and that taper varies from tree to tree, Ormerod (1973) introduced variable stem form by also modifying the exponent to an unknown:

$$d = \beta_0 (H - h)^{\beta_1} \tag{2.24}$$

Ormerod (1973) also included breast height diameter as an extra variable to account for taper not explained by $\beta_0$ and to standardise taper for different sized trees:

$$d = \beta_0 D w_D^{\beta_1} \tag{2.25}$$

Where:

$$w_D = \frac{H - h}{H - h_D}; \tag{2.26}$$

$h_D$ is height at which breast height diameter is measured.

Simple whole bole models are unable to account for inflection in stem profile and so are unlikely to generate accurate total volume estimates or diameter estimates without large localised, or within-stem stem, biases toward the stem butt or tip. This precludes their use in this research.

Several other approaches to modelling the whole bole have been taken. The most common is the empirical approach of fitting polynomial transformations of relative height. The simplest of these is the quadratic parabolic model (Kozak et al. 1969), which is given by:

$$\frac{d^2}{D^2} = \beta_0 + \beta_1 z + \beta_2 z^2 \tag{2.27}$$

The quadratic parabolic model does not well describe the neiloid at the stem base or (the potentially dramatic) changes in form within the crown with any reliability when compared to later, more complex, models; however it does reliably estimate upper stem volumes below the crown for most conifers (Kozak et al. 1969).

In an effort to better account for rapid changes in form and taper with height, numerous researchers have used higher order polynomials (e.g. Fries and Matern 1965; Bruce et al. 1968; Goulding and Murray 1976; Gordon 1983; Amidon 1984). For example, Goulding and Murray (1976) proposed a fifth order polynomial for radiata pine which was described by:

$$\frac{d^2V_p}{kH} - 2x = \beta_0 x + \beta_1 x^2 + \beta_2 x^3 + \beta_3 x^4 + \beta_4 x^R . \qquad (2.28)$$

Where:

$V_p$ is total stem volume predicted using a volume model;

$x = \frac{H-h}{H}$;

$\beta_0$ is not estimated, instead $\sum_{i=o}^{n} \frac{\beta_i}{i+1} = 0$ and $5 < R < 41$.

Goulding and Murray (1976) showed how approximate compatibility with the volume model could be enforced by using total height and estimated volume as the scaling factor rather than breast height diameter and constraining the parameter values.

Polynomial models are easy to fit. They are also usually easy to integrate to obtain volume estimates and to rearrange to obtain height estimates (Kozak 1988). However, the use of numerous polynomial transformations can easily cause multicollinearity and, as a general approach, is difficult to defend from a biological perspective (Newnham 1988). This approach is not investigated in this research.

With respect to the issue of multicollinearity, Thomas and Parresol (1991) noted that stem shape could be more parsimoniously described using trigonometric transformations of relative height that have inherent inflection points. They presented a simple taper function that included three estimated, and one fixed, parameter. This is given by:

$$\frac{d^2}{D^2} = \beta_0 (z-1) + \beta_1 \sin(c\pi z) + \beta_2 \text{cotan}(0.5\pi z) \tag{2.29}$$

Where:

$c$ is a species specific parameter.

Noting that stem profile resembles an inverted sigmoid, Biging (1984) used an inverted Chapman-Richards function to describe relative diameter. Biging constrained the model to equal zero at total height, which removes the necessity for an asymptote parameter. He also fixed one further parameter to further improve parsimony:

$$\frac{d}{D} = \beta_0 + \beta_1 \log\left[1 - \left(1 - e^{\frac{-\beta_1}{\beta_2} z^{\frac{1}{3}}}\right)\right]. \tag{2.30}$$

Neither model [eqns. (2.30) or (2.31)] adequately addresses the issue of biological realism, nor are the parameters easily interpretable. Neither approach is investigated in this research.

#### *2.3.5.2 Segmented modelling approaches*

Numerous researchers have addressed the issue of stem form complexity instead through developing models comprised of sub-functions. The sub-functions describe separate stem segments within which form is constant, while form varies between adjacent sub-functions. The sub-functions are usually constrained to coincide at their join points to produce continuous predictions along the stem. This segmented approach to modelling stem profile has been around for a long time. Demaerschalk and Kozak (1977) refer to two Swedish papers published in the 1920's which used this approach. The segmented polynomial (Goulding and Murray 1976; Max and Burkhart 1976; Cao et al. 1980; Byrne and Reed 1986; Candy 1989a; Petersson 1999) and trigonometric models (Thomas et al. 1995); the switching model (Valentine and Gregoire 2001) and the diameter point model (Ormerod 1986) are all examples of models which are comprised of sub-functions.

Ormerod (1973) presented a model containing two sub-functions that each used the following function:

$$\frac{d}{d_{0.3H}} = w_{0.3H}{}^{\beta} \tag{2.31}$$

Where:

$d_{0\,3H}$ is the measured diameter at 30 per cent of total height;

$$w_{0\,3H} = \frac{H-h}{H-(0.3H)}. \tag{2.32}$$

Demaerschalk and Kozak (1977) used a two-segment system wherein the sub-function for the lower segment gives way to that for the higher segment at the predicted inflection diameter. In contrast to Ormerod's model [model (2.32)], Demaerschalk and Kozak conditioned the model to ensure the lower sub-function passes through breast height diameter, that the upper sub-function equals zero at total height, and that each sub-function meets at the inflection height. In further contrast, the inflection diameter is predicted as a function of breast height diameter underbark and the height of inflection is estimated independently of other model parameters.

The upper sub-function is given by:

$$d = d_I \beta_0 z^{\beta_1} \beta_3^{(1-z)} \tag{2.33}$$

And the lower by:

$$d = d_I \beta_4 + \beta_5 (1-z)^{\beta_6} \tag{2.34}$$

Where:

$d_I$ is the predicted diameter at the inflection height

The following two models demonstrated the superiority of employing three sub-functions over two. In Max and Burkhart's (1976) model, the first two terms describe the upper stem segment, each further term describes adjustments to stem profile in each of the two lower segments:

$$y = \beta_0 (z-1) + \beta_1 \left(z^2 - 1\right) + \beta_2 \left(\alpha_0 - z\right)^2 I_0 + \beta_3 \left(\alpha_1 - z\right)^2 I_1 \tag{2.35}$$

Where:

$$y = \frac{d}{D} \text{ or } \frac{d^2}{D^2}$$

$\beta_{0\,\text{to}\,3}$ are model parameters describing segment form;

$\alpha_{0 \text{and} 1}$ are model parameters locating segment join points.

$$I_i = 1 \text{ for } z \geq \alpha_i, i = 0,1$$
$$= 0 \text{ for } z < \alpha_i$$

The model is essentially three polynomial terms that have been constrained so that they not only coincide at the join points but are also smooth. Sharma and Burkhart (2003) showed how Max and Burkhart's model (2.36) could be reduced to Kozak's model (2.27) through increasing the constraints upon model behaviour at the join points.

Cao et al. (1980) developed a segmented version of Goulding's (1979) polynomial profile model requiring one less parameter to be estimated than that of (2.36). This model takes the form:

$$\frac{d^2kH}{V} - 2z = \beta_0\left(3z^2 - 2z\right) + \beta_1\left(z - \alpha_0\right)^2 I_0 + \beta_2\left(z - \alpha_1\right)^2 I_1 \qquad (2.36)$$

There are two developed methods to algebraically enforce compatibility in this model [eqn. (2.37)] (Byrne and Reed 1986; McClure and Czaplewski 1986). In both models, a non-linear procedure is required for parameter estimation. Both may be algebraically integrated and inverted. Segmented approaches use easily interpretable parameters and are often linear in most, and so are worthy of investigation in this research.

#### *2.3.5.3 Variable-form modelling approaches*

Stem form and taper is often more variable between trees than profile models can account for and this variability results in prediction bias across size classes. One approach to control prediction bias has been to stratify trees according to size or age class, the principal identified causes of form and taper variation between trees. This approach is problematic however, as large datasets are required for model building and estimates of log volume then increase spasmodically as trees grow from one class to the next (Williams and Reich 1997). Reed and Byrne (1985) introduced variable-form modelling to allow form differences between trees. They fitted a simple one-parameter version of Ormerod's model (1973) to each tree in their dataset and related that recovered parameter to the ratio of breast height diameter to total height.

The one-parameter version of Ormerod's model (1973) is given by:

$$d = D\, w_D^{\beta} \tag{2.37}$$

Reed and Byrne (1985) recovered parameter values for this model and explored how they varied with breast height diameter and total height. They found that the parameter values related well to the ratio of these two variables and developed a predictive equation with fixed parameters of the form:

$$\beta = 1 - \left( \frac{H/D - 30}{120} \right) \tag{2.38}$$

Newberry and Burkhart (1986) addressed between-tree prediction bias by introducing a two-stage modelling procedure. In their model, the form and taper of the crown free bole above the butt swell for each tree is described in the first stage by fitting Ormerod's two parameter model [eqn. (2.25)] to each tree in the dataset individually. The second stage of modelling relates the recovered parameters to tree and site characteristics. In contrast to Reed and Byrne (1985), Newberry and Burkhart (1986) estimated second-stage parameters using statistical techniques to obtain an optimal solution. Used in unison, first- and second-stage models allow taper and form to vary between trees. The assumptions of ordinary least squares estimation are violated in two-stage modelling because the first-stage parameters include an estimation error component and are also often correlated, leading to unbiased, but inefficient parameter estimation in the second stage (Ferguson and Leech 1978). Methods such as random coefficients analysis and systems of equations may used to derive efficient parameter estimates (Ferguson and Leech 1978; West et al. 1984; Biging 1985). Newberry and Burkhart (1986) found that random coefficients analysis wasn't warranted, given the slight difference to ordinary least squares estimates. Many subsequent studies, which use two-stage modelling, have attempted to address the problem by instead refitting the first- and second-stage models in unison (e.g. Candy 1989a; Allen et al. 1993; Leites and Robinson 2004). Two-stage modelling offers a powerful approach to incorporate tree height and location information in profile models to account for differences between trees. This approach will be investigated in this research.

The segmented polynomial modelling approach reduces some of the bias inherent in the whole bole model approach, but at the cost of increased difficulty in both estimating the model parameters and in using these models to estimate volume and merchantable height (Kozak 1988). Constraining predictions at join points is also

problematic. While recognising the value of the slope continuity, Ormerod (1986) pointed out that that it is inconsistent to select join points at points of natural change in slope on the stem when slope continuity is enforced in the model at these very points. Constraining predictions at join points also violates assumptions about the error distribution that are required for ordinary least squares regression (Williams and Reich 1997). Many of these problems were overcome with the introduction of the variable-form (Newnham 1988; Newnham 1992) and variable-exponent (Kozak 1988) modelling approaches. In these approaches, the changes in stem shape from the ground to tip are assumed to be continuous and dependent upon a continuously changing exponent term, which itself is modelled using transformations of relative height and other tree variables. This approach has generally produced models with less local bias and greater precision when compared against segmented models (Kozak 1988; Newnham 1988; Perez et al. 1990; Newnham 1992; Kozak and Smith 1993; Muhairwe 1999; Bi and Long 2001).

Newnham (1988) argued that the outline or shape of any solid of revolution could be described using the function:

$$d^k = gh. \tag{2.39}$$

Where:

$g$ is a constant that depends on the units used for $d$ and $h$;

$k$ is one continuous function describing the continuous change in shape along the bole.

The model may be rewritten to standardise the model for different sized trees:

$$\left(\frac{d}{D}\right)^k = w_D. \tag{2.40}$$

Newnham showed how $k$ could be calculated for each measured point on the stem by rearrangement and logarithmic transformation:

$$k = \frac{\log(w_D)}{\log\left(\frac{d}{D}\right)}. \tag{2.41}$$

Newham then derived regression equations to relate $k$ to relative height and tree variables. Two-stage modelling is avoided because the influence of tree and site

characteristics are expressed in the exponent and modelled directly. Newham recommended the use of one of the two following equations:

$$k = \beta_0 + \beta_1 w_D{}^6 + \beta_2 \left(\frac{D}{H}\right) + \beta_3 w_D{}^2 \left(\frac{D}{H}\right), \tag{2.42}$$

Or:

$$k = \beta_0 + \beta_1 \left(\frac{D}{H}\right) + \beta_2 w_D \left(\frac{D}{H}\right)^2 + \beta_3 h^{-1}. \tag{2.43}$$

Kozak (1988) took a similar approach to the Newnham (1988) but his variable-exponent model varies in several critical ways. In his original model (1988), Kozak standardised his model for different sized trees about the predicted diameter at the inflection height, rather than breast height. Inflection height diameter was predicted as an allometric function of breast height diameter underbark. Partly as a result of this different formulation, he found a different set of variables to describe the exponent term. Kozak's model passes through predicted inflection diameter rather than breast height diameter so is less affected by butt swell than Newnham's model, however the height of inflection must be estimated independently and is assumed fixed for a given dataset. While both researchers used ordinary least squaes to estimate model parameter values, Newnham (1988) minimised about the exponent term, whereas Kozak (1988) instead minimised about the logarithm of inside bark diameter. Both models are constrained to ensure that $d = 0$ when $h = 0$.

Kozak's basic model (1988) takes the form:

$$d = \beta_0 D_u{}^{\beta_1} \beta_2^{D_u} \left(\frac{1-\sqrt{z}}{1-\sqrt{z_I}}\right)^k \tag{2.44}$$

Where:

$D_u$ is underbark diameter at breast height;

$$z_I = \frac{h_I}{H}; \tag{2.45}$$

$h_I$ is the height of inflection.

And the exponent term was defined by the function:

$$k = \beta_0 z^2 + \beta_1 \ln(z + 0.001) + \beta_2 \sqrt{z} + \beta_3 e^z + \beta_4 \frac{D}{H} \tag{2.46}$$

Subsequent work in numerous species has demonstrated that the formulation of the exponent term can be improved to suit alternate datasets (Perez et al. 1990; Newnham 1992; Kozak and Smith 1993; Muhairwe et al. 1994; Fang and Bailey 1999; Eerikäinen 2001), making the model more a demonstration of an approach rather than a fixed formulation useful in every situation. Moreover, the approach typically results in models requiring the estimation of numerous parameters. There are three, more practical, disadvantages to the variable-exponent modelling approach. Volume estimates can only be obtained by numerical integration, while specified height to a given diameter can only be obtained by iteration. Furthermore, no methods exist to ensure model compatibility. Some further refinements have been published.

Muhairwe (1993; 1999) removed the requirement that the height of inflection be estimated prior to model fitting by reformulating Kozak's (1988) base term such that:

$$d = \beta_0 D_u^{\beta_1} \beta_2^{D_u} (1 - \sqrt{z})^k . \tag{2.47}$$

Kozak (1997) removed the requirement by reformulating the base term of his original model (1988) to pass through breast height diameter. Both reformulations resulted in minor decline in model precision with benefits to model parsimony.

Bi (2000) and Bi and Long (2001), similarly to Thomas and Parresol (1991), sought to improve model parsimony by using trigonometric transformations of relative height in model formulation. They defined a base term by simplifying and rearranging an existing volume ratio equation (Bi 1999). This base term relates to relative diameter through the varying exponent $k$ such that:

$$\frac{d}{D} = \left( \frac{\log(\sin(0.5\pi z))}{\log\left(\sin\left(0.5\pi \frac{1.3}{H}\right)\right)} \right)^k \tag{2.48}$$

Where:

$$\begin{aligned} k = {} & \beta_0 + \beta_1 \sin(0.5\pi z) + \beta_2 z^{-1} \cos(1.5\pi z) + \beta_3 z^{-1} \sin(0.5\pi z) \\ & + \beta_4 D + \beta_5 z \sqrt{D} + \beta_6 z \sqrt{H} \end{aligned} \tag{2.49}$$

There are two important differences in this model compared with Kozak's (1988) and Newnham's (1988) formulations. One difference lies in the specification of the base term that allows the inflection point of the model to vary with tree size[8]. While most researchers have found that inflection height, while species dependent, is largely independent of other tree variables. Bi (2000) attributed much of the flexibility of the model to this feature. The second difference relates to the trigonometric functions in the exponent term which offer a parsimonious, flexible and robust method to fit an average stem shape to a wide variety of tree stems. The model has been tested on a wide variety of Eucalyptus species (Bi 2000) and proved more precise and less biased than Kozak's (1998) model. In a separate study, Bi and Long (2001) fitted the trigonometric model to radiata pine data from nine regions of N.S.W. A global fit of the same model proved more precise and less biased than regionally fitted compatible polynomial profile models.

Variable-form modelling allows will allow tree height and location information to be incorporated directly in the modelling process and will be investigated in this research.

#### *2.3.5.4 Accounting for data structure*

The parameter values of most published profile models were estimated using linear or non-linear least squares methods. There are two important characteristics of profile data that can complicate model parameter estimation. First, the sampling procedure used to assemble the data with which profile equations are developed often involves the repeated measurement of stem diameters on each sampled tree. This induces serial correlation in the response data because data points derived from the same tree are not independent of each other (Zeger et al. 1988; Gregoire et al. 1995). Secondly, while the use of relative diameter as the dependent variable helps greatly, the distribution of the dependent variable is still often heterogeneous due to the constraints that are placed on profile equation behaviour at fixed points along the stem (Czaplewski and Bruce 1990; Flewelling and Raynes 1993; Williams and Reich 1997). Examples of such constraints include that diameter equal zero at total height and equal measured breast height diameter at breast height.

It is well known that heterogeneity induces bias in the estimates of parameter standard error when it is not correctly accounted for in model formulation. In the

[8] The inflection point varied toward 10% of total height in one study Bi, H. Q. (2000). "Trigonometric Variable-Form Taper Equations for Australian Eucalypts." Forest Science **46**(3): 397 - 409..

presence of serial correlation, ordinary least squares, weighted least squares and generalised least squares estimates remain unbiased but are no longer minimum variance estimators (Laird and Ware 1982). The practical outcome of this is that least squares parameter standard deviation estimates are unreliable, so confidence intervals are incorrect and tests of significance invalid (West et al. 1984; Gregoire et al. 1995), and this can lead to model misspecification through inappropriate variable selection (Tasissa and Burkhart 1998; Garber and Maguire 2003). In contrast, maximum likelihood methods do not even generate asymptotically unbiased parameter estimates (Carroll and Ruppert 1988). Williams and Reich (1997) used a maximum likelihood technique to model stem profile and reported a significant but small increase in global model bias where serial correlation was not accounted for. Biases of the size reported by Williams and Reich (1997) are generally considered to be insignificant in practical terms (Kozak 1997). Variable selection problems, on the other hand, can deleteriously impact upon empirical model formulation and subsequent parsimony (Eerikäinen 2001); and thus predictive behaviour (Tasissa and Burkhart 1998; Garber and Maguire 2003). The practical implications are likely to be data and model formulation dependent.

While stem profile researchers were slow to adapt (Gregoire et al. 1995), the last ten years has seen most researchers presenting results of stem modelling work produced using methods which are more statistically sound (Gregoire and Schabenberger 1996; Williams and Reich 1997; Tasissa and Burkhart 1998; Eerikäinen 2001; Valentine and Gregoire 2001; Zhang et al. 2002; Garber and Maguire 2003; Leites and Robinson 2004). These methods can be categorised by the underlying modelling approach that is used (Zeger et al. 1988). The population average approach involves modelling the response variance and correlation structures explicitly. Alternately, the subject specific approach involves including random effects terms in the model. In this latter approach, random effects terms are generally assumed to adequately account for response variance and correlation structures, but further explicit modelling of these is also possible where they are not adequately accounted for using random effects terms alone (Lindstrom and Bates 1990). Random effects specification is generally achieved through mixed effects modelling (Sheiner and Beal 1980; Lindstrom and Bates 1990). Details on model specification and inference with the two approaches appear in Appendix II.

Gregoire et al. (1995) noted that mixed effects modelling was as effective in accounting for serial correlation among measurements as modelling the correlation patterns directly in a temporal growth study. With respect to profile studies,

Tasissa and Burkhart (1998) found that their profile data did not support both random effects and an explicit model for the assumed correlation pattern. Garber and Maguire (2003) found mixed effects modelling did not adequately account for serial correlation in describing profile in four species and that an autocorrelation function was also needed. Garber and Maguire (2003) also included a simple variance function to account for marginal error heterogeneity that was present in the data for some species. The findings from these profile studies suggest that both approaches may be used successfully but, in some cases, the techniques used in both may be required. Given that Tasissa and Burkhart's (1998) dataset consisted of 12 982 observations as opposed to Garber and Maguire's (2003) 215, sample size does not appear to be an important factor in successful application of both methods in unison. This latter suggestion has also been made in the general context of mixed modelling (Davidian and Giltinan 1995).

Tests on parameter significance are only valid when response variance and correlation structures are accounted for correctly. In several cases, the application of mixed effects modelling methods has demonstrated over parameterisation in models previously derived using ordinary least squares and allowed reformulation of more parsimonious models (e.g. Tasissa and Burkhart 1998; Eerikäinen 2001).

Profile researchers who have used mixed modelling methods have applied random effects to a range of model covariates that vary within the tree. Gregoire and Schabenberger (1996) modelled bole volume to specified diameter using a variant of Amateis and Burkhart's (1987) volume ratio model. That model includes a sub-function of total volume defined by total height and DBH, together with a sub-function describing the ratio of merchantable to total volume defined by DBH and diameter measurements. The latter varied in its prediction according to the distance along the stem. They applied random effects to the terms in the total volume sub function. In Tasissa and Burkhart's (1998) profile model, random effects entered the model in two sub-functions which both varied in their prediction along the stem. Those sub-functions were the form exponent, which was described only by relative height terms, and the thinning effects term, described by age, thinning age and basal area pre- and post-thinning. Garber and Maguire (2003) used a variable-exponent model similar to Kozak's model [eqn. (2.45)]. In their model, random effects were applied to the sub-functions of relative height in the exponent in all but one case, where it was applied to a breast height diameter to total height ratio term in the exponent. Leites and Robinson (2004) added random effects to the relative height terms describing upper stem profile of Max and

Burkhart's (1976) segmented model and then inspected the random effects for relations to other tree variables; in effect, using the mixed modelling approach to generate first-stage modelling parameters.

The utility of mixed effects and generalised nonlinear modelling methods in the development of stem profile models derived using tree height and location data will be investigated in this research.

#### *2.3.5.5 Summary of stem profile evaluation*

Historically, there has been an incremental increase in profile model complexity with the incremental changes in management requirements toward more specific timber utilisation information. Approaches to profile modelling have been highly varied and have included diameter prediction, and empirical or geometric approaches. Two-stage modelling methods have allowed additional tree and stand variables to be added to models to improve precision across tree size classes. Modelling the continuous form exponent directly has been proven to produce more flexible models and allows between tree differences to instead be included directly in a single modelling stage. More recently, statistical methods that account for the profile data structure, in which residual error autocorrelation and heterogeneity is typical, have been applied to modelling. This has allowed more accurate estimation of parameter standard errors, improving model parsimony and reducing prediction bias attributable to incorrect model specification. Both models forms and parameter estimation methods considered for use with have been indicated.

## 2.4 Summary

A review of remote sensing used in timber inventory and more recent remote sensing developments suggest spatially extensive survey of tree height and location may be applied to radiata pine.

A review of basal area growth in radiata pine parameterised for Tasmanian stands shows that between-tree interactions play some role in moderating growth. Previous work in radiata pine spacing trials has shown that the interaction is asymmetric with respect to stem diameter, such that breast height diameter growth is disproportionate to stem size. Most researchers believe that asymmetric growth occurs due to between-tree interactions that occur above ground and between immediate neighbours. This suggests that, in the absence of significant

silvicultural interventions that will disrupt the relationship, the stem size of a radiata pine tree should be related in some way to the size of its immediate neighbours. It should therefore be possible to improve remote stem size prediction using local density measures formulated using tree height and location that are available through processing of remotely sensed data. Stands containing trees grown to an age immediately prior to first and second thinning are identified as the best candidates for this study.

Forest managers require merchantable timber estimates. These may be derived using models of tree stem profile. Theories regarding tree growth all demonstrate that interactions between trees influence stem shape development. No single theory adequately describes the complexity of stem shape and shape may vary widely between trees so empirical approaches to stem profile modelling to facilitate inventory are required. These empirical approaches to stem profile modelling are numerous and several approaches are amenable to reformulation for use with remotely sensed data. This makes them ideal to both examine stem profile relationships to tree height and local density, and also to formulate for stem metric prediction.

*Chapter 3*

# Study area

## 3.1 Introduction

This chapter describes the radiata pine (*Pinus radiata* (D. Don)) estate that was chosen as the study area. This encompasses a description of the estate biophysical characteristics, the history of its establishment, its silvicultural management, and the effects of these factors upon stand condition.

## 3.2 Study area

### 3.2.1 Location

The Uxbridge-Moogara estate is located in southeastern Tasmania, Australia, and is centred about the Latitude of 42°47'0" and Longitude of 148°52'30". The estate lies on dissected rises between approximately 250 and 650 metres above sea level. It is bounded to the north by the Derwent River valley, and to the east and west, by the Derwent tributaries, the Plenty River and Torrent Creek respectively. The coupes comprising the estate are moderately dispersed, covering approximately 2 520 hectares over a rectangular area of approximately 10 200 hectares. Figure 3.1 presents a map of the estate and its location within the state of Tasmania, Australia.

### 3.2.2 Plantation description

Estate establishment began at the start of the 1980's on both ex-pasture and ex-forest sites. Large areas were planted each year through to the end of the 1985/1986 planting season. Smaller plantings each year have occurred since and all current establishment occurs on second rotation sites. The average coupe size is 57 hectares. At the time of sampling, a substantial proportion of the estate was at approximate ages of 15 and 20 years.

Site preparation entails site clearing and soil ripping along planting lines nominally spaced 4m apart. Trees are hand-planted at nominal 2 metre spacings along the rip lines. Residual herbicides are applied prior to planting to control subsequent grass growth. A combination fertiliser is also applied at planting.

Successful early growth is rapid. Within several years, the trees have grown free from grassy and herbaceous competition and canopy closure occurs around four to nine years after planting, dependent on realised tree spacing and site quality. At age 10 the stands are assessed. The first thinning occurs around age 15.5 decimal years dependent upon wood scheduling requirements and site quality (Pers. Comm.: Rush, M. 2002). Subsequent thinnings occur, or are planned to occur at subsequent 5 yearly intervals. Aerial fertiliser application occurs on some sites after the first thinning.

The estate was initially established to provide pulpwood to the Boyer Paper Mill, which is located on Derwent River some 20 kilometres from the estate. During the mid 1990's a pulpwood/sawlog production regime was introduced. In practice the silvicultural changes were minor since establishment methods were not altered and, at that time, very few coupes had been thinned.

### 3.2.3 Biophysical description

Land tenure and biophysical constraints have limited planting extent. Areas of gazetted State Forest surround much of the estate. Planting extent has been constrained by steep terrain and also, to a lesser degree, by poor drainage in some lower lying areas.

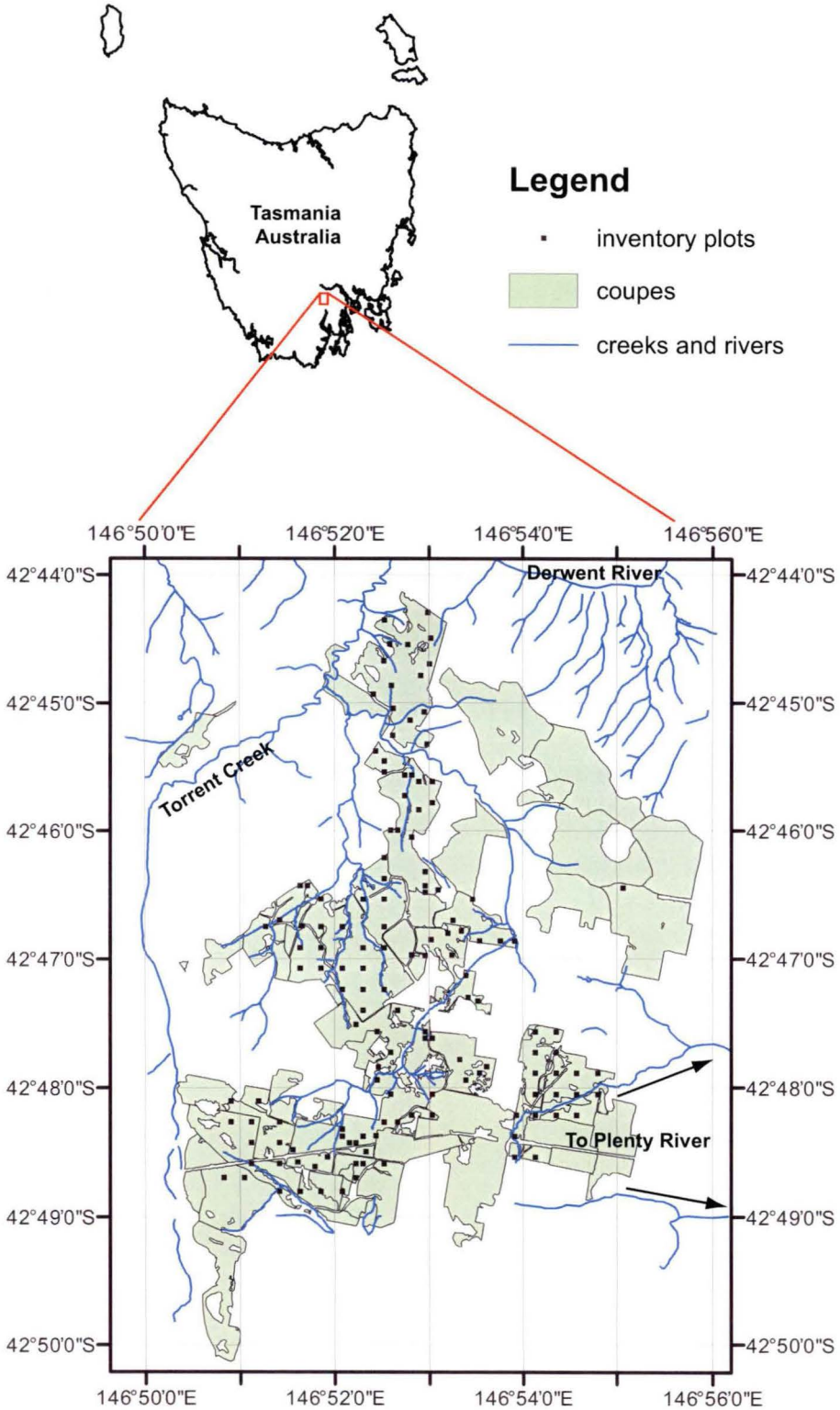


Figure 3.1 Map of the Uxbridge Moogara radiata pine Estate, located within south eastern Tasmania, Australia.

The estate soils are predominantly derived from Jurassic dolerite. These grade from well-drained shallow stony red ferrosols[1] on upper slopes, through moderately-drained brown ferrosols and dermosols on mid slopes, to moderately- or poorly-draining dermosols and texture contrast chromosols or sodosols on the lower slopes. Smaller areas carry soils derived from Permian or Triassic sediments. These soils are generally of lower fertility and tend to greater texture contrast, with higher sodicity than the dolerite soils. Dermosols and chromosols are common upslope, grading to chromosols and sodosols midslope. Sodosols are common in lower lying areas. Some smaller areas are derived from colluviums consisting of any of these parent materials, appearing alone or in combination with each other. The properties of these soils are difficult to predict, although the parent material mix and landscape position play a large role (Grant 1998).

There are no weather stations within the area. Two geographically proximate stations lie to the west and northeast of the estate and experience similar temperature and evaporation regimes throughout the year. In contrast, each station experiences quite different rainfall regimes (Bureau of Meteorology 2004). The Uxbridge Moogara estate is likely to experience similar temperature and mean evaporation regimes, and an intermediate rainfall regime. Rainfall and evaporation data for these stations are presented in Figure 3.2. Figure 3.3 presents the temperature data. Overall, the area experiences a cool temperate maritime climate. Median maximum temperatures range between ten and 15 degrees throughout the year and are highest during February. Evaporation rates peak one month earlier. Rainfall is winter-spring dominant. Tree growth is constrained by temperature and largely ceases during winter months (Pers. Comm: Bruce, J. 2003). Growth during late summer is constrained by a water deficit on some north facing slopes on the shallow and stony soils. Personal observations suggest these stands often exhibit sparse canopies. Poor drainage limits growth on some lower slope sites (Pers. Comm: Bruce, J. 2003). Snow damage is a common problem at higher altitudes to the southwest, causing butt sweep in juvenile trees, and stem and branch damage in more mature trees (Pers. Comm: Rush, M. 2003).

Establishment failure has been common and is widespread in some areas. Large contiguous areas with an absence of trees can usually be attributed to poor drainage or frost damage. Smaller cleared areas and absent individuals are more often due to poor site preparation, planting technique or browsing damage. Site preparation and planting methods are also responsible for a highly varied between-

[1] Soil terminology follows that of the Australian Soil Classification (Isbell, R. F. 1996).

tree spacing. In many areas, along row spacing varies from 1 metre or less, to 4 metres, with no apparent cause. Rip-line placement also varies considerably. Across rip-line spacing can vary from 2 metres to 6 metres or more. Figure 3.4 presents frequency histograms of stand variables in the Uxbridge Moogara estate as measured in the 137 plots located in a stratified systematic design through the estate for the age 10 inventory (Pers. COmm.: Rush 2002)[2]. Stocking commonly ranges from 400 to 1500 stems per hectare. Mean dominant height commonly ranges between 8 and 15 metres with a slight left skew to its distribution. Basal area commonly ranges from 5 square metres, or even less, through to 40 square metres and exhibits a more platykurtic distribution. These frequency histograms demonstrate the wide range in stand condition which is present in the estate.

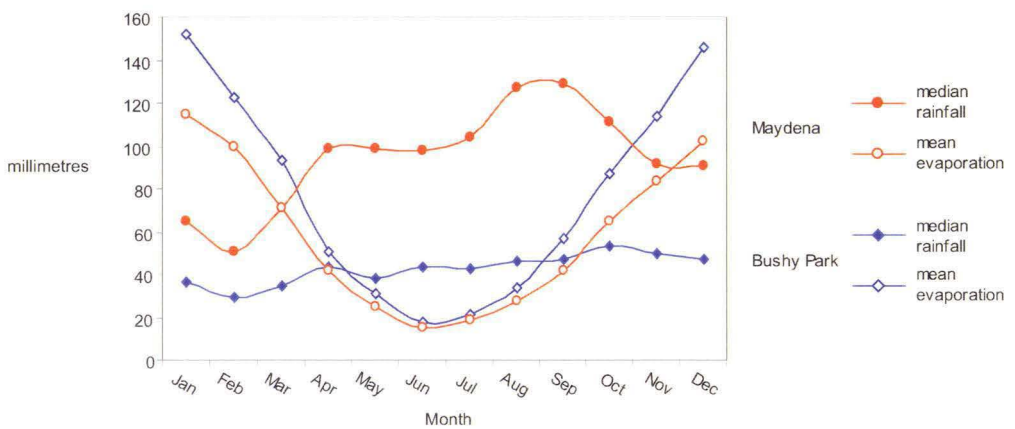


Figure 3.2 Monthly median rainfall and mean evaporation at the Bushy Park and Maydena weather stations, Tasmania

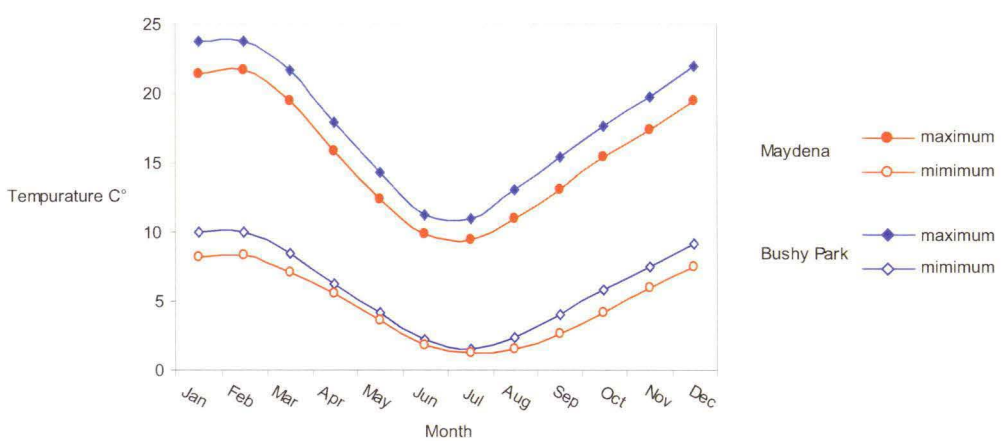


Figure 3.3 Monthly maximum and minimum temperatures at the Bushy Park and Maydena weather stations, Tasmania

[2] Strata are defined at the coupe level.

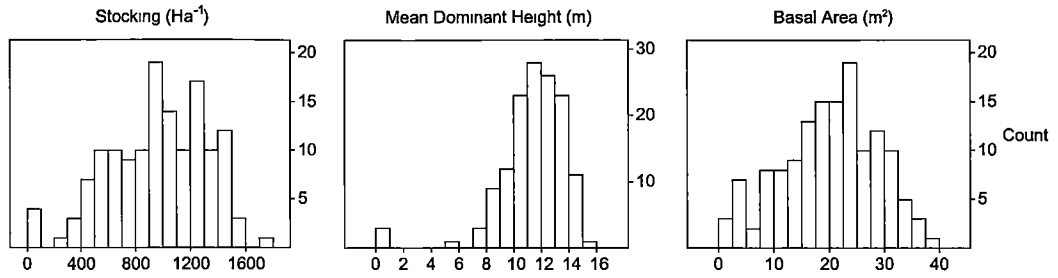


Figure 3.4 Frequency histograms of stand variables in the Uxbridge Moogara estate as measured in the 140 plots used for the age 10 inventory.

## 3.3 Summary

The Uxbridge-Moogara estate is situated in south eastern Tasmania, Australia, and is comprised of first rotation radiata pine stands of ages less than 25 years at the time of sampling. Estate silvicultural management has historically focussed upon pulpwood production. A shift to sawlog production has occurred more recently. Establishment practices, and to a lesser extent, soil type and water and frost drainage patterns, have resulted in stands of widely varying condition. Mean dominant height, basal area, and stocking each show high variability and this is demonstrated in inventory plot data.

*Chapter 4*

# Data collection

## 4.1 Introduction

This chapter describes the data collection process. This consisted of defining and implementing a sampling strategy that was designed to obtain tree-level stem profile data and local neighbourhood tree height and location data from independently selected plots across the Uxbridge Moogara estate within two age classes. Data pre-processing methods are described and justified. Some descriptive statistics are also presented.

## 4.2 Subject tree selection

The overall aim of tree selection was to obtain a sample of trees that broadly represented the variety of stand conditions and, at the individual tree level, the range of local density conditions and stem metric characteristics present in the estate. No attempt was made to ensure that the sample represented the estate in any statistical sense since the production of an actual inventory was not the focus of the project.

The existing inventory plot data was initially used to stratify the stands in an effort to broadly maximise the difference between predictor variable values in the sample, and therefore maximise the precision of predictive model parameter estimates. To that end, a sample of the age 10 inventory plots were stratified by stocking and site index and these plots were revisited to obtain trees representing the range of stand conditions. Revisited plots were easily identified in the field since each plot tree was marked at breast height during the age 10 inventory. These plots were rectangular, 25 metres by 10 metres in length.

When the plots were exhausted of suitable trees, selection focussed on four large coupes in which starting locations for tree selection were randomly sampled. The method used to randomly sample tree selection points involved placing a Cartesian grid over a map of each coupe, and matching x axis and y axis values to two lists of randomly generated numbers. Coordinate points which did not correspond to coupe extent were ignored. One tree was selected at each randomly chosen point. 60 trees were between 14.5 and 15.5 years of age when selected. Of these, 22 were selected from 6 previously measured inventory plots from 2 coupes. The additional 38 trees were selected from a further 2 coupes. 60 trees were between 19 and 20.5 years of age when selected. Of these, 48 were selected from 34 previously measured inventory plots in 3 coupes. The additional 12 trees were also selected from 1 coupe.

Subject tree selection was based upon two criteria. First, they were required be consistent with a *height* criterion. That criterion was that the subject tree needed be either height dominant (i.e. taller than 75% of neighbours within 5 metres), height codominant (i.e. of a height within the middle 50% range of neighbour height), or height subdominant (i.e. shorter than 75% of neighbours within five metres). It is important to note that stem characteristics were *not* considered during this stage and that dominance referred to tree height characteristics only. Selection aimed to collect 30 height dominant trees and 15 trees of each latter criterion. It was impractical to accurately measure the heights of each candidate and its neighbours in all circumstances so the height criterion was applied only visually in some cases. Subsequent data analysis showed that realised tree selection was near that proposed for each age class; with 29 height dominant, 18 height subdominant, and 13 height suppressed trees selected in the age 15 dataset; and 30 height dominant, 12 height subdominant, and 18 height suppressed trees selected in the age 20 dataset. The application of this criterion biased the sample since it ensures the sample does not represent the true population, it does however ensure that the range of local density existing in the population is accounted for. Such model-based sampling criteria are commonly used in studies of stem profile. Secondly, selected trees were required to have a healthy crown and one leading stem only; with no ramicorns, major branches, broken tips, major stem swellings, appreciable sweep or lean. This latter criterion proved the more difficult to fulfil since stem imperfections were very common across the estate. Again, this criterion biased the sample, but this approach was necessary in order to ensure that the stem profile data collected for each tree corresponded to a profile which could be

successfully characterised in a mathematical model. Again, the application of this criterion is common to many studies of stem profile.

Within each previously measured plot the tree selection process was as follows: One corner was chosen at random and used as a starting point to seek potential subject trees. Trees were considered for selection in increasing distances from the starting point based on the two criteria explained above. No limit was placed on the number of trees drawn from each plot. In practice, numerous plots contained none, one or two trees, since suitable trees were rare. The randomly sampled tree selection process was similar. The sampled point was located using compass and hipchain. The tree selected was that closest to the sampled point that conformed to the selection criteria. No selected trees neighboured each other or shared neighbours. This sampling schema ensured independence of local density characteristics for each tree. In a traditional plot design containing multiple subject trees, subject trees would share neighbours. This would induce correlation in the local density estimates and additional variance-covariance modelling would be required if these estimates were then to be used in further modelling (Fox 2000). In a traditional plot design, subject trees would also abut the plot boundary. Potential approaches to accounting for subject trees without neighbours include restricting subject tree selection to those which fall within a buffer around the plot boundary (e.g. Fox 2000); and the simulation of non-measured neighbour tree characteristics using edge-bias compensation models (e.g. Radtke and Burkhart 1998) Further work would be required to determine whether the latter would be appropriate in this context.

## 4.3 Subject tree data

The total height of 61 of the selected trees was measured using an Impulse 200 XL Laser range finding instrument (hereafter termed Impulse Laser).

The ground slope about the selected tree was measured using a Suunto clinometer to the nearest degree. This instrument is adequate to measure slope to this level of precision (Williams and Schreuder 2000). The aspect of the slope was measured using a Suunto compass to the nearest 5 degrees. The geographic location of the selected tree was estimated from 1: 10 000 field maps and aerial photography where available.

Selected trees were marked on the uphill side at 0.15, 0.50, 0.70, and 1.30 metres, dependent on nodal swellings. They were then felled for sectional measurement. The total stem length to the nearest 0.05 m was recorded using a measurement tape. Discs were cut orthogonal to stem length at the marked points and again at measurement points at either 2.0 metre or 10% total height intervals above 1.30 metres. These lengths were measured to the nearest 0.01 metre from the stem base toward the tip. The bark was removed from the discs and the diameter measured to the nearest millimetre using a diameter tape. Diameter tapes are biased for elliptical stems but there was no visual evidence of substantial non-circularity in any discs. Where the measurement point fell on a nodal swelling or other defect, discs were instead cut at points equidistant, usually 0.10 to 0.20 metres apart, from the measurement point. The diameter at these measurement points was then estimated as the geometric mean of the two equidistant diameter measurements. This process closely mirrors that suggested for stem profile data collection in Australia and New Zealand (Research Working Group 2 1999).

Total volume was calculated by summing the volumes of the stem sections defined by measurement points at each end. Most logs and sections of trees, regardless of species, approximate a frustum of a solid of revolution of some shape (Larson 1963). While the volume of any solid of revolution is computed from the product of its length and average cross-sectional area, the problem of volume calculation of any stem or stem section lies in determining its average cross section, given that form and taper can vary indeterminately (Husch et al. 2003, pgs. 119-132).

Smalian's formula is used commonly in profile model prediction. Smalian's formula is accurate when the shape of the log is a second-degree paraboloid, if it less than a second-degree paraboloid, (i.e. a conoid or neiloid) then Smalian's overestimates volume, if it is greater than a second-degree paraboloid Smalian's underestimates volume (Wood and Wiant 1992). Numerous alternatives to Smalian's formula exist, including Huber's and Newton's formulas (Avery and Burkhart 1994), both of which require a midpoint measurement, Bailey's (1995) overlapping bolts method, which make use of Newton's formula applied to two adjacent sections at a time, and the integration of cubic interpolated spline functions (Lahtinen and Laasasenaho 1980; Gregoire et al. 1986). Evaluation studies have demonstrated little difference between these formula's when section length is 2 metres or less (Bailey 1995; Figueiredo Filho et al. 2000). A further alternative is to estimate the shape about each stem section using multiple measurements and then to apply a

general frustum formula that incorporates a shape parameter. This latter method was used here.

The general equation to describe a frustum constrained between two measurement points is given by (Goodwin and Thompson 2003):

$$V_b = \frac{B_l L(1-\theta^{1+b})}{(1+b)(1-\theta)}. \tag{4.1}$$

Where:

$d_s$ is the small end diameter

$d_l$ is the large end diameter

$L$ is the section length

$$\theta = \left(\frac{d_s}{d_l}\right)^{\frac{2}{b}}. \tag{4.2}$$

When the section is a neiloid frustum b=3, a conic frustum b=2, and a parabolic frustum b=1.

The shape of each section was estimated by the measurements of that section and the one below it. Where the profile described by the three measurements across the two sections was concave, the upper section was assumed a neiloid frustum; where a linear profile, the section was assumed a conic frustum; and when a convex profile, it was assumed a parabolic frustum. The tip was assumed conic for which the formula simplifies to:

$$V_b = \frac{B_l L}{3} \tag{4.3}$$

Where:

$B_l$ is the large end basal area

The lowest section was always assumed neilodic. The butt section below the lowest measurement was assumed neilodic and diameter at ground level was estimated by a constrained form of Meyer's (1953) general profile equation. Meyer's general profile equation takes the form:

$$d = \left( \frac{\beta_1 - h}{\beta_2} \right)^{\frac{b}{2}} \tag{4.4}$$

The constrained version takes the form (Goodwin and Thompson 2003):

$$d_g = d_l \left( \frac{h_s - \theta h_l}{h_s - h_l} \right)^{\frac{b}{2}} \tag{4.5}$$

Where:

$d_g$ is the diameter at ground level;

$h_s$ is the height to the small end

$h_l$ is the height to the large end

$\theta$ is the as above;

$b$ is the 3 (neilodic assumption).

Figures 4.1 a) through to f) present histograms by dataset of the subject tree metrics: breast height diameter, total height and total volume determined using the general frustum formula applied to stem sections. Breast height diameter and total height are approximately normally distributed for both datasets, while total volume is strongly skewed for both datasets.

## 4.4 Neighbourhood tree data

The planar distance from the selected subject tree to all neighbouring trees within 5.5m was measured using a distance tape to the nearest 0.1 metre. The end points of these measurements were the approximate stem centres at breast height. The total height of each neighbouring tree was measured using an Impulse Laser to the nearest 0.05 metres. The bearing to each neighbour from the subject tree was measured using a Suunto compass to the nearest 5 degrees.

The bias and precision of the Impulse Laser instrument was assessed in order to determine the accuracy and precision of neighbour height measurement. This was undertaken using the total height data from the subset of subject trees which were measured using both instruments.

The difference in total height measurements is given by:

$$H_{diff} = H_T - H_L \tag{4.6}$$

Where:

$H_{diff}$ is the difference between tape and Impulse Laser measured total height,

$H_T$ is tape measured total height,

$H_L$ is Impulse Laser measured total height.

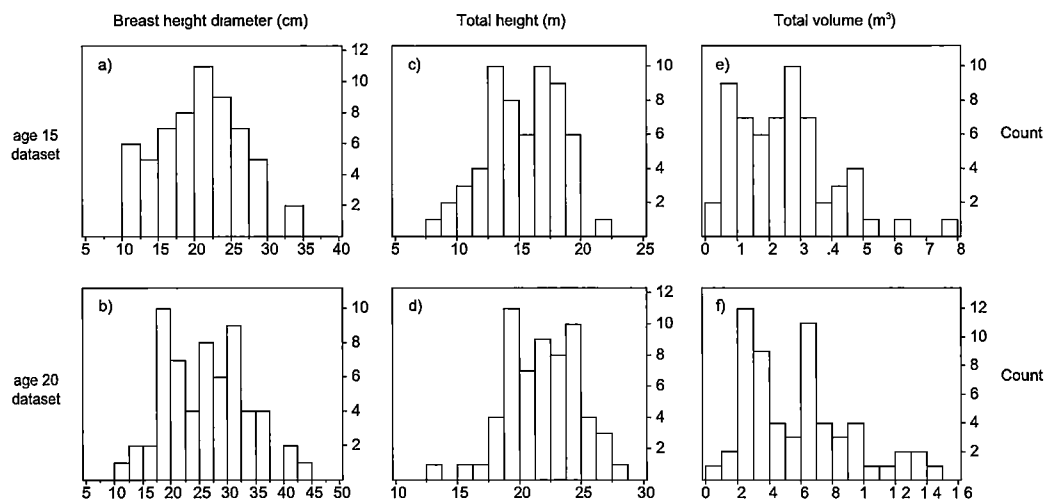


Figure 4.1 Frequency Histograms of Subject Tree data. a) and b): Breast height diameter for the age 15 and 20 datasets respectively; c) and d): Total height for the age 15 and 20 datasets respectively; e) and f): Total stem volume for the age 15 and 20 datasets respectively.

An inspection of a normal probability plot of the difference suggested it to be distributed normally and this was confirmed by formally testing the Shapiro-Wilk (1965) test statistic:

$$W_{H_{diff}} = 0.9774,$$
$$prob < W_{H_{diff}} = 0.3067$$

Where:

$W_{H_{diff}}$ is the Shapiro-Wilk statistic value of the difference between tape and Impulse Laser measured total height.

The mean value of the difference between tape and Impulse Laser measured total height was found to be not significantly different to zero according to a two sided t-test $(t = -1.6583, prob > |t| = 0.1024)$. No significant correlation was found between the difference and any other metric, including age or tape measured total height. Neighbour height measurement was therefore assumed to be unbiased. The standard deviation of the difference between tape and Impulse Laser measured total height is equal to 0.21 metres.

The distance between the neighbouring and selected trees was adjusted to account for slope in cases where the measured slope was greater than 5 degrees. Because of the small size of the plots, slope was assumed constant across the plot:

$$C_a = C_m \cos\left[S_d \cos\left(A_d - B_d\right)\right] \tag{4.7}$$

Where:

$C_a$ is the between-tree horizontal distance;

$C_m$ is the tape measured between-tree planar distance;

$S_d$ is the plot slope;

$A_d$ is the plot aspect;

$B_d$ is the bearing to neighbour tree.

Neighbouring trees at horizontal distances beyond 5 metres were discarded from the analysis.

The Cartesian planimetric position of each neighbouring tree about the selected tree was also calculated:

$$X = C_a \sin\left(B_d\right) \tag{4.8}$$

$$Y = C_a \cos\left(B_d\right) \tag{4.9}$$

Figure 4.2 a) through f) present histograms by dataset of the neighbour tree metrics: horizontal distance between neighbour and subject trees, vertical total

height difference between neighbour and subject (subject height minus neighbour height), and number of neighbours within 5 horizontal metres. The horizontal distance between neighbour and subject trees is strongly skewed as might be expected given the nonlinear relationship between plot area and radius. The vertical height difference is also slightly skewed, with a larger number of neighbours that are slightly smaller than the subject. The standard deviation of the vertical height difference is 2.85 and 4.40 metres for the age 15 and 20 datasets respectively. The number of neighbours is also slightly skewed for both datasets and also bimodal for the age 15 dataset. These distributional characteristics were unexpected given the sampling design that stratified the revisited plots by stocking.

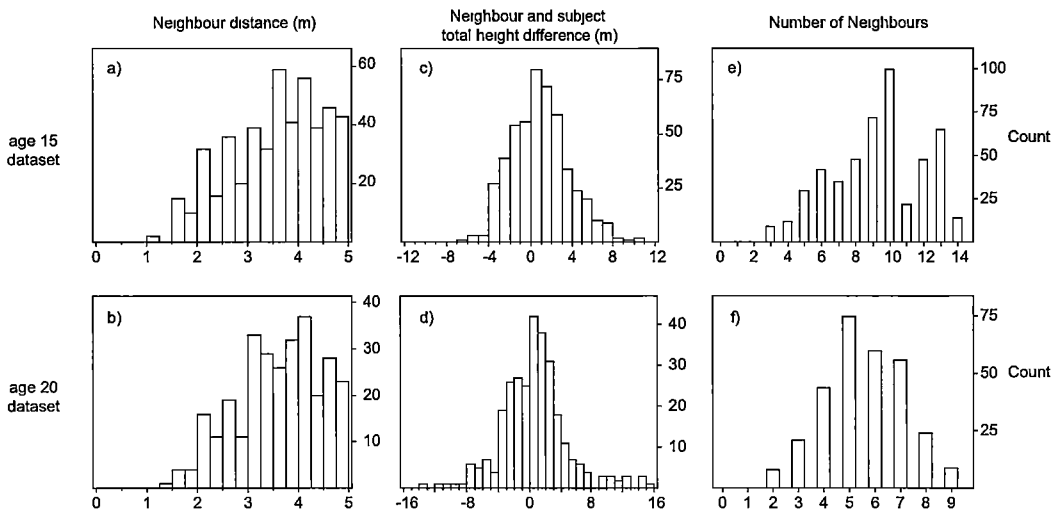


Figure 4.2 Frequency Histograms of Neighbourhood Tree data. a) and b): Horizontal distance between neighbour and subject trees for the age 15 and 20 datasets respectively; c) and d): Vertical total height difference between neighbour and subject trees for the age 15 and 20 datasets respectively; e) and f): Number of neighbours within 5 metres (horizontal distance) for the age 15 and 20 datasets respectively.

## 4.5 Summary

This chapter has explained the tree selection process and the methods used to collect the data used in subsequent analysis. It has also described some pre-processing steps; these being the determination of subject tree stem volume and the estimated height and Cartesian planimetric position of each neighbouring tree. Distributional characteristics for some data variables have also been presented using histograms.

*Chapter 5*

# Evaluating between tree interaction

## 5.1 Introduction

The objective of the study presented in this chapter is to evaluate the utility of neighbourhood tree height and location information in predicting tree DBH in thinned and unthinned stands of radiata pine. This neighbourhood information is used to derive local density indexes that are then compared using DBH prediction model statistics.

Many alternative local density indexes exist. Moreover, neighbouring trees may be excluded, or their influence modified in some way, in order to optimise the efficiency of a chosen index. Index choice is generally subjective and often informed by the mode of competitive relationships that are assumed to be present in the species or forest studied. In earlier studies, the methods used to optimise index formulations were generally subjective (De luis et al. 1998). More recently, alternative formulations have often been assessed more formally. Miina and Pukkala (2000) used a numerical routine that iterated between index modification and index evaluation. Others have used graphical methods to examine index behaviour through a sequence of formulations (e.g. De luis et al. 1998; Newton and Jolliffe 1998; Simard and Sachs 2004) or used a combination of both methods (Fox 2000). Optimisation methods generate precise index estimates. Graphical methods, while less precise, are more suitable for data exploration since the shape of the index response can inform inference regarding the mode of competition present and also help to ensure a global optimum is reached during evaluation.

In fulfilling the objective of this chapter, both index choice and sequential analysis are used to evaluate the influences of neighbour tree height, between-tree distance and neighbour spatial location. This evaluation is carried out in order to determine

index suitability, infer competitive relationships, and also determine optimum sample plot size and design so that efficient data collection can occur during remote sensing based inventory.

## 5.2 Methods

### 5.2.1 Local density index evaluation

Three distance-*independent* indexes and two distance-*dependent* indexes were compared.

The distance-independent indexes chosen were:

- a top height index, defined as the arithmetic mean height of the tallest trees in each plot (one to four tallest trees tested (MNH1,....,MNH4),
- a mean height index, defined as the arithmetic mean height of the trees in each plot (MNH), and
- the number of neighbouring trees on each plot (nNBH).

The top height and mean height indexes deserve further consideration. Because height development is largely independent of competitive effects, at least for the more dominant trees, these indexes are not expected to perform well in describing the competitive status of the more dominant (i.e. generally relatively taller) trees within the data. Where valid, all of the distance-dependent indexes were also assessed in combination with each other and with the following distance-dependent indexes.

The distance-dependent indexes chosen were the DWSR and APA indexes. These distance-dependent indexes were also further modified to facilitate further evaluation of neighbour influence.

Each distance-dependent index value was calculated using previously published SAS® software macros (Fox 2000); however several adaptations were required for this study. The APA macro was adapted to calculate bisector position and polygon area on a circular, rather than a square or rectangular plot. Each macro was adapted to calculate the index value for the subject tree only. Each macro was further adapted to incorporate the index modifiers discussed below.

Local density indexes can be assessed in a number of ways. The percentage reduction in the root mean square error of prediction (%rRMSE) achieved by incorporating an index in a DBH prediction model that already includes subject height quantifies the additional information provided by that index. This statistic is often used to compare indexes and identify the most suitable index in growth studies (e.g. Daniels et al. 1986; Biging and Dobbertin 1992; Biging and Dobbertin 1995; Fox et al. 2001). This metric is at unity with both $R^2$ and adjusted $R^2$, the other commonly used metrics where linear least squares models are compared and the Sum of Squares across models is equal.

A DBH prediction model should also display normal residual errors to ensure that the parameters are unbiased (in the case of maximum likelihood estimators) and efficient (in the case of both maximum likelihood and least squares estimators). Scatter plots of residual versus predicted DBH, together with plots of ordered residual values quantiles of the normal distribution can be constructed to visually assess residual normality and also to identify outlying values. Numerous more formal methods exist to aid in outlier identification. (Cook 1979). A simple way of assessing residual behaviour amenable to calculation across a range of sequentially assessed models involves applying a test of normality to model residuals. In this study, the Shapiro-Wilk (1965) test statistic is used to quantify residual normality and thus assess whether the assumptions of the estimator are met. Attained p-values given the degrees of freedom for the Shapiro-Wilk test statistic allow disjunctive decisions to be made regarding model suitability. In this study the test statistics themselves are used to rank competing models since the index under consideration is the only variant between models.

Together, %rRMSE and the Shapiro-Wilk test statistic may be used isolate optimum index formulations. In practical terms, any weighted combination of the two could be used, depending upon the importance given to each. In this study, they are weighted equally. The values of the two statistics are each standardised about their means and then added together. This resultant value is again standardised to generate an overall Optimum statistic. This statistic is therefore Normally distributed with mean equal to zero and variance equal to one.

## 5.2.2 Neighbourhood analysis

### *5.2.2.1 Between-tree distance*

The influence of between-tree distance was first assessed by comparing distance-independent indexes (nNBH, MNH, MNH4) with the previously published DWSR index. A secondary, sequential assessment of a modified DWSR index formulation was then employed. Previously published distance weighted indexes account for between-tree distance in contrasting ways. The DWSR index formulations assume that the competitive affect of the inverse distance between the subject and its neighbours is linear (Hamilton 1969; Hegyi 1974; Tome and Burkhart 1989), whereas the DWS index formulations (Weiner 1984; Thomas 1989) assume that the affect of the inverse distance between the subject and its neighbours is nonlinear by the addition of a power term.

In this study, the importance of inter-tree distance was explored by sequential assessment of modified versions of the DWSR index. The modified DWSR index for the subject tree is given by:

$$DSWR = \sum_{j=1}^{n} \left[ R_j A_j^{-Q} \right] \tag{5.1}$$

Where:

$R_j$ is the neighbour influence term for the *jth* neighbour described below in equation 5.2;

$Q$ is the distance modifier term. $Q$ values tested ranged from 0 to 3 by intervals of 0.5;

$A_j$ is the distance between the *jth* neighbour and the subject tree.

The distance modifier term affects the influence of neighbouring trees at different distances from the subject. When the term is set at zero the influence of each neighbour is unaffected by between-tree distance. As the term is increased, neighbours more proximate to the subject increasingly contribute to the index calculation relative to those neighbours more distant from the subject.

#### *5.2.2.2 Between-tree symmetry*

A variant of Tome and Burkhart's (1989) neighbour influence function was used to sequentially assess the affect of between-tree symmetry. Here, tree height replaces stem DBH:

$$R_j = \left( \frac{H_j}{H_i} \right)^k \tag{5.2}$$

Where:

$H_i$ is the total height of the subject tree;

$H_j$ is the total height of the neighbour tree;

$R_j$ is the neighbour influence term value for the *jth* neighbour constrained to a maximum value of four;

$k$ is the exponent term defining the degree of asymmetry. Index values were calculated using a range of $k$ term values. The $k$ term values were assessed sequentially from 0 to 4 by intervals of 0.5, and then assessed at values of 5, 6, 8 and 10.

Figure 5.1 shows the affect of a range of $k$ term values on the distribution of $R_j$ for the age 15 and age 20 datasets. The distribution of $R_j$ skews right as $k$ is increased. The variance of $R_j$ also increases as $k$ is increased. When $k = 0$ neighbour height relative to the subject tree imparts no information to the index calculation. As $k$ is increased, neighbours smaller than the subject are increasingly discounted, while neighbours larger than the subject increasingly influence index calculation. At the largest $k$ term tested, many neighbours larger than the subject contribute to index calculation equally, as the neighbour influence functions for those neighbours all equal the maximum constrained value. $R_j$ was constrained to a maximum value of four to ensure a small number of relatively larger neighbours did not overly influence index calculation. The maximum constrained value of $R_j$ was chosen because it represents the approximate ratio of the largest to smallest DBH values present in both datasets.

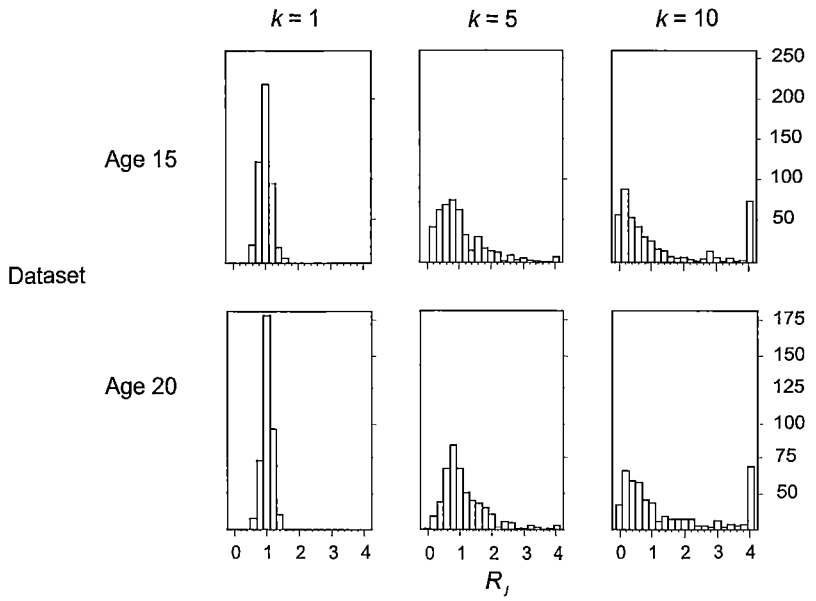


Figure 5.1 Frequency histograms of $R_j$ values for each neighbour tree calculated using different $k$ values for the age 15 and age 20 datasets.

#### *5.2.2.3 Neighbourhood size*

The influence of neighbourhood size was also assessed using the DWSR index. Because the zone of competition about each tree is dependent not only on the mode of competition but also upon the size and shape of the tree, there are considerable difficulties in defining the area over which an index should be assessed in order to include all competitors and sources of competition (e.g. Biging and Dobbertin 1992; Burton 1993; Lederman and Stage 2001). Indexes have typically been assessed over a circular area of fixed radius with the subject at the centre (De luis et al. 1998). Several researchers have found that the radius of the assessment area should be extended in stands containing older, larger individuals at wider spacings (Silander and Pacala 1985; Burton 1993; Prevósto et al. 2000; Radtke et al. 2003). While some researchers have assumed a fixed area (Hegyi 1974) or a fixed number of competitors (Van Laar 1969), others have investigated the affect of changing the area about a subject tree over which neighbours are assessed assuming that the area is a function of the subject size or a function of the neighbour size and number. While a range of methods has been tested, researchers have concluded that the optimum is approached asymptotically as the area is increased. Some researchers have fixed the area as a function of the subject and/or competitor DBH (Martin and Ek 1984; Lee and vonGadow 1997), subject height (Wimberly and Bare 1996), or subject crown radius (Lorimer 1983). Others used fixed angle gauge sweeps about the subject tree, assessing a candidate neighbouring tree as a

competitor dependent upon a combination of its DBH and distance from the subject (Daniels et al. 1986; Tome and Burkhart 1989). (Fox 2000) formalised plot radius selection by using a segmented, non-linear model which predicted the index correlation with growth as a function of the radius of the area over which the competition index was assessed. This technique yielded an asymptote value representing the optimum fixed radius.

In this study the potential neighbourhood size was constrained by the 5 metre plot radius used in data collection. Fixed plot radii defined by the distance from the subject were sequentially analysed to assess the adequacy of this radius for index calculation. Neighbours were included up to 3 to 5 meters from the subject tree by intervals of 0.5 metres.

#### *5.2.2.4 Between-tree sidedness*

The influence of between-tree sidedness was also assessed using the DWSR index. The analysis of sidedness in competition studies has been approached in several ways. Thomas (1989) modified a DWS index to include competitive sidedness by discounting the influence of neighbours smaller than the subject tree by multiplying their influence value by a number less than one. This adjustment reduces the affect of all neighbours smaller than the subject, but the reduction is greatest for those neighbours whose size is most similar to that of the subject, while competition from the larger neighbours is assumed symmetric. Others have used even simpler methods. By removing neighbours smaller than the subject, Stage's index (1973) assumes that the competitive process is totally two-sided since all neighbours are included. In contrast, Daniel et al.'s index (1986) assumes total one-sidedness since only larger neighbours are included.

In this study, a sequential neighbour analysis is used to assess neighbour sidedness (Newton and Jolliffe 1998; Simard and Sachs 2004). In sequential analysis, neighbours are assigned to an influence class. Neighbours belonging to each class are then sequentially added to an index calculation. The results of first adding the neighbours of smallest influence through to largest (upward from below) are compared against the results of first adding the neighbours of largest influence through to the smallest (downward from above). Newton and Jolliffe (1998) argued that two-sided competitive relations are evidenced by gradual changes to the prediction model density parameter value with additions of neighbours by influence class whereas one-sided competitive relations are evidenced by non-gradual changes. These differences arise due to the varying influence of neighbours under

differing sidedness conditions. The predictive utility of local density indexes is the primary interest in this study; therefore sidedness is assessed using %rRMSE and Shapiro-Wilk test statistic values. If both change gradually with sequential additions of neighbours by influence class then the competitive mode may be assumed two-sided. If additions result in non-gradual changes then the competitive mode may be assumed one-sided. Both Newton and Jolliffe (1998) and Simard and Sachs (2004) used total height to classify neighbour influence. In this study, neighbour influence is defined using both total height and distance from the subject.

#### *5.2.2.5 Tree spatial arrangement*

The importance of the spatial arrangement of neighbours was evaluated by comparing result for the DWSR index with those for the spatially explicit APA index. The APA index may also be modified to account for asymmetry and between-tree distance.

The modifications presented by Moore et al. (1973) to Brown's (1965) APA index [equation 2.3] incorporate the proportional size of all immediately proximate individuals. The index so describes two-sided, symmetric competition. In this study, the position of the bisectors in the APA index was calculated using a variant of the neighbour influence function presented by Tome and Burkhart (1989) [equation. 2.5]. Again, tree height replaces DBH as the size metric used in the function. Exponent term values [$k$ in equation 2.5] between 0 and 50 by intervals of 5 were evaluated. Where $k=0$ the bisector is set equidistant between neighbours as per Brown's (1965) original formulation. Moore et al.' (1973) formulation adjusts the equidistant position of the bisectors in a manner which is linearly related to the neighbour to subject size ratio and is calculated using $k=1$. This adjustment assumes the bisector position is symmetric to the neighbour to subject size ratio. $k$ values other than one produce APA polygons in which the bisectors are positioned asymmetrically to the neighbour to subject height ratio. $k$ values over ten reduced the APA index values to zero for some trees. Figure 5.2 presents histograms of neighbour influence values calculated using several different $k$ values. the value of the $k$ term is increased, the range of modifier values increases. At the largest $k$ value tested the neighbour influence values include numerous zeros and ones, which locate bisectors abutting the subject and neighbour trees respectively.

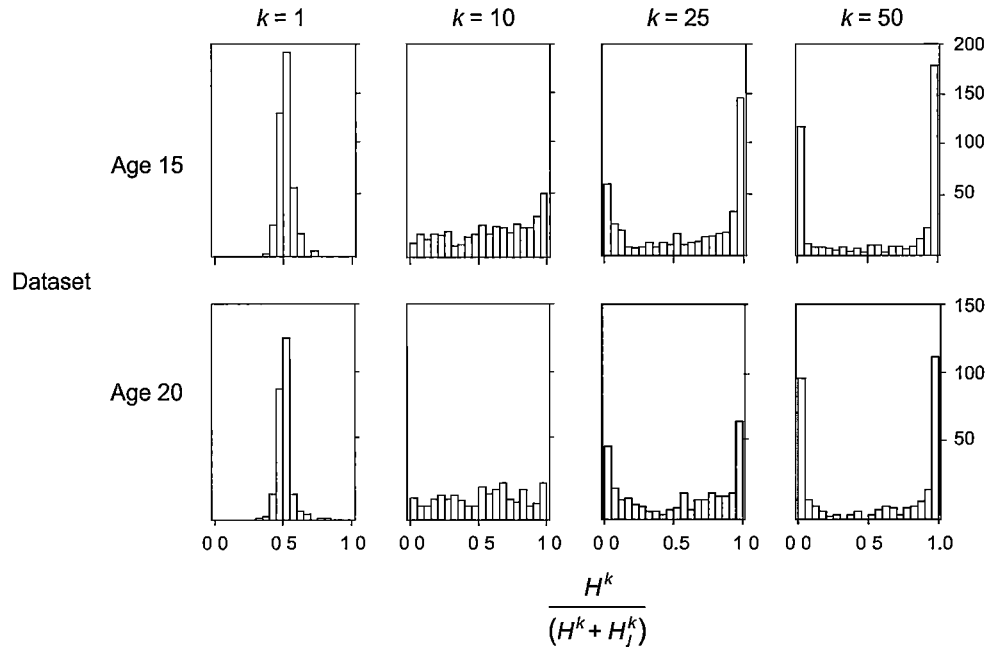


Figure 5.2 Frequency histograms of neighbour influence values for each neighbour tree calculated using different $k$ values for the age 15 and age 20 datasets.

A reformulation of Nance et al.' (1988) polygon constraint function was also used for the calculation of APA polygon values. This function is given by:

$$pc = zr\sqrt{H \Big/ \sum_{j=1}^{n} H_j} \tag{5.3}$$

Where:

$pc$ is the maximum potential area of the constrained APA polygon for subject tree;

$z$ is the polygon constraint term. $z$ values tested ranged between 0.25 and 2.5;

$r$ is the radius of the plot.

Note that tree height has been substituted for tree DBH in the size ratio component of this formula and a further polygon constraint term has been added. At the largest polygon constraint term, the index is unconstrained since the constraint lies beyond the extent of any derived polygon boundary. As the polygon constraint term is decreased, the derivation of irregular polygons is avoided as per the intent of the original formulation (Nance et al. 1988). At still smaller values, it further constrains the extent to which the bisectors define the APA boundary, first

affecting the extent to which the boundary may be shifted toward neighbours that are smaller than the subject. When the value of $k$ is small, small $z$ values ensure that the bisectors play almost no role in the APA calculation since the constraint boundary defines the polygon boundary extent. The index therefore behaves like a distance-independent index since the APA value is equivalent to the proportion of the sum tree heights on the plot that belong to the subject tree.

## 5.3 Results

### 5.3.1 Distance dependent analyses

Scatter plots were used to visually assess DBH and height relationships. Those plots showed that a simple linear model would be adequate for use as the basic DBH prediction model from which model statistics for the models incorporating density could be calculated. This linear relationship is likely to reflect the limited developmental range of these data as in datasets comprising a more expansive developmental range convex, or even sigmoidal, relationships are more common where total height is plotted on the vertical axis against DBH (Curtis 1967).

Researchers have developed numerous models to predict DBH as a function of total tree height and some metric of crown size that could serve as candidate models for this study. Many researchers have fitted models using interaction terms, presumably assuming that the affect of tree height and crown area upon DBH is synergistic. From a biological perspective, synergism implies that some feedback exists between crown and height development. For example, a positive synergy between the two could suggest that height growth facilitates greater crown exposure and therefore greater photosynthate production, allowing still greater horizontal crown development.

Examples of such synergistic models include:

$$D^2 = a + b\,H\,C \quad \text{(Aldred and Kippen 1967)} \tag{5.4}$$

$$D = a + b\,H \log_{10}(C) \quad \text{(Aldred and Sayn-Wittgenstein 1972)} \tag{5.5}$$

$$D = a + b\,H\,\sqrt{C} \quad \text{(Aldred and Sayn-Wittgenstein 1972)} \tag{5.6}$$

$$D = {HC^a}\Big/{\left(b + cH\right)} \quad \text{(Hall et al. 2001)} \tag{5.7}$$

Where:

$a$, $b$ and $c$ are model parameters

Later researchers have focussed upon selecting the 'best' of these models, among others, including models which assume no synergy between tree height and the chosen crown metric (Hall et al. 1989; Inc. 1996; Inc. 1997; Hall et al. 2001). For example, using $R^2$, RMSE and a subjective analysis of the randomness and heterogeneity of residuals to assess model fit, Hall et al. (2001) compared the predictive utility of 18 models for five different tree species and concluded that many models performed equally well, but that the best model was different for each. The models chosen included those of both additive and multiplicative, and linear and non-linear form. The distance dependent analyses in this study encompassed evaluation of the distance-independent indexes and the DWSR index in its symmetric form with a linear distance term, i.e. $Q$=1, $k$=1. This analysis showed that normal additive linear models adequately described the relationships.

No transformation of tree height or DBH was required for any model. Logarithmic transformation of the DWSR index improved model fit. The transformation has some biological meaning. The DWSR index is a modified stem count, the distribution of which is approximately Poisson where tree spatial arrangement is random and therefore approximately normalised by logarithmic transformation. Correspondingly, the distance-independent density index nNBH was also logarithmically transformed for use in the linear models. Interaction terms with tree height were tested for all the models. Their t-values indicated that they were not significant at the 0.05 level in all cases, so the results presented are for models without interaction terms. In the case of the age 15 dataset, MNH variables and nNBHs were both significant. The model statistics for only the model with the highest optimum value incorporating both MNH and nNBH variables are presented. Models were fitted using the R software package (Core R Development Team 2004).

Table 5.1 presents the model statistics for the distance dependence analysis applied to the age 15 dataset. The models are ranked according to the Optimum statistic, which is calculated using %rRMSE and Residual normality statistics from this Table only. In isolation, the distance-independent indexes perform quite poorly. In

combination, the MNH4 and nNBH behave similarly to the DWSR index. These models (8 and 9) are the most highly ranked of those tested, with good residual normality and higher %rRMSE values than those exhibited by the other tested indexes. The MNH index performs most poorly. This indicates that comparatively shorter neighbouring trees do not impart useful information in local density calculations and that local density may be one-sided in this age class.

Table 5.2 presents the model statistics for the same distance dependence analysis applied to the age 20 dataset. Again, the models are ranked according to the Optimum statistic, calculated using %rRMSE and Residual normality statistics from this Table only. In comparison to the age 15 dataset, the models show considerably lower %rRMSE values and poorer residual normality. That the relationship between local density at measurement age and subject tree DBH is weaker than that observed in the age 15 dataset is possibly evidence that the thinning five years previous has removed neighbouring trees which contributed to local density which is still expressed in measurement age DBH. Poor residual normality is evidence of the less adequate linear model. An inspection of alternate model formulations did not show any change in the rankings of residual normality statistic values. The DWSR index ranks in amongst the MNH indexes. The nNBH index performs poorly and is not significant in combination with other indexes. Since the DWSR index is a modified stem count, the poor performance of the nNBH index suggests an explanation for the less satisfactory behaviour of the DWSR index in comparison to the age 15 dataset. Again, the MNH index performs most poorly, indicating comparatively shorter neighbouring trees do not impart useful information in local density calculations and that local density may also be one-sided in this later age class.

Table 5.1 Model statistics for the distance dependence analysis applied to the age 15 dataset. A distance-independent index and DWSR index comparison.

| Model | Variable | Parameter Value (s.e.) | RMSE | %rRMSE | Residual normality | Optimum | Rank |
|---|---|---|---|---|---|---|---|
| 1 | Intercept | 3.1781 (2.7153) | 4.337 | . | 0.9693 | | 9 |
| | H | 1.2479 (0.1909) | | | | | |
| 2 | Intercept | 3.4495 (3.458) | 3.942 | 9.1 | 0.9694 | -1.455 | 8 |
| | H | 1.8553 (0.2410) | | | | | |
| | MNH | -1.1910 (0.3279) | | | | | |
| 3 | Intercept | 15.3510 (3.1954) | 3.573 | 17.6 | 0.9851 | 0.398 | 3 |
| | H | 2.2540 (0.2456) | | | | | |
| | MNH4 | -1.6566 (0.3105) | | | | | |
| 4 | Intercept | 15.6950 (3.3720) | 3.639 | 16.1 | 0.9768 | -0.203 | 5 |
| | H | 2.2260 (0.2518) | | | | | |
| | MNH3 | -1.6212 (0.3219) | | | | | |
| 5 | Intercept | 16.3597 (3.4197) | 3.615 | 16.6 | 0.9735 | -0.305 | 6 |
| | H | 2.2501 (0.2516) | | | | | |
| | MNH2 | -1.6477 (0.3204) | | | | | |
| 6 | Intercept | 16.6864 (3.5087) | 3.634 | 16.2 | 0.9576 | -1.137 | 7 |
| | H | 2.2809 (0.2594) | | | | | |
| | MNH1 | -1.6525 (0.3267) | | | | | |
| 7 | Intercept | 15.8160 (3.5845) | 3.726 | 14.1 | 0.9890 | 0.143 | 4 |
| | H | 1.3847 (0.1667) | | | | | |
| | nNBH | -6.6872 (1.4400) | | | | | |
| 8 | Intercept | 7.5311 (2.2136) | 3.359 | 22.5 | 0.9907 | 1.296 | 1 |
| | H | 1.2880 (0.1480) | | | | | |
| | DWSR | -6.1727 (0.9798) | | | | | |
| 9 | Intercept | 20.4081 (3.4335) | 3.345 | 22.9 | 0.9891 | 1.264 | 2 |
| | H | 2.0875 (0.2365) | | | | | |
| | MNH4 | -1.2374 (0.3226) | | | | | |
| | nNBH | -4.3058 (1.4341) | | | | | |

Table 5.2 Model statistics for the distance dependence analysis applied to the age 20 dataset. A distance-independent index and DWSR index comparison.

| Model | Variable | Parameter Value (s.e.) | RMSE | %rRMSE | Residual normality | Optimum | Rank |
|---|---|---|---|---|---|---|---|
| 1 | Intercept | -12.3106 (4.807) | 4.585 | . | 0.9628 | | 8 |
| | H | 1.8628 (0.2298) | | | | | |
| 2 | Intercept | -2.4304 (6.5454) | 4.448 | 3.0 | 0.9702 | 0.364 | 4 |
| | H | 2.0782 (0.2444) | | | | | |
| | MNH | -0.6641 (0.3087) | | | | | |
| 3 | Intercept | 2.4567 (5.8924) | 4.150 | 9.5 | 0.9662 | 1.087 | 1 |
| | H | 2.4101 (0.2549) | | | | | |
| | MNH4 | -1.1535 (0.3104) | | | | | |
| 4 | Intercept | 3.2553 (5.8691) | 4.108 | 10.4 | 0.9649 | 0.976 | 2 |
| | H | 2.3943 (0.2468) | | | | | |
| | MNH3 | -1.1519 (0.2950) | | | | | |
| 5 | Intercept | 3.4207 (5.9218) | 4.114 | 10.3 | 0.9594 | -0.539 | 5 |
| | H | 2.3615 (0.2430) | | | | | |
| | MNH2 | -1.1060 (0.2852) | | | | | |
| 6 | Intercept | 1.4238 (5.6863) | 4.144 | 9.6 | 0.9585 | -0.968 | 6 |
| | H | 2.3419 (0.2440) | | | | | |
| | MNH1 | -0.9820 (0.2623) | | | | | |
| 7 | Intercept | -6.2928 (5.5574) | 4.469 | 2.5 | 0.9639 | -1.481 | 7 |
| | H | 1.8358 (0.2244) | | | | | |
| | nNBH | -3.1542 (1.5666) | | | | | |
| 8 | Intercept | -6.8961 (4.6432) | 4.184 | 8.7 | 0.9651 | 0.561 | 3 |
| | H | 1.6671 (0.2168) | | | | | |
| | DWSR | -4.5234 (1.2717) | | | | | |

## 5.3.2 Neighbourhood analysis

### *5.3.2.1 Neighbourhood size, between-tree distance and symmetry analysis*

Figure 5.3 presents the results of the evaluation of neighbourhood size, between-tree distance and symmetry using the DWSR index for the age 15 dataset. In these figures, the model statistics are plotted versus DWSR index $Q$ and $k$ values. The contours represent statistic isobars. Results are shown for plot sizes between 3 and 5 metres. This was the plot size range in which %rRMSE values surpassed 15. At the minimum plot size shown, %rRMSE values are small. As it is increased there is a sudden jump in %rRMSE values toward the maximum. The maximum %rRMSE value in each plot size class is reached at increasingly larger $Q$ values. This suggests that proximate trees require greater weighting than distant trees in order to best characterise their influence upon the subject tree at larger plot sizes. In contrast to the %rRMSE statistic, the residual normality statistic shows a steady increase with increasing plot size. Apart from the results for the smallest plot size class shown, the statistic reaches is maximum within each plot size class at increasingly larger $Q$ values and so the two statistics are increasingly in accordance with each other. The largest residual normality statistic values are reached at the maximum plot size tested where two rather indistinct peaks occur. The residual normality statistic value is greater than 0.99 (alpha>0.05) in each of these peaks. This is evidence of good residual normality. The largest Optimum statistic values across plot size classes occur where $k$ is greater than one. This suggests that local density, as described by relative height, is asymmetric with respect to subject tree DBH.

In isolation, the %rRMSE statistic suggests local density will be adequately described using the relative heights of neighbours within 3 metres. The calculation of the additional residual normality statistic shows improvements to residual normality are possible by including in index calculations, both neighbouring trees more distant from the subject, and their actual distances. That the residual normality statistic reaches such a high value at larger plot sizes, while the %rRMSE statistic approaches an approximate asymptote at even smaller plot sizes, suggests the 5 metre plot radius used in data collection is adequate for this age class and is suitable for use in future inventory.

Figure 5.4 presents the results of the same analysis applied to the age 20 dataset. Again, model statistics are plotted versus DWSR index $Q$ and $k$ values in these figures. Similarly to the results of the initial density analysis, %rRMSE values are considerably lower than those shown for the age 15 dataset. At the minimum plot radius shown, optimum %rRMSE values occur at the largest $k$ value tested. The corresponding residual normality values are the poorest tested, indicating model bias across DBH classes. As the plot size is increased, %rRMSE statistic values consistently increase while residual normality statistic values appear to asymptote at the 4.5 metre plot size.

These results suggest the 5 metre plot boundary fixed during data collection may have been inadequate, although the overall poor correspondence between %rRMSE statistic and residual normality statistic values together with the results from the initial analysis indicate that the DWSR index more generally, may be inadequate for this dataset.

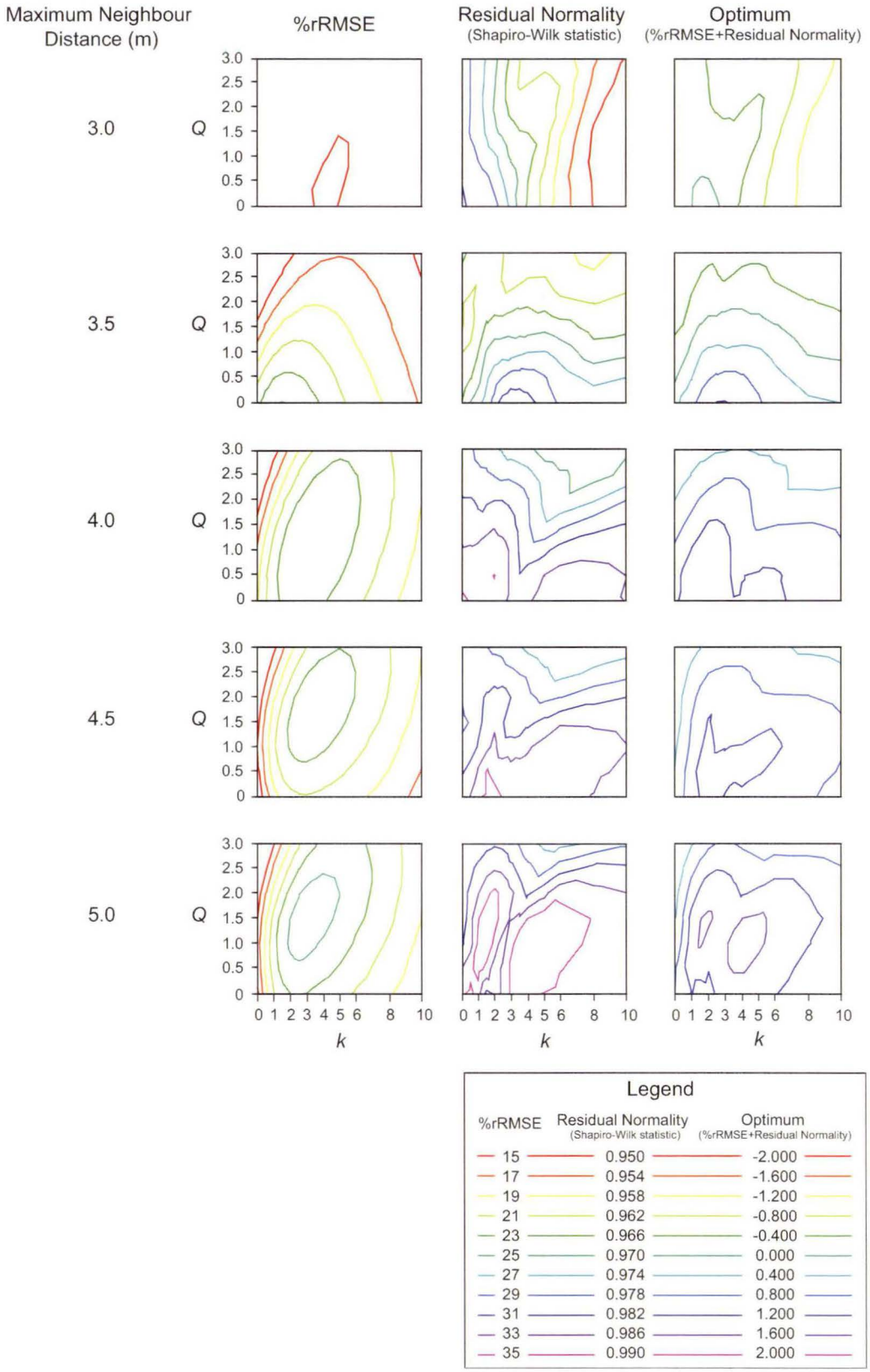


Figure 5.3 Model statistics for evaluations of neighbourhood size, between-tree distance and symmetry using the DWSR index for the age 15 dataset - %rRMSE, residual normality and Optimum statistic values versus DWSR $Q$ and $k$ terms.

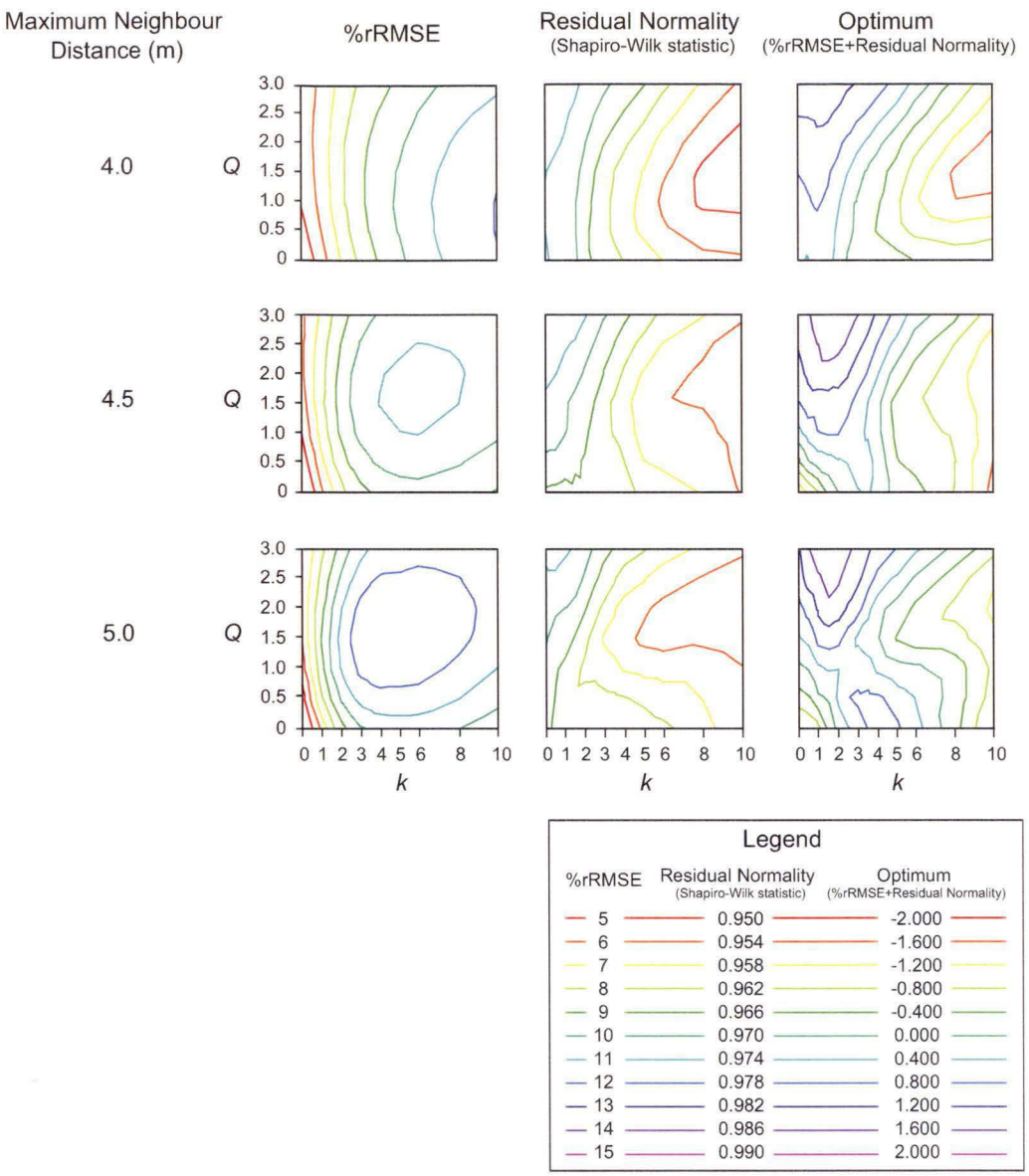


Figure 5.4 Model statistics for evaluations of neighbourhood size, between-tree distance and symmetry using the DWSR index for the age 20 dataset - %rRMSE, residual normality and Optimum statistic values versus DWSR $Q$ and $k$ terms.

#### *5.3.2.2 Between-tree sidedness*

Figure 5.5, 5.6 and 5.7 present the results of the evaluation of the influence of between-tree sidedness using the DWSR index for the age 15 dataset. Once again, the model statistics are plotted versus DWSR index $Q$ and $k$ values in these figures. Figure 5.3 shows the influence of neighbour addition from below, while Figures 5.4 and 5.5 show the influence of neighbour addition from above. Again, results are only shown for neighbour influence classes that resulted in %rRMSE values surpassing 15.

Viewing Figure 5.5, it is evident that the addition of at least 80% of the *least* influential neighbour trees is required to generate %rRMSE values greater than 15. The addition of all neighbouring trees produces the greatest reduction in RMSE and the largest residual normality statistic values. This result supports the assertion that local density in this age class is strongly one-sided, since neighbouring trees with high influence values must be included in index formulation for the index to have predictive power. The results presented in Figures 5.6 and 5.7 complement this assertion. The addition of 20% of the *most* influential trees sees %rRMSE and residual normality values reach values that are barely surpassed with further neighbour additions. In the midrange of neighbour influence classes tested, there exists a positive relationship between optimum $k$ and $Q$ values, suggesting that index behaviour is being driven by a small number of trees. Model stability improves as more neighbours are added to index formulation.

Figure 5.8, 5.9 and 5.10 present the results of the evaluation of the influence of between-tree sidedness using the DWSR index for the age 20 dataset. Figure 5.8 shows the influence of neighbour addition from below, while Figures 5.9 and 5.10 show the influence of neighbour addition from above. Results are only shown for neighbour influence classes that resulted in %rRMSE values surpassing 5.

As was the case with the age 15 dataset, local density in this age class appears to be strongly one-sided, since neighbouring trees with high influence values must be included in index formulation for the index to have any practical predictive power. Figure 5.8 shows that the addition of at least 90% of the *least* influential neighbour trees is required to generate %rRMSE values greater than 5. The results of neighbour addition downward from above presented in Figures 5.9 and 5.10 are also similar and suggest the assertion is correct. The addition of each influence class sees an incremental increase in %rRMSE values up to 50% after which this

statistic stabilises. Residual normality behaviour is less consistent and is poorly related to %rRMSE. Moreover their appears to be a strong relationship between optimum $Q$ and $k$ values within each plot, again, indicating that the model behaviour is driven by a small number of neighbouring trees. Once again, model stability improves as more neighbours are added to index formulation.

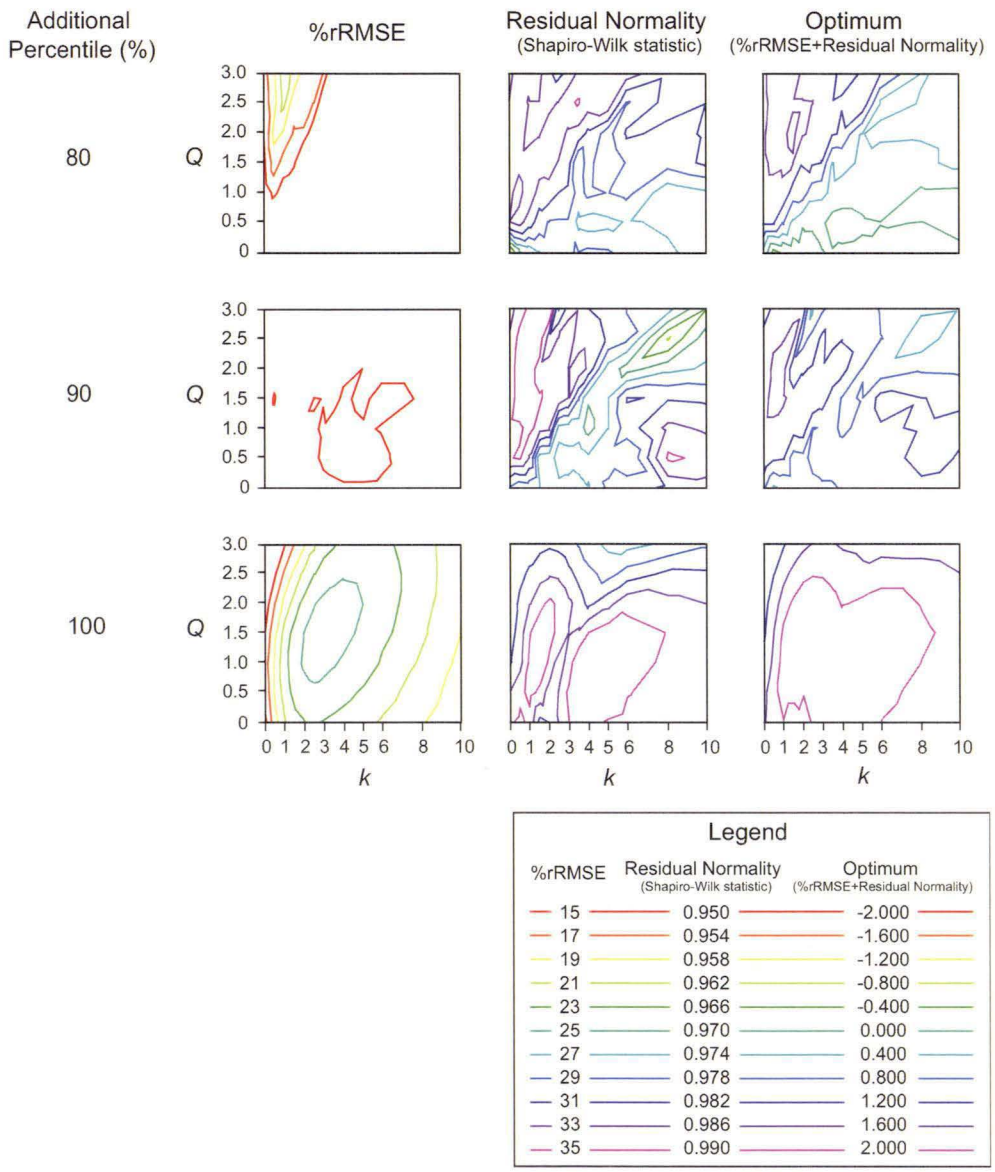


Figure 5.5 Model statistics for the evaluation of between-tree sidedness using the DWSR index for the age 15 dataset. Assessing neighbour addition upward from below - %rRMSE, residual normality and Optimum statistic values versus DWSR $Q$ and $k$ terms.

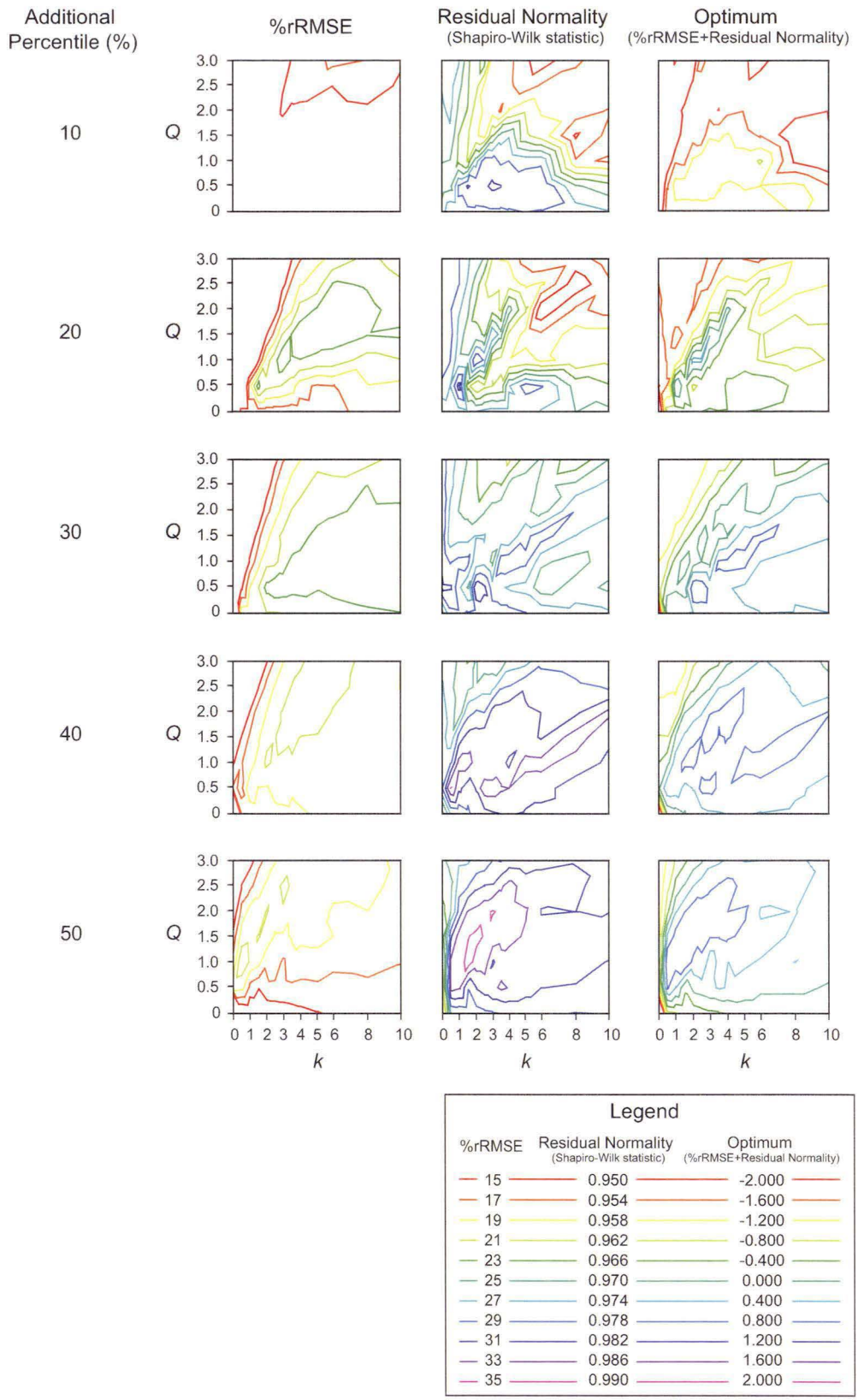


Figure 5.6 Model statistics for the evaluations of between-tree sidedness using the DWSR index for the age 15 dataset. Assessing neighbour addition downward from above. Additional neighbour percentile range 10 – 50% - %rRMSE, residual normality and Optimum statistic values versus DWSR $Q$ and $k$ terms.

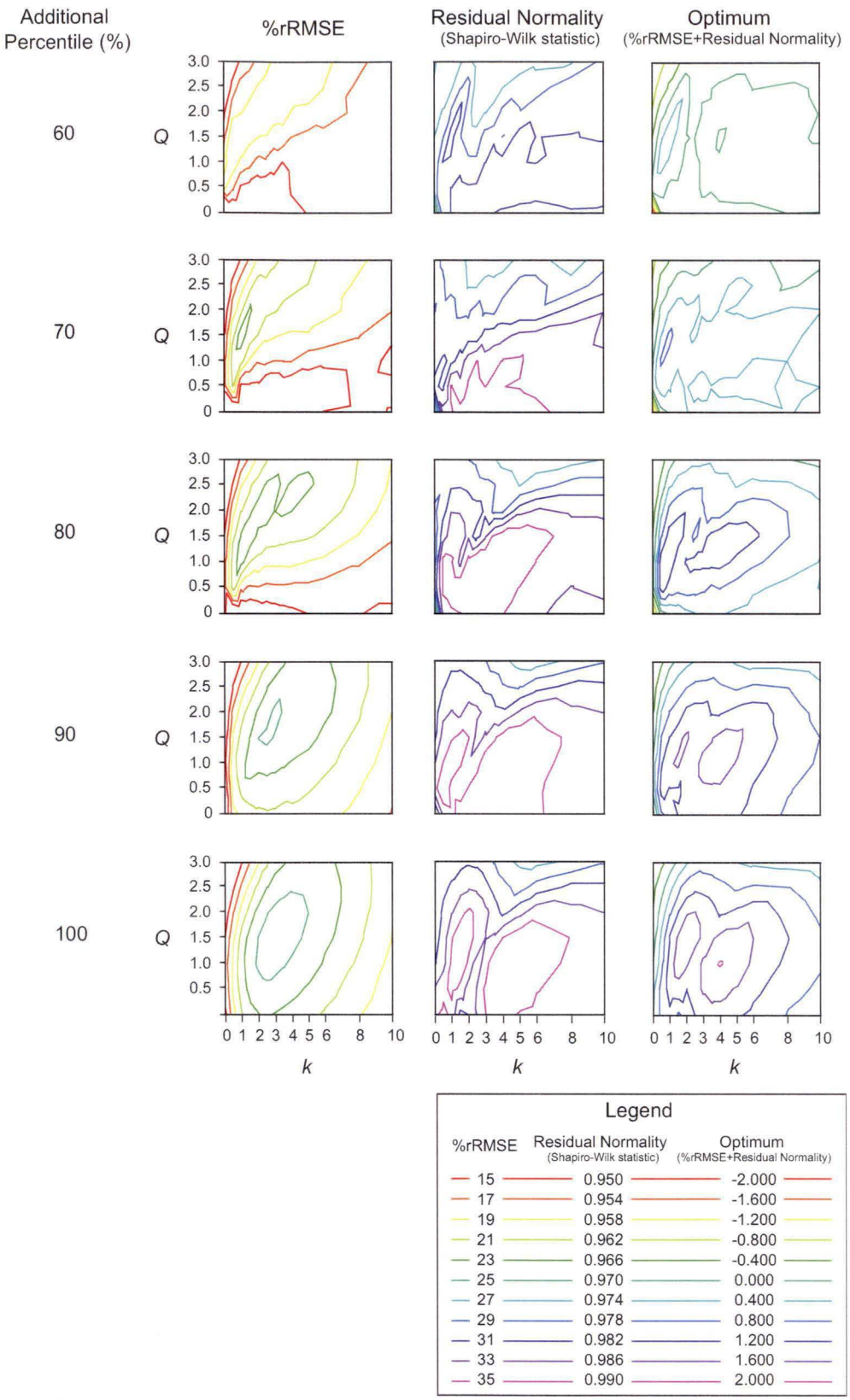


Figure 5.7 Model statistics for the evaluations of between-tree sidedness using the DWSR index for the age 15 dataset. Assessing neighbour addition downward from above. Additional neighbour percentile range 60 – 100% - %rRMSE, residual normality and Optimum statistic values versus DWSR $Q$ and $k$ terms.

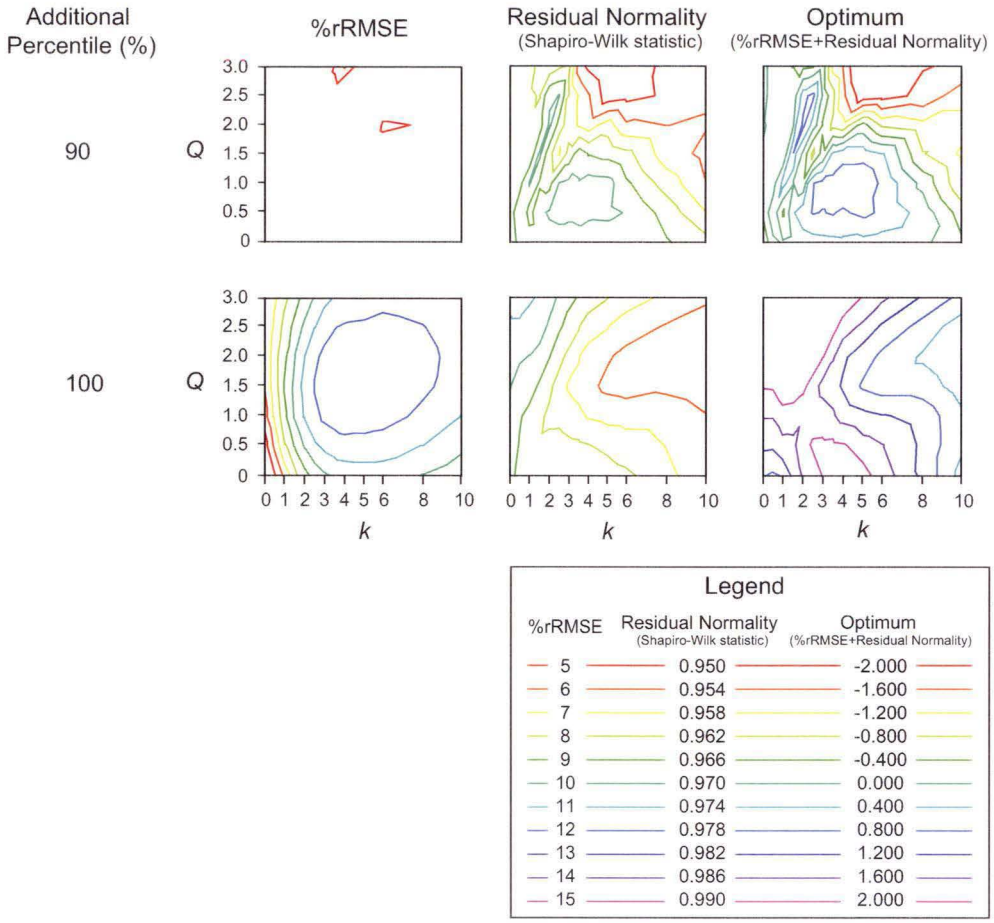


Figure 5.8 Model statistics for the evaluations of between-tree sidedness using the DWSR index for the age 20 dataset. Assessing neighbour addition upward from below - %rRMSE, residual normality and Optimum statistic values versus DWSR $Q$ and $k$ terms.

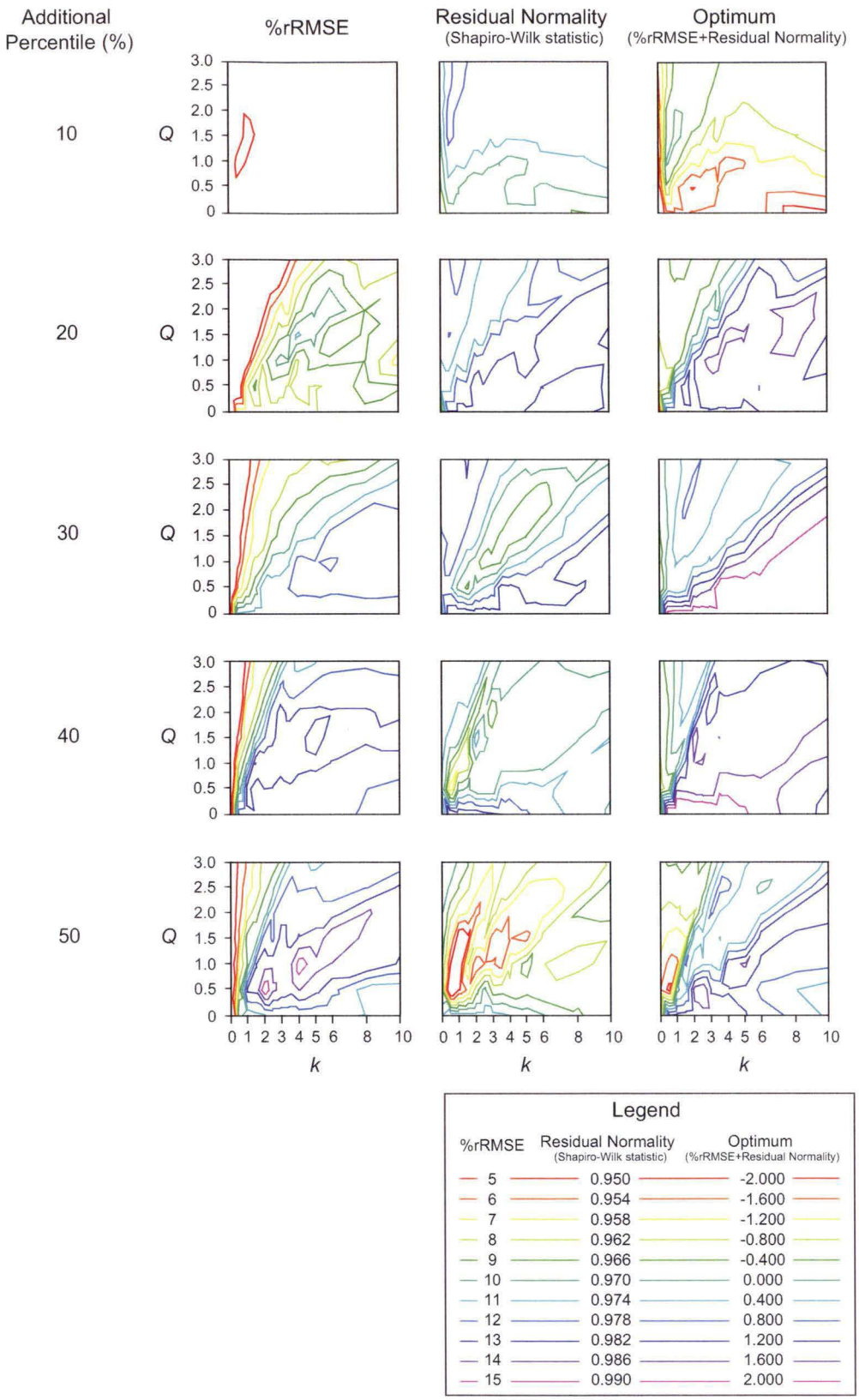


Figure 5.9 Model statistics for the evaluations of between-tree sidedness using the DWSR index for the age 20 dataset. Assessing neighbour addition downward from above. Additional neighbour percentile range 10 – 50% - %rRMSE, residual normality and Optimum statistic values versus DWSR $Q$ and $k$ terms.

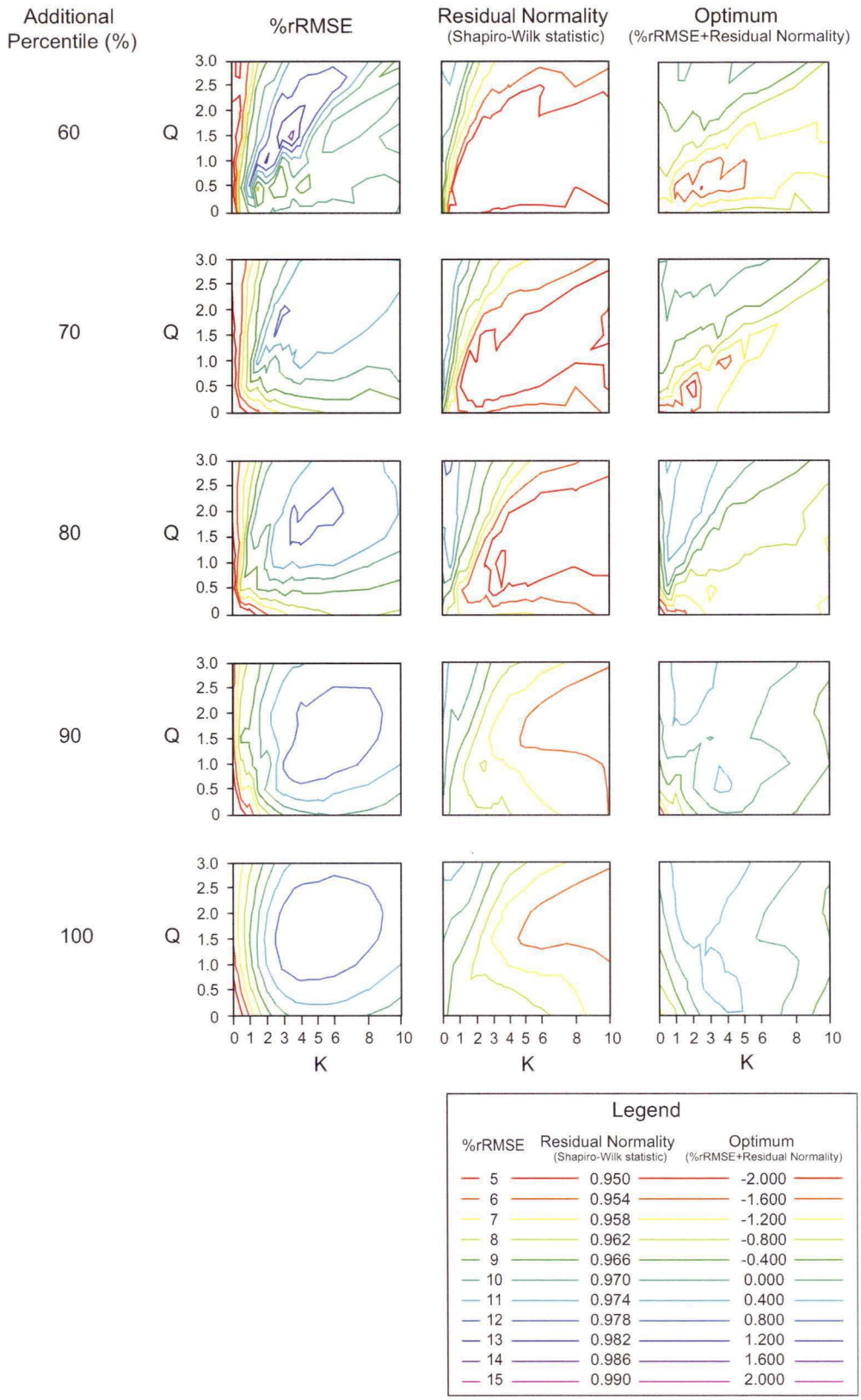


Figure 5.10 Model statistics for the between-tree sidedness evaluations using the DWSR index for the age 20 dataset. Assessing neighbour addition downward from above. Additional neighbour percentile range 60 – 100% - %rRMSE, residual normality and Optimum statistic values versus DWSR $Q$ and $k$ terms.

### *5.3.2.3 Tree spatial arrangement*

The APA index is used to evaluate the influence of tree spatial arrangement. APA index values were square root transformed. As per the DWSR index transformation, this transformation has some biological meaning. In these closed canopy stands it is reasonable to assume the APA index value approximately corresponds to crown area. The transformation normalises the relationship between the linear stem metric and the quadratic surrogate crown metric.

Figure 5.11 presents model statistics for the APA index evaluation for the age 15 dataset. The larger %rRMSE statistic values occur where $z$ is equal to 0.75 and $k$ is equal to values ranging from ten to twenty. As per the other indexes tested, the residual normality statistic is largely in accordance with the %rRMSE statistic except for the presence of two rather indistinct peaks. Maximum residual normality statistic values are greater than 0.99 (alpha>0.05), indicating good residual normality. The large $k$ value at the largest Optimum statistic value suggests that local density is asymmetric with respect to subject tree DBH. In contrast to the other distance-dependent indexes tested, maximum %rRMSE values are much larger ($\%\text{rRMSE} \simeq 35$ rather than $\%\text{rRMSE} \simeq 25$), while residual normality statistic values are similar. The results suggest neighbour spatial arrangement does influence local density.

Figure 5.12 presents model statistics for the APA index evaluation for the age 20 dataset. Here, the shape of the %rRMSE statistic response is overall very similar to that seen in the age 15 dataset (Figure 5.11) except that maximum %rRMSE statistic values are again lower. The residual normality and %rRMSE statistics are largely in accordance with each other. The large $k$ value at the largest Optimum statistic value again suggests that local density is asymmetric with respect to subject tree DBH. Similar to the age 15 dataset, maximum %rRMSE values are larger that those obtained using the other indexes, although the differences, in accordance with overall magnitude differences, are correspondingly smaller ($\%\text{rRMSE} \simeq 14.5$ rather than $\%\text{rRMSE} \simeq 11.0$). Residual normality statistic values are similar across indexes. Again, the results suggest neighbour spatial arrangement influences local density.

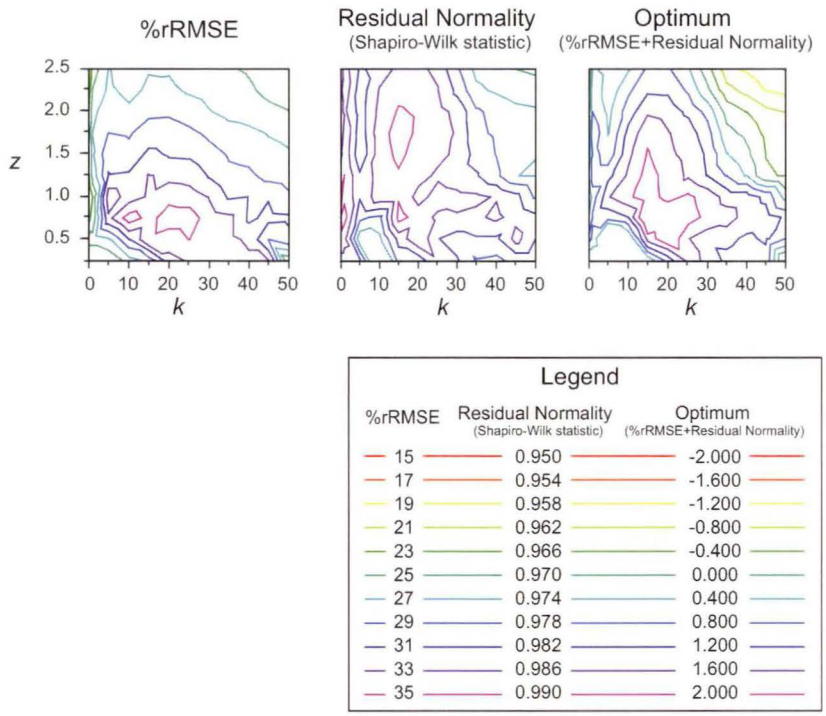


Figure 5.11 Tree spatial arrangement evaluations using the APA index for the age 15 dataset. %rRMSE, residual normality and Optimum statistic values versus APA $z$ and $k$ terms.

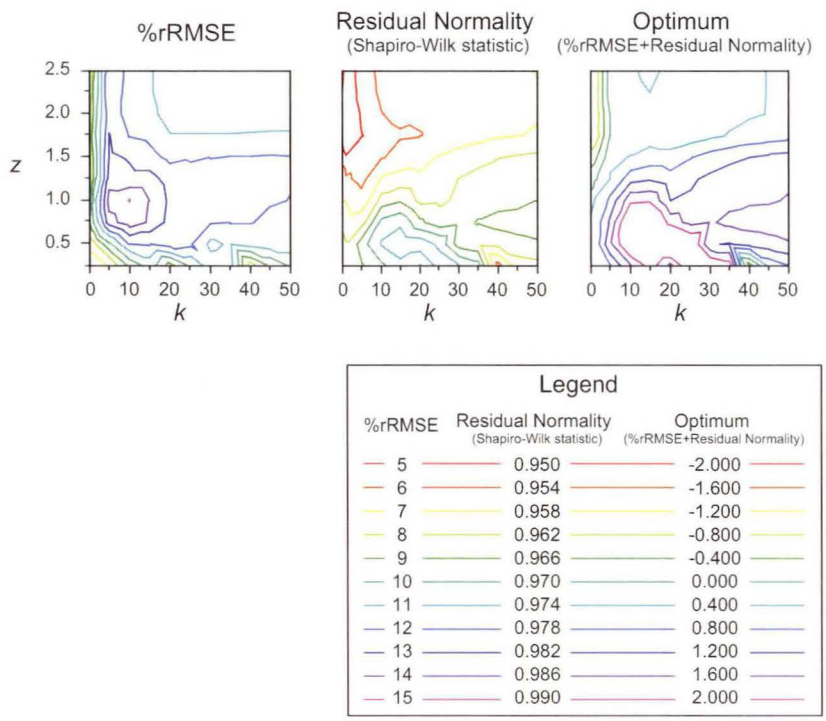


Figure 5.12 Tree spatial arrangement evaluations using the APA index for the age 20 dataset. %rRMSE, residual normality and Optimum statistic values versus APA $z$ and $k$ terms.

## 5.4 Discussion

In this study, total tree height was the input variable used to describe DBH. The degree of symmetry between height ratio and subject stem DBH was explored by comparing indexes formulated under different asymmetry assumptions. Quite high optimum asymmetry term values were found, however drawing conclusions about the nature of the density relations between trees in these stands is complicated by the manner in which neighbour/subject height ratio was used to predict subject DBH. While assumed to be a relative small component of the total, some component of the $k$ term could well be attributable to the height/DBH relationships exhibited by neighbouring trees. If DBH ratios between neighbours are not equal to their respective height ratios then their optimal $k$ term specification will not accurately describe the degree of asymmetry.

The DWSR index ranked higher than simple distance-independent indexes for the age 15 dataset but not for the age 20 dataset. The poorer responses apparent for the age 20 dataset, together with the relatively good response obtained with the simple MNH indexes, suggest that the use of distance-dependent indexes at this later age is unwarranted.

The importance of inter-tree distance was further explored in a sequential application of inter-tree distance modifier terms to the DWSR index. Optimum values between one and two were obtained, although these values varied with the number of neighbours and the plot radius. The non-zero values indicated that inter-tree distance has an influence on local density, although for the age 20 dataset, this influence was very minor.

The plot radius used in data collection was adequate for the age 15 dataset since optimum model statistic values reached an asymptote for the DWSR index prior to the inclusion of the most distant neighbours. In contrast, the results for the age 20 dataset show that the optimum plot radius was not determined, since a clear optimum or asymptote in index response was not observed.

The sequential addition of neighbours according to their influence upon the subject tree showed that the contribution of many neighbours to local density was largely restricted to improvements in model stability. This evaluation suggests that one-sided competitive relations between trees are present.

The APA index outperformed the other indexes tested, indicating that the influence of neighbour location is substantial. APA index performance was further improved by inclusion of asymmetry and polygon constraint terms. Several other studies have reported the same finding (Nance et al. 1988; Tome and Burkhart 1989; Fox 2000) but have not tested such a range of constraint values. Tome and Burkhart (1989) argued that the size of smaller neighbouring trees should enter index calculations as a negative value in order to expand differences between trees which compete asymmetrically. Both Tome and Burkhart (1989) and Fox (2000) found that the square weighted, constrained APA index outperformed other APA formulations. Wimberly and Bare (1996) argued that the costs entailed in the computational requirements of the APA index outweighed any additional benefits in terms of its predictive utility. The magnitude of the benefit shown here suggests otherwise for the age 15 dataset but not for the age 20 dataset.

At the largest polygon constraint term tested, the APA index is unconstrained and the RMSE response is relatively insensitive to the specification of the $k$ term. The magnitude of the response is similar to that of the DWSR index at its optimum $Q$ term specification. The polygon constraint function apportions plot area equally between all trees on the plot proportional to their height. Thus trees with comparatively more neighbours are afforded smaller polygons, as are trees with comparatively larger neighbours. As the polygon constraint term is decreased, large $k$ term values increasingly affect the realised polygon size of those trees with larger neighbours only, since the polygon constraint increasingly defines the polygon boundary in place of the bisectors between subject trees and their larger neighbours. The optimum index formulation is found in this region of moderate $z$ and high $k$ term values. This finding implies that the competitive relations between neighbouring trees realised in DBH in these age groups are asymmetric with respect to neighbour/subject tree height ratio. However, they also tend toward being one-sided, in that larger neighbours affect the local neighbourhood density about smaller subjects in a strongly asymmetric manner while subject trees with smaller neighbours utilise a space that is more symmetrically proportional to their height as a component of the total height of all the trees within the plot. Larger trees may be successfully competing for asymmetrically supplied resources (sunlight) but are then limited by symmetrically supplied resources (water and nutrients). As the polygon constraint term is further decreased, the k term becomes increasingly irrelevant to polygon area definition as the polygon constraint increasingly defines the polygon area in place of the bisectors.

The shapes of the response surfaces from the analysis of the distance-dependent indexes presented in Section 5.3.2 were generally very similar across age classes, with the major difference being in the magnitude of reductions in RMSE. The similarity of response surface shape between datasets provides no evidence to suggest that any shift in the nature of competitive relations is occurring as the stands mature between ages 15 and 20. The smaller responses evidenced in the age 20 dataset possibly reflect the fact that the optimum plot size was not used in their formulation. Given that the plot size was identical and adequate for index formulation at age 15, a more substantial explanation may be that these reduced responses are indicative of the reduced role of neighbours in determining subject stem size at this later age. The reduction may be due to the impact of thinning, which removes some of the neighbours responsible for earlier DBH growth trajectories.

The number of neighbours and the mean height of the 4 tallest neighbours were significant predictors of DBH in tandem for the age 15 dataset, however DBH prediction using the DWSR index resulted in a better Optimal statistic value. The distance-independent indexes were not significant predictors when employed in tandem for the age 20 dataset. These results, and those of applying the further index constraint modifications presented in Section 5.3.2, indicate that the formulated indexes offer substantial practical advantages in an inventory context. Not only may the inputs to index formulations be modified to optimise their efficiency, but these indexes offer a convenient means to summarise neighbourhood information for the prediction of stem metrics.

This study has made use of data obtained from ground-based plots that have been measured with minimal errors. The standard deviation in the height difference between subject and neighbour trees was 2.85 and 4.40 metres for the age 15 and 20 datasets respectively, while subject and neighbour tree height was measured without significant bias and with a precision of 0.05 and 0.21 metres respectively[1]. Neighbour positional error is also minor. Remotely sensed data are unlikely to be measured with precision or accuracy of similar magnitude. The effects of measurement error are likely to be complex and nonlinear, particularly since the optimum formulations were asymmetric. The results of the APA index analysis demonstrate that accurate determination of tree total height can improve the RMSE reduction from 25% to 35% and from 7% to 14% for the age 15 and age 20 datasets respectively. This suggests that optimum inventory will require remotely

[1] See Chapter 4.3 and 4.4.

sensed data that precisely determines individual tree, rather than canopy, height. The fact that the optimum formulations implied strongly asymmetric interactions suggests the accurate determination of dominant and subdominant tree location and height will be more important than the determination of location and height for trees that reach to lower heights in the canopy. It is fortuitous that the former likely comprise proportionally more of the stand timber volume.

The potential gains from both accurate determination of tree location and the restriction of tree identification errors (omission and commission) cannot by quantified without further study, however given the significance of tree location, it is likely that remote sensing systems which can accurately locate tree stems rather than delineate canopy elements are likely to be prove more useful if the APA index is to be used.

## 5.5 Summary

Local neighbour tree height and location may be used to predict DBH in radiata pine at ages 15 and 20 although there are substantial reductions in the power of the prediction at age 20. The APA index was found to outperform other indexes, suggesting that tree location is an important factor in describing the growing space afforded an individual tree.

Sequential index analysis was used to explore the sidedness and symmetry relations in the neighbourhood data and identify optimum formulations. Reformulation of the APA index to adjust the influence of the location and relative height of proximate neighbours leads to substantial improvements in its power and thus its potential utility for inventory. The reformulations help to account for the inferred asymmetric and one-sided interactions between trees. The effects of measurement error in remote sensing data are likely to be quite complex given these findings and will require further study. The results show that the approach offers a means to summarise remotely sensed data products to a form more amenable to inventory use.

*Chapter 6*

# Tree stem profile model development

## 6.1 Introduction

The objective of the study presented in this chapter is to develop models which employ total height and local density measurements to predict stem profile in thinned and unthinned stands of radiata pine.

Stem profile models are typically constructed so that the predictor variables, total height and DBH, may be used as inputs. Profile height and diameter data are transformed to a relative scale using these predictor variables, both to limit residual error heterogeneity and to allow within-tree stem form to be expressed without being masked by between-tree differences in stem size (Bruce and Max 1990). Muhairwe (1999) successfully developed profile models for use in circumstances where total height measurements are unavailable, by modelling diameter within the stem profile as a function of DBH and height above ground level. This exercise was facilitated by the fact that total height explained substantially less profile variation than did DBH, so available DBH measurements were adequate for data transformation. In constructing profile models using remotely sensed data, the diameter measurements used in transforming profile diameter are lacking.

Hall et al. (2001) used air photo estimated DBH and existing stem profile models to generate near unbiased total volume estimates for individual trees. In the absence of existing profile models, this approach is complicated by two factors. First, breast height is the reference height for diameter measurement by convention only (Wiant et al. 1989; Wood et al. 1990) and there is no evidence to suggest it will be the optimal position on the stem at which to estimate diameter using remotely sensed data. If it is suboptimal, then additional DBH model error is unnecessarily propagated through to the profile model estimates. Second, the joint estimation of DBH and stem profile model parameters requires the use of complicated methods such as random coefficients analysis or simultaneous systems

of equations in order to accommodate the possible influence of cross-equation error correlation (Ferguson and Leech 1978; West et al. 1984; Biging 1985).

In this chapter, the approach taken instead is to model stem profile directly without recourse to these more complicated methods. In doing so the utility of two approaches to accommodating the residual model error structure is explored. The chapter begins with a description of the methods used to develop the profile models. This is followed by a description of the data. Models are then developed and model fit statistics, diagnostic plots, and parameter estimates are presented. Three types of model are developed, with each development presented in a separate section. Each section is also split by the age class of the dataset used.

## 6.2 Data

The first task undertaken was to visually inspect the data for outliers and to ascertain the general stem profile. Plots of relative diameter versus relative height are presented in Figures 6.1 and 6.2 for the age 15 and age 20 datasets respectively. The plots include some annotation which is explained below.

No outliers are immediately apparent in either dataset. The age 15 data show more spread throughout the profile, which may be due to the influence of butt swell upon the scaling diameter in the smaller individuals (Bruce and Max 1990) or may indicate the occurrence of more pronounced differences in stem profile.

The data from both ages display some typical stem profile characteristics. Viewing the plots and moving from ground level up toward the stem tip ($z = 0 \rightarrow 1$), one can see pronounced concavity due to butt swell, giving way to convex curvature after an obvious inflection point ($\alpha_2$) low in the stem that occurs at around 10% of total height. This appears to be lower than that found in other work in Tasmanian radiata pine (~15%)(Candy 1989a) and more similar to that found in other segmented modelling studies (Max and Burkhart 1976; Czaplewski et al. 1989; Sharma and Burkhart 2003). In the age 20 data, the convex curve in the upper stem obviously gives way to a more linear component toward the stem tip (Figure 6.2) at a second inflection point ($\alpha_1$) at around 60% of total height. Viewing the plot of age 15 data (Figure 6.1), there is little evidence of a clear demarcation between these paraboloid and conoid segments. Trees at this age have had less time to develop their crown free bole and so may be expected to exhibit less within-tree differences in upper stem shape (Larson 1963). Overall, the age 20 dataset exhibits greater convexity in the upper stem than does the age 15 dataset.

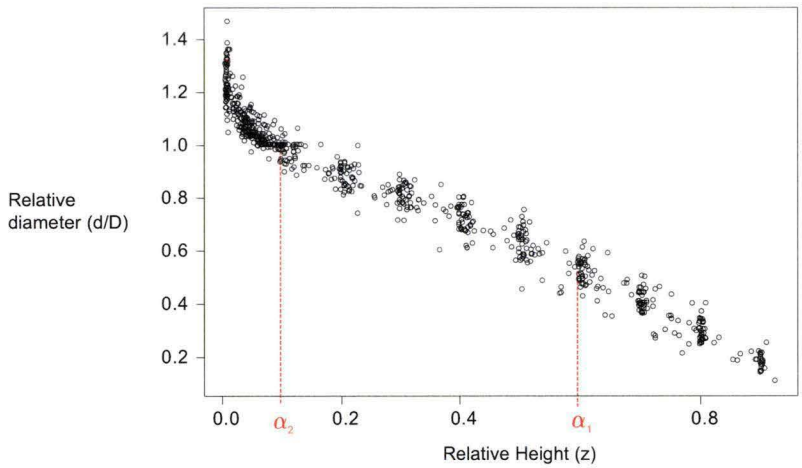


Figure 6.1 Age 15 tree stem profile - Relative diameter versus relative height

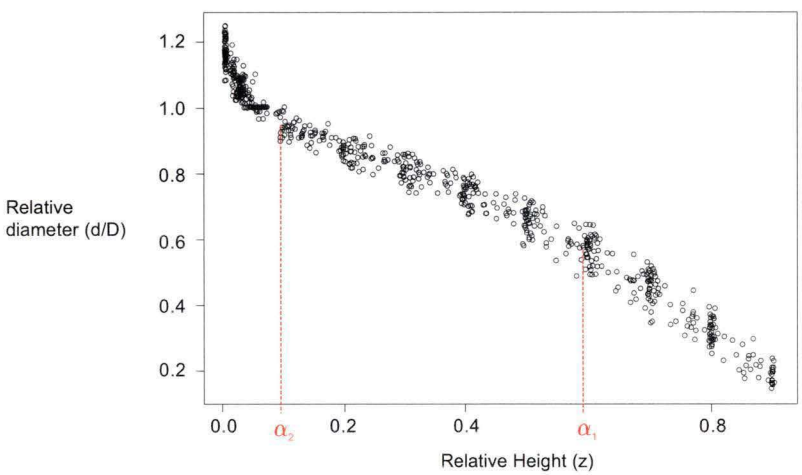


Figure 6.2 Age 20 tree stem profile - Relative diameter versus relative height

## 6.3 Methods

Model development in the first and last results sections (6.3.1 and 6.3.3) is undertaken using a two-stage, or parameter prediction, approach. In the first stage, a chosen model is fitted to the diameter data from each dataset using a nonlinear mixed effects (nlme) algorithm (Lindstrom and Bates 1990). This was implemented using the R (Core R Development Team 2004) and SPlus (MathSoft 1999) software packages. Various random effects specifications were assessed in order to determine which of the components of stem profile vary significantly between trees. The empirical best linear unbiased predictions (BLUPs) for each random effect from the first-stage models were then predicted using ordinary least squares (OLS), multiple linear regression. The candidate tree-level predictors were total height and

the optimum local density formulation[1] as determined from the analysis in Chapter 5. In each case, both tree-level predictors and their interaction were assessed. Candidate BLUP models were compared using model adjusted $R^2$ values and the t-values for the tree-level predictors. First-stage model and BLUP models were then combined with the chosen BLUP models substituting for the original fixed effects parameters. Model parameters were then again estimated using the nlme algorithm. Fitting second-stage models in this manner allows for parameter interactions and negates the requirement to use alternative two-stage fitting methods, such as seemingly unrelated regression (LeMay 1990; Davidian and Giltinan 2003). Where possible, parameter estimates were also obtained for all models using generalised nonlinear least squares (gnls) (Carroll and Ruppert 1988; Davidian and Giltinan 1995) which were fitted using appropriate parameterisations to accommodate the residual error structure. Population-average and subject-specific approaches are thus compared.

Model development in section 6.3.2 used a combination of the two-stage approach and a more simple additive approach, in which the efficacy of transformations of additional tree-level predictors are assessed by comparison to reduced models. Again, both nlme and gnls models were fitted where possible.

Where required, reformulations to improve model parsimony and predictive behaviour were considered. Akaike information criterion (AIC), Schwarz' Bayesian information criterion (BIC) and likelihood ratio tests (L.Ratio)[2] were used to formally assess the suitability of random effects (nlme) and residual error (gnls) specifications. Models with larger L.Ratio values, smaller L.Ratio p-values, and smaller AIC and BIC values are preferred (Pinheiro and Bates 2000). Normal probability plots were used to assess the distributional characteristics of the random effects. T-tests were used to assess fixed effects parameter significance. Scatter plots of standardised residual versus fitted values were used to assess residual error homogeneity.

Fitted models are consistently assigned a new number to reflect any change to their specification. Model numbering throughout the chapter reflects the consecutive order in which they were fitted.

---

[1] Since the optimum formulations at each age were near equivalent the single local density formulation was chosen. This was the APA index with formulation at k=20 and z=0.75.

[2] These criteria and tests are described in Appendix II.

## 6.4 Results

### 6.4.1 Segmented polynomial profile models

Max and Burkhart's (1976) segmented polynomial model (see Chapter 2, eqn 2.33) regularly appears in the profile model literature as a reference model against which newly developed models are compared (e.g. Kozak and Smith 1993). The model describes stem diameter using additive terms that are comprised of linear and quadratic transformations of relative height. These terms are applied to defined segments within the stem. Max and Burkhart's (1976) model is the first model fitted here for a number of reasons. First, the role of each term in determining model behaviour generally has simple interpretation, which facilitates two-stage modelling. To expand upon the comments regarding this model that appear in Chapter 2; the upper segment is described by one linear and one quadratic term; each further segment down the stem includes an additional quadratic term to describe the change in shape associated with the characteristic paraboloid and neiloid profiles in the middle and lower segments respectively; and the join points between each segment are described by join point parameters in terms of relative height. The shape parameters can also be interpreted with reference to traditional definitions of taper and form, with the linear term describing whole stem taper, and each of the quadratic terms describing stem form within each of the segments in which they appear. Each of the shape parameters also enters the model linearly. This last feature is important because the nlme algorithm is a likelihood based procedure and so the validity of hypothesis testing and inference are reliant upon the asymptotic properties of the estimated parameters.

Max and Burkhart (1976) fitted their model to both relative diameter, and relative squared diameter data. In contrast to the typical case in stem profile modelling, in this study there is no available stem diameter measurement (typically DBH) with which to scale the data. In the absence of a suitable scaling metric, the heterogeneity of the residual error may be expected to deleteriously impact upon the efficiency of the parameter estimates unless an appropriate method is used to accommodate it, be that the inclusion of additional variance functions and/or mixed effects parameters; each of which reduce model parsimony. In an effort to restrict the magnitude of the residual error variance and hence restrict model parameterisation, fits to squared diameter are not considered. In keeping with some other studies which have used Max and Burkhart's (1976) model (Williams and

Reich 1997; Sharma and Burkhart 2003), the join point parameters were initially set at fixed values after an inspection of the profile plots in Figure 6.1. These join points were set at $\alpha_1 = 0.1$ and $\alpha_2 = 0.6$ for both datasets. This reduces the number of first-stage model parameters to four.

#### *6.4.1.1 Age 15 dataset*

To begin, random effects were associated with each of shape parameters that describe profile throughout the stem. In statistical notation, Max and Burkhart's (1976) model for the $j^{th}$ $(j = 1,...,n)$ diameter observation on the $i^{th}$ $(1,...,60)$ tree is given by:

$$\begin{aligned} d_{ij} = &(\beta_0 + u_{i0})(z_{ij} - 1) + (\beta_1 + u_{i1})(z_{ij} - 1)^2 + \\ &(\beta_2 + u_{i2})(\alpha_1 - z_{ij})^2 I_{\alpha_1} + (\beta_3 + u_{i3})(\alpha_2 - z_{ij})^2 I_{\alpha_2} + \varepsilon_{ij} \end{aligned} \tag{6.1}$$

Where:

$$z_{ij} = \frac{h_{ij}}{H_i};$$

$\beta_{0 \text{ to } 3}$ are fixed effects parameters;

$u_{i0 \text{ to } i3}$ are random effects parameters;

$I_{\alpha_1} = 1$, when $z_{ij} \le \alpha_1$
$= 0$, when $z_{ij} > \alpha_1$;

$I_{\alpha_2} = 1$, when $z_{ij} \le \alpha_2$
$= 0$, when $z_{ij} > \alpha_2$.

The random effects parameters are assumed to be the $i^{th}$ independent realisation from a multivariate normal distribution with mean 0 and an unrestricted general positive-definite $4 \times 4$ variance-covariance matrix. The residual within-group errors are assumed to be independent for different $i$, independent of the random effects, and identically distributed random variables with a mean equal to zero and variance given by $\sigma^2$.

In statistical notation, these assumptions may be written:

$$\boldsymbol{u}_i \sim MVN(0,\Psi), \Psi = \begin{bmatrix} \sigma_0^2 & \sigma_{0,1} & \sigma_{0,2} & \sigma_{0,3} \\ \sigma_{0,1} & \sigma_1^2 & \sigma_{1,2} & \sigma_{1,3} \\ \sigma_{0,2} & \sigma_{1,2} & \sigma_2^2 & \sigma_{2,3} \\ \sigma_{0,3} & \sigma_{1,3} & \sigma_{2,3} & \sigma_3^2 \end{bmatrix} \text{ and } \varepsilon_{ij} \sim \mathrm{N}\left(0,\sigma^2\right)$$

Table 6.1 presents model 6.1 parameter estimates from fitting to the age 15 dataset. The format of this table requires explanation. The random effects are presented first. The random effects structure is listed. Below this, under the heading 'StdDev:', appears a column of estimated standard deviations for the random effects. Next to this is the associated approximate random effects correlation matrix under the heading "'Correlation:'. Rows correspond to the different random effects. Next to appear is the estimated residual within-group error variance. In the next section, the fixed effects are presented. The columns 'Value', 'Std.Error', 't-value', and 'p-value' respectively represent the fixed effects estimates, their approximate standard errors, the ratios between the estimates and their standard errors, and the associated p-value from a t distribution. Rows correspond to the different fixed effects. Below this is the associated approximate fixed effects correlation matrix under the heading 'Correlation:'.

T-test results show that the parameter associated with the fixed linear term is not significant.

Table 6.1 Model 6.1 parameter estimates - age 15 dataset.

```
Random effects:
Structure: General positive-definite

     StdDev:   Correlation:
u0      11.8700836          u0   u1   u2
u1      7.0084636       u1   -0.870
u2      8.5004253       u2    0.672 -0.641
u3      2.3442806       u3   -0.356 0.011 -0.002

Residual 0.4509058


Fixed effects:

    Value Std.Error  t-value p-value
b0 -2.30561 1.906975  -1.20904 0.2271
b1 -15.14444 1.162641 -13.02589 <.0001
b2 11.50975 1.652968  6.96308 <.0001
b3  4.83581 0.323426  14.95182 <.0001

Correlation:
    b0   b1   b2
b1 -0.917
b2 0.794 -0.786
b3 -0.346 0.084 -0.127
```

The influence of each random effect can be explored further by considering alternative random effects specifications. Table 6.2 presents the results of the analysis in which alternative random effects specifications were tested. Noteworthy test results appear in bold. This analysis tested the model with a full general positive-definite variance-covariance matrix specification (model 6.1) against models with variance-covariance matrices which included either less covariance terms, or less of both variance and covariance terms (all other models). The column headings require explanation. The first column lists the model number. This is a unique model identifier. The second column describes the model variance-covariance matrix. "Gen.pos.def." refers to a general positive-definite matrix in which all covariance terms are estimated. "Block Diag." refers to a block diagonal matrix in which some covariance terms are not estimated. Addition signs indicate the estimation of covariance terms for the terms either side of the sign, while commas indicate that the random effects either side of the comma are assumed independent; thus no covariance term is estimated. The numbering of the parameters is straightforward. The random effects $u_2$ are associated with the fixed effects shape parameter $\beta_2$. The third column indicates the total number of parameters estimated for the model. The next three columns provide the information criterion and log likelihood values for the model. The column titled

"Model test" indicates which models are compared using likelihood ratio tests. The final two columns provide results for these tests.

The information criterion test results presented in Table 6.2 differ slightly. The BIC test, which favours more parsimonious models than the AIC test, suggests preference for models with less complicated random effects structures. The removal of covariance terms (models 6.2 to 6.5) unequivocally results in poorer model fits for all but model 6.4, in which the covariance terms associated with the $u_2$ random effect are removed. The removal of further covariance terms (models 6.6 to 6.8) results in poorer model fit. These results suggest that each of the components of stem shape, as defined by the terms in the model, is significantly correlated, except for that describing the middle segment. The removal of random effects parameters (models 6.9 to 6.12) also results in poorer model fits, again, for all but model 6.11, in which the random effects parameter $u_2$ is removed. These results suggest there is little variation in stem shape between trees in the middle segment of the stem.

Nevertheless, the random effects BLUPs from model 6.1 were extracted and their relationships with tree-level variables analysed. This analysis was carried out using multiple linear regression. The test values derived from the multiple regressions are used only to indicate potential second stage model specifications since the influence of tree-level predictors upon random effects BLUPs is assessed in isolation from the model. Regression was chosen over scatter plot analysis because it allows a closer inspection of the interaction between tree-level predictors, and also allows a closer inspection of the leverage of each tree-level predictor. Leverage plots showed that local density requires square root transformation, as it did for $D_u$ prediction in Chapter 5.

Table 6.3 presents the results of the OLS regression analysis of the random effects BLUPs from model 6.1. Each column presents results for a different model fitted for each random effect. Shown is the ratio for each parameter between the estimate and the standard error with the associated p-value from a t distribution appearing in brackets. The table also shows the adjusted $R^2$ value for each model. Significant tree-level predictors appear in bold. Local density appears to be a highly significant predictor ($p<0.0001$) of the linear term that describes the whole stem and the quadratic term describing curvature in the butt. Trees at lower densities (thus, higher $C^{0.5}$ values) appear to show more stem taper and more butt swell. Local density is also a weaker predictor ($p<0.05$) of the quadratic term that describes the whole stem and appears to work in opposition to total height for this term, predicting trees at lower densities (higher $C^{0.5}$ values) to show less stem curvature. Total height also appears to be a weak predictor of the quadratic term that allows

for stem curvature below the upper segment. The interactions between the two tree-level predictors are not significant in any model.

Table 6.2 Tests for significance of adjusting model 6.1 with alternative random effects - age 15 dataset.

| Model | Variance-Covariance Matrix | No. of Parms. | AIC | BIC | logLike | Model test | L.Ratio | P.value |
|---|---|---|---|---|---|---|---|---|
| 6.1 | Gen.Pos.Def u0+u1+u2+u3 | 15 | 1670.50 | 1739.06 | -820.25 | | | |
| 6.2 | Block Diag. u1+u2+u3,u0 | 12 | 1700.06 | 1754.91 | -838.03 | 6.1 vs 6.2 | 35.559 | <.0001 |
| 6.3 | Block Diag. u0+u2+u3,u1 | 12 | 1704.23 | 1759.09 | -840.11 | 6.1 vs 6.3 | 39.737 | <.0001 |
| **6.4** | **Block Diag. u0+u1+u3,u2** | **12** | **1675.75** | **1730.60** | **-825.87** | | | |
| 6.5 | Block Diag. u0+u1+u2,u3 | 12 | 1701.72 | 1756.57 | -838.86 | 6.1 vs 6.5 | 37.218 | <.0001 |
| 6.6 | Block Diag. u1+u3,u0,u2 | 10 | 1709.22 | 1754.93 | -844.61 | 6.1 vs 6.6 | 48.725 | <.0001 |
| 6.7 | Block Diag. u0+u3,u1,u2 | 10 | 1700.55 | 1746.26 | -840.27 | 6.1 vs 6.7 | 40.054 | <.0001 |
| 6.8 | Block Diag. u0+u1,u2,u3 | 10 | 1704.93 | 1750.64 | -842.46 | 6.1 vs 6.8 | 44.435 | <.0001 |
| 6.9 | Gen.Pos.Def u1+u2+u3 | 11 | 1723.11 | 1773.39 | -850.55 | 6.1 vs 6.9 | 60.612 | <.0001 |
| 6.10 | Gen.Pos.Def u0+u2+u3 | 11 | 1709.75 | 1760.03 | -843.87 | 6.1 vs 6.10 | 47.252 | <.0001 |
| **6.11** | **Gen.Pos.Def u0+u1+u3** | **11** | **1677.22** | **1727.50** | **-827.61** | **6.1 vs 6.11** | **14.722** | **0.0053** |
| 6.12 | Gen.Pos.Def u0+u1+u2 | 11 | 1917.71 | 1967.99 | -947.85 | 6.1 vs 6.12 | 255.21 | <.0001 |

Table 6.3 OLS results predicting model 6.1 random effects BLUPs using tree-level variables - age 15 dataset. T-ratios for each parameter with associated p-value in brackets and adjusted $R^2$ values

| BLUPs | u0 | u1 | u2 | u3 |
|---|---|---|---|---|
| Intercept | 0.94<br>(0.3503) | 2.80<br>(0.0071) | 2.50<br>(0.0155) | -4.60<br>(<.0001) |
| H | 0.77<br>(0.4421) | **-3.51**<br>**(0.0009)** | **-2.23**<br>**(0.0298)** | **2.14**<br>**(0.0365)** |
| $C^{0.5}$ | **-5.05**<br>**(<.0001)** | **2.88**<br>**(0.0056)** | -0.14<br>(0.8880) | **6.68**<br>**(<0.0001)** |
| $H*C^{0.5}$ | 0.30<br>(0.7674) | -0.64<br>(0.5226) | -0.60<br>(0.5535) | -0.80<br>(0.4277) |
| Adj. $R^2$ | 0.327 | 0.174 | 0.058 | 0.594 |

The poor predictive behaviour of total height in describing the quadratic terms was unexpected and suggested that the random effects specification was diluting the role of total height throughout the stem. As already noted, BIC values indicate that the random effects associated with the middle segment parameter add little to the model. Plots of level one residuals versus relative height with and without these random effects (models 6.1 and 6.11 respectively) appear in Figure 6.3 and Figure 6.4 respectively. The inclusion of random effects for each of the shape parameters has removed much of the between-tree variance and facilitates a closer inspection of the biases associated with the mean model fit. Removal of the middle segment parameter random effects results in a slight increase in residual variance toward the stem tip but otherwise appears to have little effect. Given the very small diameters in this region of the stem it was decided to continue development instead with the reduced model (model 6.11).

The results of the regression analysis of the random effects BLUPs from model 6.11 are presented in Table 6.4 and show more promise for two-stage modelling. With the random effects associated with the middle segment quadratic term removed, total height becomes a highly significant predictor of the quadratic term that applies to the whole stem. Other regression models have not changed greatly.

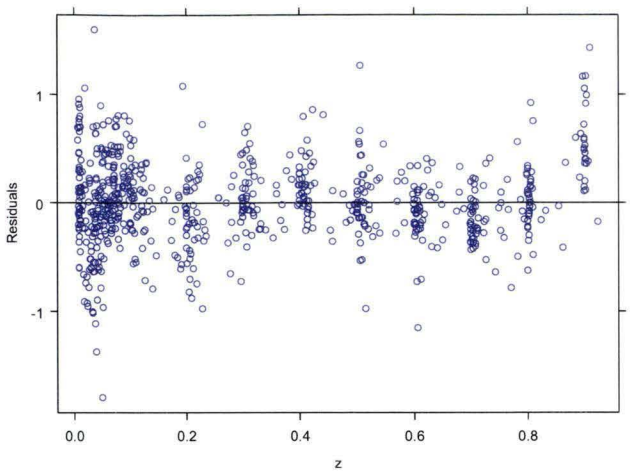


Figure 6.3 Scatter plot of model 6.1 Level 1 residuals versus relative height - age 15 dataset.

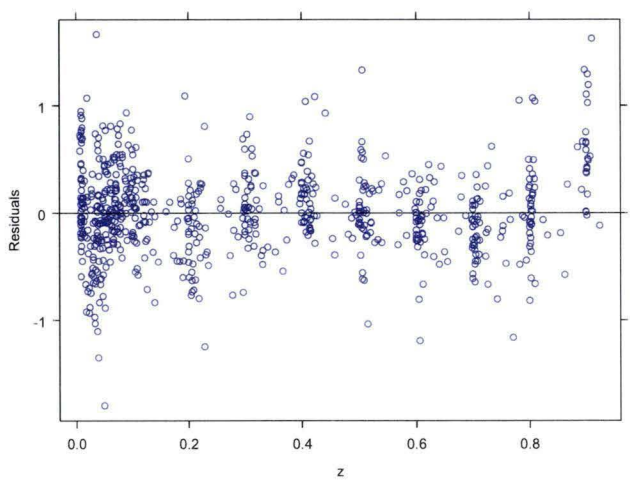


Figure 6.4 Scatter plot of model 6.11 Level 1 residuals versus relative height - age 15 dataset.

A combination of the first-stage model and linear regression models was then attempted. This entailed reformulating model 6.11 to include the additional tree-level predictors and then estimating the parameter values for this new model using the nlme algorithm. The starting value of the new parameters associated with the tree-level predictors were set to zero, while the starting values for the other parameters were set at first-stage model (6.11) estimates. The same random effects specification as that of model 6.11 was used.

This model may be written:

$$
\begin{aligned}
d_{ij} = {} & (\beta_0 + u_{i0})(z_{ij} - 1) + \beta_{01}\sqrt{C_i}\,(z_{ij} - 1) + \\
& (\beta_1 + u_{i1})(z_{ij}^{\,2} - 1) + \beta_{11} H_i\,(z_{ij}^{\,2} - 1) + \\
& \beta_2 (\alpha_1 - z_{ij})^2 I_{\alpha_1} + \\
& (\beta_3 + u_{i3})(\alpha_2 - z_{ij})^2 I_{\alpha_2} + \beta_{31}\sqrt{C_i}\,(\alpha_2 - z_{ij})^2 I_{\alpha_2}
\end{aligned}
\tag{6.13}
$$

Table 6.4 OLS results predicting model 6.11 random effects BLUPs using tree-level variables - age 15 dataset. T-ratios for each parameter with associated p-value in brackets and adjusted $R^2$ values.

| BLUPs | u0 | u1 | u2 | u3 |
|---|---|---|---|---|
| Intercept | -0.73<br>(0.4698) | 5.84<br>(<.0001) | NA | -3.91<br>(0.0003) |
| H | **2.76**<br>**(0.0077)** | **-6.58**<br>**(<.0001)** | NA | 1.65<br>(0.1048) |
| $C^{0.5}$ | **-6.50**<br>**(<.0001)** | **3.78**<br>**(0.0004)** | NA | **6.25**<br>**(<.0001)** |
| $H*C^{0.5}$ | 0.86<br>(0.3949) | -1.36<br>(0.1804) | NA | -0.85<br>(0.3998) |
| Adj. $R^2$ | 0.436 | 0.423 | NA | 0.548 |

An inspection of the statistics for the fitted second stage model showed that all of the parameters associated with the tree-level predictors were highly significant, while the first stage model parameter $\beta_0$ was not. No further additions of tree-level variables to any term was significant. In the next stage of model development the fixed join points were parameterised and the model refitted with starting values $\alpha_1 = 0.6$ and $\alpha_2 = 0.1$. This model converged to nonsensical values ($\alpha_1 > 1$) and this was attributed to the over parameterisation of the linear segment. The model converged successfully upon reformulation with the removal of $\beta_0$. An inspection of model statistics showed a further first stage model parameter ($\beta_1$) to be insignificant and again, parameter removal further improved the fit.

The resultant model is given by:

$$\begin{aligned} d_{ij} = &(\beta_0 + u_{i0})\sqrt{C_i}\left(z_{ij} - 1\right) + \\ &(\beta_1 + u_{i1})H_i\left(z_{ij}^{\,2} - 1\right) + \\ &\beta_2\left(\alpha_1 - z_{ij}\right)^2 I_{\alpha_1} + \\ &(\beta_3 + u_{i3})\left(\alpha_2 - z_{ij}\right)^2 I_{\alpha_2} + \beta_{31}\sqrt{C_i}\left(\alpha_2 - z_{ij}\right)^2 I_{\alpha_2} \end{aligned} \tag{6.14}$$

The suitability of the chosen random effects specification in accommodating the residual error structure was tested by comparison to models with the same fixed effects but different random effects specifications. Table 6.5 presents results for the test of significance for these models. The tests indicate support for model 6.15 with the blocked diagonal $3 \times 3$ variance-covariance matrix given by:

$$\boldsymbol{u}_i = \begin{bmatrix} u_{i0} \\ u_{i1} \\ u_{i3} \end{bmatrix},\ \boldsymbol{u}_i \sim \mathrm{MVN}(0, \Psi),\ \Psi = \begin{bmatrix} \sigma_0^2 & \sigma_{0,1} & 0 \\ \sigma_{0,1} & \sigma_1^2 & 0 \\ 0 & 0 & \sigma_3^2 \end{bmatrix},\ \text{and}\ \varepsilon_{ij} \sim \mathrm{N}\left(0, \sigma^2\right)$$

The removal of any other random effects or covariance terms leads to poorer model fit, as indicated by very large increases in information criterion values. This is particularly the case for the terms describing shape in all segments of the stem.

Figure 6.5 presents a standardised residual plot for model 6.15. The combination of random effects parameters and tree-level predictors appears to have adequately accommodated the residual error heterogeneity. Local biases in prediction of diameters less than approximately 8 centimetres are apparent and represent poor predictive behaviour in the stem tip. This lack of local fit represents a larger problem than does residual error heterogeneity as it indicates that bias will be present in the model parameters.

Figure 6.6 presents normal probability plots of the random effects BLUPs of model 6.15. The plots reveal that there are several outlier trees in the dataset, however the random effects otherwise acceptably follow a normal distribution.

Table 6.5 Tests for significance of adjusting model 6.14 with alternative random effects - age 15 dataset.

| Model | Variance-Covariance Matrix | No. of Parms. | AIC | BIC | logLike | Model test | L.Ratio | P.value |
|---|---|---|---|---|---|---|---|---|
| 6.14 | Gen.Pos.Def u0+u1+u3 | 14 | 1673.91 | 1737.90 | -822.95 | | | |
| **6.15** | **Block Diagonal u0+u1,u3** | **12** | **1677.36** | **1732.21** | **-826.68** | **6.14 vs 6.15** | **7.458** | **0.0240** |
| 6.16 | Block Diagonal u0+u3,u1 | 12 | 2505.45 | 2555.73 | -1241.72 | 6.14 vs 6.16 | 837.547 | <.0001 |
| 6.17 | Block Diagonal u1+u3,u0 | 12 | 2495.62 | 2550.47 | -1235.81 | 6.14 vs 6.17 | 825.721 | <.0001 |
| 6.18 | Gen.Pos.Def u0+u1 | 11 | 1817.93 | 1868.21 | -897.96 | 6.14 vs 6.18 | 150.032 | <.0001 |

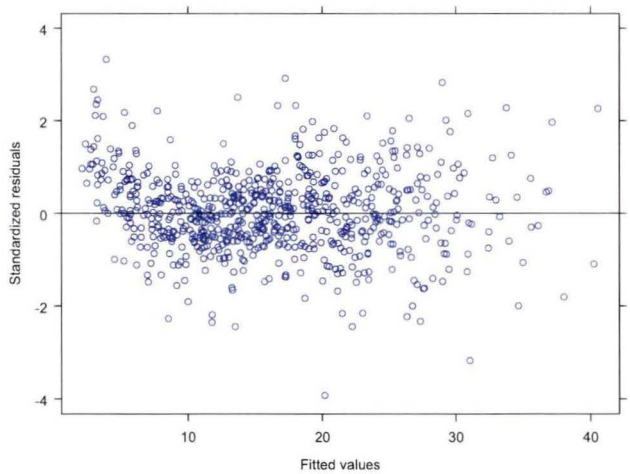


Figure 6.5 Scatter plot of model 6.15 standardised residuals versus fitted values - age 15 dataset.

Model fit statistics and parameter estimates for model 6.15 appear in Table 6.6. Information criterion values for model 6.15 are higher than for the first-stage model (6.11) but this also reflects the parameterisation of the join points. T-tests indicate that all parameters excepting $\beta_3$ are highly significant. There are several high parameter correlations that suggest the model may be over parameterised. In particular, these appear between the upper join point parameter ($\alpha_1$) and the parameter describing the middle segment ($\beta_2$), and between the two parameters describing stem shape throughout the stem. The standard error of the upper join

point parameter is an order of magnitude larger than that from the lower join point parameter, indicating the transition from upper to middle segments is estimated with considerably less reliability.

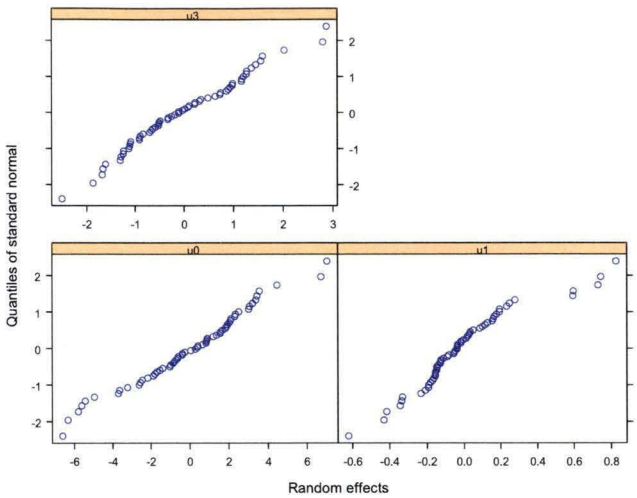


Figure 6.6 Normal probability plots of model 6.15 estimated random effects (age 15 dataset)

With respect to the second-stage parameterisation, the model seems reasonable. Generally speaking, the linear term describes the rate of change in diameter along the stem (or taper), while the quadratic terms describe stem curvature (or form). In contrast to what was expected, local density and total height entered the model through the linear and quadratic terms respectively, suggesting total height has a larger impact on stem form than does local density, and that local density is a better descriptor of stem taper than is tree height. More expected was the finding that local density also entered the model through the quadratic term that describes the neiloid in the base of the stem. The model predicts that more dominant trees will exhibit more taper and larger neiloids than less dominant ones, while taller trees exhibit more form than shorter ones.

The performance of model 6.15 fitted to the age 15 dataset is described further in Chapter 7.

Table 6.6 Model 6.15 parameter estimates and fit statistics - age 15 dataset.

```
     AIC      BIC  log likelihood

 1677.364   1732.215      -826.6821


Random effects:
Composite Structure: Blocked

      StdDev:  Correlation:

Block 1:
Structure: General positive-definite

u0    3.2304194     u0
u1    0.2873262  u1  -0.763

Block 2:
u3    1.244361

Residual 0.502791


Fixed effects:

    Value Std.Error t-value p-value
 b0 -2.686879 0.534784 -5.02424 <.0001
 b1 -0.854027 0.041941 -20.36261 <.0001
 b2 6.003763 1.048864  5.72406 <.0001
 b3 1.357779 0.355994  3.81405 0.0001
b31 1.199356 0.176960  6.77756 <.0001
 a1 0.629455 0.052132 12.07420 <.0001
 a2 0.120495 0.003587 33.58906 <.0001

 Correlation
    b0   b1   b2   b3   b31   a1
 b1 -0.782
 b2 0.065 -0.115
 b3 -0.065 0.079 -0.118
b31 0.030 -0.044 0.227 -0.734
 a1 0.183 -0.051 -0.858 0.027 -0.114
 a2 0.093 -0.076 -0.509 -0.124 -0.374 0.425
```

The population average approach is the alternative, and potentially more parsimonious, method of accommodating residual error structure. A generalised nonlinear model was fitted using the gnls algorithm with a power variance function and a first-order continuous autocorrelation function to jointly estimate residual error heterogeneity and autocorrelation. Relative height was the chosen covariate for both error functions.

In statistical notation, the expected value for a diameter observation given this model may be written:

$$E\left(d_{ij}\right) = \beta_0\sqrt{C_i}\left(z_{ij}-1\right) + \beta_1 H_i\left(z_{ij}^{\,2}-1\right) + \beta_2\left(\alpha_1 - z_{ij}\right)^2 I_{\alpha_1} + \beta_3\left(\alpha_2 - z_{ij}\right)^2 I_{\alpha_2} \tag{6.19}$$

This expected value has implied within-tree variance and correlation given by:

$$Var\left(d_j\right)_i = \sigma^2 z_{ij}{}^{\theta}, \quad Corr_i\left(d_{j1}, d_{j2}\right) = \Gamma_{i(j1,j2)}(\alpha)$$

Where:

$\theta$ is a power variance function parameter.

$\Gamma(\alpha)$ is a correlation matrix describing the correlation between adjacent observations that is comprised of first-order continuous autocorrelation functions with the autocorrelation parameter $\alpha$. This matrix is described further in Appendix X.

Achieving convergence for model 6.19 was difficult. It was only achieved by first fitting a model with a variance function only and then using the parameter estimates as starting values for the model in which the variance and autocorrelation parameters were estimated jointly. Model 6.19 converged to a nonsensical value for the upper join point parameter $\left(\alpha_1 > 1.5\right)$. The model also displayed slightly biased residual error, as shown in the standardised residual plot presented in Figure 6.7. Attempts at obtaining parameter estimates using an equally parsimonious exponent variance function failed to converge. That function was given by:

$$Var\left(d_j\right)_i = \sigma^2 \exp\left(\theta z_{ij}\right)$$

It was concluded that the approach was unsuited to the available data using this polynomial model.

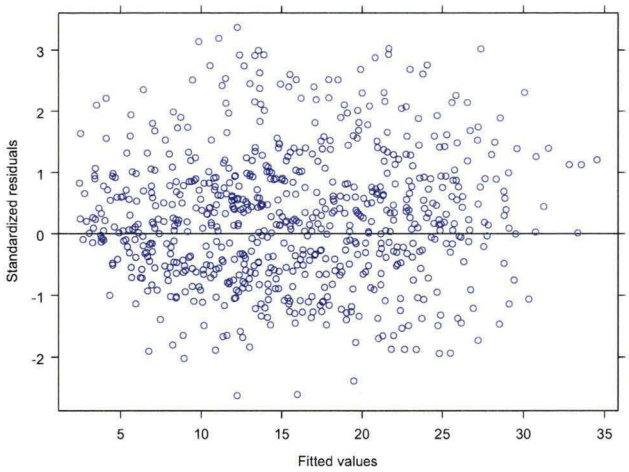


Figure 6.7 Scatter plot of model 6.19 standardised residuals versus fitted values - age 15 dataset.

### *6.4.1.2 Age 20 dataset*

Attention now turned to fitting model 6.1 to the age 20 dataset. Table 6.7 presents parameter estimates for the nlme fit of model 6.1. T-test results show that relative height may be used to predict stem profile with this model formulation.

Table 6.7 Model 6.1 parameter estimates - age 20 dataset.

```
Random effects:
Structure: General positive-definite

       StdDev:   Correlation:
u0     15.5977857          u0   u1   u2
u1     10.0943004      u1   -0.850
u2     13.4793458      u2    0.794 -0.848
u3      2.5229617      u3   -0.365 -0.123 -0.299

Residual       0.4226678


Fixed effects:

    Value Std.Error  t-value p-value
b0  6.4745 2.266457   2.85666 0.0044
b1 -26.9351 1.464930  -18.38661 <.0001
b2 14.2866 2.085746   6.84963 <.0001
b3  5.5336 0.344547  16.06052 <.0001

Correlation:
    b0   b1   b2
b1 -0.880
b2 0.957 -0.873
b3 -0.366 -0.049 -0.330
```

Table 6.8 presents the results of the analysis of alternative random effects specifications. In contrast to the case for the age 15 dataset, the significantly poorer fit of model 6.4 demonstrates that the middle segment does vary significantly between trees. However, shape in the middle of the stem appears to be independent of shape in other areas of the stem as the information criterion values of models 6.4 and 6.11 are near identical.

Table 6.8 Tests for significance of adjusting model 6.1 with alternative random effects - age 20 dataset.

| Model | Variance-Covariance Matrix | No. of Parms. | AIC | BIC | logLike | Model test | L.Ratio | P.value |
|---|---|---|---|---|---|---|---|---|
| **6.1** | **Gen.Pos.Def u0+u1+u2+u3** | **15** | **1591.44** | **1660.15** | **-780.72** | | | |
| 6.2 | Block Diag. u1+u2+u3,u0 | 12 | 1688.34 | 1743.34 | -832.18 | 6.1 vs 6.2 | 102.93 | <.0001 |
| 6.3 | Block Diag. u0+u2+u3,u1 | 12 | 1701.34 | 1756.31 | -838.67 | 6.1 vs 6.3 | 115.90 | <.0001 |
| **6.4** | **Block Diag. u0+u1+u3,u2** | **12** | **1660.93** | **1715.89** | **-818.46** | **6.3 vs 6.4** | **75.487** | **<.0001** |
| 6.5 | Block Diag. u0+u1+u2,u3 | 12 | 1164.68 | 1719.65 | -820.34 | 6.1 vs 6.5 | 79.243 | <.0001 |
| 6.6 | Block Diag. u1+u3,u0,u2 | 10 | 1691.87 | 1737.68 | -835.93 | 6.1 vs 6.6 | 110.43 | <.0001 |
| 6.7 | Block Diag. u0+u3,u1,u2 | 10 | 1729.12 | 1774.92 | -854.56 | 6.1 vs 6.7 | 147.68 | <.0001 |
| 6.8 | Block Diag. u0+u1,u2,u3 | 10 | 1730.60 | 1776.41 | -855.30 | 6.1 vs 6.8 | 149.16 | <.0001 |
| 6.9 | Gen.Pos.Def u1+u2+u3 | 11 | 1726.61 | 1776.99 | -852.30 | 6.1 vs 6.9 | 143.16 | <.0001 |
| 6.10 | Gen.Pos.Def u0+u2+u3 | 11 | 1724.29 | 1774.68 | -851.15 | 6.1 vs 6.10 | 140.85 | <.0001 |
| **6.11** | **Gen.Pos.Def u0+u1+u3** | **11** | **1658.92** | **1709.31** | **-818.46** | **6.1 vs 6.11** | **75.483** | **<.0001** |
| 6.12 | Gen.Pos.Def u0+u1+u2 | 11 | 1917.58 | 1967.97 | -947.79 | 6.1 vs 6.12 | 334.14 | <.0001 |

Table 6.9 presents the results of the OLS analysis of the random effects BLUPs from model 6.1. Each of the random effect BLUPs may be predicted using tree-level variables except those describing between-tree differences in the quadratic term for the whole stem, although the tree-level variables are weak predictors for all but the lower segment term. This term is apparently related to total height more than local density, which is in contrast to the results for the age 15 dataset.

Table 6.9 OLS results predicting model 6 1 random effects BLUPs using tree-level variables - age 20 dataset. T-ratios for each parameter with associated p-value in brackets and adjusted $R^2$ values.

| BLUPs | u0 | u1 | u2 | u3 |
|---|---|---|---|---|
| Intercept | 1.09<br>(0.2813) | 1.72<br>(0.0909) | 1.14<br>(0.0155) | -6.07<br>(<.0001) |
| H | -0.17<br>(0.8644) | -1.94<br>(0.0596) | -0.44<br>(0.6597) | **4.43**<br>**(<.0001)** |
| $C^{0.5}$ | **-2.81**<br>**(0.0067)** | 1.40<br>(0.1675) | **-2.06**<br>**(0.0444)** | **3.56**<br>**(0.0008)** |
| $H*C^{0.5}$ | -0.86<br>(0.3915) | 0.57<br>(0.5204) | -0.84<br>(0.6326) | 0.85<br>(0.3983) |
| Adj. $R^2$ | 0.150 | 0.020 | 0.092 | 0.579 |

The OLS results presented in Table 6.9 suggest two-stage modelling will be facilitated by restricting the random effects parameterisation, but a choice needs to be made about which terms should be allowed to vary and which should be fixed. While the regression results show that the quadratic term describing the whole stem cannot be predicted using tree-level variables, a comparison of information criterion values from the model in which this term is fixed while the middle segment term is allowed to vary (model 6.10) against the model in which the quadratic term describing the whole stem is allowed to vary while the middle segment term is fixed (model 6.11) shows that fixing the middle segment will allow the most flexibility.

Figures 6.8 and 6.9 present level 1 residual plots for model 6.1 and 6.11 respectively. Similar to the results of the fit to age 15 dataset, the inclusion of random effects for each of the shape parameters has removed much of the between-tree variance. Similarly to the fit to the age 15 dataset, the removal of the random effects associated with the middle segment term has increased the residual error

variance toward the stem tip but does not appear to have increased the bias. Model behaviour elsewhere in the stem appears unchanged. These plots suggest model 6.11 is acceptable for second-stage modelling.

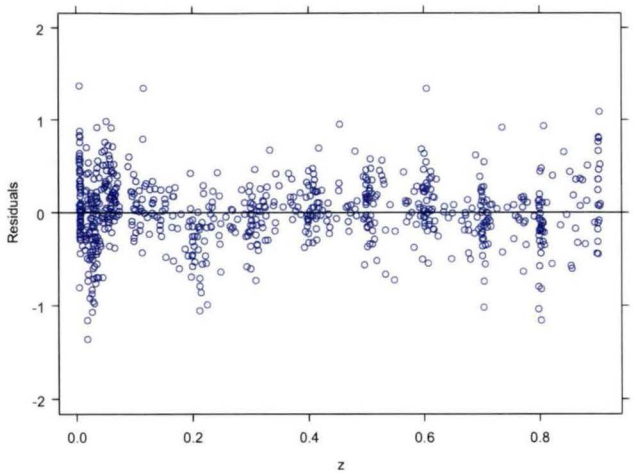


Figure 6.8 Scatter plot of model 6.1 Level 1 residuals versus relative height - age 20 dataset.

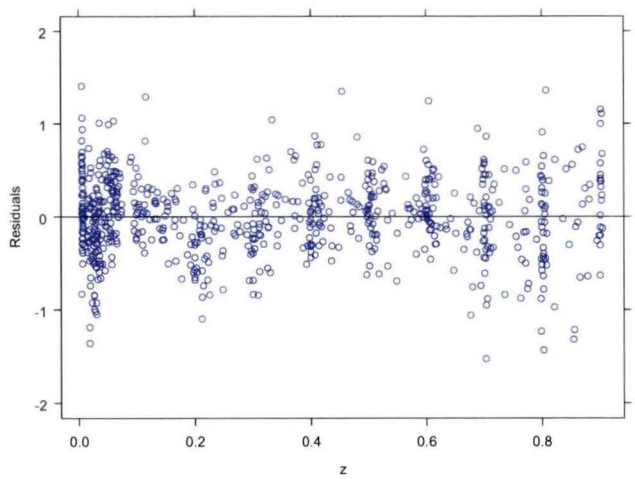


Figure 6.9 Scatter plot of model 6.11 Level 1 residuals versus relative height - age 20 dataset.

Table 6.10 presents the results of the OLS analysis of the random effects BLUPs from model 6.11. Similar to the age 15 dataset, fixing the middle segment term forces the model to account for between-tree differences in the restricted number of random effects and this results in higher adjusted $R^2$ values and more significant relationships with tree-level variables in the upper segment of the stem. Local density remains a weaker predictor than it is in the age 15 dataset while the strength of total height as a predictor is similar throughout the stem. Total height

remains the most significant predictor of the neiloid in the butt in contrast to the case for the age 15 dataset.

Table 6.10 OLS regression results predicting model 6.11 random effects BLUPs using tree-level variables - age 20 dataset. T-ratios for each parameter with associated p-value in brackets and adjusted $R^2$ values.

| BLUPs | u0 | u1 | u2 | u3 |
|---|---|---|---|---|
| Intercept | 0.61<br>(0.5440) | 5.67<br>(<.0001) | NA | -5.75<br>(<.0001) |
| H | 0.51<br>(0.6119) | **-5.12**<br>**(<.0001)** | NA | **4.37**<br>**(<.0001)** |
| $C^{0.5}$ | **-3.61**<br>**(0.0007)** | 0.04<br>(0.9710) | NA | **2.77**<br>**(0.0075)** |
| $H*C^{0.5}$ | -1.52<br>(0.1347) | 0.66<br>(0.5136) | NA | 0.56<br>(0.5776) |
| Adj. $R^2$ | 0.191 | 0.422 | NA | 0.526 |

Second stage modelling proceeded in the same manner as for the age 15 dataset. As was the case with the age 15 dataset, only one tree-level predictor proved to be a significant addition to each term in the second stage model. Parameterisation of the join points caused two terms to become insignificant and these were removed. Both total height and local density proved to be significant additions to the term describing butt swell, however models which included total height displayed poor random effects distributional characteristics. The fixed effect specification of the chosen second stage model is very similar to that of the age 15 dataset. Once again, total tree height has the largest influence upon the quadratic term, describing stem form, while local density has the largest effect upon the linear term, describing stem taper. The model includes one additional parameter to describe the component of taper throughout the stem not accounted for with local density.

It is given by:

$$d_{ij} = (\beta_0 + u_{i0})(z_{ij} - 1) + \beta_{01}\sqrt{C_i}(z_{ij} - 1) + (\beta_1 + u_{i1})H_i(z_{ij} - 1)^2 + \beta_2(\alpha_1 - z_{ij})^2 I_{\alpha_1} + (\beta_3 + u_{i3})(\alpha_2 - z_{ij})^2 I_{\alpha_2} + \beta_{31}\sqrt{C_i}(\alpha_2 - z_{ij})^2 I_{\alpha_2} + \varepsilon_{ij} \quad (6.20)$$

Tests for significance of alternative random effects specifications for the second stage model appear in Table 6.11. The results indicate support for the model with a general positive-definite variance-covariance matrix given by:

$$\boldsymbol{u}_i = \begin{bmatrix} u_{i0} \\ u_{i1} \\ u_{i3} \end{bmatrix}, \ \boldsymbol{u}_i \sim \text{MVN}(0, \Psi), \ \Psi = \begin{bmatrix} \sigma_0^2 & \sigma_{0,1} & \sigma_{0,3} \\ \sigma_{0,1} & \sigma_1^2 & \sigma_{1,3} \\ \sigma_{0,3} & \sigma_{1,3} & \sigma_3^2 \end{bmatrix}, \text{ and } \varepsilon_{ij} \sim \text{N}\left(0, \sigma^2\right)$$

In contrast to the age 15 dataset results, this result indicates that stem form in the butt region is significantly correlated with both form and taper throughout the rest of the stem.

Table 6.11 Tests for significance of adjusting model 6.20 with alternative random effects - age 20 dataset.

| Model | Variance-Covariance Matrix | No. of Parms. | AIC | BIC | logLike | Model test | L.Ratio | P.value |
|---|---|---|---|---|---|---|---|---|
| 6.20 | **Gen.Pos.Def u0+u1+u3** | **14** | **1597.82** | **1661.95** | **-784.91** | | | |
| **6.21** | Block Diagonal u0+u1,u3 | **12** | 1601.69 | 1670.40 | -785.84 | 6.20 vs 6.21 | 1.869 | 0.1715 |
| 6.22 | Block Diagonal u0+u3,u1 | 12 | 1631.42 | 1686.39 | -803.71 | 6.20 vs 6.22 | 37.601 | <.0001 |
| 6.23 | Block Diagonal u1+u3,u0 | 12 | 1657.66 | 1712.63 | -816.83 | 6.20 vs 6.23 | 63.838 | <.0001 |
| 6.24 | Gen.Pos.Def u0+u1 | 11 | 1646.58 | 1701.55 | -811.29 | 6.20 vs 6.24 | 52.757 | <.0001 |

A scatter plot of standardised residuals for model 6.20 appears in Figure 6.10. The scatter plot shows no evidence of residual model error heterogeneity. Normal probability plots of the estimated random effects from model 6.14 appear in Figure 6.11. They show that the random effects acceptably follow a normal distribution.

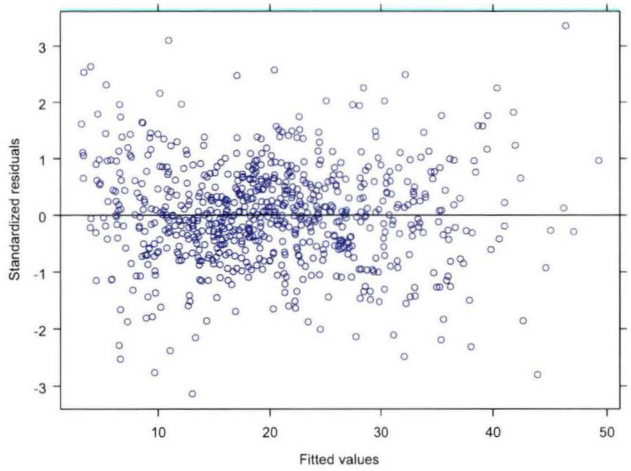


Figure 6.10 Scatter plot of model 6.20 standardised residuals versus fitted values - age 20 dataset.

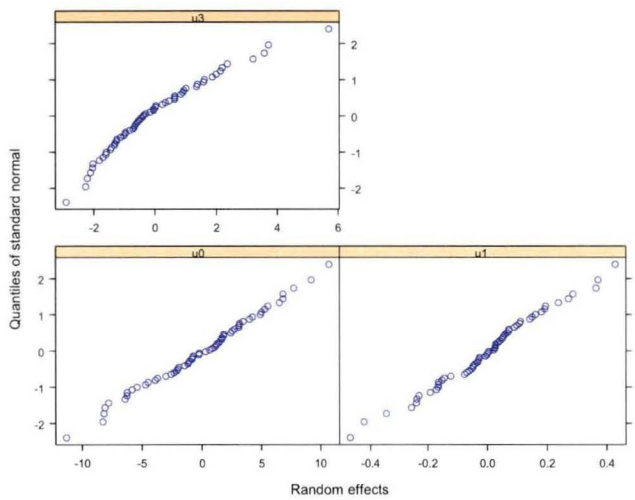


Figure 6.11 Normal probability plots of model 6.20 estimated random effects - age 20 dataset.

Model fit statistics and parameter estimates for model 6.20 appear in Table 6.12. All parameters except those describing the taper term ( $\beta_0$ and $\beta_{01}$ ) are highly significant (p value<0.001). The information criterion and log likelihood values indicate that the fit is poorer than that shown in the first-stage model (6.11) but this is a reflection of the reduced number of random effects and has no bearing on the predictive utility of the model. In many respects the model is similar to that for the age 15 dataset. The lower join point occurs at 11.7% of total height, which is slightly higher but, given the magnitude of the standard error, not significantly so. The upper join point is similarly more variable and occurs at a point lower on the stem. The parameter value found here is more similar to that reported by Candy

(1989a) for the three segment polynomial model he fitted to Tasmanian radiata pine data [$\alpha_1 = 0.3489$ (s.e. = 0.0408)]. The signs of the additional tree-level parameters suggest that trees less influenced by their neighbours are more tapered and that taller trees display more curvature throughout the stem. The performance of model 6.20 fitted to the age 20 dataset is described further in Chapter 7.

Table 6.12 Model 6.20 parameter estimates and fit statistics - age 20 dataset.

```
    AIC      BIC  log likelihood
 1603.687   1672.396     -786.8433

Random effects:
Structure: General positive-definite

       StdDev:    Correlation:

u0     4.9489490            u0   u1
u1     0.1883887  u1 -0.661
u3     1.7949882    u3 -0.039 -0.538

Residual 0.4733216

Fixed effects:

    Value Std.Error  t-value p-value
 b0  4.53478 1.342162  3.37871 0.0008
b01 -2.08158 0.377321  -5.51673 <.0001
 b1 -1.04061 0.035822 -29.04964 <.0001
 b2 16.31283 2.919598  5.58735 <.0001
 b3  2.77387 0.483255  5.73998 <.0001
b31  0.89484 0.174287  5.13432 <.0001
 a1  0.40551 0.037387  10.84620 <.0001
 a2  0.10332 0.003049  33.88430 <.0001

 Correlation:
    b0  b01   b1   b2   b3   b31  a1
b01 -0.608
 b1 -0.635 -0.066
 b2 -0.119 -0.047 0.147
 b3 -0.212 0.345 -0.187 -0.153
b31 0.279 -0.413 -0.006 0.185 -0.721
 a1 0.416 0.080 -0.513 -0.801 0.111 -0.092
 a2 0.045 0.048 -0.078 -0.574 -0.096 -0.344 0.365
```

Attempts at deriving a generalised nonlinear segmented polynomial model were not successful. The model (termed model 6.25) fitted with a power variance function only displayed biased and heterogeneous residual error, as shown in the standardised residual plot presented in Figure 6.12. Alternative variance models were tested in an effort to accommodate the residual variance. Models fitted with exponent variance functions given by $Var(d_j)_i = \sigma^2 \exp(\theta z_{ij})$ failed to converge. Models fitted with a variance function incorporating total height led to minor improvements, however subsequent attempts at jointly fitting this variance

function and a first-order continuous correlation function failed to converge. This variance function is given by:

$$Var\left(d_j\right)_i = \sigma^2 z_{ij}^{\theta_1} H_i^{\theta_2}.$$

It was concluded that the approach was unsuited to the data using this polynomial model.

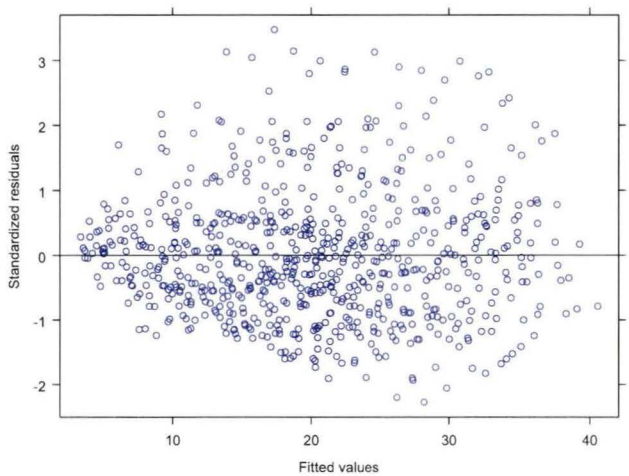


Figure 6.12 Scatter plot of model 6.25 standardised residuals versus fitted values - age 20 dataset.

### 6.4.2 Variable-exponent profile models

The segmented profile model analysis presented above is a useful method to illuminate the manner in which stem shape varies both within and between trees because the parameters of the model are readily interpretable. With respect to their predictive utility however, there are some problems. Large correlations between the parameters describing shape throughout the stem indicated that the resultant models are somewhat ill conditioned. The fit for the age 15 dataset in particular was also quite biased. Two alternative nonlinear forms were also considered for the specification of upper stem segment profile during initial exploration of the data (results not shown).

These were a simple power function given by:

$$d_{ij} = \beta_0 z_{ij}^{\beta_1} \tag{6.26}$$

And a hyperbolic function given by:

$$d_{ij} = \frac{z_{ij}}{\beta_0 + \beta_1 z_{ij}} . \tag{6.27}$$

While each showed some promise, displaying lower parameter correlations and, in the case of the hyperbola, smaller bias in the residuals, the random effects BLUPs for fits of both functions displayed severe nonlinearities, which suggested they were unsuited to second-stage modelling. As a result, both were abandoned in favour of the polynomial model.

A further problem relates to the manner in which tree-level predictors enter the model. Not only are the resultant second stage models for both datasets somewhat restrictive in their predictions, since the tree-level variables individually only entered the models through one or two parameters, the models are also not particularly realistic or interpretative in any biological sense. The models predict that trees of different height at the same density display exactly the same upper stem taper but different form, while the opposite is true for trees of different density and the same height.

In an effort to circumvent these problems, the variable-exponent approach was also considered. The variable-exponent approach is a popular alternative in profile modelling (e.g. Perez et al. 1990; Newnham 1992; Kozak and Smith 1993; Muhairwe et al. 1994; Fang and Bailey 1999; Eerikäinen 2001). Variable-exponent models typically comprise three components. The first component is the scaling function. The scaling function is typically a power function of over- or underbark DBH or a power function of a combination of total height and over- or underbark DBH. It is used to model gross between-tree differences in stem size. The scaling function is multiplied by a base term. This term is typically a transformation of relative height that evaluates to one at a specified height, such as breast or inflection height. The base term is raised to an exponent term, comprised of a suite of relative height transformation terms. The within-tree changes in form, from the stem butt to tip, are accommodated by this suite of terms. Further between-tree differences in form may also be accommodated by including tree-level predictors within the exponent term.

Published variable-exponent models include a wide variety of transformations of relative height to describe the exponent term. In this section, modified versions of the models of Kozak (1997) and Bi (2000) are each fitted to the data. Both models were chosen for their demonstrated efficacy across a range of species of regions (Kozak 1997; Bi 2000; Bi and Long 2001).

The first four terms that appear in the exponent of Kozak's (1997) model describe changes in stem form along the stem, while the last uses the ratio of the tree-level predictors, total height and overbark DBH, to describe differences in form between trees. Similarly, the first four terms in the exponent of Bi's (2000) trigonometric model describe changes in stem form along the stem, while the last three use various transformations of the tree-level predictors, total height and overbark DBH, to describe form differences between trees. In the initial analysis, the last term in the exponent of Kozak's (1997) model and the last three terms in the exponent of Bi's (2000) trigonometric model were removed. Without these terms, each is a more parsimonious, average-form model.

The simple linear additive model that was found to be adequate for predicting underbark DBH using total height and local density in Chapter 5 suggested itself as the obvious specification for the prediction of underbark DBH in these models. Kozak's (1997) model uses overbark DBH within the scaling function applied to the base term. This is adjusted to scale the base term to underbark DBH using two power functions. The datasets used here contain only underbark diameter data. If underbark DBH may be predicted using total height and local density then Kozak's (1997) model may be reformulated to:

$$d = D_u X^w \tag{6.28}$$

Where:

$$D_u = f\left(H, \sqrt{C}\right),$$

$$X = \frac{1-\sqrt{z}}{1-\sqrt{\frac{1.3}{H}}},$$

$$w = \beta_1 z^2 + \beta_2 \log(z + 0.001) + \beta_3 \sqrt{z} + \beta_4 \exp(z).$$

And:

$\beta_{1 \text{ to } 4}$ are model parameters.

In the underbark DBH prediction model used in Chapter 5, the intercept was not significantly different from zero in either age class. Initial fits of model 6.28 using the nlme specifications described below showed this to be also the case in modelling stem profile.

When model 6.28 is reformulated to exclude the intercept term, it is given by:

$$d = \alpha_0 H X^w + \alpha_1 \sqrt{C} X^w \tag{6.29}$$

Where:

$\alpha_{0 \text{ and } 1}$ are model parameters.

The trigonometric model (Bi 2000) uses underbark DBH to scale the base term. Simply by replacement this model may be reformulated to:

$$d = f\left(H, \sqrt{C}\right) B^k \tag{6.30}$$

Where:

$$B = \frac{\log\left(\sin\left(\frac{\pi}{2} z\right)\right)}{\log\left(\sin\left(\frac{\pi}{2} \frac{1.3}{H}\right)\right)};$$

$$k = \beta_1 + \beta_2 \sin\left(\frac{\pi}{2} z\right) + \beta_3 \cos\left(\frac{\pi}{2} z\right) + \beta_4 \sin\left(\frac{\pi}{2} z\right) \frac{1}{z}.$$

And:

$\beta_{1 \text{ to } 4}$ are model parameters.

Again, under the nlme specification investigated below, the intercept in the DBHUB prediction term proved to be not significant so the model may be reformulated to:

$$d = \alpha_0 H B^k + \alpha_1 \sqrt{C} B^k \tag{6.31}$$

Where:

$\alpha_{0 \text{ and } 1}$ are model parameters.

Further analysis investigated model exponent reformulations, firstly to ensure adequate exponent behaviour, and secondly to incorporate total height and local density with a view to constructing variable-form models. Methods to accommodate residual error structure were also investigated.

### *6.4.2.1 Kozak models*

#### *6.4.2.1.1 Age 15 dataset*

Model 6.29 was initially fitted using nonlinear least squares regression. That fit was found to include no exponent term parameters estimates that were significantly different from zero, indicating over parameterisation. Nevertheless, parameter estimates were used as starting values for the nlme algorithm and the model refitted with a random effect associated with the base of the total height term. Such a fit allows the model to account for gross changes in stem size that are not accounted for using the available tree-level predictors. This is given by:

$$d_{ij} = (\alpha_0 + u_{i0}) H_i X_{ij}^{w_{ij}} + \alpha_1 \sqrt{C_i} X_{ij}^{w_{ij}} + \varepsilon_{ij} \tag{6.32}$$

Where:

$u_{i0}$ is a random effects parameter.

And the residual error structure is given by:

$$u_{i0} \sim N(0, \sigma_0^2) \text{ and } \varepsilon_{ij} \sim N(0, \sigma^2)$$

As was the case with the nonlinear least squares fit, the exponent terms were again found to be not significant. A series of reduced nlme models were then tested, each with a single exponent term removed from the formulation. A combination of fixed effects parameter t-tests, L.Ratio tests, information criterion values, and plots of level 1 model residuals versus relative height were used to isolate the optimum reduced model. That analysis showed the exponent term of the optimum reduced model to be given by:

$$w = \beta_1 z^2 + \beta_2 \log(z + 0.001) + \beta_3 \sqrt{z} \tag{6.33}$$

i.e. $\beta_4 \exp(z)$ has been dropped.

Plots of level one residuals from models 6.32 and 6.33 versus relative height appear in Figure 6.13 and Figure 6.14 respectively. The two models appear virtually identical, confirming the inadequacy of the exponent term in describing additional stem form. The inclusion of the single random effects parameter in the base term associated with total height removes much of the between-tree variance and the residuals appear much as they might had overbark DBH been available to scale the

base term. The majority of residuals lie within a band approximately two centimetres wide that shows some slight cyclical bias trend with relative height. That trend appears to be more complicated than that which might be described by a simple transformation of relative height, so additional exponent terms were not used in the model.

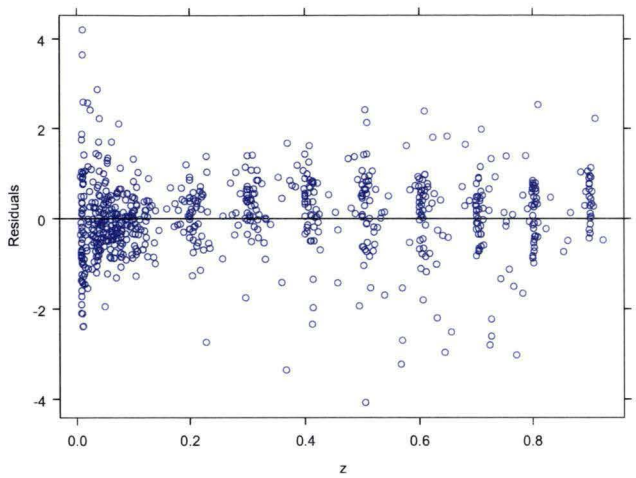


Figure 6.13 Scatter plot of model 6.32 Level 1 residuals versus relative height - age 15 dataset.

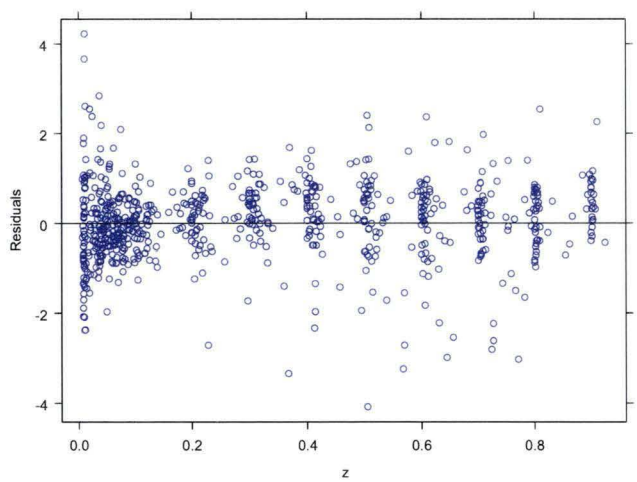


Figure 6.14 Scatter plot of model 6.33 Level 1 residuals versus relative height - age 15 dataset.

The random effects specification of model 6.33 individualises the fit through the base term. Further random effects were applied to the exponent terms to ascertain whether the between-tree variability in stem form impacted deleteriously upon the model fit. A model was fitted with random effects associated with each of the

exponent terms in an unrestricted general positive-definite $4 \times 4$ variance-covariance matrix. This exponent term is given by:

$$w_{ij} = (\beta_1 + u_{i1}) z_{ij}^{\ 2} + (\beta_2 + u_{i2}) \log(z_{ij} + 0.001) + (\beta_3 + u_{i3}) \sqrt{z_{ij}} \tag{6.34}$$

And the random effects specification for the entire model given by:

$$\boldsymbol{u}_i = \begin{bmatrix} u_{i0} \\ u_{i1} \\ u_{i2} \\ u_{i3} \end{bmatrix}, \quad \boldsymbol{u}_i \sim MVN(0, \Psi), \quad \Psi = \begin{bmatrix} \sigma_0^2 & \sigma_{0,1} & \sigma_{0,2} & \sigma_{0,3} \\ \sigma_{0,1} & \sigma_1^2 & \sigma_{1,2} & \sigma_{1,3} \\ \sigma_{0,2} & \sigma_{1,2} & \sigma_2^2 & \sigma_{2,3} \\ \sigma_{0,3} & \sigma_{1,3} & \sigma_{2,3} & \sigma_3^2 \end{bmatrix}, \text{ and } \varepsilon_{ij} \sim N(0, \sigma^2)$$

An inspection of random effects parameter correlations from model 6.34 suggested the logarithmic term that appears in the exponent was independent of other terms in the model. Tests of random effects parameter significance appear in Table 6.13. Those test results indicate that all the random effects are highly significant; however the covariance terms associated with the logarithmic term are not; thus the optimum model is 6.37. This model has random effects specified by:

$$\boldsymbol{u}_i = \begin{bmatrix} u_{i0} \\ u_{i1} \\ u_{i2} \\ u_{i3} \end{bmatrix}, \quad \boldsymbol{u}_i \sim MVN(0, \Psi), \quad \Psi = \begin{bmatrix} \sigma_0^2 & \sigma_{0,1} & \sigma_{0,3} & 0 \\ \sigma_{0,1} & \sigma_1^2 & \sigma_{1,3} & 0 \\ \sigma_{0,3} & \sigma_{1,3} & \sigma_3^2 & 0 \\ 0 & 0 & 0 & \sigma_2^2 \end{bmatrix}, \text{ and } \varepsilon_{ij} \sim N(0, \sigma^2)$$

Figure 6.15 presents a scatter plot of standardised residuals versus fitted values from model 6.37 fitted to the age 15 dataset. The heterogeneity present in the residuals is similar to that found in the fit of the segmented polynomial model (model 6.15), with larger residuals appearing to occur for the largest predictions. Again, scatter plots of standardised residuals versus relative height and versus the tree-level predictors showed no discernable trend. There appears to be an appreciable bias in the smaller predictions, as was the case with the fit of the segmented polynomial model (model 6.15). A cyclical trend is also apparent.

The normal probability plots of the estimated random effects from model 6.37 fitted to the age 15 dataset appear in Figure 6.16. The random effects are all acceptably normal, despite the fact that the parameters from the exponent term are not linear in the model. There is some slight asymmetry in the distributions of

the random effects associated with the squared and square root relative height terms ( $u_{i0}$ and $u_{i2}$ ).

Table 6.13 Tests for significance of adjusting model 6.34 with alternative random effects - age 15 dataset.

| Model | Variance-Covariance Matrix | No. of Parms. | AIC | BIC | logLike | Model test | L.Ratio | P.value |
|---|---|---|---|---|---|---|---|---|
| 6.34 | Gen.Pos.Def u0+u1+u2+u3 | 16 | 1524.92 | 1598.05 | -746.46 | | | |
| 6.35 | Block Diag. u1+u2+u3,u0 | 13 | 1564.65 | 1624.07 | -769.32 | 6.34 vs 6.35 | 45.731 | <.0001 |
| 6.36 | Block Diag. u0+u2+u3,u1 | 13 | 1565.07 | 1624.49 | -769.54 | 6.34 vs 6.36 | 46.154 | <.0001 |
| 6.37 | Block Diag. u0+u1+u3,u2 | 13 | 1522.27 | 1581.69 | -748.14 | 6.34 vs 6.37 | 3.3521 | 0.3404 |
| 6.38 | Block Diag. u0+u1+u2,u3 | 13 | 1604.27 | 1663.69 | -789.14 | 6.34 vs 6.38 | 85.353 | <.0001 |
| 6.39 | Block Diag. u1+u3,u0,u2 | 11 | 1563.68 | 1613.96 | -770.84 | 6.34 vs 6.39 | 48.766 | <.0001 |
| 6.40 | Block Diag. u0+u3,u1,u2 | 11 | 1568.00 | 1618.28 | -773.00 | 6.34 vs 6.40 | 53.084 | <.0001 |
| 6.41 | Block Diag. u0+u1,u2,u3 | 11 | 1601.85 | 1652.13 | -789.93 | 6.34 vs 6.41 | 86.935 | <.0001 |
| 6.42 | Gen.Pos.Def u0+u1+u3 | 12 | 1712.78 | 1767.63 | -844.39 | 6.34 vs 6.42 | 195.86 | <.0001 |

Parameter estimates for model 6.37 appear in Table 6.14. All parameters are highly significant but numerous fixed and random effects correlations are also very large. This colinearity is a common feature of the variable-form models (Kozak 1997). The performance of model 6.37 fitted to the age 15 dataset is described further in Chapter 7.

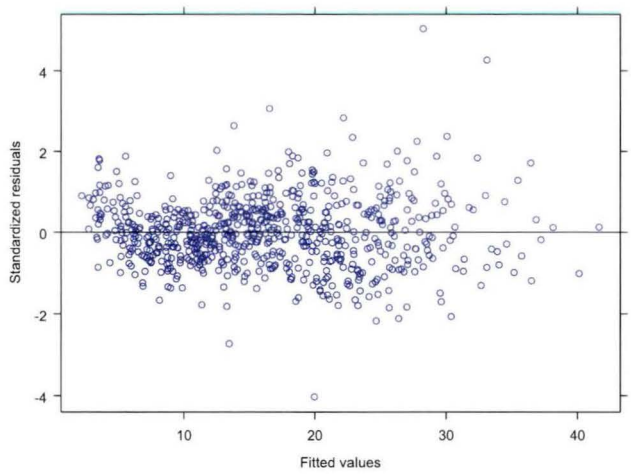


Figure 6.15 Scatter plot of model 6.37 standardised residuals versus fitted values - age 15 dataset.

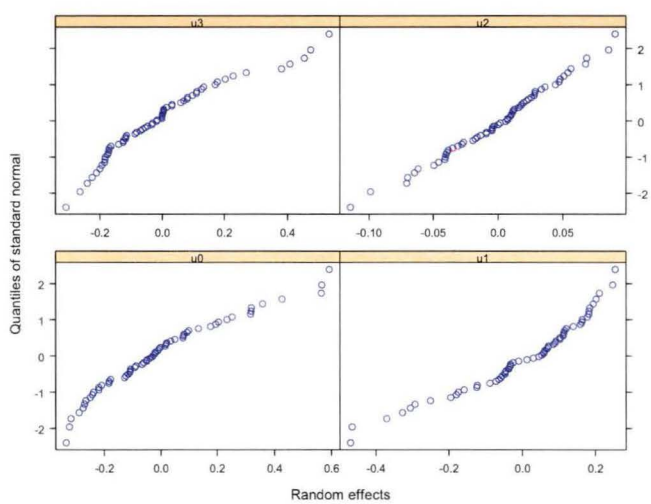


Figure 6.16 Normal probability plots of the model 6.37 estimated random effects - age 15 dataset.

Attempts at obtaining parameter estimates using gnls were more successful than they were for the segmented polynomial model. Once again, the gnls model was fitted using a power variance function and a first-order continuous autocorrelation function to jointly estimate residual error heterogeneity and autocorrelation. And again, relative height was the chosen covariate for both error functions. A comparison of information criterion, and log likelihood values between a model fitted with and without the autocorrelation term appear in Table 6.15. This comparison provides strong evidence that such a term is required for valid inference.

Table 6.14 Model 6.37 parameter estimates - age 15 dataset.

```
Random effects:
Composite Structure: Blocked

      StdDev:      Correlation:

Block 1: (General positive-definite Structure)
u0    0.2257028        u0    u1
u1    0.1941873    u1 -0.780
u3    0.1994751    u3  0.834 -0.941

Block 2:

u2    0.0454082

Residual 0.4337602

Fixed effects:

    Value Std.Error  t-value p-value
a0 1.121518 0.0428418 26.17811 <.0001
a1 2.022027 0.2669562  7.57438 <.0001
b1 0.261158 0.0322155  8.10660 <.0001
b2 -0.177944 0.0064538 -27.57175 <.0001
b3 0.495937 0.0290188 17.09021 <.0001

Correlation:
    a0    a1    b1    b2
a1 -0.729
b1 -0.387 -0.058
b2 0.481 0.037 -0.148
b3 -0.016 0.053 -0.924 0.129
```

Table 6.15 Tests for significance of adjusting model 6.43 by including an autocorrelation parameter - age 15 dataset.

| Model | Variance-Covariance Matrix | No. of Parms. | AIC | BIC | logLike | Model test | L.Ratio | P.value |
|---|---|---|---|---|---|---|---|---|
| 6.43 | VarPow | 7 | 3030.22 | 3062.22 | -1508.1 | | | |
| 6.44 | VarPow, corCAR1 | 8 | 1627.54 | 1664.11 | -805.77 | 6.45 vs 6.44 | 1404.68 | <.0001 |

A scatter plot of standardised residuals versus fitted values for model 6.44 appears in Figure 6.16. The effect of the power variance function has been quite dramatic as the residuals appear quite homogeneous, although local biases in the prediction of diameters less than approximately of eight centimetres are also apparent. These biases represent a greater problem than the minor residual heterogeneity. Model 6.44 parameter estimates and fit statistics appear in Table 6.16. The functional

parameter estimates are generally similar to those for the nlme fit except for the $\alpha_1$ parameter. The better parsimony of the gnls model is offset by slightly poorer information criterion values in comparison to those of the nlme model. The performance of model 6.44 fitted to the age 15 dataset is described further in Chapter 7.

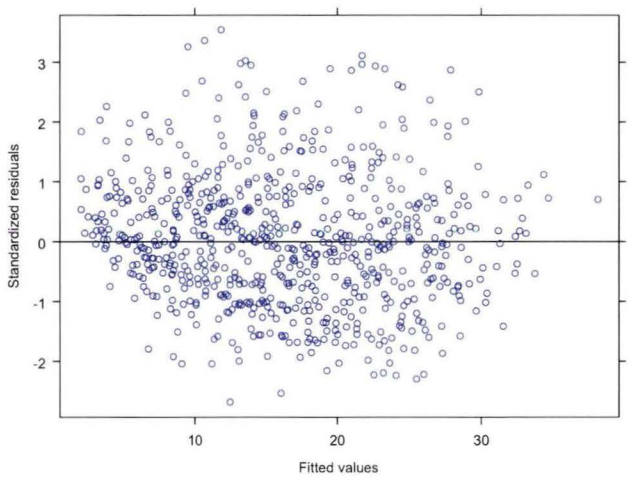


Figure 6.17 Scatter plot of model 6.44 standardised residuals versus fitted values - age 15 dataset.

Table 6.16 Model 6.44 parameter estimates and fit statistics - age 15 dataset.

```
     AIC      BIC  log Likelihood
 1627.544  1664.111     -805.7719

      lower 95%   estimate   upper 95%

Correlation Structure: Continuous AR(1)
Phi     0.1807828  0.258301   0.354668

Variance Structure: Power of variance covariate
Power  -0.3693667  -0.329912  -0.2904583

Residual Standard Error:
Error   0.8891931  1.017855   1.165134

Coefficients:
    Value Std.Error  t-value p-value
a0 1.049822 0.0295494 35.52771 <.0001
a1 2.550511 0.2046516 12.46270 <.0001
b1 0.209719 0.0378756  5.53705 <.0001
b2 -0.182692 0.0106209 -17.20114 <.0001
b3 0.546903 0.0278801 19.61625 <.0001

Correlation:
    a0    a1    b1    b2
a1 -0.786
b1 -0.090 -0.033
b2 -0.297 -0.110 -0.223
b3 0.104 0.040 -0.892 0.229
```

In models 6.37 and 6.44, differences in diameter predictions between trees are accommodated only through the base terms while the exponent is described by transformations of relative height only. In the terminology of the profile modelling literature, the terms that appear in the exponent therefore describe only average form. Kozak (1988, 1997) included the ratio of total height to overbark DBH as a further exponent term to accommodate between-tree differences in stem form. In an effort to construct a variable-form version of the model in the absence of overbark DBH, permutations of transformations of total height and local density were incorporated into the first stage model. The transformations considered were squares and square roots of the tree-level variables. Also considered were these variables multiplied by relative height. Initial parameter values for additional variables were set at zero. Parameter t-tests were used to isolate significant additional variables. Other initial parameter values were set at those of model 6.37. Information criterion values and L.Ratio tests, together with within-stem prediction bias estimates, were used to isolate the optimum model specification.

In no permutation of transformation cases did a variable multiplied by relative height prove to be a more significant variable than its non-multiplied analogue. This indicates that tree-level predictors have a stronger influence upon stem form throughout the stem than they do toward either the tip or butt. While total height was a significant variable in the exponent term, its influence was very minor and so the term was not included in the final model. Disregarding the gross changes in stem size that are predicted with the base term of the model, the parameter value for the additional local density variable that enters the model through the exponent indicates that trees growing at lower densities (i.e., higher APA values) show greater differences in form along the stem than trees grown at higher densities. The final model is given by:

$$d_{ij} = \left(\alpha_0 + u_{i0}\right) H_i X_{ij}^{\,w_{ij}} + \alpha_1 \sqrt{C_i} X_{ij}^{\,w_{ij}} + \varepsilon_{ij} \tag{6.46}$$

Where:

$$w_{ij} = \left(\beta_1 + u_{i1}\right) z_{ij}^{\,2} + \left(\beta_2 + u_{i2}\right) \log\left(z_{ij} + 0.001\right) + \left(\beta_3 + u_{i3}\right) \sqrt{z_{ij}} + \beta_4 \sqrt{C_i}$$

And the residual error structure is given by:

$$\boldsymbol{u}_i = \begin{bmatrix} u_{i0} \\ u_{i1} \\ u_{i2} \\ u_{i3} \end{bmatrix}, \quad \boldsymbol{u}_i \sim MVN(0, \Psi), \quad \Psi = \begin{bmatrix} \sigma_0^2 & \sigma_{0,1} & \sigma_{0,3} & 0 \\ \sigma_{0,1} & \sigma_1^2 & \sigma_{1,3} & 0 \\ \sigma_{0,3} & \sigma_{1,3} & \sigma_3^2 & 0 \\ 0 & 0 & 0 & \sigma_2^2 \end{bmatrix}, \quad \text{and} \quad \varepsilon_{ij} \sim N\left(0, \sigma^2\right)$$

Diagnostic plots for model 6.46 were near identical to those shown for the average-form version (model 6.37) and so are not shown. Model fit statistics and parameter estimates for model 6.46 appear in Table 6.17. Large decreases in information criterion and log likelihood values demonstrate the significance of including the local density predictor in the exponent term. The magnitude of each of the random effects has declined slightly as some between-tree variance is absorbed by the additional tree-level predictor appearing in the exponent term. The performance of model 6.46 fitted to the age 15 dataset is described further in Chapter 7.

Table 6.17 Model 6.46 fit statistics and parameter estimates - age 15 dataset.

```
    AIC     BIC  log Likelihood
 1499.249  1563.241    -735.6243

Random effects:
Composite Structure: Blocked

      StdDev:    Correlation:

Block 1: (General positive-definite Structure)
u0    0.2085599     u0    u1
u1    0.1896181  u1 -0.726
u3    0.1889499  u3 0.780 -0.951

Block 2:
b2    0.04115582

Residual 0.4330692


Fixed effects:

    Value Std.Error  t-value p-value
a0 0.997394 0.0471987 21.13180 <.0001
a1 3.080654 0.3298112  9.34066 <.0001
b1 0.287821 0.0322337  8.92918 <.0001
b2 -0.161784 0.0066997 -24.14797 <.0001
b3 0.386975 0.0348087 11.11720 <.0001
b4 0.044164 0.0083576  5.28431 <.0001

Correlation:
    a0    a1    b1    b2    b3
a1 -0.819
b1 -0.381 0.063
b2 -0.230 0.293 -0.062
b3 0.586 -0.320 -0.840 -0.172
b4 -0.479 0.584 0.176 0.458 -0.601
```

A generalised nonlinear least squares version of model 6.46 also converged successfully. A scatter plot of standardised residuals versus fitted values for this model (6.47) appears in Figure 6.18. Again, the effect of the power variance function has been quite dramatic. Fit statistics and parameter estimates for model 6.47 appear in Table 6.18. Again, the parameter estimates, excepting that for $\alpha_0$, are all similar to the fixed effects parameters derived using nlme (model 6.46). Once again, the greater model parsimony of the gnls model is offset by slightly poorer information criterion values compared to those of the nlme model. The performance of model 6.47 fitted to the age 15 dataset is described further in Chapter 7.

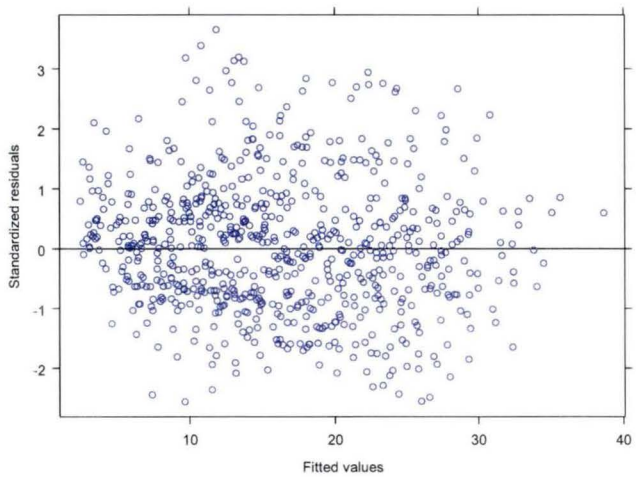


Figure 6.18 Scatter plot of model 6.47 standardised residuals versus fitted values - age 15 dataset.

#### *6.4.2.1.2 Age 20 dataset*

Analysis of the age 20 dataset proceeded in the same manner as for the age 15 dataset. The nonlinear least squares fit of model 6.29 and the nlme fit of model 6.32 both exhibited entirely non significant exponent terms just as they did when fitted to the age 15 dataset. Tests of reduced models again showed the exponent formulation of model 6.33 to be most suitable. This model was initially fitted with the random effects specification given by 6.34. An inspection of the resulting random effects parameter correlations from model 6.34 suggested the random effects associated with the base term and the logarithmic term that appears in the exponent were independent of other terms in the model. Tests of random effects parameter significance appear in Table 6.19. Those test results indicate that all the random effects are highly significant and, once again, some covariance terms are

not. In this case, the optimum model is 6.39, suggesting the independence of stem size and form, as described by $\beta_0$ and $\beta_{1\text{ to }3}$, respectively. This model has a random effects specification given by:

$$\boldsymbol{u}_i = \begin{bmatrix} u_{i0} \\ u_{i1} \\ u_{i2} \\ u_{i3} \end{bmatrix}, \quad \boldsymbol{u}_i \sim MVN(0, \Psi), \quad \Psi = \begin{bmatrix} \sigma_0^2 & 0 & 0 & 0 \\ 0 & \sigma_2^2 & 0 & 0 \\ 0 & 0 & \sigma_1^2 & \sigma_{1,3} \\ 0 & 0 & \sigma_{1,3} & \sigma_3^2 \end{bmatrix}, \text{ and } \varepsilon_{ij} \sim N\left(0, \sigma^2\right)$$

Table 6.18 Model 6.47 fit statistics and parameter estimates - age 15 dataset.

```
    AIC      BIC  log Likelihood
1610.313  1651.451     -796.1567


     lower 95%   estimate   upper 95%

Correlation Structure: Continuous AR(1)
Phi    0.1714074  0.2466974  0.3414312

Variance Structure: Power of variance covariate
power  -0.3701713  -0.3298992  -0.289627

Residual Standard Error:
Error   0.8655219  0.9905173  1.133564

Coefficients:

    Value Std.Error  t-value p-value
a0 0.998872 0.0307386 32.49570 <.0001
a1 2.949631 0.2177182 13.54793 <.0001
b1 0.259402 0.0394788  6.57066 <.0001
b2 -0.163147 0.0115132 -14.17038 <.0001
b3 0.403061 0.0426850  9.44270 <.0001
b4 0.046790 0.0106224  4.40489 <.0001

Correlation:

    a0   a1   b1   b2   b3
a1 -0.815
b1 0.106 -0.211
b2 0.060 -0.397 -0.068
b3 -0.298 0.379 -0.783 -0.187
b4 0.404 -0.396 0.304 0.425 -0.762
```

Table 6.19 Tests for significance of adjusting model 6.34 with alternative random effects - age 20 dataset.

| Model | Variance-Covariance Matrix | No. of Parms. | AIC | BIC | logLike | Model test | L.Ratio | P.value |
|---|---|---|---|---|---|---|---|---|
| 6.34 | Gen.Pos.Def u0+u1+u2+u3 | 16 | 1508.40 | 1581.69 | -738.20 | | | |
| 6.35 | Block Diag. u1+u2+u3,u0 | 13 | 1515.62 | 1575.17 | -744.81 | 6.34 vs 6.35 | 13.2181 | 0.0042 |
| 6.36 | Block Diag. u0+u2+u3,u1 | 13 | 1528.34 | 1587.89 | -751.17 | 6.34 vs 6.36 | 25.9384 | <.0001 |
| 6.37 | Block Diag. u0+u1+u3,u2 | 13 | 1518.79 | 1578.34 | -746.39 | 6.34 vs 6.37 | 16.3917 | 0.0009 |
| 6.38 | Block Diag. u0+u1+u2,u3 | 13 | 1528.93 | 1588.47 | -751.46 | 6.34 vs 6.38 | 26.5263 | <.0001 |
| 6.39 | Block Diag. u1+u3,u0,u2 | 11 | 1519.25 | 1569.64 | -748.63 | 6.34 vs 6.39 | 20.8475 | 0.0009 |
| 6.48 | Block Diag. u1+u3,u0 | 10 | 1582.87 | 1689.26 | -811.43 | 6.34 vs 6.48 | 147.045 | <.0001 |
| 6.49 | Block Diag. u1+u3,u2 | 10 | 3608.49 | 3654.30 | -1794.2 | 6.34 vs 6.49 | 2112.09 | <.0001 |

Figure 6.19 presents a scatter plot of standardised residuals versus fitted values from model 6.39. The plot provides no evidence of any residual error heterogeneity. The normal probability plots of the estimated random effects from model 6.39 appear in Figure 6.20. The asymmetry in the distribution of each of the random effects is similar to that found in the fit to the age 15 dataset.

Model 6.39 parameter estimates appear in Table 6.21. All parameters are highly significant and, as was the case with the age 15 dataset, the fixed and random effects correlations are also very large. The performance of model 6.39 fitted to the age 20 dataset is described further in Chapter 7.

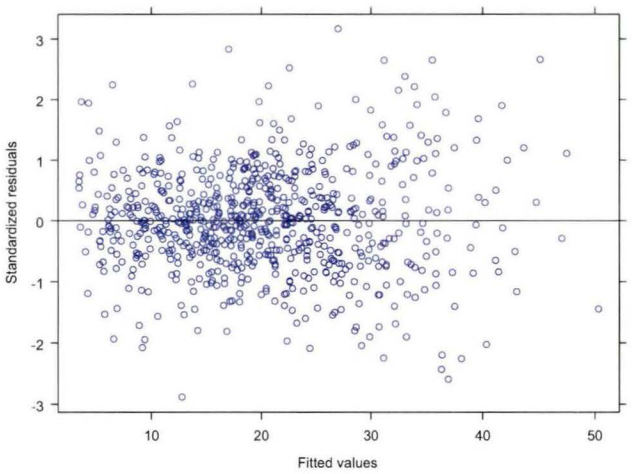


Figure 6.19 Scatter plot of model 6.39 standardised residuals versus fitted values (age 20 dataset

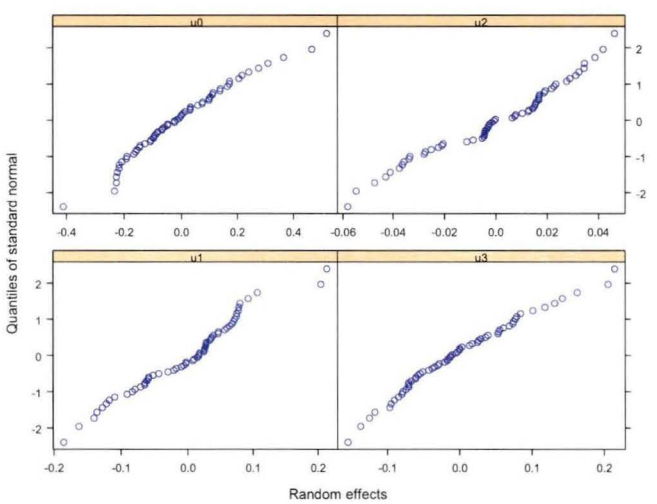


Figure 6.20 Normal probability plots of the model 6.39 estimated random effects (age 20 dataset

Attempts at obtaining parameter estimates using gnls were less successful. A model fitted jointly with a power variance function and a first-order continuous autocorrelation function failed to accommodate the residual error heterogeneity. A plot of standardised residuals versus fitted values for this model, termed model 6.50 , appears in Figure 6.21. Scatter plots of standardised residuals versus tree-level predictors showed no discernable trends. It was concluded that gnls modelling was inappropriate for profile prediction given the available data and this type of profile model.

Table 6.20 Model 6.39 parameter estimates - age 20 dataset.

```
Random effects:
Composite Structure: Blocked

      StdDev:   Correlation:

Block 1: (General positive-definite Structure)
u1    0.10969826        u1
u3    0.09606441    u3 -0.793

Block 2:
u2    0.02882667

Block 3:
u0    0.1799493

Residual 0.41619860


Fixed effects:

    Value Std.Error  t-value p-value
a0 0.944342 0.0496881 19.00539 <.0001
a1 2.286040 0.4160392  5.49477 <.0001
b1 0.413620 0.0199590 20.72348 <.0001
b2 -0.161903 0.0043573 -37.15681 <.0001
b3 0.309378 0.0155924 19.84156 <.0001

 Correlation:

    a0   a1   b1   b2
a1 -0.883
b1 0.000 -0.010
b2 0.000 0.007 -0.225
b3 -0.001 0.011 -0.854 0.225
```

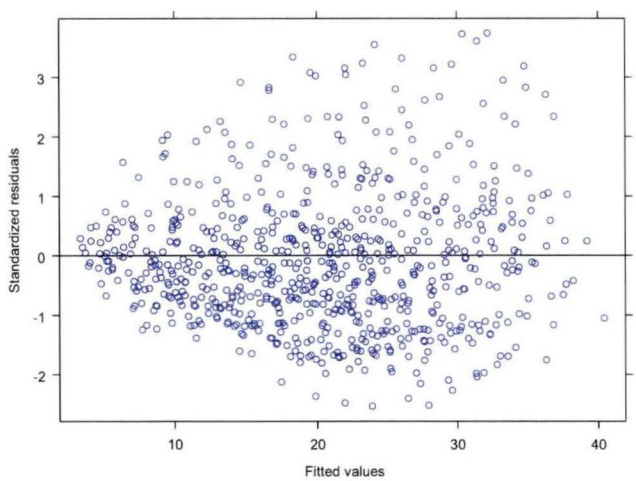


Figure 6.21 Scatter plot of model 6.50 standardised residuals versus fitted values - age 20 dataset.

The incorporation into model 6.39 of the same permutations of transformations of total height and local density that were tested for the age 15 dataset was then attempted in an effort to construct a variable-form version of the model. The

results of this process were very similar to those for the age 15 dataset. Only local density proved to be a significant addition in the final model. This model (6.51) is identical to model 6.46 in every respect except for the random effects structure, which was unchanged from that of the average-form version of the model fitted to the age 20 dataset (model 6.39).

Fit statistics and parameter estimates for model 6.51 appear in Table 6.21. All parameters are highly significant but, once again, fixed and random effects correlations are also very large. The performance of model 6.51 fitted to the age 20 dataset is described further in Chapter 7.

Table 6.21 Model 6.51 fit statistics and parameter estimates - age 20 dataset.

```
   AIC    BIC  log Likelihood
1502.202  1557.17     -739.101

Random effects:
Composite Structure: Blocked

      StdDev:  Correlation:

Block 1: (General positive-definite Structure)
u1    0.1181621       u1
u3    0.1036647   u3 -0.858

Block 2:
u2   0.02697783

Block 3:
u0    0.1802636

Residual 0.4125328


Fixed effects:

    Value Std.Error  t-value p-value
a0 0.943119 0.0498049 18.93627 <.0001
a1 2.302677 0.4170276  5.52164 <.0001
b1 0.434052 0.0211752 20.49806 <.0001
b2 -0.151213 0.0047750 -31.66787 <.0001
b3 0.237496 0.0227354 10.44609 <.0001
b4 0.022089 0.0048573  4.54762 <.0001

Correlation:

    a0   a1   b1   b2   b3
a1 -0.883
b1 -0.011 0.002
b2 0.004 0.004 -0.087
b3 0.011 -0.006 -0.771 -0.206
b4 -0.005 0.008 0.210 0.497 -0.694
```

Again, attempts at obtaining parameter estimates using gnls were less successful. A model fitted with a power variance function failed to accommodate the residual error heterogeneity and no trends were apparent with any available predictor (plots

not shown). A model which included a further autocorrelation term failed to converge, so the approach was abandoned.

### *6.4.2.2 Trigonometric models*

#### *6.4.2.2.1 Age 15 dataset*

Nonlinear least squares regression was used to generate initial fixed effects parameter values for the nlme algorithm. The initial attempt at fitting model 6.31 using a full general positive-definite random effects specification failed to converge. While acknowledging that the least squares estimators of NLS parameters are only asymptotically normal (Jennrich 1969), an inspection of the parameter correlations from the NLS fit revealed extreme colinearity in the parameters describing the exponent terms, and convergence failure was attributed to this model characteristic. A series of models with reduced random effects specifications was then assessed. Initially, random effects were included for the exponent intercept term ($\beta_0$) to explain differences in stem form that are not accounted for using the relative height terms. Random effects were also initially included for the base term parameter ($\alpha_1$) to accommodate gross changes in stem size not accounted for using total height and local density. The test results that appear in Table 6.22 show preference for models with additional random effects associated with the exponent terms. Test values also indicate support for models with a fully symmetric matrix structure, indicating significant correlations occur between stem size (accommodated through $u_{i0}$) and the various stem form components (accommodated through $u_{i1}$). While the lowest information criterion values were found with a model with three exponent random effects, the distributional characteristics of these random effects were poor. The best compromise between information criterion values and random effects normality suggested model 6.52 to be optimum. This is given by:

$$d_{ij} = (\alpha_0 + u_{i0}) H_i B_{ij}^{k_{ij}} + \alpha_1 \sqrt{C_i} B_{ij}^{k_{ij}} + \varepsilon_{ij} \tag{6.52}$$

Where:

$$k_{ij} = (\beta_1 + u_{i1}) + (\beta_2 + u_{i2}) \sin\left(\frac{\pi}{2} z_{ij}\right) + \beta_3 \cos\left(\frac{3\pi}{2} z_{ij}\right) + \beta_4 \sin\left(\frac{\pi}{2} z_{ij}\right) \frac{1}{z_{ij}}.$$

And:

$$\boldsymbol{u}_i = \begin{bmatrix} u_{i0} \\ u_{i1} \\ u_{i2} \end{bmatrix}, \ \boldsymbol{u}_i \sim MVN(0, \Psi), \ \Psi = \begin{bmatrix} \sigma_0^2 & \sigma_{0,1} & \sigma_{0,2} \\ \sigma_{0,1} & \sigma_1^2 & \sigma_{1,2} \\ \sigma_{0,2} & \sigma_{1,2} & \sigma_2^2 \end{bmatrix}, \text{ and } \varepsilon_{ij} \sim N\left(0, \sigma^2\right).$$

Table 6.22 Tests for significance of adjusting model 6.31 with alternative random effects - age 15 dataset.

| Model | Variance-Covariance Matrix | No. of Parms | AIC | BIC | logLike | Model test | L.Ratio | P.value |
|---|---|---|---|---|---|---|---|---|
| 6.31 | Gen.Pos.Def. u0+u1 | 10 | 1641.67 | 1687.38 | -810.83 | | | |
| 6.52 | Gen.Pos.Def. u0+u1+u2 | 13 | 1536.38 | 1595.80 | -755.19 | 6.31 vs 6.52 | 111.28 | <.0001 |
| 6.53 | Gen.Pos.Def. u0+u1+u3 | 13 | 1567.32 | 1626.74 | -770.66 | 6.31 vs 6.53 | 80.349 | <.0001 |
| 6.54 | Gen.Pos.Def. u0+u1+u4 | 13 | 1573.85 | 1633.27 | -773.92 | 6.31 vs 6.54 | 73.816 | <.0001 |
| 6.55 | Gen.Pos.Def. u0+u1+u2+u3 | 17 | 1536.11 | 1613.82 | -751.05 | 6.31 vs 6.55 | 119.55 | <.0001 |
| 6.56 | Gen.Pos.Def. u0+u1+u2+u4 | 17 | 1505.54 | 1583.25 | -735.77 | 6.31 vs 6.56 | 150.12 | <.0001 |
| 6.57 | Block Diag. u1+u2,u0 | 11 | 1567.49 | 1617.77 | -772.74 | 6.31 vs 6.57 | 76.177 | <.0001 |
| 6.58 | Block Diag. u0+u2,u1 | 11 | 1592.79 | 1643.07 | -785.39 | 6.31 vs 6.58 | 50.876 | <.0001 |
| 6.59 | Block Diag. u0+u1,u2 | 11 | 1586.12 | 1636.40 | -782.06 | 6.31 vs 6.59 | 57.548 | <.0001 |

The scatter plot of standardised residuals versus fitted values from model 6.52 fitted to the age 15 dataset were nearly indistinguishable from those of the first and second stage variable-exponent models (6.37 and 6.46) and so are not shown. The normal probability plots of the estimated random effects from model 6.52 fitted to the age 15 dataset appear in Figure 6.22. In contrast to the case with the variable-exponent models, the random effects show no evidence of asymmetry.

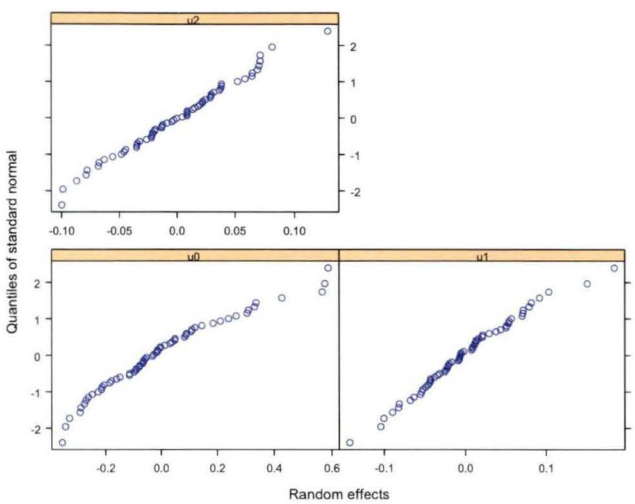


Figure 6.22 Normal probability plots of the model 6.52 estimated random effects - age 15 dataset.

The parameter estimates from model 6.52 fitted to the age 15 dataset appear in Table 6.23. All of the model parameters are highly significant however large fixed and random defects correlations are again present. The performance of model 6.52 fitted to the age 15 dataset is described further in Chapter 7.

A gnls version of model 6.52 (termed model 6.60) fitted with both a power variance function and a first-order continuous autocorrelation function converged without difficulty. The scatter plot of the model residuals appears in Figure 6.23 and suggests that residual error homogeneity is reasonable. Fit statistics and parameter estimates for model 6.60 appear in Table 6.24. Error variance and covariance parameters are similar to those obtained for the gnls variable-exponent models presented in the previous section. In other respects the model is similar to the nlme fitted version, with larger information criterion values indicating that better model parsimony comes at a cost of poorer model fit. The performance of model 6.60 fitted to the age 15 dataset is described further in Chapter 7.

Table 6.23 Model 6.52 parameter estimates - age 15 dataset.

```
Random effects: (General positive-definite structure)

     StdDev:        Correlation:

u0    0.22716849              u0   u1
u1    0.06408807          u1 0.487
u2    0.05583302          u2 0.103 -0.700

Residual 0.45567595


Fixed effects:

    Value Std.Error  t-value p-value

a0 1.155651 0.0440292  26.24736 <.0001
a1 1.671441 0.2786769   5.99778 <.0001
b1 1.413828 0.0641264  22.04752 <.0001
b2 -0.376145 0.0321666 -11.69366 <.0001
b3 -0.076764 0.0080653  -9.51777 <.0001
b4 -0.660852 0.0340936 -19.38347 <.0001

 Correlation:

    a0   a1   b1   b2   b3
a1 -0.742
b1 -0.021 0.027
b2 0.025 0.027 -0.951
b3 0.015 0.012 -0.843 0.923
b4 0.021 0.015 -0.988 0.914 0.810
```

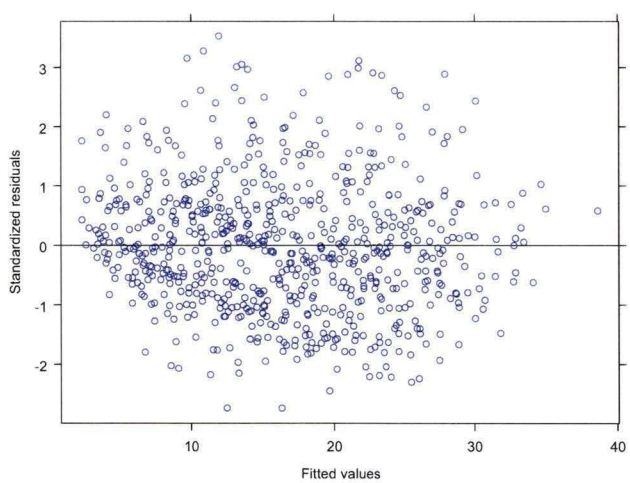


Figure 6.23 Scatter plot of model 6.60 standardised residuals versus fitted values - age 15 dataset.

Table 6.24 Model 6.60 fit statistics and parameter estimates - age 15 dataset.

```
    AIC     BIC  log Likelihood
1610.493  1651.631     -796.2467


     lower 95%   estimate   upper 95%

Correlation Structure: Continuous AR(1)
Phi    0.1844335  0.2625768  0.3592449

Variance Structure: Power of variance covariate
power  -0.3740781  -0.334741  -0.2954039

Residual Standard Error:
Error   0.8737886  1.000852   1.146392


Coefficients:
    Value Std.Error  t-value p-value
a0 1.046154 0.0287687 36.36424 <.0001
a1 2.562013 0.2002472 12.79425 <.0001
b1 1.454656 0.1384260 10.50854 <.0001
b2 -0.405015 0.0674588 -6.00389 <.0001
b3 -0.083514 0.0144924 -5.76259 <.0001
b4 -0.672041 0.0730097 -9.20481 <.0001

 Correlation:
    a0   a1   b1   b2   b3
a1 -0.791
b1 0.030 0.080
b2 -0.044 -0.118 -0.974
b3 -0.030 -0.084 -0.893 0.943
b4 -0.017 -0.046 -0.994 0.948 0.869
```

As per the variable-exponent models fitted in section 6.4.2.1, further between-tree variation can be accounted for by including further tree-level predictors in the exponent term. An inspection of the regression analysis results for the prediction of model 6.52 random effect BLUPs using tree-level variables, presented in Table 6.25, reveals evidence that both tree-level variables influence stem form in some way. Partial leverage plots did not suggest that the influence was nonlinear, but the technique is not suitable for determining whether the influence of the tree-level variables varies within the stem. In an effort to construct a variable-form version of the model, the same permutations of transformations of total height and local density as that tested in section 6.4.2.1 were incorporated into model 6.52. The results of that analysis were very similar, with both optimum tree-level predictors entering the model without multiplication by relative height. Again, an inspection of model performance indicated that the influence of total height was very minor so it was not included in the final model.

Table 6.25 OLS regression result predicting model 6.52 random effects BLUPs using tree-level variables - age 15 dataset. T-ratios for each parameter with associated p-value in brackets and adjusted $R^2$ values.

| BLUPs | u1 |
|---|---|
| Intercept | 1.52<br>(0.1330) |
| H | -2.93<br>(0.0048) |
| $C^{0.5}$ | 4.95<br>(<.0001) |
| $H*C^{0.5}$ | -1.49<br>(0.1425) |
| Adj. $R^2$ | 0.331 |

The optimum exponent term of the variable-form model is given by:

$$k_{ij} = (\beta_1 + u_{i1}) + (\beta_2 + u_{i2}) \sin\left(\frac{\pi}{2} z_{ij}\right) + \beta_3 \cos\left(\frac{3\pi}{2} z_{ij}\right) + \beta_4 \sin\left(\frac{\pi}{2} z_{ij}\right) \frac{1}{z_{ij}} + \beta_5 \sqrt{C_i} \tag{6.61}$$

The form of the base term is unchanged from that of model 6.52. Tests for changes to the random effects specification showed little difference from that found to best suit the average form version and so are not shown. Similarly, the diagnostic plots were also largely unchanged and so are also not shown. The fit statistics and parameter estimates for model 6.61 fitted to the age 15 dataset appear in Table 6.26. The parameters associated with the exponent terms that also appear in model 6.52 are very similar, indicating that the addition of the tree-level predictors to the exponent has not greatly changed the average stem form prediction. The parameters associated with the base terms have changed in a similar fashion to that observed in the variable-exponent model, with the parameters and t-values associated with local density larger and those of total height smaller. The performance of model 6.61 fitted to the age 15 dataset is described further in Chapter 7.

Table 6.26 Model 6.61 fit statistics and parameter estimates - age 15 dataset.

```
    AIC    BIC  log Likelihood
 1518.094  1582.086     -745.0469

Random effects: (General positive-definite Structure)

      StdDev:       Correlation:

   u0 0.20099708             u0   u1
   u1 0.05606480    u1 0.351
   u2 0.05517897    u2 0.182 -0.723

Residual 0.45604389

Fixed effects:

    Value Std.Error  t-value p-value
a0 1.007054 0.0495312 20.33169 <.0001
a1 2.935249 0.3583756  8.19043 <.0001
b1 1.375777 0.0646005 21.29670 <.0001
b2 -0.379249 0.0321965 -11.77920 <.0001
b3 -0.077238 0.0080782 -9.56129 <.0001
b4 -0.662674 0.0341431 -19.40875 <.0001
b5 0.022854 0.0046218  4.94479 <.0001

Correlation:
    a0   a1   b1   b2   b3   b4
a1 -0.849
b1 -0.096 0.075
b2 0.011 0.039 -0.942
b3 0.007 0.015 -0.836 0.923
b4 0.012 0.017 -0.981 0.914 0.810
b5 0.637 -0.542 -0.125 -0.013 -0.008 -0.006
```

The results of fitting a gnls version of this model (termed model 6.62) were very similar to those for the average-form versions. The scatter plot (not shown) indicated acceptable residual error homogeneity. Fit statistics and parameter estimates for model 6.62 appear in Table 6.27. The performance of model 6.62 fitted to the age 15 dataset is described further in Chapter 7.

#### *6.4.2.2.2 Age 20 dataset*

With respect to the nlme models, the results of the fitting process for the age 20 dataset were very similar. Convergence of the nlme algorithm was not achieved when random effects were applied to each term in the exponent. Reduced models converged without difficulty and the convergence problems could be attributed to the high colinearity of the terms in the exponent of the model. In contrast to the case with the age 15 dataset, the optimum model was not found to include the full positive definite variance-covariance matrix; rather that the random effects associated with the base term were independent of those associated with the terms that appear in the exponent. This suggests that stem size and stem form, as

described by the model, is independent. Test results for the specification of model random effects appear in Table 6.28.

Table 6.27 Model 6.62 fit statistics and parameters estimates - age 15 dataset.

```
    AIC     BIC  log Likelihood
1593.432  1639.141     -786.7161


     lower 95%   estimate   upper 95%

Correlation Structure: Continuous AR(1)
Phi    0.1738877  0.2493689  0.3439725

Variance Structure: Power of variance covariate
power   -0.3775180 -0.3373659  -0.2972138

Residual Standard Error:
Error   0.8456949  0.9677379  1.107393


Coefficients:
    Value Std.Error  t-value p-value
a0 0.988902 0.0305186 32.40330 <.0001
a1 3.022235 0.2199848 13.73838 <.0001
b1 1.410033 0.1374609 10.25771 <.0001
b2 -0.406574 0.0666881 -6.09665 <.0001
b3 -0.083311 0.0143229 -5.81662 <.0001
b4 -0.676007 0.0722782 -9.35284 <.0001
b5 0.023340 0.0053491  4.36344 <.0001

 Correlation:
    a0   a1   b1   b2   b3   b4
a1 -0.827
b1 0.005 0.090
b2 -0.051 -0.092 -0.972
b3 -0.032 -0.067 -0.891 0.943
b4 -0.035 -0.019 -0.990 0.949 0.870
b5 0.469 -0.446 -0.081 0.012 0.011 -0.012
```

The random effects structure of the optimum model (termed model 6.57) may be written:

$$\boldsymbol{u}_i = \begin{bmatrix} u_{i0} \\ u_{i1} \\ u_{i2} \end{bmatrix},\ \boldsymbol{u}_i \sim MVN(0,\Psi),\ \Psi = \begin{bmatrix} \sigma_0^2 & 0 & 0 \\ 0 & \sigma_1^2 & \sigma_{1,2} \\ 0 & \sigma_{1,2} & \sigma_2^2 \end{bmatrix},\ \text{and}\ \varepsilon_{ij} \sim N\left(0,\sigma^2\right)$$

Normal probability plots for the random effects of the model 6.57 fit appear in Figure 6.24. The optimum model was found to exhibit quite asymmetric random effects for the relative height transformation that appears in the exponent term ($\mu_{i1}$). This suggests the standard error estimates for this parameter should be

viewed with some caution. Estimates of model standard errors and other parameters appear in Table 6.29. As per the fit to the age 15 data, the parameters appearing in the exponent term display very high colinearity. Colinearity of similar magnitude was also found in the model fitted with a full positive definite variance-covariance matrix. These results suggest the colinearity is a feature of the trigonometric model. The performance of model 6.57 fitted to the age 20 dataset is described further in Chapter 7.

Table 6.28 Tests for significance of adjusting model 6.31 with alternative random effects - age 20 dataset.

| Model | Variance-Covariance Matrix | No. of Parms | AIC | BIC | logLike | Model test | L.Ratio | P.value |
|---|---|---|---|---|---|---|---|---|
| 6.31 | Gen.Pos.Def. u0+u1 | 10 | 1602.03 | 1647.83 | -791.01 | | | |
| 6.52 | Gen.Pos.Def. u0+u1+u2 | 13 | 1488.93 | 1548.48 | -731.46 | 6.31 vs 6.52 | 129.32 | <.0001 |
| 6.53 | Gen.Pos.Def. u0+u1+u3 | 13 | 1508.55 | 1568.10 | -741.27 | 6.31 vs 6.53 | 99.478 | <.0001 |
| 6.54 | Gen.Pos.Def. u0+u1+u4 | 13 | 1518.21 | 1577.76 | -746.11 | 6.31 vs 6.54 | 89.814 | <.0001 |
| 6.55 | Gen.Pos.Def. u0+u1+u2+u3 | 17 | 1478.10 | 1555.97 | -722.05 | 6.31 vs 6.55 | 148.14 | <.0001 |
| 6.56 | Gen.Pos.Def. u0+u1+u2+u4 | 17 | 1460.65 | 1538.52 | -713.32 | 6.31 vs 6.56 | 165.59 | <.0001 |
| 6.57 | Block Diag. u1+u2,u0 | 11 | 1497.81 | 1548.24 | -737.91 | 6.31 vs 6.57 | 116.44 | <.0001 |
| 6.58 | Block Diag. u0+u2,u1 | 11 | 1528.38 | 1578.77 | -753.19 | 6.31 vs 6.58 | 75.643 | <.0001 |
| 6.59 | Block Diag. u0+u1,u2 | 11 | 1516.82 | 1567.21 | -747.41 | 6.31 vs 6.59 | 87.203 | <.0001 |

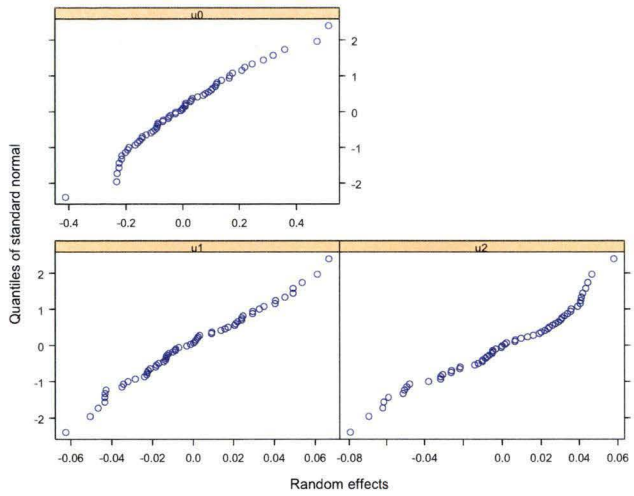


Figure 6.24 Normal probability plots of the model 6.57 estimated random effects - age 20 dataset.

Table 6.29 Model 6.57 parameter estimates - age 20 dataset.

```
Random effects:
Composite Structure: Blocked

      StdDev:  Correlation:

Block 1: (General positive-definite Structure)

u1    0.03344136        u1
u2    0.03932754    u2 -0.712

Block 2:
u0    0.1803598

Residual 0.4287236


Fixed effects: a0 + a1 + b0 + b1 + b2 + b3 ~ 1
    Value Std.Error  t-value p-value
a0 0.943448 0.0498292  18.93365 <.0001
a1 2.295206 0.4171874  5.50162 <.0001
b1 1.313187 0.0466573  28.14535 <.0001
b2 -0.282669 0.0236037 -11.97562 <.0001
b3 -0.036849 0.0055766  -6.60787 <.0001
b4 -0.655209 0.0246248 -26.60764 <.0001

 Correlation:
    a0   a1   b1   b2   b3
a1 -0.883
b1 -0.006 -0.016
b2 0.005 0.016 -0.959
b3 0.005 0.013 -0.868 0.928
b4 0.006 0.016 -0.993 0.929 0.839
```

Attempts to obtain parameter estimates using gnls were less successful than was the case in fitting these models to the age 15 dataset. While convergence was possible for a model which included only a power variance function, a scatter plot

of the residuals from this model showed large heterogeneity was present. A model fitted jointly with a power variance function and a first-order continuous autocorrelation function failed to converge. The approach was abandoned for the dataset using this type of model.

The result of the OLS regression analysis for the prediction of the exponent random effect BLUPs from model 6.57 appears in Table 6.30. There appears to be an extremely weak relationship between local density and stem form, as described by the varying exponent intercept term. This was borne out by the subsequent analysis in which the suites of tree-level variable transformations were assessed as additional terms in the exponent of the model. In no case was total height significant. The best local density term was again the square root transformation. The final model has the same fixed effects specification as that for the age 15 dataset. It had the same random effects specification as model 6.57. The fit statistics and parameter estimates for the final model (model 6.63) appear in Table 6.31. The addition of local density to the model has very little effect upon the estimates of other parameters. The local density parameter itself is only moderately significant. The influence of local density upon model behavior is described further in Chapter 7 where model performance is analysed. Attempts at constructing a gnls version of this model also failed.

Table 6.30 OLS regression result predicting model 6.57 random effects BLUPs using tree-level variables - age 20 dataset. T-ratios for each parameter with associated p-value in brackets and adjusted $R^2$ values.

| BLUPs | u1 |
|---|---|
| Intercept | -0.77<br>(0.4428) |
| H | 0.04<br>(0.9682) |
| $C^{0.5}$ | 2.09<br>(0.0407) |
| $H*C^{0.5}$ | -1.39<br>(0.1693) |
| Adj. $R^2$ | 0.062 |

Table 6.31 Model 6.63 fit statistics and parameter estimates - age 20 dataset.

```
    AIC    BIC  log Likelihood
 1489.833  1544.801    -732.9165

Random effects:
Composite Structure: Blocked

     StdDev:        Correlation:

Block 1: (General positive-definite Structure)
u1    0.03209777       u1
u2    0.03920386   u2 -0.747

Block 2:
u0    0.1803782

Residual 0.4289872


Fixed effects:

    Value Std.Error  t-value p-value
a0 0.942633 0.0498697  18.90192 <.0001
a1 2.301744 0.4175264  5.51281 <.0001
b1 1.296202 0.0469784  27.59145 <.0001
b2 -0.283423 0.0236294 -11.99447 <.0001
b3 -0.037065 0.0055838  -6.63793 <.0001
b4 -0.655749 0.0246553 -26.59666 <.0001
b5 0.007478 0.0022632  3.30435  0.001

 Correlation:
    a0   a1   b1   b2   b3   b4
a1 -0.883
b1 -0.006 -0.015
b2 0.005 0.016 -0.953
b3 0.005 0.013 -0.861 0.929
b4 0.006 0.016 -0.986 0.929 0.839
b5 0.005 -0.006 -0.109 -0.009 -0.011 -0.008
```

### 6.4.3 Reduced segmented profile models

A comparison of information criterion values for the segmented and variable-exponent models presented above in sections 6.4.1 and 6.4.2 suggests that the variable-exponent models allow a closer fit to the data. Variable-exponent modelling is also very flexible, as the manner in which the models are constructed facilitates the development of models with degrees of complexity suited to the data. Average-form models that describe average stem form may be constructed by using tree-level predictors to scale the base term. Variable-form models that describe additional between-tree differences in stem form may be constructed by incorporating additional tree-level predictor transformations within the exponent term. Attempts at the latter in this work were not entirely successful. The multiple regression analysis undertaken in the segmented polynomial model development

suggested local density and, to a lesser extent, total height impacted particularly upon stem form in the stem butt, yet total height proved to be insignificant and the influence of local density was not related to relative height in the second-stage variable-form models. The variable-exponent models are also lacking in other ways. The parameters of the transformations of relative height that appear in the exponent terms in both investigated models exhibit high colinearity and also lack interpretability. These parameters are also nonlinear and the random effects for some of these models were not normally distributed, violating a mixed effects modelling assumption.

In this section, alternative models are developed in an effort to circumvent the problems associated with both the segmented polynomial and variable-exponent models. There were two aims. The first was to develop models in which the tree-level predictors enter through a single parameter, as they did through the base term in each of the variable-exponent models. The second was to maintain parameter interpretability to facilitate further second-stage modelling of between-tree differences in stem form. In order to do this, a segmented model was developed that comprised a flexible function with interpretable parameters to describe the main bole of the stem and an additional exponent term to describe an additional component of profile in the stem butt. The reduced segmented model is given by:

$$d = \left(\beta_0 + \beta_1 \left(z - \beta_4\right)\right)\left(\frac{1-z}{1-\beta_4}\right)^{\beta_2} + \left(\exp\left(1 - \frac{z}{\beta_4}\right) - 1\right)^{\beta_3} I \qquad (6.64)$$

Where:

$\beta_{0\text{to}4}$ are model parameters;

$I = 0$ for $z > \beta_4$ and $I = 1$ for $z \leq \beta_4$.

The model may be decomposed to three constituent components to facilitate a visual description:

$$A = \beta_0 \left(\frac{1-z}{1-\beta_4}\right)^{\beta_2}$$

$$B = \beta_1 \left(z - \beta_4\right)\left(\frac{1-z}{1-\beta_4}\right)^{\beta_2}$$

$$C = \left(\exp\left(1 - \frac{z}{\beta_4}\right) - 1\right)^{\beta_3} I$$

Model 6.64 may be then be written as:

$$d = A + B + C$$

A plot of model 6.64 components for a representative tree appears in Figure 6.25.

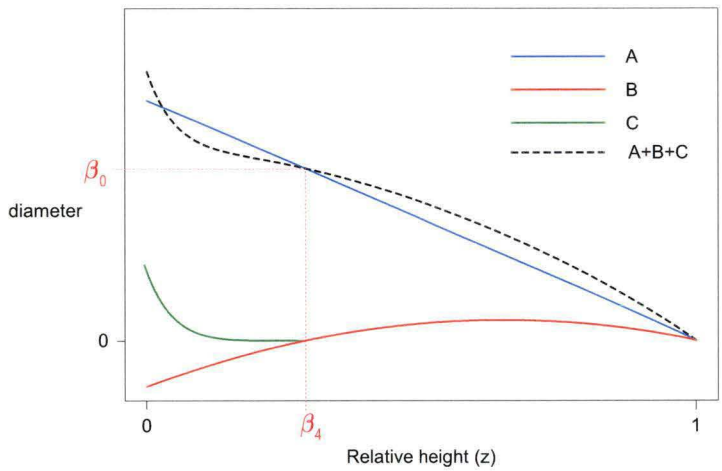


Figure 6.25 Components of model 6.64 for a representative tree[3]

The model is largely linear in its parameters, including one nonlinear shape parameter in the upper stem, one in the lower stem, and one nonlinear join point parameter to complicate two-stage modelling. The use of the exponent term for the description of profile below the join point means the model cannot be integrated algebraically. This concession was judged to be appropriate after considering an alternative formulation which instead employed a polynomial term below the join point. That alternative was acceptable for the age 20 dataset, but suffered from between-tree bias when fitted to the age 15 dataset.

In other respects the model has some appealing characteristics. The prediction is continuous about the join point. The slope of the prediction in the region about the join point does not need to include zero. While not algebraically monotonic, the constraint that the prediction passes through a join point diameter ensures that it is so in practice. While not algebraically constrained to ensure that diameter at the stem tip is equal to zero, this constraint is ensured when $\beta_2 > 0$, something that also occurs in practice. The parameters also have simple interpretation: $\beta_0$ describes the diameter prediction at the join point, which occurs at relative height $\beta_4$. $\beta_1$ is a shape parameter describing decreasing amounts of stem curvature as one moves up the stem toward the tip; $\beta_2$ is a shape parameter describing

[3] See text for a definition of the model components.

decreasing amounts of stem curvature as one moves down the stem from the tip; and $\beta_3$ is a shape parameter describing curvature below the join point. The parameterisation for the upper stem allows for some flexibility in shape in that it can describe paraboloids, conoids or neiloids bounded away from the stem tip and join point with only two parameters that behave in an increasingly independent fashion as upper stem shapes within a tree are increasingly distinguished from one another. When the lower region of the upper stem segment bounded away from the join point is a conoid $\beta_1 = 0$, when it is a neiloid $\beta_1 < 0$, and when a paraboloid $\beta_1 > 0$. When the upper region of the upper stem segment bounded away from the stem tip is a conoid $\beta_2 = 1$, when it is a neiloid $\beta_2 > 1$, and when a paraboloid $\beta_2 < 1$.

In the following two sections, model development is split by the age class of the dataset.

### *6.4.3.1 Age 15 dataset*

The development of the segmented polynomial models in section 6.3.1 suggested random effects should be associated with all the model shape parameters. Initial analysis suggested the inflection height should also be allowed to vary between trees. To ensure maximum flexibility in the initial fit, the variance-covariance matrix was specified to be positive-definite. The development of the variable-form models in section 6.4.2 suggested that the parameter describing the diameter at the inflection point should be specified as an additive linear function of total height and local density. Therefore the model may be reformulated to:

$$d = \alpha_0 H\left(\frac{1-z}{1-\beta_4}\right)^{\beta_2} + \alpha_1\sqrt{C}\left(\frac{1-z}{1-\beta_4}\right)^{\beta_2} + \beta_1\left(z-\beta_4\right)\left(\frac{1-z}{1-\beta_4}\right)^{\beta_2} + \left(\exp\left(1-\frac{z}{\beta_4}\right)-1\right)^{\beta_3} I \tag{6.65}$$

In statistical notation, the model is given by:

$$\begin{aligned} d_{ij} = {} & \left(\alpha_0 + u_{i0}\right) H_i\left(\frac{1-z_{ij}}{1-\left(\beta_4 + u_{i4}\right)}\right)^{\left(\beta_2+u_{i2}\right)} + \alpha_1\sqrt{C}_i\left(\frac{1-z_{ij}}{1-\left(\beta_4 + u_{i4}\right)}\right)^{\left(\beta_2+u_{i2}\right)} + \\ & \left(\beta_1 + u_{i1}\right)\left(z_{ij} - \left(\beta_4 + u_{i4}\right)\right)\left(\frac{1-z_{ij}}{1-\left(\beta_4 + u_{i4}\right)}\right)^{\left(\beta_2+u_{i2}\right)} + \\ & \left(\exp\left(1-\frac{z_{ij}}{\left(\beta_4 + u_{i4}\right)}\right)-1\right)^{\left(\beta_3+u_{i3}\right)} I + \varepsilon_{ij} \end{aligned} \tag{6.66}$$

And:

$$\boldsymbol{u}_i = \begin{bmatrix} u_{i0} \\ u_{i1} \\ u_{i2} \\ u_{i3} \\ u_{i4} \end{bmatrix}, \quad \boldsymbol{u}_i \sim MVN(0, \Psi), \quad \Psi = \begin{bmatrix} \sigma_0^2 & \sigma_{0,1} & \sigma_{0,2} & \sigma_{0,3} & \sigma_{0,4} \\ \sigma_{0,1} & \sigma_1^2 & \sigma_{1,2} & \sigma_{1,3} & \sigma_{1,4} \\ \sigma_{0,2} & \sigma_{1,2} & \sigma_2^2 & \sigma_{2,3} & \sigma_{2,4} \\ \sigma_{0,3} & \sigma_{1,3} & \sigma_{2,3} & \sigma_3^2 & \sigma_{3,4} \\ \sigma_{0,4} & \sigma_{1,4} & \sigma_{2,4} & \sigma_{3,4} & \sigma_4^2 \end{bmatrix}, \text{ and } \varepsilon_{ij} \sim N\left(0, \sigma^2\right)$$

Initial attempts at fitting the model using this full matrix failed to converge. Subsequent attempts using reduced block diagonal matrices were more successful. The important tests of random effects parameter significance appear in Table 6.32. An inspection of the 95% confidence intervals for the covariance parameters of the fit of model 6.70 suggested many of the random effects were independent of each other. The model statistics presented show that models with reduced block-diagonal or diagonal matrices are more suitable, indicating independence between most, but not all, random effects. The statistics also show that all of the random effects parameters in the model are significant. Final model selection was based upon an analysis of normal probability plots of the random effects and an inspection of within-stem prediction bias estimates. That analysis isolated model 6.72 as the optimum average-form version of the reduced segmented model. The stipulated error structure of model 6.72 is given by:

$$\boldsymbol{u}_i = \begin{bmatrix} u_{i0} \\ u_{i1} \\ u_{i2} \\ u_{i3} \\ u_{i4} \end{bmatrix}, \quad \boldsymbol{u}_i \sim MVN(0, \Psi), \quad \Psi = \begin{bmatrix} \sigma_0^2 & 0 & 0 & 0 & 0 \\ 0 & \sigma_1^2 & \sigma_{1,2} & 0 & 0 \\ 0 & \sigma_{1,2} & \sigma_2^2 & 0 & 0 \\ 0 & 0 & 0 & \sigma_3^2 & 0 \\ 0 & 0 & 0 & 0 & \sigma_4^2 \end{bmatrix}, \text{ and } \varepsilon_{ij} \sim N\left(0, \sigma^2\right)$$

Table 6.32 Tests for significance of adjusting model 6.66 with alternative random effects - age 15 dataset.

| Model | Variance-Covariance Matrix | No. of Parms | AIC | BIC | logLike | Model test | L.Ratio | p.value |
|---|---|---|---|---|---|---|---|---|
| 6.66 | Gen.Pos.Def u0+u1+u2+u3+u4 | | | | | | | |
| 6.67 | Block Diag. u0,u1+u2+u3+u4 | 18 | 1545.02 | 1627.30 | -754.51 | | | |
| 6.68 | Block Diag. u1,u0+u2+u3+u4 | 18 | 1549.61 | 1631.89 | -756.81 | | | |
| 6.69 | Block Diag. u2,u0+u1+u3+u4 | 18 | 1546.39 | 1628.66 | -755.19 | | | |
| 6.70 | Block Diag. u3, u0+u1+u2+u4 | 18 | 1535.68 | 1617.95 | -749.84 | | | |
| 6.71 | Block Diag. u4, u0+u1+u2+u3 | 18 | 1537.41 | 1619.69 | -750.71 | | | |
| 6.72 | Block Diag. u1+u2,u0,u3,u4 | 13 | **1546.84** | **1606.26** | **-760.42** | 6.67 vs 6.72 | 11.8177 | 0.0374 |
| 6.73 | Diag. u0,u1,u2,u3,u4 | 12 | 1554.80 | 1609.65 | -765.40 | 6.67 vs 6.73 | 21.7763 | 0.0013 |
| 6.74 | Diag. u0,u1,u2,u3 | 11 | 1766.27 | 1816.55 | -872.14 | 6.67 vs 6.74 | 235.251 | <.0001 |
| 6.75 | Diag. u0,u1,u2,u4 | 11 | 1600.93 | 1651.21 | -789.46 | 6.67 vs 6.75 | 69.9067 | <.0001 |
| 6.76 | Diag. u0,u1,u3,u4 | 11 | 1568.42 | 1618.70 | -773.21 | 6.67 vs 6.76 | 37.4040 | <.0001 |
| 6.77 | Diag. u0,u2,u3,u4 | 11 | 1588.33 | 1638.61 | -783.16 | 6.67 vs 6.77 | 57.3055 | <.0001 |

Figure 6.26 presents a scatter plot of standardised residuals versus fitted values from model 6.72 fitted to the age 15 dataset. The heterogeneity present in the residuals is similar to that found in the fit of the segmented polynomial model (model 6.15), with larger residuals appearing to occur for the largest predictions. The patterned bias is also similar, appearing largest for predictions less than approximately 8 centimetres. The model evidently suffers from local bias within this region of the stem, a problem typical of segmented models tested. Again, scatter plots of standardised residuals versus relative height and versus the tree-level predictors showed no discernable trend.

The normal probability plots of the estimated random effects from model 6.72 fitted to the age 15 dataset appear in Figure 6.27. These plots demonstrate that the random effects are all acceptably normally distributed.

The parameter estimates for model 6.72 appear in Table 6.33. Both the fixed and random effects correlations are quite small, although relatively large correlations between the upper stem shape parameters are apparent. The join point occurs at approximately 23% of total height and the magnitude of the associated random effects BLUP standard deviations suggests this varies by an average of approximately 8.5% of the total between trees. The values for the upper stem shape parameters indicate that average upper stem shape is parabolic ($\beta_2 < 1$, and $\beta_1 > 0$), while the magnitude of the associated random effects BLUP standard deviations suggest neiloid upper stem shapes are also present in the data. The performance of model 6.72 fitted to the age 15 dataset is described further in Chapter 7.

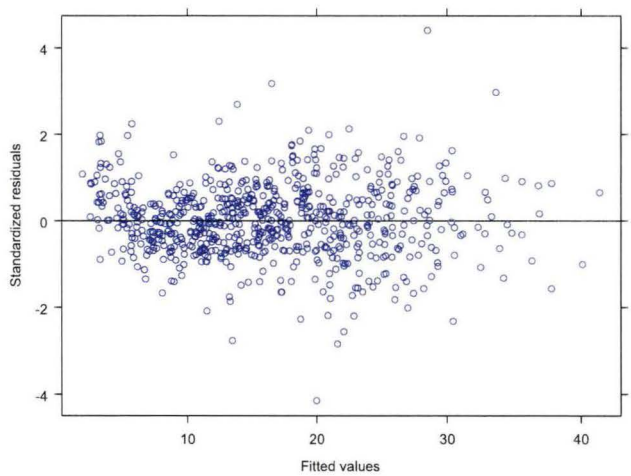


Figure 6.26 Scatter plot of model 6.72 standardised residuals versus fitted values - age 15 dataset.

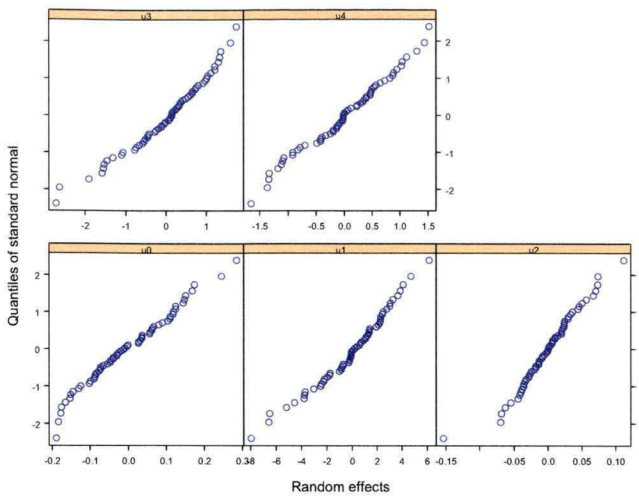


Figure 6.27 Normal probability plots of the model 6.72 estimated random effects - age 15 dataset.

Table 6.33 Model 6.72 parameter estimates - age 15 dataset.

```
Random effects:
Composite Structure: Blocked

    StdDev:   Correlation:
Block 1: (General positive-definite Structure)
u1    4.5751760       u1
u2    0.1043612  u2  0.647

Block 2:
u0    0.1179409

Block 3:
u3   0.08452397

Block 4:
u4    0.7762147

Residual 0.3996230


Fixed effects:

   Value Std.Error  t-value p-value
a0 0.916451 0.0356834 24.88693 <.0001
a1 1.939134 0.2687483  7.62138 <.0001
b1 4.496426 0.7666976  6.04061 <.0001
b2 0.901405 0.0201475 44.99823 <.0001
b3 3.220887 0.1111992 16.81187 <.0001
b4 0.231248 0.0143192 28.96501 <.0001

Correlation:
    a0    a1    b1    b2    b3
a1 -0.845
b1 -0.052 -0.057
b2 -0.032 -0.068 0.782
b3 0.006 -0.066 0.141 0.144
b4 -0.017 -0.183 0.237 0.235  0.132
```

Convergence of gnls version of model 6.72 (termed model 6.78) was achieved without difficulty. The scatter plot of standardised residuals versus fitted values that appears in Figure 6.28 shows some consistent bias in the fit. Very weak correlations between standardised residuals from the model and tree-level predictors were observed, however these were not significant enough to warrant additional variance modelling. Fit statistics and parameter estimates from model 6.78 appear in Table 6.34. The model predicts the join point to occur at a point lower on the stem. The estimates for parameters $\beta_1$ and $\beta_3$ are slightly smaller, indicating that the model predicts less curvature through the middle and lower stem regions. The performance of model 6.78 fitted to the age 15 dataset is described further in Chapter 7.

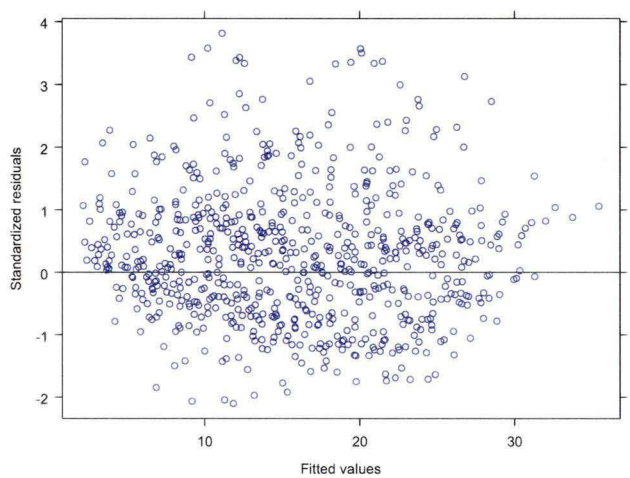


Figure 6.28 Scatter plot of model 6.78 standardised residuals versus fitted values - age 15 dataset.

OLS regression analysis of the relationships between random effects BLUPs from model 6.72 and the tree-level predictors suggested the potential existed to construct a variable-form version of the model. The results of this analysis appear in Table 6.35. Despite the use of the diameter prediction model to constrain the fit, there still remains a large component of the BLUPs variance which may be explained using tree-level predictors. The candidate predictors, total height and local density, appear to respectively dominate the prediction of the $\beta_1$ term; thus describing curvature through the middle of the stem, and the $\beta_3$ term; thus describing curvature in the stem butt. Stem form in the tip ( $\beta_2$ ) appears to be unrelated to either tree-level predictor. The height of inflection $\beta_4$ is very weakly related to local density.

Table 6.34 Model 6.78 fit statistics and parameter estimates - age 15 dataset.

```
   AIC    BIC  log Likelihood
1658.942  1700.08    -820.4708


     lower 95%   estimate   upper 95%

Correlation Structure: Continuous AR(1)
Phi    0.2006112  0.2820165  0.3807223

Variance Structure: Power of variance covariate
power   -0.3895617 -0.3516940  -0.3138263

Residual Standard Error:
Error   0.8964918  1.027912   1.178599


Coefficients:
   Value Std.Error t-value p-value
a0 0.932479 0.031136 29.94831 <.0001
a1 2.137666 0.182289 11.72682 <.0001
b1 3.711315 1.184701 3.13270 0.0018
b2 0.891440 0.031917 27.92988 <.0001
b3 2.746235 0.217521 12.62516 <.0001
b4 0.168654 0.019000 8.87672 <.0001

 Correlation:
    a0   a1   b1   b2   b3
a1 -0.557
b1 -0.041 -0.377
b2 -0.023 -0.290 0.889
b3 -0.153 -0.014 -0.076 -0.034
b4 -0.243 -0.528 0.329 0.256 0.544
```

Table 6.35 OLS regression result predicting model 6.72 random effects BLUPs using tree-level variables - age 15 dataset. T-ratios for each parameter with associated p-value in brackets and adjusted $R^2$ values.

| BLUPs | u1 | u2 | u3 | u4 |
|---|---|---|---|---|
| Intercept | -4.72<br>(<.0001) | -1.80<br>(0.0776) | -1.64<br>(0.1063) | 1.51<br>(0.1377) |
| H | 5.39<br>(<.0001) | 1.55<br>(0.1267) | -0.27<br>(0.7885) | -2.27<br>(0.0269) |
| $C^{0.5}$ | -3.45<br>(0.0011) | 0.16<br>(0.8723) | 5.70<br>(<.0001) | 2.37<br>(0.0211) |
| $H*C^{0.5}$ | 1.75<br>(0.0862) | 0.81<br>(0.4234) | -1.03<br>(0.3060) | 0.82<br>(0.4174) |
| Adj. $R^2$ | 0.346 | 0.009 | 0.430 | 0.074 |

After some exploration, the second stage model was defined as:

$$d_{ij} = (\alpha_0 + u_{i0}) H_i \left( \frac{1 - z_{ij}}{1 - (\beta_4 + u_4)} \right)^{(\beta_2 + u_{i2})} + \alpha_1 \sqrt{C_i} \left( \frac{1 - z_{ij}}{1 - (\beta_4 + u_4)} \right)^{(\beta_2 + u_{i2})} + (\beta_1 + u_{i1}) H_i \left( z_{ij} - (\beta_4 + u_4) \right) \left( \frac{1 - z_{ij}}{1 - (\beta_4 + u_4)} \right)^{(\beta_2 + u_{i2})} + \left( \exp\left( 1 - \frac{z_{ij}}{(\beta_4 + u_4)} \right) - 1 \right)^{((\beta_3 + u_3) + \beta_{31}\sqrt{C_i})} I + \varepsilon_{ij} \tag{6.79}$$

Model 6.79 was initially fitted using the same random effects specification as that of model 6.72. Tests of random effects significance appear in table 6.36. The addition of the tree-level predictors has little impact upon the optimal covariance structure of the model and the optimum remains block diagonal with modelled covariance between the upper stem form parameters. The residual error scatter plots for this variable-form version of the model was not distinguishable from that for the average-form version (model 6.72) and so is not shown. The parameter estimates for model 6.79 appear in table 6.37. The performance of model 6.79 fitted to the age 15 dataset is described further in Chapter 7.

The gnls version of model 6.79 (termed model 6.80) converged without difficulty. The scatter plot of standardised residuals versus fitted values (not shown) was very similar to that of the average-form version in showing some consistent bias in the fit. Once again, very weak correlations between standardised residuals from the model and tree-level predictors were observed, however these were not significant enough to warrant additional variance modelling. Fit statistics and parameter estimates from model 6.80 appear in Table 6.38. The performance of model 6.80 fitted to the age 15 dataset is described further in Chapter 7.

### *6.4.3.2 Age 20 dataset*

Analysis of the age 20 dataset proceeded in the same manner as for the age 15 dataset. An inspection of the 95% confidence limits of the covariance parameters for model 6.66 suggested independence between random effects other than those describing differences in form in the upper stem. Test results for reduced random effects models appear in Table 6.39. The results confirm the significance of the random effects covariance parameters but subsequent analysis of within-stem bias suggested they had little positive effect while inflating model prediction error. The

results shown in Table 6.39 also confirm the significance of each random effect. Again, model 6.72 was chosen as the average-form model.

Table 6.36 Tests for significance of adjusting model 6.79 with alternative random effects - age 15 dataset.

| Model | Variance-Covariance Matrix | No. of Parms | AIC | BIC | logLike | Model test | L.Ratio | p.value |
|---|---|---|---|---|---|---|---|---|
| 6.79 | Block Diag. u1+u2,u0,u3,u4 | **14** | **1504.40** | **1568.40** | **-738.20** | | | |
| 6.81 | Diag. u0,u1,u2,u3,u4 | 13 | 1511.34 | 1570.76 | -742.67 | 6.79 vs 6.81 | 8.93206 | 0.0028 |
| 6.82 | Diag. u0,u1,u2,u3 | 12 | 1561.41 | 1616.26 | -768.70 | 6.79 vs 6.82 | 61.0055 | <.0001 |
| 6.83 | Diag. u0,u1,u2,u4 | 12 | 1585.14 | 1639.99 | -780.57 | 6.79 vs 6.83 | 84.7329 | <.0001 |
| 6.84 | Diag. u0,u1,u3,u4 | 12 | 1529.98 | 1584.83 | -752.99 | 6.79 vs 6.84 | 29.5748 | <.0001 |
| 6.85 | Diag. u0,u2,u3,u4 | 12 | 1532.59 | 1587.44 | -754.29 | 6.79 vs 6.85 | 32.1819 | <.0001 |

The diagnostic plots for the fit of model 6.72 appear in Figures 6.29 and 6.30. The plots show no evidence of residual error heterogeneity or violation of the random effects normality assumption. Estimated parameter values for the fit of model 6.72 to the age 20 dataset appear in table 6.40. They indicate that, in comparison to the fit of the same model to the age 15 dataset, the join point occurs at a higher point on the stem, at approximately 26% of total height. Stem shape is also generally more paraboloid throughout the stem as estimated values for the shape parameters are somewhat larger. The performance of model 6.72 fitted to the age 20 dataset is described further in Chapter 7.

Table 6.37 Model 6.79 parameter estimates - age 15 dataset.

```
Random effects:
Composite Structure: Blocked

    StdDev:   Correlation:
Block 1: (General positive-definite Structure)
u1    0.2965778       u1
u2    0.1177069  u2  0.671

Block 2:
u0    0.1307387

Block 3:
u3    0.5358653

Block 4:
u4   0.089109074

Residual 0.3926803


Fixed effects:

    Value Std.Error  t-value p-value
 a0 0.917905 0.0336907 26.20977 <.0001
 a1 1.812582 0.2503995  7.80670 <.0001
 b1 0.330953 0.0402843  6.51186 <.0001
 b2 0.921303 0.0178167 42.83984 <.0001
 b3 2.132370 0.1763871 12.17798 <.0001
b31 0.580605 0.0778926  7.12327 <.0001
 b4 0.241578 0.0150400 16.14728 <.0001

Correlation:
    a0   a1   b1   b2   b3  b31
 a1 -0.839
 b1 -0.048 -0.105
 b2 -0.029 -0.104 0.645
 b3 0.082 -0.157 0.204 0.185
b31 -0.089 0.125 -0.096 -0.089 -0.881
 b4 -0.004 -0.229 0.327 0.298 0.184 -0.106
```

Table 6.38 Model 6.80 fit statistics and parameter estimates (age 15 dataset)

```
   AIC     BIC  log Likelihood
 1644.4  1690.109     -812.200


     lower 95%   estimate  upper 95%

Correlation Structure: Continuous AR(1)
Phi    0.2234051 0.3087515  0.4095096

Variance Structure: Power of variance covariate
power   -0.3746310 -0.3375056 -0.3003802

Residual Standard Error:
Error   0.9376073 1.074755  1.2319630


Coefficients:
    Value Std.Error t-value p-value
 a0 2.412762 0.2147941 11.23291 <.0001
 a1 0.804965 0.0318706 25.25733 <.0001
 b1 0.432450 0.0711921 6.07441 <.0001
 b2 0.973631 0.0337439 28.85352 <.0001
 b3 0.240098 0.0249108 9.63830 <.0001
 b4 1.764334 0.3776713 4.67161 <.0001
b41 0.564325 0.1415005 3.98815 0.0001

 Correlation:
    a0   a1   b1   b2   b3   b4
 a1 -0.460
 b1 -0.201 -0.263
 b2 -0.181 -0.253 0.894
 b3 -0.383 -0.561 0.421 0.386
 b4 -0.470 0.245 0.049 0.054 0.284
b41 0.509 -0.391 -0.019 -0.013 -0.048 -0.880
```

Table 6.39 Tests for significance of adjusting model 6.66 with alternative random effects - age 20 dataset.

| Model | Variance-Covariance Matrix | No. of Parms | AIC | BIC | logLike | Model test | L.Ratio | p.value |
|---|---|---|---|---|---|---|---|---|
| 6.66 | Gen.Pos.Def u0+u1+u2+u3+u4 | 22 | 1500.38 | 1601.15 | -728.19 | | | |
| 6.72 | Block Diag. u1+u2,u0,u3,u4 | 13 | **1539.19** | **1598.74** | **-756.60** | 6.66 vs 6.72 | 56.8125 | <.0001 |
| 6.73 | Diag. u0,u1,u2,u3,u4 | 12 | 1559.56 | 1614.52 | -767.78 | 6.66 vs 6.73 | 79.1766 | <.0001 |
| 6.74 | Diag. u0,u1,u2,u3 | 11 | 1582.21 | 1632.60 | -780.11 | 6.66 vs 6.74 | 103.834 | <.0001 |
| 6.75 | Diag. u0,u1,u2,u4 | 11 | 1768.17 | 1818.56 | -873.09 | 6.66 vs 6.75 | 289.794 | <.0001 |
| 6.76 | Diag. u0,u1,u3,u4 | 11 | 1597.26 | 1647.65 | -787.63 | 6.66 vs 6.76 | 118.882 | <.0001 |
| 6.77 | Diag. u0,u2,u3,u4 | 11 | 1611.58 | 1661.97 | -794.79 | 6.66 vs 6.77 | 133.205 | <.0001 |

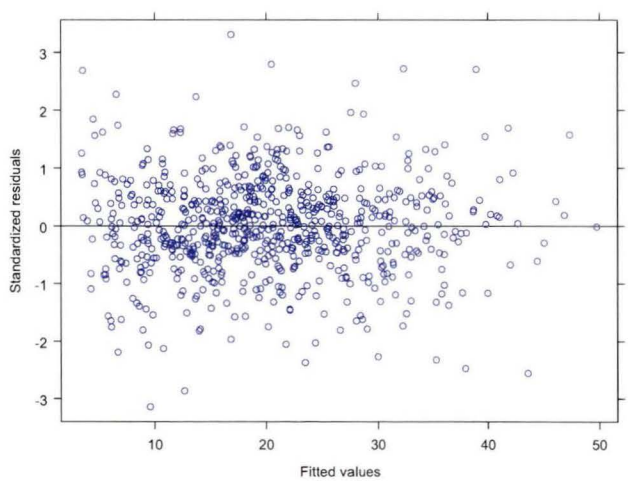


Figure 6.29 Scatter plot of model 6.72 standardised residuals versus fitted values - age 20 dataset.

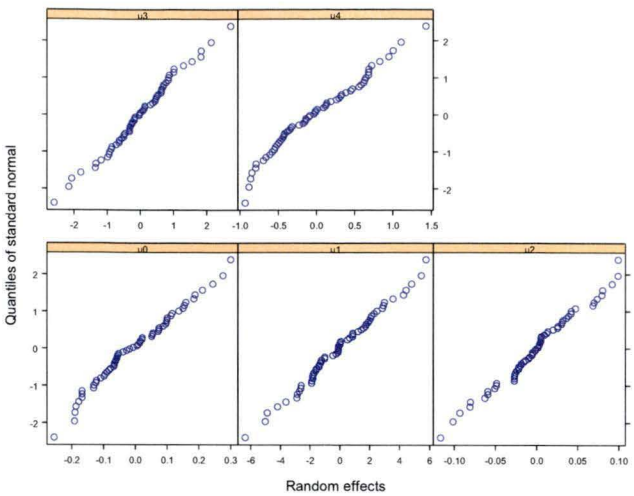


Figure 6.30 Normal probability plots of the model 6.72 estimated random effects - age 20 dataset.

Table 6.40 Model 6.72 parameter estimates - age 20 dataset.

```
Random effects:
Composite Structure: Blocked

    StdDev:   Correlation:

Block 1: (General positive-definite Structure)
u1    4.74290844      u1
u2    0.09809695  u2  0.766

Block 2:
u0    0.1303576

Block 3:
u3    0.6731811

Block 4:
u4   0.08070666

Residual 0.3704636


Fixed effects:

   Value Std.Error  t-value p-value
a0 0.79573 0.0383086 20.55944 <.0001
a1 1.87115 0.3172094  6.35150 <.0001
b1 12.13879 0.6858461 17.77191 <.0001
b2 0.93198 0.0153688 60.83661 <.0001
b3 3.42653 0.0964704 18.37593 <.0001
b4 0.26067 0.0141826 35.62871 <.0001

Correlation:
    a0   a1   b1   b2   b3
a1 -0.878
b1 -0.015 -0.030
b2 -0.001 -0.059 0.789
b3 0.016 -0.064 0.137 0.154
b4 0.034 -0.161 0.165 0.229  0.174
```

A gnls version of model 6.72 (termed model 6.86) fitted using the power variance function and an autocorrelation term converged without difficulty, however the residual error was consistently biased and quite heterogeneous, as shown in Figure 6.31. The magnitude of the prediction bias was large enough to preclude further analysis of this model using the available data.

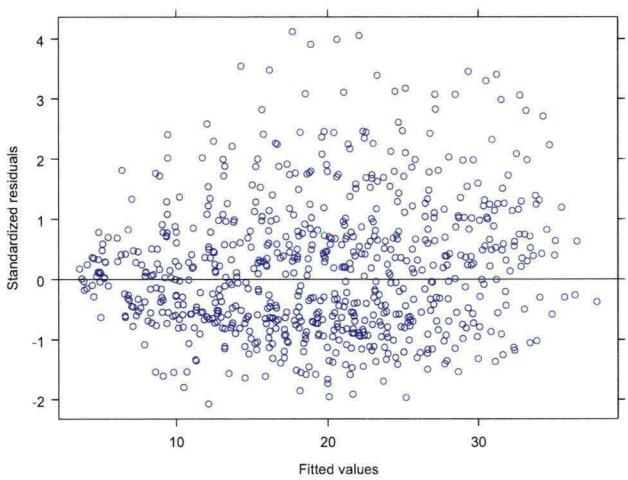


Figure 6.31 Scatter plot of model 6.86 standardised residuals versus fitted values (age 20 dataset

The results of the multiple regression analysis of the relationships between the random effects BLUPs from model 6.72 fitted to the age 20 dataset and the tree-level predictors appear in Table 6.41. The results are very similar to those of the age 15 dataset, although the strength of the relationships, as defined by adjusted $R^2$, are weaker. Again, between-tree variation appears to be manifested through the random effects associated with the parameters describing stem shape through the middle ($\beta_1$) and base of the stem ($\beta_3$). Stem shape bounded away from the tip ($\beta_2$) and the height of the join point ($\beta_4$) appear to be largely independent of tree-level influences.

Variable-form modelling using the reduced segmented model was conducted in the same manner as it was for the age 15 dataset. The optimum fixed effects specification was found to be identical. The results of the tests carried out to determine the optimum random effects specification for this model appear in Table 6.42. The optimum specification remained the same as that of the average-form version and appears in this table as model 6.79.

Table 6.41 OLS regression results predicting model 6.72 random effects BLUPs using tree-level variables - age 20 dataset. T-ratios for each parameter with associated p-value in brackets and adjusted $R^2$ values.

| BLUPs | u1 | u2 | u3 | u4 |
|---|---|---|---|---|
| Intercept | -3.68<br>(0.0005) | -0.80<br>(0.4265) | -4.30<br>(<.0001) | -0.17<br>(0.8673) |
| H | 3.21<br>(0.0022) | 0.36<br>(0.7223) | 2.97<br>(0.0044) | 0.24<br>(0.8097) |
| $C^{0.5}$ | 0.41<br>(0.6819) | 1.38<br>(0.1740) | 2.96<br>(0.0045) | -0.65<br>(0.5175) |
| $H*C^{0.5}$ | -0.45<br>(0.6563) | -0.03<br>(0.9773) | 1.33<br>(0.1902) | 1.07<br>(0.2877) |
| Adj. $R^2$ | 0.242 | 0.030 | 0.409 | 0.006 |

Table 6.42 Tests for significance of adjusting model 6.79 with alternative random effects - age 20 dataset.

| Model | Variance-Covariance Matrix | No. of Parms | AIC | BIC | logLike | Model test | L.Ratio | p.value |
|---|---|---|---|---|---|---|---|---|
| 6.79 | Block Diag. u1+u2,u0,u3,u4 | 14 | **1484.80** | **1558.09** | **-726.40** | | | |
| 6.81 | Diag. u0,u1,u2,u3,u4 | 13 | 1506.55 | 1566.10 | -740.27 | 6.79 vs 6.81 | 27.7490 | <.0001 |
| 6.87 | Diag. u0,u1,u2,u3 | 13 | 1525.99 | 1580.96 | -751.00 | 6.79 vs 6.87 | 49.1951 | <.0001 |
| 6.88 | Diag. u0,u1,u2,u4 | 13 | 1696.19 | 1751.16 | -836.09 | 6.79 vs 6.88 | 219.390 | <.0001 |
| 6.89 | Diag. u0,u1,u3,u4 | 13 | 1553.41 | 1608.38 | -764.70 | 6.79 vs 6.89 | 76.6097 | <.0001 |
| 6.85 | Diag. u0,u2,u3,u4 | 12 | 1526.75 | 1581.72 | -751.38 | 6.79 vs 6.85 | 49.9526 | <.0001 |

As was the case with the fit to the age 15 dataset, the diagnostic plots for this variable-form version of the reduced segmented model (model 6.79) were not distinguishable from those for the average-form version (model 6.72) and so are not shown. The parameter estimates for model 6.79 appear in Table 6.43. The performance of model 6.79 fitted to the age 20 dataset is described further in Chapter 7. Convergence of a gnls version of this model was rapid but the results were similarly strongly biased and the model abandoned.

Table 6.43 Model 6.79 parameter estimates - age 20 dataset.

```
Random effects:
Composite Structure: Blocked

    StdDev:   Correlation:

Block 1: (General positive-definite Structure)
u1    0.15687460      u1
u2    0.08909702  u2  0.736

Block 2:
u0    0.1336979

Block 3:
u3    1.372947

Block 4:
u4    0.4991890

Residual 0.3831441


Fixed effects:

   Value Std.Error  t-value p-value
a0 0.764692 0.0394893 19.36454 <.0001
a1 1.998920 0.3249065 6.15229 <.0001
b1 0.580581 0.0260001 22.32995 <.0001
b2 0.948511 0.0150096 63.19364 <.0001
b3 2.612772 0.1678534 15.56580 <.0001
b31 0.305352 0.0577675 5.28588 <.0001
b4 0.269657 0.0127681 21.11964 <.0001

Correlation:

    a0   a1   b1   b2   b3  b31
 a1 -0.873
 b1 -0.014 -0.040
 b2 -0.001 -0.066 0.815
 b3 0.063 -0.113 0.157 0.171
b31 -0.065 0.086 -0.064 -0.084 -0.888
 b4 0.031 -0.189 0.233 0.290 0.230 -0.123
```

## 6.5 Summary

This chapter has presented the development of stem profile models which employ tree height and local density in their formulation. Both mixed effects and generalized nonlinear modelling methods have been used to obtain parameter estimates. The lack of a precise estimate of diameter with which to transform the data to a relative scale has impeded the use of generalized nonlinear modelling methods in some circumstances and required the use of numerous random effects within the mixed effects modelling framework. Three previously published models have been adapted and applied to the data. A new model has been derived and applied. The performance and utility of these models is discussed in the following chapter.

*Chapter 7*

# Tree stem profile model evaluation

## 7.1 Introduction

The objective of the study presented in this chapter is to evaluate the models which were developed in the previous chapter. Model performance is evaluated by comparing their utility for predicting diameter and volume within relative height classes, total volume within total volume classes, and merchantable height within upper stem diameter classes. A discussion of model performance is then presented.

## 7.2 Model evaluation methods

Model performance was evaluated using the bias and precision statistics suggested by Kozak and Smith (1993). These were used to determine model utility in predicting the following metrics: diameter by relative height class, cumulative volume by relative height class, height to small end diameter by diameter class, cumulative volume to small end diameter by diameter class and, finally, total volume by total volume size class. The latter represents the assessment of between–tree model utility, while each of the former represent the assessment of within-tree model utility.

Relative height classes were defined to contain approximately similar numbers of observations. The range of relative height values in each class and number of observations per class in each dataset is presented in Table 7.1.

Table 7.1 Relative height class membership by dataset

| Age 15 dataset z range | z class | n | Age 20 dataset z range | z class | n |
|---|---|---|---|---|---|
| $z<0.025$ | 0.0125 | 70 | $z<0.0175$ | 0.0075 | 62 |
| $0.025 \leq z < 0.050$ | 0.0375 | 72 | $0.0175 \leq z < 0.0375$ | 0.0275 | 80 |
| $0.050 \leq z < 0.075$ | 0.0625 | 69 | $0.0375 \leq z < 0.0625$ | 0.05 | 56 |
| $0.075 \leq z < 0.125$ | 0.1 | 81 | $0.0625 \leq z < 0.125$ | 0.1 | 56 |
| $0.125 \leq z < 0.225$ | 0.2 | 64 | $0.125 \leq z < 0.225$ | 0.2 | 65 |
| $0.225 \leq z < 0.350$ | 0.3 | 61 | $0.225 \leq z < 0.350$ | 0.3 | 75 |
| $0.350 \leq z < 0.450$ | 0.4 | 56 | $0.350 \leq z < 0.450$ | 0.4 | 59 |
| $0.450 \leq z < 0.550$ | 0.5 | 57 | $0.450 \leq z < 0.550$ | 0.5 | 62 |
| $0.550 \leq z < 0.650$ | 0.6 | 56 | $0.550 \leq z < 0.650$ | 0.6 | 61 |
| $0.650 \leq z < 0.750$ | 0.7 | 51 | $0.650 \leq z < 0.750$ | 0.7 | 57 |
| $z \geq 0.750$ | 0.85 | 77 | $z \geq 0.750$ | 0.85 | 88 |
| | TOTAL | 714 | | TOTAL | 721 |

Diameter classes were used for estimation of merchantable height to an upper diameter limit and volume to an upper diameter limit. The classes were defined to contain observations measured at an above ground height of 3.3 metres or more. This is the current minimum log length used in the estate. Stump height was not accounted for as this varies with slope and the type of equipment used in harvest. The range of diameter values in each class and number of observations per class in each dataset is presented in Table 7.2.

Table 7.2 Diameter class membership by dataset. Observations are from upper fifty per cent of relative height only.

| diameter range (cm) | Diameter class | Age 15 dataset n | Age 20 dataset n |
|---|---|---|---|
| $6.25 < d$ | 5 | 66 | 33 |
| $6.25 \leq d < 8.75$ | 7.5 | 67 | 43 |
| $8.75 \leq d < 11.25$ | 10 | 68 | 46 |
| $11.25 \leq d < 13.25$ | 12.5 | 52 | 62 |
| | TOTAL | 253 | 184 |

Four total volume size classes were defined, comprising fifteen trees in each class for each dataset. Total actual, and estimated volume from each model, were calculated using the sectional volume calculation method presented in Chapter 4 (Bruce and Max 1990).

Bias was defined as the average deviation of predicted values from the actual observations. This is given by:

$$Bias = \frac{\sum_{i=1}^{n}\left(Y_i - \hat{Y}_i\right)}{n} . \tag{7.1}$$

Where:

$Y_i$ is the actual observation;

$\hat{Y}_i$ is the predicted value of the actual observation[1];

$n$ is the number of observations.

Precision was defined two ways.

The standardised estimated error (or residual variance), which is the penalised average squared deviation of predicted values from the actual observations, is given by:

$$SEE = \frac{\sum_{i=1}^{n}\left(Y_i - \hat{Y}_i\right)^2}{n-k} . \tag{7.2}$$

Where:

$SEE$ is the standardised estimated error;

$k$ is the number of parameters used in the model.

[1] The predictions for nlme fitted models are obtained using the estimated fixed effects parameters only.

The estimated coefficient of determination is given by:

$$I^2 = \frac{SS_y - SS_{res}}{SS_y}.$$

Where:

$$SS_{res} = \sum_{i=1}^{n} \left(Y_i - \hat{Y}_i\right)^2, \tag{7.3}$$

$$SS_Y = \sum_{i=1}^{n} \left(Y_i - \bar{Y}\right)^2, \tag{7.4}$$

$\bar{Y}$ is the average untransformed observation.

Since the estimated coefficient of determination is an unpenalised measure of fit, this was only calculated for whole-tree estimates of diameter and volume.

All prediction bias and SEE estimates were rounded to the nearest significant value. Diameter prediction bias and SEE estimates were rounded to the nearest 0.1 centimetres, which is equal to the precision of the diameter tape used in measurement. The precision of this measurement at breast height for trees of average breast height diameter drawn from the age 15 and age 20 datasets is equal to 0.49% and 0.38% respectively. The coefficient of determination for diameter prediction was therefore rounded to the nearest 0.05 for both datasets.

Other estimates were rounded to values that were calculated by propagation of variance estimates for total height and diameter measurement errors. First, nonlinear least squares were used to estimate the parameters of Max and Burkhart's (1976) polynomial model (see model 2.33). A single model was fitted to the combined age 15 and 20 datasets. Relative diameter squared was chosen as the dependent variable. The model displayed a coefficient of determination of 0.9505 and the residual error distribution was acceptable for the chosen purpose. This model was then used to propagate measurement errors in cumulative and total volume, and merchantable height.

Max and Burkhart's (1976) polynomial model may be rearranged to predict volume between any specified upper and lower diameter limit. Assuming the lower limit occurs at ground level, the volume prediction model is given by:

$$V = KD^2H\left(\frac{\beta_2}{3}\frac{h_u^3}{H^3} + \frac{\beta_1}{2}\frac{h_u^2}{H^2} - (\beta_1+\beta_2)\frac{h_u}{H} - \frac{\beta_3}{3}\left(\alpha_1 - \frac{h_u}{H}\right)^3 I_1\alpha_1^3 - \frac{\beta_4}{3}\left(\alpha_2 - \frac{h_u}{H}\right)^3 I_2\alpha_2^3\right) \tag{7.5}$$

Where:

$h_u$ is the specified upper height limit;

$$I_1 = 1, \text{when} \frac{h_u}{H} \le \alpha_1$$
$$= 0, \text{when} \frac{h_u}{H} > \alpha_1;$$
$$I_2 = 1, \text{when} \frac{h_u}{H} \le \alpha_2$$
$$= 0, \text{when} \frac{h_u}{H} > \alpha_2;$$

If the errors in total height and breast height diameter measurement are assumed to be independent, then they may be propagated to estimate cumulative volume measurement error by:

$$\sigma_V = \sqrt{\frac{\delta V}{\delta H}^2 \sigma_H^2 + \frac{\delta V}{\delta D}^2 \sigma_D^2} \tag{7.6}$$

Where:

$$\frac{\delta V}{\delta D} = 2KDH\left(\frac{\beta_2}{3}\frac{h_u^3}{H^3} + \frac{\beta_1}{2}\frac{h_u^2}{H^2} - (\beta_1+\beta_2)\frac{h_u}{H} - \frac{\beta_3}{3}\left(\alpha_1 - \frac{h_u}{H}\right)^3 I_1\alpha_1^3 - \frac{\beta_4}{3}\left(\alpha_2 - \frac{h_u}{H}\right)^3 I_2\alpha_2^3\right) \tag{7.7}$$

$$\frac{\delta V}{\delta H} = KD^2\left(\begin{array}{l}\left(\frac{\beta_2}{3}\frac{h_u^3}{H^3} + \frac{\beta_1}{2}\frac{h_u^2}{H^2} - (\beta_1+\beta_2)\frac{h_u}{H} - \frac{\beta_3}{3}\left(\alpha_2 - \frac{h_u}{H}\right)^3 I_1\alpha_1^3 - \frac{\beta_4}{3}\left(\alpha_2 - \frac{h_u}{H}\right)^3 I_2\alpha_2^3\right) - \\ \frac{h_u}{H}\left(\beta_1\frac{h_u}{H} + \beta_2\frac{h_u^2}{H^2} - (\beta_1+\beta_2) + \beta_3\left(\alpha_1 - \frac{h_u}{H}\right)^2 I_1 + \beta_4\left(\alpha_2 - \frac{h_u}{H}\right)^2 I_2\right)\end{array}\right) \tag{7.8}$$

$\sigma_H$ = 0.05 metres and $\sigma_D$ = 0.1 centimetres

Figure 7.1 presents a line plot depicting the estimated propagated error in cumulative volume prediction and the associated significant values versus relative height for trees of average total height and breast height diameter drawn from the age 15 and age 20 datasets. The estimated propagated error increases with the relative height of prediction. At and below 30% of total height, the prediction bias and SEE statistics were rounded to the nearest 1.25 and $2.5 \times 10^{-3}$ metres$^3$ for the age 15 and 20 datasets respectively. Above 30% of total height, they were rounded to the nearest 2.5 and $5 \times 10^{-3}$ metres$^3$ respectively. The total volume bias and SEE estimates were also rounded to these latter values. The propagated error for trees of average total height and breast height diameter drawn from the age 15 and age 20 datasets is equal to 1.03% and 0.80% respectively. The coefficient of determination was therefore rounded to the nearest 0.01 for both datasets.

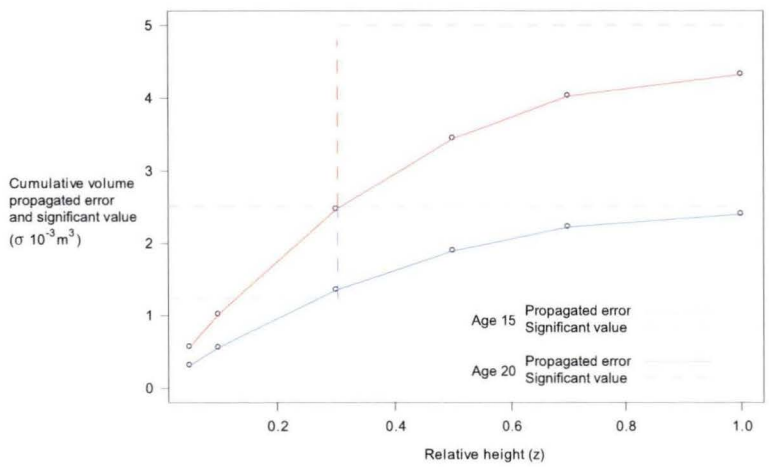


Figure 7.1 Estimated propagated error in cumulative volume prediction and associated significant values versus relative height for trees of average total height and breast height diameter drawn from the age 15 and age 20 datasets.

Max and Burkhart's (1976) polynomial model may also be rearranged to predict merchantable height to any specified upper diameter limit.

If the specified upper limit is assumed to occur at a relative height greater than the lower join point, then the merchantable height prediction model is given by:

$$h_m = H\frac{-B-\sqrt{B^2-4AC}}{2A} \tag{7.9}$$

Where:

$h_m$ is merchantable height,

$d_u$ is the specified diameter at merchantable height,

$$A = \beta_1 + P\beta_2\,, \tag{7.10}$$

$$B = \beta_0 + 2P\alpha_1\beta_2\,, \tag{7.11}$$

$$C = -\beta_0 - \beta_1 - \frac{d_u^{\,2}}{D^2} + P\alpha_1^{\,2}\beta_2\,, \tag{7.12}$$

$d_1$ is the estimated diameter at the upper join point $\left(h = \alpha_1 H\right)$,

$P = 1$, when $d_u \geq d_1$
$= 0$, when $d_u < d_1$.

And:

$$d_1 = D\sqrt{\beta_0\left(\alpha_1 - 1\right) + \beta_1\left(\alpha_1^{\,2} - 1\right)} \tag{7.13}$$

If the errors in total height and breast height diameter measurement are assumed to be independent, then they may be propagated to estimate merchantable height measurement error by:

$$\sigma_{h_m} = \sqrt{\frac{\delta h_m}{\delta H}^2 \sigma_H^2 + \frac{\delta h_m}{\delta D}^2 \sigma_D^2} \tag{7.14}$$

Where:

$$\frac{\delta h_m}{\delta H} = \frac{-B-\sqrt{B^2-4AC}}{2A} \tag{7.15}$$

$$\frac{\delta h_m}{\delta D} = H\frac{2d_u^{\,2}}{D^3}\left(B^2 - 4AC\right)^{-0.5} \tag{7.16}$$

$\sigma_H = 0.05$ metres and $\sigma_D = 0.1$ centimetres

Measurement errors averaged between 4.7 and 4.8 centimetres for the trees of average total height and breast height diameter in both datasets across the assessed range of upper diameter limits. They also varied through less than 0.5 centimetres in both datasets. The merchantable height estimates were therefore rounded to the nearest 5 centimetres in both datasets.

The small size of each dataset precluded subdivision into fit and prediction sets. Instead, cross validation was used to generate predictions (Snee 1977). Each dataset was randomly split into 6 sets (10 trees per set). The models were refitted without each set in turn, and the refitted parameter estimates used to generate predictions for each set in turn. Hence, predictions for all trees are derived from observations unused in model fitting.

To facilitate description, the developed models are referred to according to their functional form. Where the Kozak and trigonometric models behave in a similar manner they may be referred to as the variable-exponent models. Other model titles and the number assigned during model development appear in Table 7.3. Note that the term 'average-form' will only be used to describe models that use tree-level predictors to scale the base term only; while the term 'variable-form' will only be used to describe models that accommodate additional between-tree differences in stem form through the incorporation of additional tree-level predictors elsewhere within the model.

Table 7.3 Model number by dataset and model titles used in model assessment

| Fitting method | Age 15 dataset | | Age 20 dataset | Average- or variable-form | Model title | Abbreviated Model Title |
|---|---|---|---|---|---|---|
| | nlme | gnls | nlme | | | |
| Model number | 6.15 | NA | 6.20 | NA | Segmented polynomial | SegPoly |
| | 6.37 | 6.44 | 6.39 | Average- | Kozak | Kozak Av-form |
| | 6.46 | 6.56 | 6.51 | Variable- | Kozak | Kozak Var-form |
| | 6.52 | 6.60 | 6.57 | Average- | Trigonometric | Trig Av-form |
| | 6.61 | 6.62 | 6.63 | Variable- | Trigonometric | Trig Var-form |
| | 6.72 | 6.78 | 6.72 | Average- | Reduced segmented | RedSeg Av-form |
| | 6.79 | 6.85 | 6.79 | Variable- | Reduced segmented | RedSeg Var-form |

## 7.3 Results

The presentation of the results of the analysis of model performance is split by age class.

### 7.3.1 Age 15 dataset

#### *7.3.1.1 Within-tree prediction*

Table 7.4 presents bias estimates for the prediction of diameter. All models behave relatively poorly in the base of the stem, displaying biases between -1 and 2.1 centimetres in either the 0.0125 or 0.0375 relative height class. In other regions of the stem, the segmented polynomial model and the gnls fitted reduced segmented models display pronounced positive bias, particularly below 0.5 of total height, which sums to an overall bias in excess of 0.5 centimetres for the former and 0.8 centimetres for the latter. The nlme fitted variable-exponent models display smaller overall biases of -0.2 centimetres, while the nlme fitted reduced segmented models and the gnls fitted variable-exponent models display overall biases that are smaller again, at or less than 0.1 centimetres. Within relative height classes these latter models behave very well, displaying approximate biases generally less than 0.2 centimetres in the relative height classes above the two classes in the stem base. The average-form versions of the nlme fitted models are generally more biased than their variable-form counterparts. The gnls fitted average- and variable-form variable-exponent models are similar, while the average-form version of gnls fitted reduced segmented model displays less bias than its variable-form counterpart. These results overall point to the variable-form versions of the nlme fitted reduced segmented model and the gnls fitted variable-exponent models as being optimal.

Estimates of standardised error (SEE) for the prediction of diameter are presented in Table 7.5. SEE estimates for all models decrease with increasing relative height class from approximate values of 4.2 to 5.1 centimetres down to values between 0.8 and 1.0 centimetres. The gnls fitted models generally display slightly lower SEE estimates than their nlme fitted counterparts. Variable-form models generally display lower SEE values than their average-form counterparts in the lower third of relative height, with the differences between average- and variable-form being more pronounced in the nlme fitted models than in the gnls fitted models. Overall, the

average SEE estimates range between approximately 2.5 and 2.8 centimetres, with estimated coefficients of determination ($I^2$) ranging between 0.875 and 0.895. The gnls fitted models do not display lower SEE values or higher $I^2$ values overall than their nlme fitted counterparts, suggesting the lower SEE estimates in individual relative height classes are attributable to the better parsimony of the gnls fitted models. Average-form, nlme fitted models consistently display larger SEE and smaller $I^2$ estimates than their variable-form counterparts. Only the average-form gnls fitted reduced segmented model displays a smaller $I^2$ estimate than its variable-form counterpart. These results suggest preference for the nlme fitted variable-form models and the gnls fitted variable-exponent models.

Table 7.6 presents cumulative volume prediction bias estimates. The segmented polynomial model and the gnls fitted reduced segmented models show a trend of increasing positive bias from low in the stem toward the tip. The former model displays an average bias of approximately $7.9 \times 10^{-3}$ cubic metres, which amounts to a bias of $15.6 \times 10^{-3}$ cubic metres in total, while the latter display average biases between $9.1 \times 10^{-3}$ and $10.7 \times 10^{-3}$ cubic metres, amounting to biases between $16.9 \times 10^{-3}$ and $19.8 \times 10^{-3}$ cubic metres in total. The Kozak models also display notable bias, with the nlme fitted versions tending to negative bias in the upper half of the stem, while the gnls fitted versions tend to positive bias throughout. In comparison, the other models are all relatively unbiased. Variable-form models are slightly more biased on average and in total than their average-form counterparts, with variable-form models generally only displaying lower biases in the lower third of the stem. These results point to the trigonometric models and the nlme fitted reduced segmented models as being optimum.

The SEE estimates for the prediction of cumulative volume appear in Table 7.7. The trend is one of increasing SEE with increasing cumulative volume from stem butt to tip. The SEE estimates range from approximate values of $3.75 \times 10^{-3}$ to $5.00 \times 10^{-3}$ cubic metres in the base of the stem, accumulating to approximate values between $62.5 \times 10^{-3}$ and $70.0 \times 10^{-3}$ cubic metres for total stem volume. The gnls fitted models generally outperform the nlme fitted models within relative height classes. Overall, they also outperform the nlme fitted models with respect to SEE but the differences are not apparent in terms of $I^2$. $I^2$ values for cumulative volume prediction are slightly larger than those for diameter prediction, but their range is slightly smaller. The best $I^2$ value is recorded for the gnls fitted version of the variable-form reduced segmented model, with the differences between other models subsumed by measurement error. The nlme fitted versions of the average–form models are consistently poorer performers than their variable-form

counterparts, particularly in the lower half of the stem. The results of variable-form modelling using gnls are more mixed, with the average-from versions of the variable-exponent model generally outperforming their variable-form counterparts while the opposite is the case for the gnls fitted reduced segmented models. The segmented polynomial model is generally equivalent to the nlme fitted, average-form models. Overall, these results suggest preference for gnls fitted models.

Table 7.8 presents bias estimates for the prediction of merchantable height by diameter class. Biases range between values of -0.45 and 0.30 metres. The segmented polynomial model and the gnls fitted reduced segmented models generally display positive bias that is quite varied in its range. The nlme fitted variable-exponent and gnls variable-form variable-exponent models are generally negatively biased. The other models are generally unbiased, and the range of bias estimates between classes is smaller. Average- and variable-form models are often different from each other, but these differences are not consistent across classes. The gnls fitted versions of the variable-exponent models generally show the smallest range in bias estimates across classes. The results suggest preference for these models.

The SEE estimates for the prediction of merchantable height by diameter class appear in Table 7.9. The trend is generally one of increasing SEE estimates with diameter class, from approximate values between 0.55 and 0.70 metres to approximate values between 1.15 and 1.40 metres. As is the case in the bias estimate, neither average- or variable-form versions of any nlme-fitted model is appreciably superior. In contrast, the gnls fitted average-form variable-exponent models are consistently superior to their variable-form counterparts. The gnls fitted version of the variable-form reduced segmented model performs poorly throughout, while the segmented polynomial performs poorly in the largest diameter class only. The results again suggest preference for the gnls fitted variable-exponent models, but here the preference is for the average-form versions.

Bias estimates for the prediction of cumulative volume by diameter class are presented in Table 7.10. Both the segmented polynomial model and the gnls fitted reduced segmented models display consistent positive bias. The latter is more biased in its average-form specification than its variable-form specification. All other models display equivalent or lower biases in their variable-form specifications. The nlme fitted variable-exponent models are somewhat negatively biased, while all other models generally behave well across diameter classes. The result suggest preference for these latter models: the gnls fitted variable-exponent models and the nlme fitted reduced segmented models.

Table 7.11 presents SEE estimates for the prediction of cumulative volume by diameter class. Estimates are generally somewhat lower for the gnls fitted models, reflecting their parsimony. However the differences are rather minor. Variable-form modelling only consistently leads to reductions in SEE for the nlme fitted reduced segmented model, in all other cases, the effects of variable-from modelling are not consistent. The results do not suggest strong preference for any model.

#### *7.3.1.2 Between-tree prediction*

Estimates of between-stem total volume prediction bias appear in Table 7.12. While the average total volumes for the total volume classes 1 to 4 range from $85.0 \times 10^{-3}$ to $475.5 \times 10^{-3}$ cubic metres, the prediction biases range between -35.0 and $67.5 \times 10^{-3}$ cubic metres. Larger biases are apparent in class 1 and 4 than in classes 2 and 3. The models are evidently all incapable of predicting the full range of observations in the data so biases are larger for trees with total volumes more distant from the population mean. Within that bias range, some models behave better than others. Perhaps the best performer is the nlme fitted variable-form reduced segmented model, which displays approximate biases ranging from between $-17.5 \times 10^{-3}$ cubic metres for class 1, to $32.5 \times 10^{-3}$ cubic metres for class 4, with approximate biases of $-2.5 \times 10^{-3}$ cubic metres for classes 2 and 3. The segmented polynomial model is quite acceptable for classes 1 to 3 but is inadequate for describing volume in class 4 trees. All of the gnls fitted models also show large positive prediction biases in class 4. Variable-form modelling leads to generally consistent reductions in bias in the nlme fitted reduced segmented models and the gnls fitted variable-exponent models. In other cases, the effects of variable-form modelling are mixed. In particular, nlme fitted variable-form variable-exponent models show large negative biases in class 3. These biases are offset by improvements from large negative biases in average-form versions of these models in class 1.

Table 7.4 Diameter prediction bias by relative height class for the age 15 dataset (cm).

| z class | n | average diameter | **Model Form Method** | SegPoly nlme | Kozak av nlme | Kozak var nlme | Trig av nlme | Trig var nlme | RedSeg av nlme | RedSeg var nlme | Kozak av gnls | Kozak var gnls | Trig av gnls | Trig var gnls | RedSeg av gnls | RedSeg var gnls |
|---|---|---|---|---|---|---|---|---|---|---|---|---|---|---|---|---|
| 0.0125 | 70 | 26.1 | | 1.2 | 0.2 | 0.1 | 0.3 | **0.0** | 0.5 | 0.4 | 0.2 | 0.3 | **0.0** | 0.1 | 1.8 | 2.1 |
| 0.0375 | 72 | 22.6 | | -0.3 | -0.9 | -0.9 | -0.9 | -0.8 | -1.0 | -0.9 | -0.7 | -0.6 | -0.9 | -0.7 | **0.2** | 0.4 |
| 0.0625 | 69 | 21.7 | | 0.5 | -0.2 | -0.3 | -0.1 | -0.2 | -0.1 | **0.0** | -0.1 | -0.1 | -0.2 | -0.1 | 0.8 | 0.9 |
| 0.1 | 81 | 19.2 | | 0.7 | -0.4 | -0.4 | -0.2 | -0.3 | **0.1** | **0.1** | -0.2 | -0.2 | -0.2 | **-0.1** | 0.7 | 0.9 |
| 0.2 | 64 | 18.0 | | 0.7 | -0.1 | **0.0** | **0.0** | **0.0** | 0.2 | 0.3 | 0.1 | 0.2 | 0.1 | 0.1 | 0.6 | 1.0 |
| 0.3 | 61 | 16.5 | | 0.6 | **0.0** | 0.1 | **0.0** | **0.0** | 0.2 | 0.3 | 0.3 | 0.4 | 0.1 | 0.1 | 0.6 | 0.8 |
| 0.4 | 56 | 14.9 | | 0.5 | -0.1 | **0.0** | -0.1 | -0.1 | 0.1 | 0.1 | 0.3 | 0.3 | 0.1 | **0.0** | 0.5 | 0.6 |
| 0.5 | 57 | 12.5 | | 0.3 | -0.3 | -0.2 | -0.3 | -0.2 | -0.1 | -0.1 | 0.1 | **0.0** | **0.0** | -0.1 | 0.3 | 0.3 |
| 0.6 | 56 | 10.5 | | 0.2 | -0.3 | -0.3 | -0.2 | -0.1 | -0.1 | -0.1 | **0.0** | **0.0** | **0.0** | **0.0** | 0.2 | 0.3 |
| 0.7 | 51 | 8.2 | | 0.2 | -0.2 | -0.2 | -0.1 | **0.0** | -0.1 | -0.1 | 0.1 | **0.0** | 0.1 | **0.0** | 0.2 | 0.3 |
| 0.85 | 77 | 5.4 | | 0.4 | **0.1** | 0.2 | **0.1** | **0.1** | 0.2 | 0.2 | 0.3 | 0.2 | 0.2 | **0.1** | 0.3 | 0.5 |
| TOTAL | 714 | 15.9 | | 0.5 | -0.2 | -0.2 | -0.2 | -0.2 | **0.0** | **0.0** | **0.0** | **0.0** | -0.1 | -0.1 | 0.6 | 0.8 |

Table 7.5 Diameter prediction SEE by relative height class for the age 15 dataset (cm).

| z class | n | diameter std.dev. | **Model Form Method** | SegPoly nlme | Kozak av nlme | Kozak var nlme | Trig av nlme | Trig var nlme | RedSeg av nlme | RedSeg var nlme | Kozak av gnls | Kozak var gnls | Trig av gnls | Trig var gnls | RedSeg av gnls | RedSeg var gnls |
|---|---|---|---|---|---|---|---|---|---|---|---|---|---|---|---|---|
| 0.0125 | 70 | 7.2 | | 4.3 | 4.8 | 4.3 | 5.1 | 4.4 | 4.8 | 4.4 | 4.3 | **4.2** | 4.4 | **4.2** | 4.9 | 4.6 |
| 0.0375 | 72 | 5.9 | | 3.6 | 3.9 | 3.8 | 4.0 | 3.8 | 3.9 | 3.8 | 3.6 | 3.6 | 3.7 | 3.7 | **3.4** | **3.4** |
| 0.0625 | 69 | 5.4 | | 3.2 | 3.5 | 3.3 | 3.7 | 3.3 | 3.6 | 3.5 | 3.2 | **3.1** | 3.2 | 3.2 | 3.4 | 3.2 |
| 0.1 | 81 | 5.2 | | 3.6 | 3.7 | 3.6 | 3.8 | 3.5 | 3.8 | 3.8 | **3.4** | **3.4** | **3.4** | **3.4** | 3.5 | 3.5 |
| 0.2 | 64 | 4.6 | | 2.8 | 2.7 | 2.7 | 2.8 | 2.7 | 2.9 | 2.9 | **2.5** | 2.6 | 2.6 | 2.6 | 2.7 | 2.8 |
| 0.3 | 61 | 4.1 | | 2.3 | 2.3 | 2.2 | 2.4 | 2.2 | 2.3 | 2.4 | **2.1** | 2.2 | **2.1** | **2.1** | 2.2 | 2.3 |
| 0.4 | 56 | 3.5 | | 1.9 | 1.9 | 1.9 | 1.9 | 1.9 | 1.9 | 1.9 | **1.8** | **1.8** | **1.8** | **1.8** | **1.8** | 1.9 |
| 0.5 | 57 | 2.9 | | 1.5 | 1.6 | 1.6 | 1.6 | 1.6 | 1.5 | 1.6 | 1.5 | 1.5 | 1.5 | 1.5 | **1.4** | 1.5 |
| 0.6 | 56 | 2.3 | | 1.3 | 1.4 | 1.4 | 1.4 | 1.4 | 1.3 | 1.3 | 1.3 | 1.3 | 1.3 | 1.3 | **1.2** | 1.3 |
| 0.7 | 51 | 2.0 | | 1.1 | 1.1 | 1.2 | 1.1 | 1.2 | 1.1 | 1.1 | 1.1 | 1.1 | 1.1 | 1.1 | **1.0** | 1.1 |
| 0.85 | 77 | 1.5 | | 1.0 | 0.9 | 0.9 | **0.8** | **0.8** | 0.9 | 0.9 | 0.9 | **0.8** | 0.9 | **0.8** | 0.9 | 1.0 |
| Average | 714 | 9.0 | | **2.5** | 2.6 | **2.5** | 2.8 | **2.5** | 2.7 | **2.5** | **2.5** | **2.5** | **2.5** | **2.5** | 2.6 | 2.6 |
| Isqrd | | | | **0.895** | 0.885 | **0.895** | 0.875 | **0.895** | 0.880 | **0.895** | **0.895** | **0.895** | **0.895** | **0.895** | 0.885 | 0.890 |

Table 7.6 Cumulative volume prediction bias by relative height class for the age 15 dataset $(10^{-3}m^3)$

| z class | n | average cum.volume | **Model Form** **Method** | SegPoly nlme | Kozak av nlme | Kozak var nlme | Trig av nlme | Trig var nlme | RedSeg av nlme | RedSeg var nlme | Kozak av gnls | Kozak var gnls | Trig av gnls | Trig var gnls | RedSeg av gnls | RedSeg var gnls |
|---|---|---|---|---|---|---|---|---|---|---|---|---|---|---|---|---|
| 0.0125 | 70 | 11.25 | | 1.25 | 1.25 | **0.00** | 1.25 | **0.00** | 1.25 | 1.25 | 1.25 | 1.25 | **0.00** | **0.00** | 2.50 | 2.50 |
| 0.0375 | 72 | 31.25 | | **1.25** | **-1.25** | **-1.25** | **-1.25** | **-1.25** | **-1.25** | **-1.25** | **-1.25** | **-1.25** | **-1.25** | **-1.25** | 2.50 | 2.50 |
| 0.0625 | 69 | 48.75 | | 2.50 | **0.00** | **0.00** | 1.25 | **0.00** | 1.25 | 1.25 | **0.00** | **0.00** | **0.00** | **0.00** | 5.00 | 5.00 |
| 0.1 | 81 | 60.00 | | 3.75 | 1.25 | -1.25 | 1.25 | **0.00** | 1.25 | 1.25 | 1.25 | 1.25 | **0.00** | **0.00** | 6.25 | 6.25 |
| 0.2 | 64 | 110.00 | | 7.50 | -1.25 | -2.50 | **0.00** | -1.25 | **0.00** | **0.00** | **0.00** | **0.00** | **0.00** | -1.25 | 7.50 | 10.00 |
| 0.3 | 61 | 156.25 | | 12.50 | 1.25 | -1.25 | 2.50 | **0.00** | 2.50 | 3.75 | 3.75 | 3.75 | 2.50 | 1.25 | 12.50 | 15.00 |
| 0.4 | 56 | 200.0 | | 12.5 | **0.0** | -2.5 | 2.5 | **0.0** | 2.5 | 2.5 | 2.5 | 5.0 | 2.5 | **0.0** | 15.0 | 17.5 |
| 0.5 | 57 | 217.5 | | 10.0 | -5.0 | -5.0 | -2.5 | -5.0 | -2.5 | -2.5 | **0.0** | **0.0** | -2.5 | -2.5 | 10.0 | 15.0 |
| 0.6 | 56 | 237.5 | | 12.5 | -5.0 | -5.0 | -2.5 | -5.0 | -2.5 | **0.0** | **0.0** | 2.5 | -2.5 | -2.5 | 12.5 | 15.0 |
| 0.7 | 51 | 247.5 | | 12.5 | -2.5 | -5.0 | -2.5 | -2.5 | **0.0** | **0.0** | 2.5 | 2.5 | **0.0** | **0.0** | 15.0 | 17.5 |
| 0.85 | 77 | 255.0 | | 15.0 | -5.0 | -5.0 | **0.0** | -2.5 | -2.5 | -2.5 | 2.5 | 5.0 | **0.0** | **0.0** | 15.0 | 17.5 |
| TOTAL | 714 | 280.0 | | 15.0 | -2.5 | -2.5 | **0.0** | -2.5 | **0.0** | 2.5 | 5.0 | 5.0 | 2.5 | 2.5 | 17.5 | 20.0 |
| AVERAGE | | 137.5 | | 7.5 | -2.5 | -2.5 | **0.0** | -2.5 | **0.0** | **0.0** | 2.5 | 2.5 | **0.0** | **0.0** | 10.0 | 10.0 |

Table 7.7 Cumulative volume prediction SEE by relative height class for the age 15 dataset $(10^{-3}m^3)$

| z class | n | cum.volume std.dev. | **Model Form Method** | SegPoly nlme | Kozak av nlme | Kozak var nlme | Trig av nlme | Trig var nlme | RedSeg av nlme | RedSeg var nlme | Kozak av gnls | Kozak var gnls | Trig av gnls | Trig var gnls | RedSeg av gnls | RedSeg var gnls |
|---|---|---|---|---|---|---|---|---|---|---|---|---|---|---|---|---|
| 0.0125 | 70 | 11.25 | | 5.00 | 5.00 | **3.75** | 5.00 | **3.75** | 5.00 | **3.75** | **3.75** | **3.75** | **3.75** | **3.75** | 5.00 | 5.00 |
| 0.0375 | 72 | 21.25 | | **10.00** | **10.00** | **10.00** | **10.00** | **10.00** | **10.00** | **10.00** | **10.00** | **10.00** | **10.00** | **10.00** | **10.00** | **10.00** |
| 0.0625 | 69 | 27.50 | | **13.75** | 15.00 | **13.75** | 15.00 | **13.75** | 15.00 | 13.75 | **13.75** | **13.75** | **13.75** | **13.75** | 15.00 | **13.75** |
| 0.1 | 81 | 40.00 | | 21.25 | 22.50 | 21.25 | 22.50 | 21.25 | 22.50 | 21.25 | 21.25 | **20.00** | 21.25 | 21.25 | 21.25 | 21.25 |
| 0.2 | 64 | 73.75 | | 33.75 | 35.00 | 33.75 | 36.25 | 33.75 | 33.75 | 33.75 | **32.50** | **32.50** | **32.50** | **32.50** | **32.50** | **32.50** |
| 0.3 | 61 | 95.00 | | 47.50 | 48.75 | 46.25 | 51.25 | 46.25 | 48.75 | 47.50 | **45.00** | **45.00** | **45.00** | **45.00** | 46.25 | **45.00** |
| 0.4 | 56 | 115.0 | | 57.5 | 57.5 | 57.5 | 60.0 | 57.5 | 57.5 | 57.5 | **55.0** | **55.0** | **55.0** | **55.0** | **55.0** | **55.0** |
| 0.5 | 57 | 132.5 | | 57.5 | 57.5 | 60.0 | 62.5 | 60.0 | 57.5 | 57.5 | **55.0** | **55.0** | **55.0** | **57.5** | **55.0** | **55.0** |
| 0.6 | 56 | 132.5 | | 62.5 | 62.5 | 62.5 | 65.0 | 62.5 | 62.5 | 62.5 | **57.5** | 60.0 | 60.0 | 60.0 | **57.5** | 60.0 |
| 0.7 | 51 | 152.5 | | 67.5 | 70.0 | 67.5 | 75.0 | 67.5 | 70.0 | 70.0 | **62.5** | 65.0 | **62.5** | 65.0 | 65.0 | **62.5** |
| 0.85 | 77 | 155.0 | | 65.0 | 62.5 | 65.0 | 62.5 | 65.0 | 62.5 | 62.5 | 62.5 | 62.5 | 62.5 | 65.0 | **60.0** | 62.5 |
| TOTAL | 714 | 155.0 | | 67.5 | 67.5 | 67.5 | 70.0 | 67.5 | 67.5 | 67.5 | **62.5** | 65.0 | 65.0 | 65.0 | 65.0 | 65.0 |
| Isqrd | | | | 0.91 | 0.91 | 0.91 | 0.91 | 0.91 | 0.91 | 0.91 | 0.91 | 0.91 | 0.91 | 0.91 | 0.91 | **0.92** |

Table 7.8 Merchantable height prediction bias by diameter class for the age 15 dataset (m).

| Diameter class | n | average m.height | **Model Form** | SegPoly | Kozak av | Kozak var | Trig av | Trig var | RedSeg av | RedSeg var | Kozak av | Kozak var | Trig av | Trig var | RedSeg av | RedSeg var |
|---|---|---|---|---|---|---|---|---|---|---|---|---|---|---|---|---|
| | | | **Method** | nlme | nlme | nlme | nlme | nlme | nlme | nlme | gnls | gnls | gnls | gnls | gnls | gnls |
| 5.0 | 66 | 12.20 | | 0.20 | -0.05 | -0.05 | -0.10 | -0.10 | **0.00** | 0.05 | 0.10 | -0.05 | 0.05 | -0.10 | 0.15 | 0.30 |
| 7.5 | 67 | 10.25 | | **-0.05** | -0.40 | -0.30 | -0.40 | -0.30 | -0.25 | -0.25 | -0.15 | -0.25 | -0.15 | -0.25 | **-0.05** | 0.15 |
| 10.0 | 68 | 8.60 | | 0.20 | -0.30 | -0.15 | -0.30 | -0.15 | -0.10 | -0.10 | 0.05 | -0.05 | **0.00** | -0.05 | 0.20 | 0.45 |
| 12.5 | 52 | 7.80 | | **0.05** | -0.45 | -0.25 | -0.45 | -0.25 | -0.20 | -0.25 | -0.15 | -0.10 | -0.20 | -0.15 | 0.10 | 0.20 |

Table 7.9 Merchantable height prediction bias by diameter class for the age 15 dataset (m).

| Diameter class | n | m.height std.dev. | **Model Form** | SegPoly | Kozak av | Kozak var | Trig av | Trig var | RedSeg av | RedSeg var | Kozak av | Kozak var | Trig av | Trig var | RedSeg av | RedSeg var |
|---|---|---|---|---|---|---|---|---|---|---|---|---|---|---|---|---|
| | | | **Method** | nlme | nlme | nlme | nlme | nlme | nlme | nlme | gnls | gnls | gnls | gnls | gnls | gnls |
| 5.0 | 66 | 1.80 | | 0.65 | 0.60 | 0.65 | 0.60 | 0.65 | 0.60 | 0.60 | **0.55** | 0.60 | **0.55** | 0.60 | 0.60 | 0.70 |
| 7.5 | 67 | 1.85 | | 0.90 | 1.00 | 0.95 | 1.05 | 0.95 | 0.95 | 0.95 | **0.85** | 0.90 | **0.85** | 0.90 | **0.85** | 0.90 |
| 10.0 | 68 | 1.70 | | 1.25 | 1.20 | 1.25 | 1.25 | 1.20 | 1.20 | 1.20 | **1.15** | 1.20 | **1.15** | 1.20 | 1.20 | 1.40 |
| 12.5 | 52 | 1.70 | | 1.30 | 1.30 | 1.35 | 1.30 | 1.35 | 1.30 | 1.30 | **1.15** | 1.25 | 1.20 | 1.30 | 1.25 | 1.40 |

Table 7.10 Cumulative volume prediction bias by diameter class for the age 15 dataset $(10^{-3}m^3)$

| Diameter class | n | average cum.vol. | **Model Form** **Method** | SegPoly nlme | Kozak av nlme | Kozak var nlme | Trig av nlme | Trig var nlme | RedSeg av nlme | RedSeg var nlme | Kozak av gnls | Kozak var gnls | Trig av gnls | Trig var gnls | RedSeg av gnls | RedSeg var gnls |
|---|---|---|---|---|---|---|---|---|---|---|---|---|---|---|---|---|
| 5.0 | 66 | 210.0 | | **5.0** | -15.0 | -12.5 | -12.5 | -12.5 | -10.0 | -7.5 | -7.5 | **-5.0** | -10.0 | -7.5 | **5.0** | 10.0 |
| 7.5 | 67 | 225.0 | | 10.0 | -7.5 | -7.5 | -5.0 | -5.0 | -2.5 | -2.5 | **0.0** | **0.0** | -2.5 | -2.5 | 12.5 | 15.0 |
| 10.0 | 68 | 197.5 | | 7.5 | -10.0 | -7.5 | -7.5 | -7.5 | -5.0 | -2.5 | -2.5 | **0.0** | -5.0 | -2.5 | 10.0 | 12.5 |
| 12.5 | 52 | 230.0 | | 12.5 | -2.5 | -5.0 | 0.0 | -2.5 | 0.0 | 0.0 | 2.5 | 2.5 | 0.0 | 0.0 | 12.5 | 15.0 |

Table 7.11 Cumulative volume prediction SEE by diameter class for the age 15 dataset $(10^{-3}m^3)$

| Diameter class | n | cum.vol. std.dev. | **Model Form** **Method** | SegPoly nlme | Kozak av nlme | Kozak var nlme | Trig av nlme | Trig var nlme | RedSeg av nlme | RedSeg var nlme | Kozak av gnls | Kozak var gnls | Trig av gnls | Trig var gnls | RedSeg av gnls | RedSeg var gnls |
|---|---|---|---|---|---|---|---|---|---|---|---|---|---|---|---|---|
| 5.0 | 66 | 147.5 | | 52.5 | 55.0 | 55.0 | 55.0 | 55.0 | 52.5 | 50.0 | 50.0 | 52.5 | 50.0 | 52.5 | **47.5** | **47.5** |
| 7.5 | 67 | 155.0 | | 65.0 | 65.0 | 65.0 | 67.5 | 65.0 | 65.0 | 62.5 | 62.5 | 62.5 | 62.5 | 62.5 | 62.5 | **60.0** |
| 10.0 | 68 | 120.0 | | 50.0 | 52.5 | 55.0 | 52.5 | 52.5 | 52.5 | 50.0 | 50.0 | 50.0 | 50.0 | 52.5 | **47.5** | 50.0 |
| 12.5 | 52 | 145.0 | | 62.5 | 65.0 | 62.5 | 67.5 | 62.5 | 65.0 | 60.0 | 57.5 | 60.0 | 57.5 | 60.0 | 60.0 | 57.5 |

The SEE estimates for between-stem total volume prediction appear in Table 7.13. There is an increase in SEE estimates with increasing total volume class, from values between $27.5 \times 10^{-3}$ and $52.5 \times 10^{-3}$ cubic metres, through to values between $80.0 \times 10^{-3}$ and $92.5 \times 10^{-3}$ cubic metres. This increase is in line with increases in the standard deviation of within-class total volume. The nlme fitted average-form variable-exponent models are appreciably worse than their variable-form counterparts in class 1 and otherwise near equivalent. The segmented polynomial model, the gnls fitted average-form Kozak model, and the gnls fitted reduced segmented models all perform poorly in class 4. All the other models perform in a similar manner. Thus, the results suggest preference for the nlme fitted variable-form variable-exponent models, the nlme fitted reduced segmented models and the gnls fitted variable-exponent models.

## 7.3.2 Age 20 dataset

### *7.3.2.1 Within-tree prediction*

The age 20 dataset bias estimates for the prediction of diameter within relative height classes are presented in Table 7.14. The segmented polynomial model and the reduced segmented models behave poorly in the smallest two relative height classes, with biases ranging between -0.5 and 0.5 centimetres. The variable-exponent models display biases in this stem region of 0.2 centimetres or less. All models behave remarkably well throughout the rest of the stem, displaying biases of 0.2 centimetres or less in all but one case. There are no appreciable differences between average- and variable-form models. Overall, the biases are smaller than those recorded for the age 15 dataset, with all models except the variable-form reduced segmented models displaying overall biases of magnitude less than the measurement precision. The results do not indicate preference for any particular model.

SEE estimates for the prediction of diameter within relative height classes are presented in Table 7.15. As was the case for the age 15 dataset, the magnitude of the SEE estimates for all models decreases with increasing relative height class. The SEE estimates are generally larger, as might be expected given the generally larger diameter observations within each class. The differences between models however, are smaller than those for the age 15 dataset.

Table 7.12 Total volume prediction bias by total volume class for the age 15 dataset $(10^{-3}m^3)$

| t. volume class | n | average t.volume | **Model Form** | SegPoly | Kozak | Kozak | Trig | Trig | RedSeg | RedSeg | Kozak | Kozak | Trig | Trig | RedSeg | RedSeg |
|---|---|---|---|---|---|---|---|---|---|---|---|---|---|---|---|---|
| | | | | | av | var | av | var | av | var | av | var | av | var | av | var |
| | | | **Method** | nlme | nlme | nlme | nlme | nlme | nlme | nlme | gnls | gnls | gnls | gnls | gnls | gnls |
| 1 | 15 | 85.0 | | -7.5 | -30.0 | -17.5 | -35.0 | -20.0 | -20.0 | -17.5 | -17.5 | -17.5 | -17.5 | -17.5 | -10.0 | **2.5** |
| 2 | 15 | 187.5 | | 10.0 | -12.5 | -15.0 | -12.5 | -15.0 | -5.0 | **-2.5** | -5.0 | **-2.5** | -10.0 | -7.5 | 12.5 | 17.5 |
| 3 | 15 | 292.5 | | 10.0 | -5.0 | -25.0 | 5.0 | -20.0 | -5.0 | **-2.5** | -10.0 | -7.5 | -17.5 | -12.5 | 17.5 | 12.5 |
| 4 | 15 | 457.5 | | 65.0 | 35.0 | 40.0 | 42.5 | 42.5 | **32.5** | **32.5** | 57.5 | 50.0 | 50.0 | 45.0 | 65.0 | 67.5 |

Table 7.13 Total volume prediction SEE by total volume class for the age 15 dataset $(10^{-3}m^3)$

| t.volume class | n | t.volume std.dev. | **Model Form** | SegPoly | Kozak | Kozak | Trig | Trig | RedSeg | RedSeg | Kozak | Kozak | Trig | Trig | RedSeg | RedSeg |
|---|---|---|---|---|---|---|---|---|---|---|---|---|---|---|---|---|
| | | | | | av | var | av | var | av | var | av | var | av | var | av | var |
| | | | **Method** | nlme | nlme | nlme | nlme | nlme | nlme | nlme | gnls | gnls | gnls | gnls | gnls | gnls |
| 1 | 15 | 30.0 | | 32.5 | 45.0 | 37.5 | 52.5 | 40.0 | 40.0 | 37.5 | 35.0 | 35.0 | 35.0 | 37.5 | 32.5 | **27.5** |
| 2 | 15 | 30.0 | | **55.0** | 62.5 | 60.0 | 62.5 | 60.0 | 60.0 | 60.0 | **55.0** | 57.5 | 57.5 | 57.5 | **55.0** | **55.0** |
| 3 | 15 | 25.0 | | 77.5 | 77.5 | 77.5 | 80.0 | 77.5 | **75.0** | **75.0** | **75.0** | 77.5 | 77.5 | 77.5 | **75.0** | **75.0** |
| 4 | 15 | 117.5 | | 92.5 | **80.0** | **80.0** | 82.5 | **80.0** | 85.0 | 85.0 | 87.5 | 82.5 | 85.0 | **80.0** | 90.0 | 90.0 |

The SEE estimates range from 5.6 to 5.8 centimetres down to values of 1.3 and 1.4 centimetres. Overall, the models are indistinguishable, displaying average SEE estimates of 3.3 centimetres and $I^2$ estimates of 0.865. Within relative height classes, the average-form models are generally equivalent or better than their variable-form counterparts. For example, the variable-form Kozak model displays SEE values 0.1 centimetres larger than the average-form version in six of the 11 relative height classes. These results suggest variable-form modelling is not supported by the available data. The segmented model behaves more poorly in the lower half of the stem than other models. The results indicate that average-form models are preferred.

The bias estimates for the prediction of cumulative volume within relative height classes appear in Table 7.16. All models display an appreciable positive bias above the lowest relative height class. These biases are larger than those recorded for the age 15 dataset and this may in part reflect the fact that average cumulative volumes within each class are substantially larger. Biases range from $2.5 \times 10^{-3}$ cubic metres in the 0.0375 relative height class through to values from $15 \times 10^{-3}$ to $25 \times 10^{-3}$ cubic metres in total. The segmented polynomial model consistently displays the lowest SEE estimates, however overall the estimate for this model is equivalent to, or near equivalent to those of several other models. In particular, the average-form variable-exponent models and the reduced segmented models are quite similar, while the variable-form variable-exponent models are generally worse. The results suggest preference for the segmented polynomial model and the average-form models.

Table 7.17 presents SEE estimates for the prediction of cumulative volume. The magnitude of the estimates is considerably larger than that recorded for the age 15 dataset, but so too is the magnitude of the cumulative volume standard deviation within each class. They range from $7.5 \times 10^{-3}$ cubic metres in the smallest relative height class through to values between $205 \times 10^{-3}$ and $210 \times 10^{-3}$ cubic metres in total. Variable-form models and the segmented polynomial model are increasingly poor performers with increasing relative height. This may reflect their poorer parsimony, as the SEE and $I^2$ estimates for total volume are near equivalent across models. Only the variable-form variable-exponent models are consistently poorer in terms of both overall SEE and $I^2$. The other models are equivalent to each other.

Bias estimates in the prediction of merchantable height within diameter class for the age 20 dataset is presented in Table 7.18. In contrast to the case for the age 15 dataset, there is a consistent bias trend, with a slightly increasing negative bias recorded with increasing diameter class. It is assumed that this trend is a

consequence of the relatively limited ability of the models to adequately describe the range of diameter in the data; thus the smaller observations in the dataset, from which the observations comprising the diameter classes are drawn, are under predicted. Biases range from -0.20 to -0.10 metres for the smallest diameter class, through to values between -0.45 and -0.55 metres for the largest diameter class. The variable-form version of the reduced segmented model displays lower biases than its average-form counterpart, whereas the situation for the variable-exponent models is reversed. The segmented polynomial model, the average-form variable-exponent models, and the variable-form reduced segmented model show the smallest biases. The results suggest preference for these models.

The SEE estimates for the prediction of height within diameter class for the age 20 dataset appear in Table 7.19. The trend is similar to that of bias, with larger diameter classes displaying larger SEE estimates. These estimates range from between 0.55 and 0.65 metres in class 1 to between 1.65 and 1.75 metres in class 4. The differences between models are quite small. The variable-form variable-exponent models and the average-form reduced segmented model behave more poorly than others.

The bias estimates for the prediction of cumulative volume within diameter classes for the age 20 dataset appear in Table 7.20. Bias estimates for the smallest diameter class are substantially larger than for other classes, however this may be an aberrant statistic. A smaller number of observation were available for statistic calculation in this class. Biases range from $-40\times10^{-3}$ through to $10\times10^{-3}$ cubic metres across models and classes. All the models behave is similar manner, yet show a slight preference for the reduced segmented models.

Table 7.21 presents SEE estimates for the prediction of cumulative volume within diameter classes for the age 20 dataset. SEE increases slightly in line with increases in the standard deviation of cumulative volume within diameter classes, from values between $150\times10^{-3}$ and $160\times10^{-3}$ cubic metres in diameter class 5, through to values of $190\times10^{-3}$ or $195\times10^{-3}$ in diameter class 12.5. Variable-form modelling using variable-exponent models leads to reductions in SEE in the smallest diameter class and increases in the largest classes, with no estimable effect otherwise. It reduces SEE in two out four classes for the reduced segmented model, again, with no estimable effect otherwise. The results are very similar for all models but show some slight preference for the variable-exponent models.

Table 7.14 Diameter prediction bias by relative height class for the age 20 dataset (cm).

| z class | n | average diameter | **Model Form** **Method** | SegPoly nlme | Kozak av nlme | Kozak var nlme | Trig av nlme | Trig var nlme | RedSeg av nlme | RedSeg var nlme |
|---|---|---|---|---|---|---|---|---|---|---|
| 0.0075 | 62 | 30.4 | | 0.4 | **0.2** | **0.2** | **0.2** | **0.2** | 0.5 | 0.5 |
| 0.0275 | 80 | 28.5 | | -0.5 | 0.1 | 0.1 | **0.0** | **0.0** | -0.3 | -0.3 |
| 0.05 | 56 | 27.2 | | -0.1 | **0.0** | **0.0** | **0.0** | **0.0** | -0.1 | **0.0** |
| 0.1 | 56 | 22.9 | | 0.2 | -0.2 | -0.2 | -0.2 | **-0.1** | 0.3 | **0.1** |
| 0.2 | 65 | 23.2 | | **0.0** | -0.1 | **0.0** | **0.0** | 0.1 | 0.1 | 0.2 |
| 0.3 | 75 | 21.4 | | **0.0** | -0.1 | **0.0** | -0.1 | **0.0** | -0.1 | -0.1 |
| 0.4 | 59 | 19.5 | | 0.1 | **0.0** | 0.1 | **0.0** | **0.0** | 0.1 | 0.1 |
| 0.5 | 62 | 17.2 | | 0.1 | **0.0** | 0.1 | **0.0** | **0.0** | 0.1 | 0.1 |
| 0.6 | 61 | 14.7 | | **0.1** | **0.1** | **0.1** | **0.1** | **0.1** | **0.1** | 0.2 |
| 0.7 | 57 | 11.9 | | **0.0** | -0.1 | **0.0** | **0.0** | **0.0** | **0.0** | **0.0** |
| 0.85 | 88 | 7.4 | | 0.1 | **0.0** | 0.1 | **0.0** | 0.1 | **0.0** | **0.0** |
| TOTAL | 721 | 19.5 | | **0.0** | **0.0** | **0.0** | **0.0** | **0.0** | **0.0** | 0.1 |

Table 7.15 Diameter prediction SEE by relative height class for the age 20 dataset (cm).

| z class | n | diameter std.dev. | **Model Form Method** | SegPoly nlme | Kozak av nlme | Kozak var nlme | Trig av nlme | Trig var nlme | RedSeg av nlme | RedSeg var nlme |
|---|---|---|---|---|---|---|---|---|---|---|
| 0.0075 | 62 | 8.1 | | 5.8 | **5.6** | 5.7 | **5.6** | 5.7 | 5.8 | 5.8 |
| 0.0275 | 80 | 7.3 | | 4.8 | **4.7** | **4.7** | **4.7** | **4.7** | **4.7** | 4.8 |
| 0.05 | 56 | 7.3 | | 5.3 | **5.1** | 5.2 | **5.1** | 5.2 | 5.2 | 5.3 |
| 0.1 | 56 | 6.3 | | 4.1 | **3.9** | 4.0 | **3.9** | 4.0 | 4.0 | 4.0 |
| 0.2 | 65 | 5.8 | | 3.8 | **3.7** | **3.7** | **3.7** | **3.7** | **3.7** | **3.7** |
| 0.3 | 75 | 5.3 | | 3.4 | **3.3** | 3.4 | **3.3** | 3.4 | **3.3** | **3.3** |
| 0.4 | 59 | 4.8 | | 3.2 | **3.1** | 3.2 | **3.1** | 3.2 | 3.2 | **3.1** |
| 0.5 | 62 | 4.3 | | 2.9 | **2.8** | 2.9 | **2.8** | 2.9 | 2.9 | 2.9 |
| 0.6 | 61 | 3.6 | | **2.4** | **2.4** | **2.4** | **2.4** | **2.4** | **2.4** | **2.4** |
| 0.7 | 57 | 2.7 | | **2.1** | **2.1** | **2.1** | **2.1** | **2.1** | **2.1** | **2.1** |
| 0.85 | 88 | 2.4 | | **1.3** | 1.4 | 1.4 | 1.4 | 1.4 | **1.3** | **1.3** |
| TOTAL | 721 | 10.6 | | **3.3** | **3.3** | **3.3** | **3.3** | **3.3** | **3.3** | **3.3** |
| Isqrd | | | | **0.865** | **0.865** | **0.865** | **0.865** | **0.865** | **0.865** | **0.865** |

Table 7.16 Cumulative volume prediction bias by relative height class for the age 20 dataset $(10^{-3}\,m^3)$

| z class | n | average cum.volume | **Model Form Method** | SegPoly nlme | Kozak av nlme | Kozak var nlme | Trig av nlme | Trig var nlme | RedSeg av nlme | RedSeg var nlme |
|---|---|---|---|---|---|---|---|---|---|---|
| 0.0125 | 62 | 12.5 | | **0.0** | **0.0** | **0.0** | **0.0** | **0.0** | **0.0** | **0.0** |
| 0.0375 | 80 | 47.5 | | **2.5** | **2.5** | **2.5** | **2.5** | **2.5** | **2.5** | **2.5** |
| 0.0625 | 56 | 90.0 | | **5.0** | 7.5 | 7.5 | 7.5 | **5.0** | **5.0** | **5.0** |
| 0.1 | 56 | 107.5 | | **2.5** | **2.5** | **2.5** | **2.5** | **2.5** | **2.5** | **2.5** |
| 0.2 | 65 | 232.5 | | **7.5** | 10.0 | 10.0 | 10.0 | 10.0 | 10.0 | 12.5 |
| 0.3 | 75 | 335.0 | | **7.5** | **7.5** | 10.0 | 10.0 | 10.0 | 10.0 | 10.0 |
| 0.4 | 59 | 425 | | **10** | 15 | 15 | 15 | 15 | 15 | 15 |
| 0.5 | 62 | 490 | | **15** | 20 | 20 | 20 | 20 | 20 | 20 |
| 0.6 | 61 | 535 | | **15** | **15** | 20 | 20 | 20 | 20 | 20 |
| 0.7 | 57 | 585 | | **15** | 20 | 25 | 20 | 25 | 25 | 25 |
| 0.85 | 88 | 595 | | **15** | 20 | 25 | 20 | 25 | 25 | 25 |
| TOTAL | 60 | 635 | | **15** | **15** | 25 | 20 | 25 | 20 | 20 |
| Average | | 320 | | **10** | **10** | 15 | **10** | 15 | **10** | **10** |

Table 7.17 Cumulative volume prediction SEE by relative height class for the age 20 dataset $(10^{-3}m^3)$

| Z class | n | cum.volume std.dev. | **Model Form Method** | SegPoly nlme | Kozak av nlme | Kozak var nlme | Trig av nlme | Trig var nlme | RedSeg av nlme | RedSeg var nlme |
|---|---|---|---|---|---|---|---|---|---|---|
| 0.0125 | 70 | 10.0 | | **7.5** | **7.5** | **7.5** | **7.5** | **7.5** | **7.5** | **7.5** |
| 0.0375 | 72 | 27.5 | | 20.0 | **17.5** | **17.5** | **17.5** | **17.5** | **17.5** | 20.0 |
| 0.0625 | 69 | 55.0 | | 40.0 | **37.5** | **37.5** | **37.5** | **37.5** | **37.5** | 40.0 |
| 0.1 | 81 | 85.0 | | **45.0** | **45.0** | **45.0** | **45.0** | **45.0** | **45.0** | **45.0** |
| 0.2 | 64 | 142.5 | | 85.0 | **82.5** | 85.0 | **82.5** | 85.0 | **82.5** | 85.0 |
| 0.3 | 61 | 190.0 | | 115.0 | **112.5** | 115.0 | **112.5** | 115.0 | **112.5** | 115.0 |
| 0.4 | 56 | 245 | | 155 | **150** | **150** | **150** | **150** | **150** | 155 |
| 0.5 | 57 | 280 | | 175 | **170** | 175 | **170** | 175 | **170** | 175 |
| 0.6 | 56 | 305 | | **185** | **185** | **185** | **185** | **185** | **185** | **185** |
| 0.7 | 51 | 320 | | 210 | **205** | 210 | **205** | 210 | **205** | 210 |
| 0.85 | 77 | 325 | | 200 | **195** | 200 | **195** | 200 | 200 | 200 |
| Average | 60 | 340 | | 210 | **205** | 210 | **205** | 210 | 210 | 210 |
| Isqrd | | | | **0.85** | 0.84 | 0.84 | 0.84 | 0.84 | **0.85** | **0.85** |

Table 7.18 Merchantable height prediction bias by diameter class for the age 20 dataset (m).

| Diameter class | n | average m.height | **Model Form** | SegPoly | Kozak | Kozak | Trig | Trig | RedSeg | RedSeg |
|---|---|---|---|---|---|---|---|---|---|---|
| | | | | | av | var | av | var | av | var |
| | | | **Method** | nlme | nlme | nlme | nlme | nlme | nlme | nlme |
| 5.0 | 33 | 19.30 | | **-0.10** | -0.15 | -0.20 | -0.15 | -0.15 | -0.20 | -0.15 |
| 7.5 | 43 | 15.55 | | **-0.25** | -0.30 | -0.45 | -0.30 | -0.40 | -0.50 | -0.30 |
| 10.0 | 46 | 15.25 | | **-0.35** | -0.40 | -0.45 | -0.40 | -0.45 | -0.50 | -0.40 |
| 12.5 | 62 | 13.15 | | **-0.45** | **-0.45** | -0.55 | **-0.45** | -0.50 | -0.50 | **-0.45** |

Table 7.19 Merchantable height prediction SEE by diameter class for the age 20 dataset (m).

| Diameter class | n | m.height std.dev. | **Model Form** | SegPoly | Kozak | Kozak | Trig | Trig | RedSeg | RedSeg |
|---|---|---|---|---|---|---|---|---|---|---|
| | | | | | av | var | av | var | av | var |
| | | | **Method** | nlme | nlme | nlme | nlme | nlme | nlme | nlme |
| 5.0 | 33 | 2.65 | | **0.55** | 0.65 | 0.60 | 0.65 | 0.60 | 0.65 | 0.60 |
| 7.5 | 43 | 4.10 | | **1.00** | **1.00** | 1.15 | 1.05 | 1.10 | 1.25 | 1.05 |
| 10.0 | 46 | 3.95 | | **1.10** | 1.15 | 1.25 | 1.15 | 1.25 | 1.30 | 1.15 |
| 12.5 | 62 | 4.00 | | 1.70 | **1.65** | 1.70 | **1.65** | 1.70 | 1.75 | **1.65** |

Table 7.20 Cumulative volume prediction bias by diameter class for the age 20 dataset $(10^{-3}\,m^3)$

| Diameter class | n | average cum.vol. | **Model Form** **Method** | SegPoly nlme | Kozak av nlme | Kozak var nlme | Trig av nlme | Trig var nlme | RedSeg av nlme | RedSeg var nlme |
|---|---|---|---|---|---|---|---|---|---|---|
| | 33 | 535 | | -50 | -45 | **-40** | -45 | **-40** | **-40** | **-40** |
| 5.0 | 43 | 425 | | **0** | -5 | -5 | -5 | -5 | **0** | **0** |
| 7.5 | 46 | 490 | | -25 | -25 | **-20** | -25 | -20 | **-20** | **-20** |
| 10.0 | 62 | 475 | | **5** | **5** | 10 | **5** | 10 | 10 | 10 |
| 12.5 | | | | | | | | | | |

Table 7.21 Cumulative volume prediction SEE by diameter class for the age 20 dataset $(10^{-3}\,m^3)$

| Diameter class | n | cum.vol. std.dev. | **Model Form** **Method** | SegPoly nlme | Kozak av nlme | Kozak var nlme | Trig av nlme | Trig var nlme | RedSeg av nlme | RedSeg var nlme |
|---|---|---|---|---|---|---|---|---|---|---|
| 5.0 | 33 | 290 | | 155 | 155 | **150** | 155 | **150** | 160 | 155 |
| 7.5 | 43 | 290 | | 170 | **165** | **165** | **165** | **165** | 170 | 170 |
| 10.0 | 46 | 305 | | 165 | **160** | **160** | **160** | **160** | 165 | **160** |
| 12.5 | 62 | 335 | | **190** | **190** | 195 | **190** | 195 | **190** | **190** |

#### *7.3.2.2 Between-tree prediction*

Table 7.22 presents estimates of between-stem bias in total volume prediction for the age 20 dataset. As was the case with the analysis of the age 15 dataset, larger biases are apparent in total volume classes 1 and 4 than in 2 and 3, and this is attributable to the inability of the models to accurately predict total volume across the range of observations in the data. In contrast to the case for the age 15 dataset, class 4, which comprises the trees with largest total volumes, exhibits particularly large bias estimates. Classes 2 and 3 are also far more biased, showing that the models are inadequate at accurately predicting any size class outside the mean. The average total volumes for the total volume classes 1 to 4 range from $230\times10^{-3}$ to $1070\times10^{-3}$ cubic metres. The concordant prediction biases range between $-75\times10^{-3}$ and $-55\times10^{-3}$ cubic metres through to values between $205\times10^{-3}$ and $250\times10^{-3}$ cubic metres. In classes 1, 2 and 4 the segmented polynomial model displays the smallest bias. Both versions of the reduced segmented models also perform well in these classes, while the variable-exponent and trigonometric models generally perform less well. These latter models show larger biases in their variable-form specifications in these classes. In class 3, the variable–form versions of these models perform best, while their average-form counterparts and the segmented polynomial model perform badly. Both versions of the reduced segmented models are both adequate performers in this class. The analysis suggests that variable-form modelling using the variable-exponent and trigonometric models improves total volume estimation in only a small range of tree sizes and this improvement comes at the expense of model behaviour elsewhere in the data. The segmented polynomial model is generally very good although it is somewhat inconsistent. The reduced segmented models perform quite well throughout the range of classes.

The SEE estimates for between-stem total volume prediction appear in Table 7.23. SEE estimates increase with increasing total volume class from values between $90\times10^{-3}$ and $105\times10^{-3}$ cubic metres, through to values between approximately $310\times10^{-3}$ and $335\times10^{-3}$ cubic metres. Generally, the segmented polynomial model performs best. Again, the reduced segmented models are generally consistent performers across classes. Variable-form modelling using either the variable-exponent or trigonometric model has little impact upon SEE in class 1 and 2, while leading to decreases in class 3 and increases in class 4.

Table 7.22 Total volume prediction bias by total volume class for the age 20 dataset $(10^{-3}m^3)$

| t. volume class | n | average t.volume | **Model Form** **Method** | SegPoly nlme | Kozak av nlme | Kozak var nlme | Trig av nlme | Trig var nlme | RedSeg av nlme | RedSeg var nlme |
|---|---|---|---|---|---|---|---|---|---|---|
| 1 | 15 | 230 | | **-55** | -65 | -75 | -65 | -70 | -65 | -60 |
| 2 | 15 | 405 | | **-45** | -60 | -65 | -60 | -60 | -55 | -50 |
| 3 | 15 | 670 | | -20 | -15 | **-5** | -15 | **-5** | **-5** | **-5** |
| 4 | 15 | 1070 | | **205** | 230 | 255 | 230 | 250 | 230 | 230 |

Table 7.23 Total volume prediction SEE by total volume class for the age 20 dataset $(10^{-3}m^3)$

| t.volume class | n | t.volume Std.dev. | **Model Form** **Method** | SegPoly nlme | Kozak av nlme | Kozak var nlme | Trig av nlme | Trig var nlme | RedSeg av nlme | RedSeg var nlme |
|---|---|---|---|---|---|---|---|---|---|---|
| 1 | 15 | 70 | | **90** | 105 | 105 | 105 | 105 | 100 | 95 |
| 2 | 15 | 70 | | **145** | 150 | **145** | 150 | **145** | **145** | **145** |
| 3 | 15 | 45 | | 200 | 180 | **175** | 180 | **175** | 185 | 180 |
| 4 | 15 | 225 | | **310** | 325 | 335 | 325 | 335 | 325 | 325 |

## 7.4 Discussion

The analysis of within-tree model performance demonstrates that models may be constructed for the age 15 dataset which are not biased in practical terms. More substantial within-tree biases occur in the age 20 dataset in both merchantable height prediction and cumulative volume prediction by relative height and diameter class. However these biases too, are still minor in practical terms. These results are important because the decision making process undertaken to schedule harvest for a particular stand during strategic planning is typically a disjunctive one in which the key determinant is an estimate of stand merchantable yield. Such a yield may be determined by calculating the number of trees in the stand which contain logs of length and diameter at merchantable size or greater. The developed models may be used estimate this quantity with known confidence (Cox 1998); thus quantifying risk in this decision making process. Moreover, in using these models, such yields may be determined under varying log length or diameter specifications without recourse to remodelling available data.

The analysis of between-tree model performance demonstrates that the precision of the total volume estimates degrades as the mean total volume within the class increases. These between-tree evaluation results show the tested models have more limited utility for predicting the merchantable volume of trees within a sampled population that belong to particular volume classes. The degree of bias across volume classes is still quite minor for the age 15 dataset but is considerably more pronounced in the age 20 dataset. Predicting log assortments at harvest is typically a secondary consideration after harvest scheduling and the utility of the models is more restricted in this respect.

Models have been fitted to the age 15 dataset using both mixed effects, and generalised, nonlinear modelling methods. The model development statistics (information criterion and log likelihood values) indicate preference for the mixed effects models, suggesting that mixed effects specifications are better suited to accommodating the structure of the residual error. Yet the model performance statistics (bias, SEE and $I^2$) suggest the practical benefits of mixed effects modelling are specific to the type of model considered. Fitted models also show performance differences in terms of both precision and bias. In contrast, generalised nonlinear modelling methods have not been successfully applied to the age 20 dataset. These models have either failed to converge, or have estimated stem metrics with large biases. The models that are fitted successfully to the age 20

dataset using mixed effects modelling methods show substantially less bias and precision divergence than those that are fitted to the age 15 dataset. Higher $I^2$ values have been achieved in modelling the age 15 data, indicating that the models account for more between-tree variability. The greater divergence in behaviour between models in the age 15 dataset is perhaps attributable to the smaller within-tree differences in form being modelled. A comparison of the form parameters from the average-form reduced segmented models fitted to each of the datasets reveals that the age 15 model predicts less form throughout the stem and does so with less certainty, with both smaller estimates and smaller t-values for the form parameters: $\beta_1, \beta_2$ and $\beta_3$. This is the modelling paradox. Average- and variable-form models may be constructed for the age 15 data using either mixed effects or generalised least squares methods, facilitated by access to local density information that correlates well with both stem size and form. However, the trees at this age exhibit less within-stem changes in form, leading to less stable stem form parameter estimates and a greater likelihood of within-stem prediction bias.

The results demonstrate the performance of Max and Burkhart's (1976) segmented polynomial model to be poor for the age 15 dataset but very good for the age 20 dataset. In both cases, only mixed effects modelling generates realistic predictions, and obtaining sensible join point parameter estimates requires a two-stage approach in which tree-level predictors are first incorporated with fixed join points. Within-tree precision is generally acceptable when fitted to the age 15 dataset, but the model shows consistent within-tree bias. Between-tree bias is also evident, with the largest volume class predictions being strongly biased. In contrast, both the within- and between-tree precision and bias of the model fitted to the age 20 dataset suggest it to be one of the best models. Gross between-tree differences in diameter are accommodated through the first two terms of the model that apply to the whole stem. Total height and local density each enter the model separately through these terms, so the models do not depict the populations in a realistic manner. These terms are also very collinear. The other model parameters have simple interpretation and show that a further component of stem shape lower in the stem is related to local density and total height.

A model specification that is more stable across datasets allows gross size differences between stems to be accommodated through a single term. This approach has been assessed in fitting both the variable-exponent and the reduced segmented models. These models may also be formulated in a more flexible manner since additional tree-level predictors may be added to accommodate between-tree

differences in form should they occur. The study demonstrates this flexibility by constructing average- and variable-form versions of these models.

The performance differences between tested variable-exponent models are generally slight, betraying the similarities of their formulation. An average-form version of Kozak's (1997) model requires reformulation of the exponent term, while the trigonometric model does not, supporting Bi and Long's (2001) assertion that exponent terms comprised of a suite of trigonometric functions of relative height are more stable and less data driven. The variable-exponent models include some parameters that are not biologically interpretable, nor are they all linear in the model. These parameter features impede variable-form modelling in a mixed effects framework (Leites and Robinson 2004). The lack of interpretability limits the utility of second-stage models as relationships between mixed effects BLUPS and tree-level covariates are spurious, while parameter nonlinearities lead to violation of the normality assumption for mixed effects BLUPS (Gregoire and Schabenberger 1996). Variable-exponent models generally perform well in both datasets. However, no model performs well in all respects and no single model or fitting method is optimal to both datasets. The gnls fitted models generally outperform the nlme fitted models in the age 15 dataset with no substantial advantages apparent in variable-form modelling. These gnls fitted models are biased total volume predictors across size classes but otherwise perform very well. The nlme models are slightly biased predictors of within-stem diameter, with the average-form versions of these being also both less precise within-stem diameter predictors and biased total volume predictors across size classes. The gnls fitting method is unsuited to the age 20 dataset. Variable-form modelling increases cumulative volume prediction bias with no attendant improvement in precision. The total volume prediction bias also increases across size classes. There are minor improvements to precision in merchantable height prediction with variable-form modelling, and this is the one area where the average-form variable-exponent models perform poorly in this dataset. In other respects these average-form models are very good.

The reduced segmented model has been derived in an attempt to circumvent the problems encountered in both the segmented polynomial and variable-exponent models. The gross differences in stem size may be accommodated through modification of a single term and the other parameters in the model have a biological interpretation, which helps to ensure the model will behave appropriately outside the range of the data. These parameters, for the most part, enter the model linearly, which also facilitates second-stage modelling. The reduced segmented model is only fitted successfully using nlme, generating strongly biased estimates

when fitted using gnls. It is the only model that performs consistently across age classes. In the age 15 dataset there are less differences between nlme fitted average- and variable-form versions than are apparent in the nlme fitted variable-exponent models, with the variable-form version displaying better precision in diameter estimation within the stem and less bias in total volume across size classes. In the age 20 dataset, the variable-form version of the model performs slightly better than the average-form version in that the precision of the merchantable height prediction is superior. In other respects it is very similar. It is the only model tested that showed any support for variable-form modelling in this later age dataset.

The stem profiles of the trees comprising the available data conform to a shape that is sufficiently regular to be characterised using empirical models which use inputs that are potentially available through remote sensing. Profile differences that are not a function of the measured variables produce residual model errors that are correlated within trees and also heterogeneous, violating regression assumptions. Mixed effects modelling methods may be used to account for residual error structure because the structure may be expressed in tree-level model parameters that are, generally speaking, normally distributed. The population-average approach, in which the structure is modelled directly, has also been assessed and appears to generate adequate prediction models in some limited cases. In every type of model tested, information criterion values provide strong evidence that approaches are required which account for residual error structure. Past modelling attempts that have addressed this issue have shown such models to be no more accurate or precise predictors for practical purposes (Williams and Reich 1997), but are preferred for the validity of hypothesis testing and inference (Gregoire and Schabenberger 1996; Valentine and Gregoire 2001). The methods used may even result in more parsimonious models (Tasissa and Burkhart 1998; Eerikäinen 2001). In this work, model parsimony was not affected but confidence in hypothesis testing and inference, in light of residuals that are otherwise strongly structured, is assured.

All tested models are acceptable for the prediction of certain stem metrics, however few are acceptable for the prediction of all metrics in both datasets. The behaviour of the segmented polynomial model is inconsistent across datasets. The optimum fitting method for the variable-exponent models is inconsistent across datasets, as is the specified complexity of form modelling. The reduced segmented model is a consistent performer in both datasets in a variable-form specification that is fitted using nlme. This model is rarely optimum for any one stem metric yet neither does it behave poorly in the measurement of any one metric. The stability of this model

can probably be attributed to the manner in which the tree-level predictors enter the model and the manner in which the model may be parameterised to obtain a mixed effects solution. Being tested on such a small dataset it is not possible to argue that it will be applicable in a wider range of situations but it is evidently acceptable for the radiata pine total height and local density data against which it was assessed in this study.

The study data was acquired during a restricted time frame from one estate in an effort to restrict the influence of environmental and genotypic factors upon stem size and profile. Local density has been used in place of breast height diameter and ratios of total height to breast height diameter, which are commonly used in profile modelling studies to describe between-tree profile differences. Additional tree metrics were not considered as covariates in the modelling process. The study made use of local density metrics which could not be standardised across thinning events so the datasets were treated separately. Were data available for the same stand before and after thinning, a thinning index (Liu et al. 1995) might be used to modify local density values. This would increase the effective size of the dataset and allow the use of age as an additional model covariate. Whether or not this would lead to smaller prediction errors or more stable parameter estimates is not known. The greater data range in a combined dataset would have allowed more powerful second-stage models to be constructed, so facilitating variable-form modelling. However, the marked differences in optimum model formulation between age classes indicate that stem shape is substantially different between ages and suggest that prediction biases across age classes would be large. The inconsistent results of previous studies which have attempted to incorporate additional covariates such as age (Muhairwe et al. 1994; Kozak 1998; Petersson 1999; Valentine and Gregoire 2001) also suggest the combination of datasets may not result in improved models. In any case, these ruminations are rather immaterial since the silvicultural system employed in radiata pine, with its fixed age planning allows the use of fixed age models.

Recent studies suggest that terrestrial laser scanners may become appropriate tools for non-destructive stem profile sampling (Simonse et al. 2003; Aschoff et al. 2004; Pfeifer et al. 2004). A profile system that made use of scanner acquired data without an additional sampling stage would also require a bark thickness model. (Gordon 1983) showed that stem bark profile in radiata pine is largely a function of total height, breast height diameter and relative height. Whether stem wood and bark profile could be estimated jointly (Eerikäinen 2001) using local density and total height metrics requires further study.

Profile modelling has focussed upon empirical approaches because the theoretical foundations of stem development are numerous and the interactions between the theorised determinants of stem growth are too poorly understood to allow practical application. The lack of data relating stem form to canopy processes and broader scale environmental conditions have also contributed to the popularity of the empirical approach. The developed models have interpretable parameters and are designed for use with spatially extensive remotely sensed data. They provide the opportunity to explore how stem profile varies at both canopy and landscape scales, with potential implications for process-based stem profile modelling.

## 7.5 Summary

Models of stem profile may be constructed using total height and local density data. Model fit statistics demonstrate the importance of accommodating residual error structure for valid inference. Mixed effects and generalised nonlinear modelling methods have been compared. The latter is only suited to the variable-exponent models which are fitted to the age 15 dataset. Otherwise, these models either fail to converge or generate strongly biased estimates. Mixed effects nonlinear modelling is suited to both datasets and is more intuitively reasonable, accommodating the heterogeneity and variance of the residual error by allowing model parameters to vary randomly between trees. Mixed effects nonlinear modelling is still inadequate in fitting the segmented polynomial model at age 15 but adequate for all other models. Both segmented polynomial and variable-exponent models fail to adequately represent the data across stem sizes. A reduced segmented model was derived which was simple, interpretable and allowed between-tree differences to be accommodated in a biologically reasonable manner. This model fits both datasets well and performs consistently well for a range of tasks. Variable-form modelling generally led to improvements in model precision in the age 15 dataset but did not do so for the age 20 dataset, with only the variable-form reduced segmented model showing any improvement in this later age class. Overall the best models predict diameter and cumulative volume at relative height, and merchantable height to specified diameter with acceptably small bias and error. Between stem prediction is poorer, particularly for the age 20 dataset, which suggests the utility of the models, particularly for the latter age dataset, is restricted to predicting population averages rather than particular stem size classes. It is suggested that these models may be used to support harvest scheduling.

# *Chapter 8*

# Conclusions

Traditional strategic inventory techniques often fail to reliably estimate timber volumes within individual (or small groups of) coupes due to spatial variability in plantation condition. The thesis proposed that recent developments in remote sensing offer data products suited to tree-level timber volume inventory in such circumstances. Models were developed to predict merchantable timber volume in radiata pine plantations through the application of tree-level metrics which may be measured remotely. This development demonstrates a potential use for emergent remote sensing technologies and represents a new approach to tree-level remote sensing based inventory.

In the following summary, the key conclusions drawn from addressing each of the specific aims of the thesis are presented.

Aim 1) *Identify potential remotely sensed data products suited to stem profile prediction and optimal age of data capture through a review of recent remote sensing developments and growth processes in radiata pine timber plantations.*

Remote sensing developments have seen the introduction of automated data analysis methods that allow the spatially extensive assessment of forest canopy and crown metrics. Prior to the deceleration of height growth with the onset of maturity, the relationships between crown and stem metrics in radiata pine are strong. However, the complex shape and interlocking nature of radiata pine tree crowns suggests the precision of crown delineation will be poor, both in remotely sensed and ground truthed data. The location of tree stems in remotely sensed data offers more promise and has been successfully applied in radiata pine. The growth trajectories of proximate radiata pine trees after the onset of between-tree interactions and prior to maturity are disproportionate to size. This may be attributed to the strongly asymmetric character of the interactions that occur

between proximate neighbours as a consequence of competition for light. That between-tree interactions are local and occur above ground suggests that tree-level proximate neighbour height and location information be used to augment stem metric predictions. Opportunities for data capture are limited, as thinning activities disrupt between-tree interactions and consequently disrupt local density characterisation. Optimal data capture is identified as being prior to first or second thinning.

Aim 2) *Develop and evaluate indexes both to capture the information content in potential remotely sensed data products and to efficiently summarise these potential products to a form amenable to further modelling.*

Local tree density indexes were adapted for use with remotely sensed data products and a number of formulations of these indexes were evaluated in sequence. The sequential evaluation was used to quantify neighbourhood influences on the development to felling age of subject tree diameter at breast height (DBH) by examining their contribution to a DBH prediction model employing a local density index and total height. The influences evaluated were neighbour tree total height, between-tree distance and neighbour spatial location. This evaluation was also used to determine the optimum index and the optimum sample plot size. The use of graphical methods in the sequential evaluation allowed the contributions of the neighbourhood metrics to be examined more closely and ensured that the results could be used to infer the nature and effect of between-tree interactions upon the development of subject tree DBH to the age of felling. The evaluation identified the percentage reduction in root mean square error (RMSE) and the residual model error normality in subject tree DBH prediction that could be obtained using each index. Together, these statistics described both the power of each index formulation in reducing prediction error, and their applicability across the range of observations in the data.

The results of the local tree density index evaluation demonstrated that local neighbour tree height and location may be used to predict DBH in radiata pine at ages 15 and 20, although there were substantial reductions in the power of the prediction at age 20. The optimum density index formulations led to reductions in RMSE of 35% and 14% for the age 15 and age 20 datasets respectively. In both datasets, residual model errors were acceptably normally distributed.

The sequential addition and removal of neighbour trees from distance weighted size ratio (DWSR) index formulations, according to their distance from the subject tree, demonstrated that plots with a radius of 5 metres were adequate for the age 15

dataset as only proximate trees contributed to reductions in RMSE, although more distant trees contributed to the normality of the model error. The same analysis of the age 20 dataset showed that all neighbour trees contributed to index utility, suggesting that the optimum plot radius was not determined, although the slight improvements observed with inclusion of the most distant neighbours suggested the optimum plot radius was only slightly larger than five metres.

The sequential addition and removal of neighbour trees from DWSR index formulations according to their height demonstrated that only a small component of the neighbour cohort had any influence on the development to felling age of subject tree DBH in both datasets. That component was comprised of trees which were taller than the subject. This finding suggests that local density was very one-sided.

Sequential adjustments to the influence of subject to neighbour distance in DWSR index formulations demonstrated its influence was nonlinear in both datasets, with the influence of more proximate neighbours being proportionally greater than less proximate neighbours. This finding supports the contention that asymmetric interactions dominate DBH development since it suggests neighbour proximity is also an important factor in local density description.

Sequential adjustments to the influence of neighbour tree height in both DWSR and area potentially available (APA) indexes demonstrated that its influence was also asymmetric in both datasets, with taller neighbours influencing the development to felling age of subject tree DBH in a manner which was disproportionately greater than the subject to neighbour height ratio. The extent to which this asymmetry may be attributed to between-tree interactions, as opposed to nonlinearities in the height and diameter relationship, cannot be determined using the available data. This was not considered to be an important factor in light of the proposed index application.

For the age 15 dataset, reformulated versions of the DWSR indexes were superior predictors of subject tree DBH than were the number of neighbours and the mean height of the four tallest neighbours. DWSR indexes were not superior to these simple neighbour metrics for the age 20 dataset. The APA index outperformed other indexes considered for both datasets. The APA index employs tree height and location in its formulation, rather than tree height and inter-tree distance, suggesting that tree location is an important driver of local density in these stands, and demonstrating that the index offers a method to efficiently summarise a

number of potentially remotely sensed tree metrics to a form amenable to further modelling. Reformulations to account for sidedness and asymmetry also improved the utility of this index, offering support for the contention that these characteristics of local density are not dependent on the type of index employed.

Plot derived data were analysed in a deliberate attempt to identify the influences of neighbour metrics without these influences being obscured by remote sensing measurement errors. The effects of measurement error in remote sensing data are likely to be quite complex given the degree of sidedness and asymmetry in between-tree interactions that was encountered. These effects require further study. However, the results suggest that the measurement of individual tree height, rather than canopy height, and the determination of tree stem location, will lead to substantial improvements in tree stem assessment, as the relative heights and locations of neighbouring trees both have a substantial influence upon the development of subject tree DBH. Potential improvements in assessment gained through canopy element delineation have not been considered.

Aim 3) *Develop and evaluate stem profile prediction models utilising the local density indexes and tree height data.*

In keeping with numerous other profile studies, the lack of a suitable unifying theoretical framework obligated the development of empirical stem profile models. These were applied to the available tree profile data using generalised and mixed effects nonlinear modelling methods. Model fit statistics and diagnostic plots were used to show that stem profile models may be developed that employ total height and local density measurements to predict stem profile in thinned and unthinned stands of radiata pine without recourse to two-stage parameter estimation methods such as random coefficients analysis or simultaneous systems of equations.

Three terms of Max and Burkhart's (1976) segmented polynomial model were augmented by the available tree-level variables, total height and local density. Two variable-exponent models, those of Kozak (1988; 1997) and Bi (2000), were also adapted for use by reformulating the base term of each to incorporate total height and local density rather than DBH. An average-form version of each variable-exponent model was derived by simplifying the exponent terms to describe only within-tree form differences. Variable-form versions were also derived in which local density was incorporated into the exponent terms. A reduced segmented model was developed that included interpretable parameters describing within-stem form. It also expressed gross between-tree differences in stem size through a single model term. This model also supported variable-form formulations through adjustments

to form parameters using tree-level variables. The profile models were compared by evaluating their utility in estimating diameter and cumulative volume to given relative heights, merchantable height and cumulative volume to given small end diameters, and total volume within stem size classes.

The type of model chosen had less influence upon stem metric predictions than did the method used to obtain parameter estimates, an indication of the influence of model residual error structure in this high variance data. Indeed, the generalised versions of all models either failed to solve or generated very large prediction biases when fitted to the age 20 dataset and only suited the variable-exponent models in the age 15 dataset, otherwise generating models with large prediction biases. The mixed effects version of Max and Burkhart's (1976) segmented polynomial and the generalised version of reduced segmented models fitted to the age 15 dataset also displayed large prediction biases. The reduced segmented model fitted using mixed effects methods performed consistently well for a range of tasks in both datasets.

Variable-form modelling generally led to improvement in model precision in the age 15 dataset but did not do so for the age 20 dataset, with only the variable-form reduced segmented model showing any improvement in this later age class. Model bias was generally unaffected by variable-form modelling in the age 15 dataset, while being detrimental to prediction bias in some models in the age 20 dataset.

The variable-form reduced segmented model predicted diameter and cumulative volume at relative height, and merchantable height and volume to a specified diameter limit, with acceptably small bias and error in both datasets. The model is well suited to stem profile description in circumstances where access to small datasets with large variance in the dependent variable would be the norm. The model is also easily adaptable to management demands, in that average- and variable-form models are easily constructed. Average diameter prediction biases within relative height classes above 5% of total height were less than 0.35 and 0.15 centimetres for the age 15 and 20 datasets respectively. In terms of precision, the models displayed estimated coefficients of determination for diameter prediction of 0.895 and 0.865 respectively. Only the age 20 model showed any consistent bias in merchantable height estimation, but even this model did not generate consistently biased volume estimates to an upper diameter limit, indicating that adequate quantities of variance were explained to estimate average merchantable timber volumes. Between-stem predictions were somewhat poorer. This was particularly true of the models fitted to the age 20 dataset and suggests that the utility of the models fitted to this dataset is restricted to predicting population average metrics

rather than metrics belonging to particular stem size classes. Total volume estimates within size classes defined by actual total volume showed biases of up to $32.5\times10^{-3}$ and $230\times10^{-3}$ cubic metres for the age 15 and 20 datasets respectively, while the precision of these estimates, defined by SEE, was as low as $85\times10^{-3}$ and $325\times10^{-3}$ cubic metres respectively.

While the research has investigated one plantation species and identified suitable age cohorts, the nature of between-tree interactions and features of stem form are likely to be similar in a number of other timber plantation species. The developed methods are likely to be applicable to inventory in a wider range of settings and the results suggest research into its application elsewhere is appropriate. In particular, the potential exists to incorporate the developed models into decision support systems tailored to harvest scheduling as the models are well suited to support disjunctive decision making. In identifying methods suitable for condensing remotely sensed information and in developing a simple, yet flexible profile model, the research has contributed to the field of forest inventory, offering a new approach to timber assessment in spatially variable, even-aged timber stands.

# Bibliography


Aarssen, L. W. (1995). 'Hypotheses for the evolution of apical dominance in plants: implications for the interpretation of overcompensation.' Oikos **74**: 149 - 156.

Aldred, A. H. and F. W. Kippen (1967). 'Plot volumes form large-scale 70-mm air photographs.' Forest Science **12**: 419 - 427.

Aldred, A. H. and L. Sayn-Wittgenstein (1972). Tree diameters and volumes from large-scale aerial photographs. Canadian Forest Service, Ottawa: 34pp.

Alemdag, I. S. (1978). Evaluation of some competition indices for the prediction of diameter increment in planted white spruce. Canadian Forest Service, Forest Management Institute., Information Report FMR-X-108

Allen, P. J., N. B. Henry and P. Gordon (1993). 'Polynomial taper model for Queensland plantation hoop pine.' Australian Forestry **55**: 9-14.

Amateis, R. L. and H. E. Burkhart (1987). 'Cubic-foot volume equations for loblolly pine trees in cutover site prepared plantations.' Southern Journal of Applied Forestry **11**(4): 190 - 192.

Amidon, E. L. (1984). 'A general taper function form to predict bole volume for five mixed-conifer species in California.' Forest Science **30**: 166 - 171.

Anderson, H., S. E. Reutebuch and G. F. Schreuder (2001). Use of Automated Individual Tree Crown Recognition and Measurement Algorithms in Forest Inventories. *In*: First International Precision Forestry Symposium, Washington.

Andrew, R. M., C. M. Trotter, B. K. Hock and A. Dunningham (1999). Inventory of plantation forests using crown delineation techniques. *In*: Fourth international airborne remote sensing conference and exhibition / 21st Canadian symposium on remote sensing, Ottawa, Ontario, Canada: 131 - 138

Aschoff, T., M. Thies and H. Spiecker (2004). Describing forest stands using Terrestrial Laser-scanning. *In*: ISPRS XXth Congress, Istanbul, Turkey: 237 - 242

Assman, E. (1970). The principles of forest yield study. New York, Pergamon Press: 506pp.

Avery, T. E. (1971). 'Two cameras for parallax height measurements.' Photogrammetric Engineering **37**(4): 576.

Avery, T. E. and H. E. Burkhart (1994). Forest Measurements. McGraw-Hill: 408pp.

Avery, T. E. and J. Canning (1973). 'Tree measurements on large scale aerial photographs.' New Zealand Journal of Forestry **18**(2): 252-264.

Avery, T. E. and J. Canning (1974). 'Air photo measurements of New Zealand pines.' Photogrammetric Engineering **40**(8): 957 - 959.

Bailey, R. L. (1995). 'Upper Stem Volumes from Stem Analysis Data - an Overlapping Bolts Method.' Canadian Journal of Forest Research **25**(1): 170-173.

Ballaré, C. L., A. L. Scopel and R. A. Sanchez (1990). 'Far-red radiation reflected from adjacent leaves: an early signal of competition in plant canopies.' Science **247**: 329 - 332.

Ballaré, C. L., R. A. Sánchez, A. L. Scopel, J. J. Casal and C. M. Ghersa (1987). 'Early detection of neighbour plants by phytochrome perception of spectral changes in reflected sunlight.' Plant, Cell and Environment **10**: 551 - 557.

Barker, J. E. (1979). 'Growth and wood properties of pinus radiata in relation to applied ethylene.' New Zealand Journal of Forestry Science **9**: 15 - 19.

Barker, J. E. (1980). 'Bole growth patterns of Pinus radiata d. don in relation to fertilization, bending stress, and crown growth.' New Zealand Journal of Forestry Science **10**(2): 445-459.

Begon, M. (1984). 'Density and individual fitness: asymmetric competition.' *In*: Evolutionary ecology, Ed: B. Shorrocks, Blackwell Scientific Publications, Oxford: 175 - 194.

Behre, C. E. (1923). 'Preliminary notes on studies of tree form.' Journal of Forestry **21**: 507-511.

Bella, I. E. (1971). 'A new competition model for individual trees.' Forest Science **17**: 364 - 372.

Berntson, G. M. and P. M. Wayne (2000). 'Characterizing the size dependence of resource acquisition within crowded plant populations.' Ecology **81**(4): 1072-1085.

Bi, H. (1989). Growth in pinus radiata (D. Don) stands in relation to intra- and inter-specific competition. PhD thesis, University of Melbourne: 181pp.

Bi, H. (1999). 'Predicting stem volume to any height limit for native tree species in Southern New South Wales and Victoria.' New Zealand Journal of Forest Science **29**: 318 - 331.

Bi, H. and J. Turner (1994). 'Long-term effects of superphosphate fertilization on stem form, taper and stem volume estimation of Pinus radiata.' Forest Ecology and Management **70**(1-3): 285-297.

Bi, H. Q. (2000). 'Trigonometric Variable-Form Taper Equations for Australian Eucalypts.' Forest Science **46**(3): 397 - 409.

Bi, H. Q. and Y. S. Long (2001). 'Flexible taper equation for site-specific management of Pinus radiata in New South Wales, Australia.' Forest Ecology and Management **148**(1-3): 79-91.

Biggs, P. H. (1990). Estimating timber resources using aerial photography: A guide to selected literature, School of Forestry, University of Melbourne: 102pp.

Biging, G. S. (1984). 'Taper equations for second-growth mixed conifers of Northern California.' Forest Science **26**: 71 - 80.

Biging, G. S. (1985). 'Improving estimates of site index curves using a varying-parameter model.' Forest Science **31**: 248 - 259.

Biging, G. S. and M. Dobbertin (1992). 'A comparison of distance-dependent competition measures for height and basal area growth of individual conifer trees.' Forest Science **38**(3): 695-720.

Biging, G. S. and M. Dobbertin (1995). 'Evaluation of competition indices in individual tree growth models.' Forest Science **41**(2): 360 - 377.

Bliss, C. I. and K. A. Reinker (1964). 'A log-normal approach to diameter distributions in even-aged stands.' Forest Science **10**: 350 - 360.

Bolduc, P., K. Lowell and G. Edwards (1999). 'Automated estimation of localized forest volume from large-scale aerial photographs and ancillary cartographic information in a boreal forest.' International Journal of Remote Sensing **20**(18): 3611 - 3624.

Bonnor, G. M. (1964). 'The influence of stand density on the correlation of stem diameter with crown width and height for lodgepole pine.' Forestry Chronicle **40**(3): 347 - 349.

Boyd, J. (1950). 'Tree growth stresses. I: Growth stress evaluation.' Australian journal of scientific research, Series B: Biological sciences **3**: 270 - 293.

Brand, D. G. and S. Magnussen (1988). 'Asymmetric, two sided competition in even-aged monocultures of red pine.' Canadian Journal of Forest Research **18**: 901 - 910.

Broad, L. and G. C. Wake (1995). 'Derivative based methods for constructing volume-ratio and taper equations.' Forest Science **41**: 157 - 167.

Brown, G. S. (1965). 'Point density in stems per acre.' New Zealand Forest Research Notes **38**: 11pp.

Brown, K. M. and A. C. Leopold (1973). 'Ethylene and the regulation of growth in pine.' Canadian Journal of Forest Research **3**: 143 - 145.

Bruce, D. and T. A. Max (1990). Use of profile equations in tree estimation. *In*: State of the art methodology for forest inventory: A symposium proceedings, U.S. Forest Service General technical report: PNW-GTR-263.

Bruce, D., R. O. Curtis and C. VanCoevering (1968). 'Development of a system of taper and volume tables for red alder.' Forest Science **14**: 339 - 350.

Burton, P. J. (1993). 'Some limitations inherent to static indices of plant competition.' Canadian Journal of Forest Research **23**: 2141 - 2152.

Byrne, J. C. and D. D. Reed (1986). 'Complex compatible taper and volume estimation systems for red and loblolly pine.' Forest Science **32**(2): 423-443.

Candy, S. G. (1989a). 'Compatible tree volume and variable form stem taper models for Pinus radiata in Tasmania.' New Zealand Journal of Forestry Science **19**(1): 97-111.

Candy, S. G. (1989b). 'Growth and yield models for Pinus radiata plantations in Tasmania.' New Zealand Journal of Forestry Science **19**: 112 - 133.

Candy, S. G. (1999). Gumboot. Hobart: Growth and yield models for Radiata pine in the Uxbridge Moogara estate.

Cannell, M. G. R., P. Rothery and E. D. Ford (1984). 'Competition within stands of Picea sitchensis and Pinus contorta.' Annals of Botany **53**: 349 - 362.

Cao, Q. V., H. E. Burkhart and T. A. Max (1980). 'Evaluation of two methods of cubic volume prediction of loblolly pine to any merchantable limit.' Forest Science **26**: 71-80.

Carroll, R. J. and D. Ruppert (1988). Transformation and weighting in regression. New York, Chapman and Hall: 264pp.

Carron, L. T. and N. Hall (1954). 'National forest inventory: Beech forest (Victoria) military mapsheet area - western half.' Australian Forestry **18**(2): 128 - 140.

Casper, B. B. and R. B. Jackson (1997). 'Plant competition underground.' Annual review of ecology and systematics **28**: 545-570.

Chiba, Y., T. Fujimori and Y. Kiyono (1988). 'Another interpretation of the profile diagram and its availability with consideration of the growth process of forest trees.' Journal of the Japanese Forestry Society **70**: 245 - 254.

Cook, R. D. (1979). 'Influential observations in linear regression.' Journal of the American Statistical Association **72**: 863 - 866.

Cromer, D. A. N. and J. D. Aitkin (1948). 'An aerial inventory of Norfolk Island pine.' Australian Forestry **12**(2): 82 - 87.

Culvenor, D. S. (2000). Development of a tree delineation algorithm for application to high spatial resolution imagery of Australian native forest. PhD thesis, University of Melbourne: 355pp.

Czaplewski, R. L. and D. Bruce (1990). 'Retransformation bias in a stem profile model.' Canadian Journal of Forest Research **20**(10): 1623-1630.

Czaplewski, R. L., A. S. Brown and R. C. Walker (1989). Profile models for estimating log end diameters in the Rocky Mountain region, USDA Forest Service: 7pp.

Daniels, R. F., H. E. Burkhart and T. R. Clason (1986). 'A comparison of competition measures for predicting growth in loblolly pine trees.' Canadian Journal of Forest Research **16**: 1230 - 1237.

Daniels, R. F., H. E. Burkhart and T. R. Clason (1986). 'A comparison of competition measures for predicting growth in loblolly pine trees.' Canadian Journal of Forest Research **16**: 1230 - 1237.

Davidian, M. and D. M. Giltinan (1995). Nonlinear Models for Repeated Measurement Data. CRC Press: 359pp

Davidian, M. and D. M. Giltinan (2003). 'Nonlinear models for repeated measurement data: An overview and update.' Journal of Agricultural and Environmental statistics **4**: 387-419.

De luis, M., J. Raventós, J. Cortina, M. J. Moro and J. Bellot (1998). 'Assessing components of a competition index to predict growth in an even-aged Pinus nigra stand.' New Forests **15**(3): 223-242.

Dean, T. J. and J. N. Long (1986a). 'Validity of constant-stress and elastic-instability principals of stem formation in Pinus contorta and Trifolium pratense.' Annals of Botany (London) **58**: 833 - 840.

Dean, T. J., S. D. Roberts, D. W. Gilmore, D. A. Maguire, J. N. Long, K. L. O'Hara and R. S. Seymour (2002). 'An evaluation of the uniform stress hypothesis based on stem geometry in selected North American conifers.' Trees-Structure and Function **16**(8): 559-568.

Deleuze, C. and F. Houllier (2002). 'A flexible radial increment taper equation derived from a process-based carbon partitioning model.' Annals of Forest Science **59**(2): 141-154.

Demaerschalk, J. P. (1971). 'Taper equations that can be converted to volume equations and point sampling factors.' Forestry Chronicle **47**(6): 352 - 354.

Demaerschalk, J. P. (1972). 'Converting volume equations to compatible taper equations.' Forest Science **18**: 241 - 245.

Demaerschalk, J. P. (1973). 'Integrated systems for the estimation of tree taper and volume.' Canadian Journal of Forest Research **3**: 90 - 94.

Demaerschalk, J. P. and A. Kozak (1977). 'The whole-bole system: a conditioned dual-equation system for precise prediction of tree profiles.' Canadian Journal of Forest Research **7**: 488-497.

Dendron Resource Surveys Inc (1996). Equations for estimating diameter at breast height from large scale photo tree measurements. Sault Ste. Marie, Canadian Forest Service, Great lakes Forestry Centre Report 20: 16pp

Dendron Resource Surveys Inc (1997). Enhancing Ontario's forest resource inventory using large scale sampling photographs. Toronto, Ontario Canada, Ontario ministry of natural resources: 24pp.

Diggle, P. J. (1976). 'A spatial stochastic model of inter-plant competition.' Journal of applied probability **13**: 662-671.

Donald, C. M. (1963). 'Competition among crop and pasture plants.' Advances in Agronomy **15**: 1-118.

Downes, G. M., G. A. Moore and N. D. Turvey (1994). 'Variations in response to induced stem bending in seedlings of Pinus radiata.' Trees-Structure and Function **8**: 151 - 159.

Drever, C. R. and K. P. Lertzman (2001). 'Light-growth responses of coastal Douglas-fir and western red cedar saplings under different regimes of soil moisture and nutrients.' Canadian Journal of Forest Research **31**: 2124 - 2133.

Eerikäinen, K. (2001). 'Stem volume models with random coefficients for Pinus keysia in Tanzania, Zambia, and Zimbabwe.' Canadian Journal of Forest Research **31**: 879 - 888.

Evans, D. L., S. D. Roberts, J. W. McCombs and R. L. Harrington (2001). 'Detection of regularly spaced targets in small-footprint LIDAR data: research issues for consideration.' Photogrammetric Engineering and Remote Sensing **67**(10): 1133 - 1136.

Fang, Z. X. and R. L. Bailey (1999). 'Compatible volume and taper models with coefficients for tropical species on Hainan Island in Southern China.' Forest Science **54**(1): 85 - 100.

Fang, Z. X., B. E. Borders and R. L. Bailey (2000). 'Compatible volume-taper models for loblolly and slash pine based on a system with segmented-stem form factors.' Forest Science **46**(1): 1-12.

Ferguson, I. S. and J. W. Leech (1978). 'Generalized least squares estimation of yield functions.' Forest Science **1**: 27-44.

Ferguson, I. S., J. Fox, T. Baker, D. Stackpole and I. Wild (2002). Australian and regional wood availability, 2001 - 2044. Consultants report for the 2002 National Plantation Inventory. Canberra, Australia, Bureau of Rural Sciences: 88pp.

Figueiredo Filho, A., S. A. Machado and M. R. A. Carneiro (2000). 'Testing accuracy of log volume calculation procedures against water displacement techniques (xylometer).' Canadian Journal of Forest Research **30**(6): 990 - 997.

Flewelling, J. W. and L. M. Raynes (1993). 'Variable-shape stem-profile predictions for western hemlock. Part I. Predictions from DBH and total height.' Canadian Journal of Forest Research **23**(3): 520-536.

Ford, E. D. (1975). 'Competition and stand structure in some even-aged plant monocultures.' Journal of Ecology **63**: 311-333.

Fourcaud, T. and P. Lac (2003). 'Numerical modelling of shape regulation and growth stresses in trees I. An incremental static finite element formulation.' Trees - Structure and Function **17**(1): 23 - 30.

Fourcaud, T., F. Blaise, P. Lac, P. Castéra and d. R. P. (2003). 'Numerical modelling of shape regulation and growth stresses in trees II. Implementation in the AMAPpara software and simulation of tree growth.' Trees - Structure and Function **17**(1): 31 - 39.

Fox, J. (2000). Spatial dependence and individual tree growth models in Eucalyptus pilulris (Smith). PhD thesis, University of Melbourne.

Fox, J. C., P. K. Ades and H. Bi (2001). 'Review: Stochastic structure and individual-tree growth models.' Forest Ecology and Management **154**(1): 261 - 276.

Fries, J. and B. Matern (1965). On the use of multivariate methods for the construction of tree taper curves. In: IUFRO Advisory Group of Forest Statisticians Conference, Stockholm, Sweden: 85 - 117

Gál, J. and I. E. Bella (1995). 'Evaluation of stem taper functions for estimating log volume assortments.' The Forestry Chronicle **71**(6): 743 - 746.

Garber, S. M. and D. A. Maguire (2003). 'Modeling stem taper of three central Oregon species using nonlinear mixed effects models and autoregressive error structures.' Forest Ecology and Management **179**: 507 - 522.

Gates, D. J. (1978). 'Bimodality in even-aged plant monocultures.' Journal of Theoretical Biology **71**: 525-540.

Gates, D. J. and M. Westcott (1982). 'Competition and skewness in plantations.' Journal of Theoretical Biology. **94**: 909 - 922.

Gates, D. J., R. McMurtrie and C. J. Borough (1983). 'Skewness reversal of distribution of stem diameter in plantations of Pinus radiata.' Australian Forest Research **13**: 267-270.

Gerrard (1969). 'Competition quotient: A new measure of the competition affecting individual forest trees.' Michigan State University Agricultural Research Station Research Bulletin. **20**: 1 - 32.

Gifford, R. M. and L. T. Evans (1981). 'Photosynthesis, carbon partitioning, and yield.' Annual review of plant physiology **32**: 485 - 509.

Goodwin, A. and D. N. Thompson (2003). A modified hyperbolic tree taper model. *Unpublished.*

Gordon, A. D. (1983). 'Comparison of compatible polynomial taper equations.' New Zealand Journal of Forestry Science **13**(2): 146 - 155.

Gordon, A. D. (1983). 'Estimating bark thickness of Pinus radiata.' New Zealand Journal of Forestry Science **13**: 340 – 353

Gougeon, F. A. (1995). 'A crown-following approach to the automatic delineation of individual tree crowns in high spatial resolution aerial images.' Canadian Journal of Remote Sensing **21**(3): 274-284.

Gougeon, F. A. and D. G. Leckie (1999). Forest regeneration: individual tree crown detection techniques for density and stocking assessments. *In*: Proceedings automated interpretation of high resolution digital imagery for forestry, Victoria, British Columbia.

Goulding, C. J. (1979). 'Cubic spline curves and calculation of volume of sectionally measured trees.' New Zealand Journal of Forest Science **9**: 89 - 99.

Goulding, C. J. and J. C. Murray (1976). 'Polynomial taper equations that are compatible with tree volume equations.' New Zealand Journal of Forestry Science **5**(313-322).

Goulding, C. J., C. M. Trotter, B. K. Hock and S. Hitchcock (2000). 'Determining the location of trees and their log products within a stand.' New Zealand Journal of Forestry **45**(1): 34 - 39.

Gray, H. R. (1956). 'The form and taper of forest-tree stems.' Oxford University Imperial Forestry Institute Paper 32: 1-74.

Gregoire, T. G. and O. Schabenberger (1996). 'Nonlinear mixed-effects modeling of cumulative bole volume with spatially correlated within-tree data.' Journal of agricultural, biological, and environmental statistics **1**(1): 107 - 119.

Gregoire, T. G., H. T. Valentine and G. M. Furnival (1986). 'Estimation of bole volume by importance sampling.' Canadian Journal of Forest Research **16**(3): 554 - 557.

Gregoire, T. G., O. Schabenberger and J. P. Barrett (1995). 'Linear modeling of irregularly spaced, unbalanced, longitudinal data from permanent plot measurements.' Canadian Journal of Forest Research **25**: 137 - 156.

Grosenbaugh, L. R. (1966). 'Tree form: definition, interpolation, extrapolation.' Forestry Chronicle **42**: 444 - 457.

Hall, R. J., R. T. Morton and R. N. Nesby (1989). 'A comparison of existing models for DBH estimation from large-scale photos.' Forestry Chronicle **62**(2): 114 -120.

Hall, R. J., Y. Wang and D. J. Morgan (2001). 'Estimating Tree Diameter and Volume with a Taper Model and Large-Scale Photo Measurements.' Northern Journal of Applied Forestry **18**(4): 110 - 118.

Hamilton, G. J. (1969). 'The dependence of volume increment of individual trees on dominance, crown dimensions, and competition.' Forestry **42**: 133 - 144.

Hara, T. (1984). 'A stochastic model and the moment dynamics of the growth and size distribution in plant populations.' Journal of theoretical biology **109**: 173 - 190.

Hara, T. (1984). 'Dynamics of stand structure in plant monocultures.' Journal of Theoretical Biology **110**: 223-239.

Harper, J. L. (1967). 'A Darwinian approach to plant ecology.' Journal of Ecology **55**: 247-270.

Harper, J. L. (1977). Population Biology of Plants. New York, Academic Press London: 892pp.

Harrison, B. A. and D. L. B. Jupp (1989). An introduction to remotely sensed data. Canberra, CSIRO: 141pp.

Hatch, C. R., D. J. Gerrard and J. C. Tappeiner II (1975). 'Exposed crown surface area: a mathematical index of individual tree growth potential.' Canadian Journal of Forest Research **5**: 224 - 228.

Hegyi, F. (1974). 'A simulation model for managing jack-pine stands. Growth models for tree and stand simulation.' Stockholm Royal College of Forestry Research Notes **20**: 74 - 90.

Henry, H. A. L. and L. W. Aarssen (1999). 'The interpretation of stem diameter-height allometry in trees: biomechanical constraints, neighbour effects, or biased regressions?' Ecology Letters **2**(2): 89-97.

Proceedings of the international forum on automated interpretation of high spatial resolution digital imagery for forestry, (1998). *Eds*: Hill, D. and D. G. Leckie, Victoria, B.C. Canada, Canadian Forest Service.

Holbrook, N. M. and F. E. Putz (1989). 'The influence of neighbors on tree form: effect of lateral shade and prevention of sway on the allometry of Liquidambar styraciflua (sweet gum).' American Journal of Botany **76**: 1740-1749.

Hopkins, J. C. and R. J. Leipold (1996). 'On the dangers of adjusting the parameter values of mechanism based mathematical models.' Journal of theoretical biology **183**(4): 417 - 427.

Husch, B., T. W. Beers and J. Kershaw, J.A. (2003). Forest Mensuration. Hoboken, New Jersey, John Wiley and Sons: 434pp

Hyyppä, J., O. Kelle, M. Lehikoinen and M. Inkinen (2001). 'A segmentation-based method to retrieve stem volume estimates from 3-D tree height models produced by laser scanners.' IEEE Transactions on Geoscience and Remote Sensing **39**: 969 - 975.

Jackson, D. S., H. H. Gifford and J. Chittenden (1976). 'Environmental variables influencing the increment of Pinus radiata: (2) Effects of seasonal drought on height and diameter increment.' New Zealand Journal of Forestry Science **5**: 265 - 286.

Jacobs, M. R. (1954). 'The effect of wind sway on the form and development of Pinus radiata.' Australian Journal of Botany **2**: 35-51.

Jennrich, R. (1969). 'Asymptotic Properties of Non-Linear Least Squares Estimators.' Annals of Statistics **40**(2): 633 - 643.

Jonas, D. (2004). 'Maximum possible pulse rate using current ALS technology is 100 000 Hz.' Personal comment made at a AAMHatch presentation to CenSIS on ALS technologies. Hobart.

Keddy, P. A. (1989). Competition. London, Chapman and Hall: 202pp

Kershaw, J. A. and D. A. Maguire (2000). 'Influence of vertical foliage structure on the distribution of stem cross-sectional area increment in western hemlock and balsam fir.' Forest Science **46**(1): 86-94.

Kilkki, P., M. Saramäki and M. Varmola (1978). 'A simultaneous equation model to determine taper curve.' Silva Fennica **12**: 120 - 125.

King, D. A. and O. L. Loucks (1978). 'The theory of tree bole and branch form.' Radiation and Environmental Biophysics **15**: 141 - 165.

Kozak, A. (1988). 'A variable-exponent taper equation.' Canadian Journal of Forest Research **18**(11): 1363-1368.

Kozak, A. (1997). 'Effects of multicollinearity and autocorrelation on the variable-exponent taper functions.' Canadian Journal of Forest Research **27**(5): 619-629.

Kozak, A. (1998). 'Effects of upper stem measurements on the predictive ability of a variable-exponent taper equation.' Canadian Journal of Forest Research **28**(7): 1078-1083.

Kozak, A. and J. H. G. Smith (1993). 'Standards for evaluating taper estimating systems.' Forestry Chronicle **69**(4): 438-444.

Kozak, A., D. D. Munro and J. H. G. Smith (1969). 'Taper functions and their application in forest inventory.' Forestry Chronicle **42**: 278 - 283.

Kramer, P. J. and T. T. Kozlowski (1979). Physiology of woody plants. London, Academic Press: 811pp

Lahtinen, A. and J. Laasasenaho (1980). 'On the construction of taper curves by using spline functions.' Julkaisuja - Metsantutkimuslaitos. = Communications - Finnish Forest Research Institute **95**(1): 1 - 63.

Laird, N. M. and H. Ware (1982). 'Random effects models for longitudinal data.' Biometrics **38**: 963 - 974.

Lanner, R. M. (1976). 'Patterns of shoot development in Pinus and their relationship to growth potential.' *In*: Tree physiology and yield improvement, London, Academic Press: 567pp

Lanner, R. M. (1985). 'On the insensitivity of height growth to spacing.' Forest Ecology and Management **13**: 143 - 148.

Lappi, J. (1986). 'Mixed linear models for analyzing and predicting stem form variation of Scots pine.' Communicationes Instituti Forestalis Fenniiae **134**: 1-69.

Larsen, M. (1998). 'Finding an optimal match window for Spruce top detection based on an optical tree model.' In: Proceedings of the international forum on automated interpretation of high spatial resolution digital imagery for forestry, Victoria, B.C. Canada, Canadian Forest Service: 55 - 66

Larson, P. R. (1962). 'Auxin gradients and the regulation of tree growth.' In: Tree growth (Ed: T. T. Kozlowski) New York, The Ronald Press Company: 97 - 117.

Larson, P. R. (1963). 'Stem form development of forest trees.' Forest Science Monograph **5**: 1 - 41.

Larson, P. R. (1965). 'Stem form development of young Larix trees as influenced by wind and pruning.' Forest Science **11**: 412 - 424.

Lawrence, P. R. and B. B. Walker (1954). 'Methods and results of forest assessment using random sampling units in photo-interpreted strata.' Australian Forestry **18**(2): 107 - 127.

Leckie, D. G. (1990). 'Advances in remote sensing technologies for forest surveys and management.' Canadian Journal of Forest Research **20**(4): 464 - 483.

Leckie, D. G., F. Gougeon, D. Hill, R. Quinn, L. Armstrong and R. Shreenan (2003). 'Combined high-density lidar and multispectral imagery for individual tree crown analysis.' Canadian Journal of Remote Sensing **29**(5): 633 – 649.

Lederman, T. and A. R. Stage (2001). 'Effects of competitor spacing in individual-tree indices of competition.' Canadian Journal of Forest Research **31**(12): 2143-2150.

Lee, W. K. and K. von Gadow (1997). 'Iterative selection of competitor trees in Pinus densiflora stands.' Allgemeine Forst Und Jagdzeitung **168**(3-4): 41-45.

Lee, W. K., J.-H. Seo, Y. M. Son, K. H. Lee and K. von Gadow (2003). 'Modeling stem profiles for Pinus densiflora in Korea.' Forest Ecology and Management **172**(1): 69-77.

Lefsky, M. A., W. B. Cohen, S. A. Acker, G. C. Parker, T. A. Spies and D. J. Harding (1999). 'Lidar remote sensing of the canopy structure and biophysical properties of Douglas-fir western hemlock forests.' Remote Sensing of Environment **70**: 339 - 361.

Leites, L. P. and A. P. Robinson (2004). 'Improving taper equations of Loblolly pine with crown dimensions in a mixed-effects modelling framework.' Forest Science **50**(2): 204 - 212.

LeMay, V. M. (1990). 'MSLS: A linear least squares technique for fitting a simultaneous system of equations with a generalized error structure.' Canadian Journal of Forest Research **20**: 1830 - 1839.

Leopold, A. C., K. M. Brown and F. H. Emerson (1972). 'Ethylene in the wood of stressed trees.' Horticultural science **7**: 175.

Lindstrom, M. J. and D. M. Bates (1990). 'Nonlinear mixed effects models for repeated measures data.' Biometrics **46**: 673 - 687.

Liu, J., H. E. Burkhart and R. L. Amateis (1995). 'Projecting crown measures for loblolly pine trees using a generalized thinning response function.' Forest Science **41**: 43 - 53.

Long, J. N., F. W. Smith and D. R. M. Scott (1981). 'The role of Douglas-fir sapwood and heartwood in the mechanical and physiological support of crowns and the development of stem form.' Canadian Journal of Forest Research **11**: 459 - 464.

Lorimer, C. G. (1983). 'Tests of age-independent competition indices for individual trees in natural hardwood stands.' Forest Ecology and Management **6**: 343-360.

Lyons, E. H. (1964). 'Recent developments in 70mm stereo-photography form helicopters.' Photogrammetric Engineering **30**(5): 750 - 756.

Makela, A. (2002). 'Derivation of stem taper from the pipe theory in a carbon balance framework.' Tree Physiology **22**(13): 891-905.

Makela, A. and P. Hari (1986). 'Stand growth model based on carbon uptake and allocation in individual trees.' Ecological Modelling **33**: 205 - 229.

Martin, G. L. and A. R. Ek (1984). 'A comparison of competition measures and growth models for predicting plantation red pine diameter and height growth.' Forest science **30**(3): 731-743.

Max, T. A. and H. E. Burkhart (1976). 'Segmented polynomial regression applied to taper equations.' Forest Science **22**(3): 283-289.

McClure, J. P. and R. L. Czaplewski (1986). 'Compatible taper equation for loblolly pine.' Canadian Journal of Forest Research **16**: 1272 - 1277.

McMahon, T. A. (1973). 'The mechanical design of trees.' Science **233**: 92 - 102.

McMahon, T. A. and R. E. Kronauer (1976). 'Tree structure: deducing the principle of mechanical design.' Journal of Theoretical Biology **59**: 443 - 466.

McTague, J. P. and R. L. Bailey (1987). 'Simultaneous total and merchantable volume equations and a compatible taper function for loblolly pine.' Canadian Journal of Forest Research **17**: 87 - 92.

Metzger, K. (1894). 'Die absoluten Schaftformzahlem der Fichte.' Mundener Forstl **6**: 87-93.

Meyer, H. A. (1953). Forest Mensuration. Penns Valley Publishers, Inc. State College Pennsylvania.

Miina, J. and T. Pukkala (2000). 'Using numerical optimization for specifying individual-tree competition models.' Forest Science **46**(2): 277 - 283.

Monserud, R. A. and A. R. Ek (1974). 'Plot edge bias in forest stand growth simulation models.' Canadian Journal of Forest Research **4**: 419 - 423.

Moore, J. A., C. A. Budelsky and R. C. Schlesinger (1973). 'A new index representing individual tree competitive status.' Canadian Journal of Forest Research **7**: 495 - 500.

Morgan, J. and M. G. R. Cannell (1994). 'Shape of Tree Stems - a Reexamination of the Uniform Stress Hypothesis.' Tree Physiology **14**(1): 49-62.

Morsdorf, F., E. Meier, B. Kotz, K. I. Itten, M. Dobbertin and B. Allgower (2004). 'LIDAR-based geometric reconstruction of boreal type forest stands at single tree level for forest and wildland fire management.' Remote Sensing of Environment **92**(3): 353-362.

Muhairwe, C. K. (1993). Examination and modelling of tree form over time for interior lodgepole pine. PhD thesis, University of British Columbia, Canada.

Muhairwe, C. K. (1994). 'Tree form and taper variation over time for interior lodgepole pine.' Canadian Journal of Forest Research **24**(9): 1904-1913.

Muhairwe, C. K. (1999). 'Taper equations for Eucalyptus pilularis and Eucalyptus grandis for the north coast in New South Wales, Australia.' Forest Ecology and Management **113**(2-3): 251-269.

Muhairwe, C. K., V. M. LeMay and A. Kozak (1994). 'Effects of adding tree, stand, and site variables to Kozak's variable-exponent taper equation.' Canadian Journal of Forest Research **24**(2): 252-259.

Myers, B. J. (1974). 'Stocking assessment in young pine plantations using 70 mm aerial photographs.' Australian Forest Research **6**(3): 35 - 42.

Nance, W. L., J. E. Grissom and W. R. Smith (1988). 'A new competition index based on weighted and constrained area potentially available.' USDA Forest Service general technical report **120**: 134-142.

Neilsen, W. A. E. (1990). Plantation handbook, Forestry Commission, Tasmania: 270pp

Nelson, R., R. Swift and W. Krabill (1988). 'Using airborne lasers to estimate forest canopy and stand characteristics.' Journal of Forestry **86**(10): 31-38.

Newberry, J. D. and H. E. Burkhart (1986). 'Variable-form stem profile models for loblolly pine.' Canadian Journal of Forest Research **16**: 109-114.

Newnham, R. M. (1965). Stem form and the variation of taper with age and thinning regime. Forestry **38**: 218-224.

Newnham, R. M. (1988). A variable-form taper function. Chalk River, Ontario, Petawawa National Forestry Institute, Forestry Canada, Information Report PI-X-83

Newnham, R. M. (1992). 'Variable-form taper functions for four Alberta tree species.' Canadian Journal of Forest Research **22**(2): 210-223.

Newton, P. F. and P. A. Jolliffe (1998). 'Aboveground modular component responses to intraspecific competition within density-stressed black spruce stands.' Canadian Journal of Forest Research **28**(11): 1587-1610.

Newton, P. F. and P. A. Jolliffe (1998). 'Assessing Processes of Intraspecific Competition within Spatially Heterogeneous Black Spruce Stands.' Canadian Journal of Forest Research **28**(2): 259-275.

Niklas, K. J. (1994). Plant allometry: the scaling of form and process. University of Chicago Press, Chicago: 395pp

Nilsson, M. (1996). 'Estimation of Tree Weights and Stand Volume Using an Airborne Lidar System.' Remote Sensing of Environment **56**(1): 1-7.

O'Brien, S. T., S. P. Hubbell, P. Spiro, R. Condit and R. B. Foster (1995). 'Diameter, height, crown, and age relationships in eight neotropical tree species.' Ecology **76**(6): 1926-1939.

Ojansuu, R. (1993). 'Prediction of Scots pine increment using a multivariate variance component model.' Acta Forestalia Fennica **239**: 72pp.

Opie, J. E. (1968). 'The predictability of individual tree growth using various definitions of competing basal area.' Forest Science **14**: 314 - 323.

Ormerod, D. W. (1973). 'A simple bole model.' Forestry Chronicle **49**: 136-138.

Ormerod, D. W. (1986). 'The diameter-point method for tree taper description.' Canadian Journal of Forest Research **16**: 484-490.

Osawa, A. (1993). 'Effects of mechanical stresses and photsynthetic production on stem form development of Populus maximowiczii.' Annals of Botany **71**: 489 - 494.

Osawa, A., M. Ishizuka and Y. Kanazawa (1991). 'A profile theory of tree growth.' Forest ecology and management **41**: 33 - 63.

Osler, G. H. R., P. W. West and G. M. Downes (1996). 'Effects of bending stress on taper and growth of stems of young Eucalyptus regnans trees.' Trees-Structure and Function **10**(4): 239-246.

Parsons, M., M. Gavran and A. Gerrand (2004). National Forest Inventory, National Plantation Inventory Update – March 2004. Bureau of Rural Sciences, Australian Government, Canberra: 8 pp.

Pelz, D. R. (1978). 'Estimating individual tree growth with tree polygons.' In: Growth models for long term forecasting of timber yields. Report VPI FWS 1-78.

Pelz, D. R. (1993). 'National forest inventories: past developments and future prospects.' In: Forest Resource Inventory and Monitoring and Remote Sensing Technology, Proceedings of the IUFRO Centennial Meeting, Berlin: 11-18

Perez, D. N., H. E. Burkhart and C. T. Stiff (1990). 'A variable-form taper function for Pinus oocarpa (Schiede) in central Honduras.' Forest Science **36**: 186 - 191.

Perry, D. A. (1985). 'The competition process in forest stands.' In: Attributes of trees as crop plants. Midlothian, Scotland, Institute of Terrestrial Ecology, Natural Environment Research Council: 481 - 506

Persson, A., J. Holmgren and U. Söderman (2002). 'Detecting and measuring individual trees using an airborne laser scanner.' Photogrammetric Engineering and Remote Sensing **68**(9): 925 - 932.

Petersson, H. (1999). 'A segmented stem profile model for Pinus sylvestris.' Forest Ecology and Management **124**(1): 13-26.

Pfeifer, N., B. Gorte and D. Winterhalder (2004). 'Automatic Reconstruction of Single Trees From Terrestrial Laser Scanner Data.' In: ISPRS XXth Congress, Istanbul, Turkey: 114 - 119

Pinheiro, J. C. and D. M. Bates (2000). Mixed-effects models in S and S-PLUS. Springer, New York: 528pp

Pinz, A. (1998). 'Tree isolation and species classification.' *In:* Proceedings of the international forum on automated interpretation of high spatial resolution digital imagery for forestry, Victoria, B.C. Canada, Canadian Forest Service: 127 - 140

Pollock, R. (1999). 'Individual tree recognition based on a synthetic tree crown image model.' *In:* Proceedings of the international forum on automated

interpretation of high spatial resolution digital imagery for forestry, Victoria, B.C. Canada, Canadian Forest Service: 41 - 54

Popescu, S. C., R. H. Wynne and R. F. Nelson (2002). 'Estimating plot-level tree heights with lidar: local filtering with a canopy-height based variable window size.' Computers and electronics in agriculture **37**(1-3): 71 - 95.

Prevósto, B., T. Curt, J. Gueugnot and P. Coquillard (2000). 'Modeling mid-elevation Scots pine growth on a volcanic substrate.' Forest Ecology and Management **131**(1-3): 223 - 237.

Pukkala, T. and T. Kolstrom (1987). 'Competition indices and the prediction of radial growth in scots pine.' Silva Fennica **21**(1): 55 - 67.

Quirk, J. T. and F. Freese (1976). 'Effects of mechanical stress on growth and anatomical structure of red pine: compression stress.' Canadian Journal of Forest Research **6**: 195 - 202.

R Core Development Team (2004). R: A Language and Environment for Statistical Computing. Vienna, Austria, R Foundation for Statistical Computing.

Radtke, P. J. and H. E. Burkhart (1998). 'A Comparison of methods for edge-bias compensation.' Canadian Journal of Forest Research **28**(6): 942-945.

Radtke, P. J. and H. E. Burkhart (1999). 'Basal area growth and crown closure in a loblolly pine spacing trial.' Forest Science **45**(1): 35-44.

Radtke, P. J., J. A. Westfall and H. E. Burkhart (2003). 'Conditioning a distance-dependent competition index to indicate the onset of inter-tree competition.' Forest Ecology and Management **175**(1-3): 17-30.

Reed, D. D. and E. J. Green (1984). 'Compatible stem taper and volume ratio equations.' Forest Science **30**(4): 977-990.

Reed, D. D. and J. C. Byrne (1985). 'A simple, variable form volume estimation system.' Forestry Chronicle **61**: 87 - 90.

Rennolls, K. (1994). 'Pipe-model theory of stem-profile development.' Forest Ecology and Management **69**(1-3): 41-55.

Research Working Group 2. (1999). Code of Forest Mensuration Practice: A guide to good tree measurement practice in Australia and New Zealand. *Eds*: G. B. Wood, B. J. Turner and C. L. Brack, url: http://www.anu.edu.au/Forestry/mensuration/rwg2/code

Rich, P. M. (1986). 'Mechanical architecture of arborescent rain of forest palms.' Principes **30**: 117 - 131.

Rich, P. M., K. Helenurm, D. Kearns, S. R. Morse, W. M. Palmer and L. Short (1986). Journal of the Torrey Botanical Club **113**: 241 - 246.

Ross, M. A. and J. L. Harper (1972). 'Occupation of biological space during seedling establishment.' Journal of Ecology **60**: 77 - 88.

Royston, J. P. (1982). 'An Extension of Shapiro and Wilk's W Test for Normality to Large Samples.' Applied Statistics **31**: 115–124.

Royston, J. P. (1992). 'Approximating the Shapiro-Wilk's W-Test for Non-normality.' Statistics and Computing **2**: 117-119.

Rudemo, M. (1999). 'Spatial tree pattern analysis from maxima of smoothed aerial photographs.' *In*: International Forum on the Automated Interpretation Of High Spatial Resolution Digital Imagery For Forestry: 35 - 40

Rush, M. (2002). A summary of inventory data for the Uxbridge Moogara estate.

Rush, M. (2003). Personal communication: First thinning age in the Norske Skog estate is 15 to 16 years.

Sayn-Wittgenstein, L. and A. H. Aldred (1967). 'Tree volumes from large-scale photos.' Photogrammetric Engineering **33**(1): 69 - 73.

Schwinning, S. (1996). 'Decomposition analysis of competitive symmetry and size structure dynamics.' Annals of Botany **77**(1): 47-57.

Schwinning, S. and J. Weiner (1998). 'Mechanisms determining the degree of size asymmetry in competition among plants.' Oecologia **113**(4): 447-455.

Shapiro, S. S. and M. B. Wilk (1965). 'An analysis of variance test for normality (complete samples).' Biometrika **52**(3,4): 591-611.

Sharma, M. and H. E. Burkhart (2003). 'Selecting a level of conditioning for the segmented polynomial taper equation.' Forest Science **49**(3): 324 - 330.

Sheiner, L. B. and S. L. Beal (1980). 'Evaluation of methods for estimating population pharmacokinetic parameters. I. Michalis-Menten model: Routine clinical pharmacokinetic data.' Journal of Pharmacokinetics and Biopharmaceutics **8**(6): 553 - 571.

Shinozaki, K., K. Yoda, K. Hozumi and T. Kira (1964). 'A quantitative analysis of plant form - The pipe model theory. I. Basic analysis.' Japanese journal of ecology **14**: 97 - 105.

Shinozaki, K., K. Yoda, K. Hozumi and T. Kira (1964). 'A quantitative analysis of plant form - The pipe model theory. II. Further evidence of the theory and its application in forest ecology.' Japanese journal of ecology **14**: 133 - 139.

Silander, J. A. and S. W. Pacala (1985). 'Neighborhood predictors of plant size.' Oecologia **66**: 256 - 263.

Simard, S. W. and D. L. Sachs (2004). 'Assessment of interspecific competition using relative height and distance indices in an age sequence of seral interior cedar–hemlock forests in British Columbia.' Canadian Journal of Forest Research **34**(6): 1228 - 1240.

Simonse, M., T. Aschoff, H. Spiecker and M. Thies (2003). 'Automatic Determination of Forest Inventory Parameters Using Terrestrial Laserscanning.' *In*: Proceedings of the ScandLaser Scientific Workshop on Airborne Laser Scanning of Forests. Umeå, Sweden: 251- 257

Smith, H. and G. C. Whitelam (1997). 'The shade avoidance syndrome: multiple responses mediated by multiple phytochromes.' Plant, Cell and Environment **20**: 840 - 844.

Snee, R. D. (1977). 'Validation of regression models: Methods and examples.' Technometrics **19**: 415 - 428.

Sokal, R. R. and F. J. Rohlf (1995). Biometry: the principles and practice of statistics in biological research. Freeman, New York: 887pp

Spencer, R. D. (1972). Plantation management studies from supplementary aerial photographs. Masters Thesis, University of Melbourne, Melbourne, Australia: 258.

Spencer, R. D. (1979). 'Fixed-base large-scale photographs for forest sampling.' Photogrammetria **35**: 117 - 140.

Spurr, S. H. (1962). 'A measure of point density.' Forest Science **8**: 85 - 96.

Stage, A. R. (1973). Prognosis model for stand development USDA U.S. Intermountain Forest and Range Experiment Station: 32pp.

St-Onge, B. and C. Vega (2003). 'Combining stereo-photogrammetry and LIDAR to map forest canopy height.' *In*: Proceedings of the ISPRS working group III/3 workshop '3-D reconstruction from airborne laserscanner and InSAR data', Dresden, Germany: 7pp

Tasissa, G. and H. E. Burkhart (1998). 'An Application of Mixed Effects Analysis to Modeling Thinning Effects On Stem Profile of Loblolly Pine.' Forest Ecology and Management **103**(1): 87-101.

Thomas, C. E. and B. R. Parresol (1991). 'Simple, flexible, trigonometric taper equations.' Canadian Journal of Forest Research **21**(7): 1132-1137.

Thomas, C. E., B. R. Parresol, K. H. N. Lê and R. E. Lohrey (1995). 'Biomass and taper for trees in thinned and unthinned longleaf pine plantations.' Southern Journal of Applied Forestry **19**: 29 - 35.

Thomas, S. C. a. W., J. (1989). 'Including competitive asymmetry in measures of local interference in plant populations.' Oecologia **80**: 349 - 355.

Thompson, D. N. (2000). 'Stratified sampling based on photo-interpreted forest types reduces the cost of strategic forest inventory.' Tasforests **12**: 77 - 82.

Thompson, E. J. (1976). 'Optimum photo-plot size for estimating stocking in young pine plantations.' Australian Forest Research **7**(2): 47 - 51.

Thornley, J. H. M. (1999). 'Modelling stem height and diameter growth in plants.' Annals of Botany **84**(2): 195 - 205.

Tome, M. and H. E. Burkhart (1989). 'Distance-dependent competition measures for predicting growth of individual trees.' Forest Science **35**(3): 816-831.

Valentine, H. T. (1985). 'Tree-growth models: derivations employing the pipe theory.' Journal of theoretical biology **117**: 579 - 585.

Valentine, H. T. and T. G. Gregoire (2001). 'A switching model of bole taper.' Canadian Journal of Forest Research **31**: 1400 - 1409.

Valinger, E. (1992). 'Effects of wind sway on stem form and crown development of Scots pine (Pinus sylvestris L.).' Australian Forestry **55**: 15-21.

Van Laar, A. (1969). 'Influence of tree parameters and stand density on diameter growth of Pinus radiata.' South African Forestry Journal **70**: 5-14.

Vanclay, J. K. (1994). Modelling forest growth and yield: applications to mixed tropical forests. CAB International, Wallingford: 312pp

Walsworth, N. A. and D. J. King (1999). 'Image modelling of forest changes associated with acid mine drainage.' Computers and Geosciences **25**(5): 567 - 580.

Wareing, P. F. (1982). 'A plant physiology odessey.' Annual review of plant physiology **33**: 1 - 26.

Weiner, J. (1984). 'Neighborhood interference amongst Pinus rigida individuals.' Journal of Ecology **72**: 183 -195.

Weiner, J. (1985). 'Size hierarchy in experimental populations of annual plants.' Ecology **66**: 743 - 752.

Weiner, J. (1990). 'Asymmetric competition in plant populations.' Trends in ecology and evolution **5**: 360-364.

Weiner, J. and S. C. Thomas (1986). 'Size variability and competition in plant monocultures.' Oikos **47**: 211-222.

West, P. W. (1981). 'Simulation of diameter growth and mortality in regrowth eucalypt forest of southern Tasmania.' Forest Science **27**: 603 - 616.

West, P. W. and C. J. Borough (1983). 'Tree suppression and the self-thinning rule in a monoculture of Pinus radiata D. Don.' Annals of Botany **52**(2): 149-158.

West, P. W., D. A. Ratkowsky and A. W. Davis (1984). 'Problems of hypothesis testing of regressions with multiple measurements from individual sampling units.' Forest Ecology and Management **7**: 207 - 224.

West, P. W., D. R. Jackett and C. J. Borough (1989). 'Competitive processes in a monoculture of Pinus radiata D. Don.' Oecologia **81**(1): 57-61.

West, P. W., D. R. Jackett and S. J. Sykes (1989). 'Stresses in, and the shape of, tree stems in forest monoculture.' Journal of Theoretical Biology **140**(3): 327-343.

Westoby, M. (1982). 'Frequency distributions of plant size during competitive growth of stands: the operation of distribution modifying functions.' Annals of Botany **50**: 733-735.

Westoby, M. (1984). 'The self-thinning rule.' Advances in Ecological Research **14**: 167-225.

Whyte, A. G. D. and R. C. Woolons (1992). 'Diameter distribution growth and yield modelling: Recent revisions and perspectives.' In: Integrating Forest Information Over Space and Time IUFRO Conference, Canberra, Australia, ANUTECH Pty Ltd.

Wiant, J., . H.V., G. B. Wood and J. A. Miles (1989). 'Estimating the volume of a radiata pine stand using importance sampling.' Australian Forestry **52**(4): 286 - 292.

Wijanarto, A. (2001). Digital photogrammetric mapping of canopy height in a Radiata pine plantation. PhD Thesis, University of Tasmania, Hobart.

Williams, M. S. and R. M. Reich (1997). 'Exploring the error structure of taper equations.' Forest Science **43**(3): 378-386.

Wilson, B. F. and R. R. Archer (1979). 'Tree design: some biological solutions to mechanical problems.' Bioscience **29**: 293 - 298.

Wimberly, M. C. and B. B. Bare (1996). 'Distance-Dependent and Distance-Independent Models of Douglas-Fir and Western Hemlock Basal Area Growth Following Silvicultural Treatment.' Forest Ecology and Management **89**(1-3): 1-11.

Wood, G. B. and H. V. Wiant (1992). 'Test of Application of Centroid and Importance Sampling in a Point-3p Forest Inventory.' Forest Ecology and Management **53**: 107.

Wood, G. B., H. V. Wiant, R. J. Loy and J. A. Miles (1990). 'Centroid sampling: a variant of importance sampling for estimating the volume of sample trees of radiata pine.' Forest Ecology and Management **36**: 233 - 243.

Wright, E. F., K. D. Coates, C. D. Canham and P. Bartemucci (1998). 'Species variability in growth response to light across climatic regions in northwestern British Columbia.' Canadian Journal of Forest Research **28**: 871 - 886.

Zeger, S. L., K. Liang and P. Albert (1988). 'Models for longitudinal data: A generalized estimating equation approach.' Biometrics **44**: 1049 - 1060.

Zhang, Y., B. E. Borders and R. L. Bailey (2002). 'Derivation, fitting and implication of a compatible stem taper-volume-weight system for intensively managed, fast growing loblolly pine.' Forest Science **48**(3): 595 - 607.

Zimble, D. A., D. L. Evans, G. C. Carlson, R. C. Parker, S. C. Grado and P. D. Gerard (2003). 'Characterizing vertical forest structure using small-footprint airborne LiDAR.' Remote Sensing of Environment **87**(2-3): 171-182.

# *Appendix I*

# Basal area growth and mortality

This appendix presents:

- the second-stage basal area growth models (with their component models);
- the mortality model; and,
- the derivation of the second partial derivative of the basal area growth model.

The curves presented in Figure 1 Chapter 2 are of basal area growth for the median inventory plot data in the Uxbridge Moogara estate. Total basal area is given by predictions from equations AI.9, AI.2 and AI.3. The rate of basal area growth is given by predictions from equations AI.1, AI.2 and AI.3.

The scatter plots presented in Figure 2 Chapter 2 are of mean dominant height versus stocking at measurement age, and the same projected to thinning age, for the inventory plot data in the Uxbridge Moogara estate. The projected values at thinning age are given by predictions from equations AI.4 and AI.6 for mean dominant height and stocking respectively. Symbol colours represent the percentage basal area growth at the specified age which is predicted to have grown after trajectory inflection. This percentage is calculated using equations AI.1, AI.9, AI.2 and AI.3.

# AI.1 Second-stage basal area growth models

In projection form, the Gompertz model used to estimate radiata pine basal area increment in Tasmania (Candy 1989b) is given by:

$$G_{t_k} = G_{t_{k-j}} \times e^{e^{\alpha+\beta+\log(t_{k-j})}} - e^{e^{\alpha+\beta+\log(t_k)}} \qquad \text{(AI.1)}$$

Where:

$G_k$ is projected basal area at age $t_k$;

$G_{t_{k-1}}$ is basal area at age $t_{k-j}$[1].

Two second-stage equations were defined to describe the model parameters and thus localise the model (Candy 1989b, 1999). The models are given respectively by:

$$\alpha = \lambda_0 + \lambda_1 S + \lambda_2 L + \lambda_3 L^2 + \lambda_4 \frac{G_t}{N_t}. \qquad \text{(AI.2)}$$

And:

$$\beta = \lambda_5 + \lambda_6 S + \lambda_7 L. \qquad \text{(AI.3)}$$

Where:

$G_t$ is basal area at measurement age $t$;

$N_t$ is stocking at measurement age $t$;

$S$ is site index;

$L$ is Lawrence's stand density index ;

$\lambda_{0\,\text{to}\,7}$ are model parameters.

Site index and Lawrence's stand density index may be estimated from the inventory data using two further models.

---

[1] Age $t_{k-j}$ is typically measurement age.

## AI.2 Mean dominant height growth

In projection form, the model used to estimate radiata pine mean dominant height increment in Tasmania (Candy 1989b) is given by:

$$M_{t_k} = M_{t_{k-j}} \left( \frac{1 - e^{\delta_1 t_k}}{1 - e^{\delta_1 t_{k-j}}} \right)^{\delta_2} . \qquad \text{(AI.4)}$$

Where:

$M_{t_k}$ is projected mean dominant height at age $t_k$;

$M_{t_{k-j}}$ is mean dominant height at age $t_{k-j}$;

$\delta_{1 \text{ and } 2}$ are model parameters.

Site index is calculated using this model where $t_k = 20$.

## AI.3 Lawrence' stand density index

Lawrence (1976) developed his stand density index using data from 790 Tasmanian permanent yield plots. The index relates the basal area of a given plot given its mean dominant height to the predicted basal area of that plot were it at full stocking. Lawrence defined full stocking as the mean basal area of the 5% of permanent yield plots with the largest basal areas in each 1.5 metre mean dominant height class.

Lawrence's index takes the form:

$$L = 100 \times \frac{G}{\gamma_1 \times \log\left(\gamma_2 - \frac{\gamma_3}{\exp\left(M/\gamma_4\right)}\right)} \qquad \text{(AI.5)}$$

Where:

$L$ is Lawrence's stand density index;

$\gamma_{1\text{to}4}$ are model parameters.

## AI.4 Mortality

The second stage models do not explicitly include changes to stocking due to mortality. Candy (1989b) modelled tree mortality by fitting a survival model with a log-linear hazard to the Tasmanian permanent yield plot data. The general form of the model is given by:

$$N_k = N_{k-j}\left(1 - e^{-\int_{k-j}^{k} \eta(t)dt}\right). \qquad \text{(AI.6)}$$

The derivative term is approximated by:

$$\int_{t_{k-1}}^{t_k} \eta(t)dt \cong T \times e^{\beta_0+\beta_1 S+\beta_2 T_M+\beta_3 T_M^2}. \qquad \text{(AI.7)}$$

Where:

$$T = t_k - t_{k-2} \text{ and } T_M = \frac{t_k + t_{k-1}}{2}.$$

# AI.5 Partial derivatives of the basal area growth model

The first partial derivative of the Gompertz basal area growth model in projection form with respect to age is given by:

$$\frac{dG_{t_k}}{dt} = -G_{t_{k-1}} e^{e^{\alpha+\beta\log(t_{k-1})}-e^{\alpha+\beta\log(t_k)}} e^{\alpha+\beta\log(t_k)} \beta \frac{1}{t_k}$$

$$= -G_{t_{k-1}} \frac{\beta}{t_k} e^{\alpha+\beta\log(t_k)+e^{\alpha+\beta\log(t_{k-1})}-e^{\alpha+\beta\log(t_k)}}. \qquad \text{(AI.8)}$$

The second partial derivative of basal area with respect to age is given by:

$$\frac{dG_{t_k}^{\ 2}}{d^2t} = G_{t_{k-1}} \frac{\beta}{t_k^{\ 2}} e^{\alpha+\beta\log(t_k)+e^{\alpha+\beta\log(t_{k-1})}-e^{\alpha+\beta\log(t_k)}}$$

$$- G_{t_{k-1}} \frac{\beta}{t_k} \left( e^{\alpha+\beta\log(t_k)+e^{\alpha+\beta\log(t_{k-1})}-e^{\alpha+\beta\log(t_k)}} \beta \frac{1}{t_k} - e^{\alpha+\beta\log(t_k)} \beta \frac{1}{t_k} \right)$$

$$= G_{t_{k-1}} \frac{\beta}{t_k^{\ 2}} e^{\alpha+\beta\log(t_k)+e^{\alpha+\beta\log(t_{k-1})}-e^{\alpha+\beta\log(t_k)}} \left(1 - \beta\left(1 - e^{\alpha+\beta\log(t_k)}\right)\right) \qquad \text{(AI.9)}$$

# *Appendix II*

# Stem profile model fitting methods

## AII.1 The stem profile model with unstructured error

The stem profile model for the *jth* of $n$ total diameter observations on the *ith* of $m$ trees that assumes no serial correlation or error heterogeneity can be defined as:

$$d_{ij} = f\left(\boldsymbol{\beta}, \boldsymbol{x}_{ij}\right) + \varepsilon_{ij} . \qquad \text{(AII.1)}$$

Where:

$d_{ij}$ is the *jth* observed diameter on the *ith* tree;

$\boldsymbol{\beta}$ is a vector of parameters of length $p \times 1$; [1]

$\boldsymbol{x}_{ij}$ is a vector of predictors for the *jth* observation on the *ith* tree;

$f(.)$ is a linear or nonlinear function of the parameter and predictor vectors;

$\varepsilon_{ij}$ is the error term. The vector of errors $\boldsymbol{\varepsilon} = [\varepsilon_{ij1}, \ldots, \varepsilon_{ijn}]$ is independent and identically normal, i.e.:

$\boldsymbol{\varepsilon} \sim N\left(0, \sigma^2\right)$.

[1] The parameter vector $p$ may be as short as one (e.g. Gray 1956), but is typically of a length between three (e.g. Biging 1984; Thomas and Parresol 1991) and seven (e.g. Bi 2000).

Where:

$\sigma^2$ is the mean error variance.

Under this model, response is assumed to be normally distributed, with mean and variance given by:

$$E(d_{ij}) = f(\boldsymbol{\beta}, \boldsymbol{x}_{ij}),\ Var(d_{ij}) = \sigma^2. \qquad \text{(AII.2)}$$

Numerous early profile models were formulated under this modelling assumption (Gregoire and Schabenberger 1996). Methods which account for serial correlation and/or error heterogeneity represent alterations to this model.

# AII.2 The stem profile model with structured error

Broadly, there are two approaches to account for serial correlation and/or error heterogeneity. First, additional correlation and/or variance models may be estimated jointly with functional parameters in a generalisation of the classical least squares model. This is termed the population average approach by Zeger, Liang and Albert (1988). In the second approach, additional random effects are included in the model to more closely depict the hierarchical nature of the data. In circumstances where random effects fail to adequately account for residual error serial correlation and/or heterogeneity, further covariance structures may also be specified. Zeger, Liang and Albert (1988) termed this the subject specific approach. The following discussion explores these approaches.

## A2.1 Population average approaches

### *A2.1.1 Accounting for serial correlation*

Where correlations between observations occur within trees, the within-tree error correlation is non zero and a correlation pattern must be included for valid inference. When variance is constant, the error covariance can be adjusted using a correlation matrix (Davidian and Giltinan 1995, pg. 24) i.e.:

$$\mathrm{Cov}(\boldsymbol{\varepsilon}) = \sigma^2 \boldsymbol{\Gamma}(\boldsymbol{\alpha}). \qquad \text{(AII.3)}$$

Where:

$\boldsymbol{\Gamma}(\boldsymbol{\alpha})$ is correlation matrix that is a function of the vector of correlation parameters $\boldsymbol{\alpha}$ with length $s \times 1$ [2].

One approach, which has been used successfully in profile modelling (Gregoire and Schabenberger 1996; Garber and Maguire 2003), models within-subject error covariance by assuming continuous, first-order serial correlation between measurements[3] (Liang and Zeger 1986). If the *j1th* and *j2th* diameter measurements are taken at adjacent stem heights then continuous, first-order serial correlation can be defined by:

$$Corr\left(\varepsilon_{j_1}\varepsilon_{j_2}\right) = \exp\left(\frac{-\sqrt{\left(S_{j_1 j_2}\right)^2}}{\alpha}\right). \qquad \text{(AII.4)}$$

Where:

$S_{j_1 j_2}$ is a distance metric separating adjacent measurements;

$\alpha$ is the correlation parameter.

---

[2] In profile modelling where serial correlation occurs in one dimension, the correlation parameter vector length is typically one.

[3] This is termed the CAR(1) model (e.g. Pinheiro, J. C. and D. M. Bates 2000).

The correlation matrix for this model can be shown in upper triangular form:

$$\Gamma(\alpha) = \begin{bmatrix} 1 & \exp\left(\frac{-\sqrt{\left(S_{j_1 j_2}\right)^2}}{\alpha}\right) & \cdots & \cdots & \exp\left(\frac{-\sqrt{\left(S_{j_1 j_n}\right)^2}}{\alpha}\right) \\ & 1 & \exp\left(\frac{-\sqrt{\left(S_{j_1 j_2}\right)^2}}{\alpha}\right) & \cdots & \exp\left(\frac{-\sqrt{\left(S_{j_1 j_{n-1}}\right)^2}}{\alpha}\right) \\ & & \ddots & \ddots & \cdots \\ & & & \ddots & \exp\left(\frac{-\sqrt{\left(S_{j_1 j_2}\right)^2}}{\alpha}\right) \\ & & & & 1 \end{bmatrix}. \quad \text{(AII.5)}$$

This correlation structure is suitable for use where the distance between measurements is unequal within the tree. In profile studies where measurements are taken at fixed, equidistant intervals, many alternate autoregressive functions are available. For example, Tasissa and Burkhart (1998) used a non-continuous, first-order model in their study that made use of equidistant interval profile data.

### *A2.1.2 Accounting for heterogeneity*

Broadly, two methods may be used to address error heterogeneity. Resampling methods may be used to estimate model parameters since these methods are generally immune to its impacts (Efron and Tibshirani 1986). Alternately, the degree of heterogeneity can be estimated in the fitting process and parameter estimates derived or adjusted to account for its presence (Gregoire and Dyer 1989). The latter methods have been used extensively in profile modelling.

The profile model which includes heterogeneous variance can be written as:

$$E\left(d_{ij}\right) = \mu_{ij}, Var\left(d_{ij}\right) = \sigma^2 g^2\left(\mu_{ij}, \boldsymbol{v}_{ij}, \boldsymbol{\theta}\right). \tag{AII.6}$$

Where:

$\boldsymbol{\beta}$ and $\mathbf{x}_{ij}$ are as defined earlier;

$$\mu_{ij} = f\left(\boldsymbol{\beta}, \mathbf{x}_{ij}\right); \tag{AII.7}$$

$\boldsymbol{v}_{ij}$ is a vector comprised of one or more components of $\mathbf{x}_{ij}$;

$\boldsymbol{\theta}$ is a variance function parameter vector of length $q \times 1$;

$g^2$ is a variance function which may depend on one or more of $\mu_{ij}$, $\boldsymbol{v}_{ij}$, and $\boldsymbol{\theta}$.

Profile modellers have investigated quite complicated model forms for the variance function. For example, Czaplewski and Bruce (1990) derived variance functions for use with profile models in the context of a re-transformation bias study. In that study, Max and Burkhart's (1976) segmented model was fitted by ordinary least squares. Variance heterogeneity was then modelled as functions of relative height using multiple least squares. An example of a derived variance function is given by:

$$g^2 = \theta_0\left(1 - z_{ij}\right)^2 - \theta_1\left(1 - z_{ij}\right)^3 + \theta_2\left(\theta_3 - z_{ij}\right)I. \tag{AII.8}$$

Where:

$$I = \begin{cases} 1 \, for \, z_{ij} < \theta_4 \\ 0 \; otherwise \end{cases}.$$

Williams and Reich (1997) investigated variance functions which were continuously differentiable along their length, again with application to Max and Burkhart's (1976) segmented model. An example of one suggested variance function was:

$$g^2 = \theta_0\left(\exp\left(\theta_1 z_{ij}\right) + \theta_2 z_{ki}^{\theta_3}\left(1 - z_{ij}\right)^{\theta_4}\right). \tag{AII.9}$$

### *A2.1.3 Accounting for serial correlation and heterogeneity jointly*

A diagonal variance matrix can be defined by:

$$\boldsymbol{G}(\beta,\theta) = diag\left[g^2(\mu_{i1},v_{i1},\theta),.....,g^2(\mu_{in},v_{in},\theta)\right]. \qquad \text{(AII.10)}$$

Where the correlation structure is defined by a correlation matrix, for example, as above in equation AII.10, the error covariance under simultaneous specification of a variance function and a correlation structure may be accommodated by:

$$\begin{aligned}\mathrm{Cov}(\varepsilon) &= \sigma^2\left\{\boldsymbol{G}(\beta,\theta)\right\}^{\frac{1}{2}}\boldsymbol{\Gamma}(\alpha)\left\{\boldsymbol{G}(\beta,\theta)\right\}^{\frac{1}{2}} \\ &= \boldsymbol{R}(\beta,\xi)\ ,\ \xi = [\sigma,\theta',\alpha']^T.\end{aligned} \qquad \text{(AII.11)}$$

Where:

$\xi$ is the combined vector of all within-tree covariance parameters of length $\{(q+s+1)\times 1\}$.

This covariance matrix specification implies within-tree variance and correlation given by:

$$Var(d_j)_i = \sigma^2 g^2{}_i(\mu_j,v_j,\theta),\quad Corr_i(d_{j1},d_{j2}) = \boldsymbol{\Gamma}_{i(j1,j2)}(\alpha). \qquad \text{(AII.12)}$$

### *A2.1.4 Inference in population average models*

Czaplewski and Bruce (1990) derived variance function parameters from ordinary least squares (OLS) residuals and used the function to adjust the profile model predictions outright. Variance parameters have also been estimated iteratively for improved efficiency. Cormier, Reich, Czaplewski et al. (1992), and Flewelling and Raynes (1993) used a manual iterative fitting process in which initial OLS residuals were used to derive variance function parameters. The variance function was then used as a weighting term in a weighted least squares estimation. Broad and Wake (1995) used iteratively reweighted least squares in a generalised least squares (GLS) formulation to determine variance parameters. More recently, researchers have made use of GLS formulations and the restricted maximum likelihood method to jointly estimate variance and correlation parameters (Garber and Maguire 2003). This method will now be described further.

The covariance structure presented in equation AII.12 can be reformulated to allow its expression as a weight matrix for use in a GLS formulation. To do this the functional and non-functional covariance parameters are first divorced from each other by:

$$\boldsymbol{R}(\beta,\xi) = \sigma^2 \boldsymbol{S}(\beta,\gamma),\ \gamma = \left[\theta', \alpha'\right]^T. \qquad \text{(AII.13)}$$

Where:

$\gamma$ is the vector of functional variance parameters of length $q + s$.

The functional variance parameter vector can now be solved jointly together with the model vector in the following iterative steps (Davidian and Giltinan 1995, pgs. 35-36).

Step 1 Obtain a preliminary estimate of the model vector $\beta$, denoted $\hat{\beta}^{(p)}$. This is generally achieved using the OLS method.

Step 2 Obtain an estimate of the functional variance parameter vector by pseudo likelihood or restricted maximum likelihood methods, defined respectively by:

$$PL\left(\hat{\beta}^{(p)}, \sigma, \hat{\gamma}\right) = \log\left|\sigma^2 \boldsymbol{S}\left(\hat{\beta}^{(p)}, \hat{\gamma}\right)\right| + \frac{\left\{d - f\left(\hat{\beta}^{(p)}\right)\right\}^T \boldsymbol{S}^{-1}\left(\hat{\beta}^{(p)}, \hat{\gamma}\right)\left\{d - f\left(\hat{\beta}^{(p)}\right)\right\}}{\sigma^2}. \qquad \text{(AII.14)}$$

Where:

$$f\left(\hat{\beta}^{(p)}\right) = \left[f\left(x_1, \hat{\beta}^{(p)}\right), \ldots, f\left(x_n, \hat{\beta}^{(p)}\right)\right]^T. \qquad \text{(AII.15)}$$

And:

$$REML\left(\hat{\boldsymbol{\beta}}^{(p)},\sigma,\hat{\boldsymbol{\gamma}}\right) = PL\left(\hat{\boldsymbol{\beta}}^{(p)},\sigma,\hat{\boldsymbol{\gamma}}\right) - p\log\sigma^2 + \log|\,\boldsymbol{X}'\left(\hat{\boldsymbol{\beta}}^{(p)}\right)\boldsymbol{S}^{-1}\left(\hat{\boldsymbol{\beta}}^{(p)},\hat{\boldsymbol{\gamma}}\right)\boldsymbol{X}\left(\hat{\boldsymbol{\beta}}^{(p)}\right)|\,. \tag{AII.16}$$

Where:

$\boldsymbol{X}(\boldsymbol{\beta})$ is the matrix whose *jth* element is given by $f_{\boldsymbol{\beta}}{}^{T}\left(\mathbf{x}_j,\boldsymbol{\beta}\right)$ of length $(n\times p)$.

Step 3 Form the estimated weight matrix using the preliminary model and functional variance parameter vector estimates:

$$\hat{\boldsymbol{W}} = \boldsymbol{S}^{-1}\left(\hat{\boldsymbol{\beta}}^{(p)},\hat{\boldsymbol{\gamma}}\right). \tag{AII.17}$$

Step 4 Solve the $p$-dimensional set of estimating equations for $\hat{\boldsymbol{\beta}}^{(p)}$:

$$\mathbf{X}'\left(\hat{\boldsymbol{\beta}}^{(p)}\right)\hat{\boldsymbol{W}}\left\{d - f\left(\hat{\boldsymbol{\beta}}^{(p)}\right)\right\} = 0\,. \tag{AII.18}$$

Step 5 Iterate steps 2 through 5 replacing the preliminary $\boldsymbol{\beta}$ estimate with the new $\boldsymbol{\beta}$ estimate derived in Step 4, denoted $\boldsymbol{\beta}_{GLS}$, until an appropriate level of convergence is obtained.

The final variance estimate is given by:

$$\sigma^2 = \frac{1}{n-p}\left\{d - f\left(\hat{\boldsymbol{\beta}}_{GLS}\right)\right\}^{T}\boldsymbol{S}^{-1}\left(\hat{\boldsymbol{\beta}}_{GLS},\hat{\boldsymbol{\gamma}}\right)\left\{d - f\left(\hat{\boldsymbol{\beta}}_{GLS}\right)\right\}. \tag{AII.19}$$

## A2.2 Subject specific approaches[4]

The mixed effects stem profile model can be defined as follows (after Davidian and Giltinan 1995, pgs. 108-109).

If $\boldsymbol{d}_i$ is the vector of diameter responses of length $(n \times 1)$ for the *ith* individual, $\boldsymbol{\varepsilon}_i$ is the vector of within-tree errors of the same length, and there exists a model vector for that tree of the form $\boldsymbol{f}_i(\boldsymbol{\beta}_i) = f\left(\mathbf{x}_{i1}, \boldsymbol{\beta}_i, \ldots\ldots, \mathbf{x}_{in}, \boldsymbol{\beta}_i\right)'$ which is dependent on the model parameter vector $\boldsymbol{\beta}_i$ with length $p \times 1$ specific to the individual, then a within-tree error expectation and covariance may be specified respectively as:

$$E(\boldsymbol{\varepsilon}_i \mid \boldsymbol{\beta}_i) = 0. \tag{AII.20}$$

And:

$$\begin{aligned} \mathrm{Cov}(\boldsymbol{\varepsilon}_i \mid \boldsymbol{\beta}_i) &= \sigma^2 \left\{\boldsymbol{G}_i(\boldsymbol{\beta}_i, \boldsymbol{\theta})\right\}^{\frac{1}{2}} \boldsymbol{\Gamma}_i(\boldsymbol{\alpha}) \left\{\boldsymbol{G}_i(\boldsymbol{\beta}_i, \boldsymbol{\theta})\right\}^{\frac{1}{2}} \\ &= \boldsymbol{R}_i(\boldsymbol{\beta}_i, \boldsymbol{\xi}), \ \boldsymbol{\xi} = \left[\sigma, \boldsymbol{\theta}', \boldsymbol{\alpha}'\right]^T. \end{aligned} \tag{AII.21}$$

Where:

$\boldsymbol{G}_i(\boldsymbol{\beta}_i, \boldsymbol{\theta})$ is the diagonal matrix describing within-tree variance of length $(n_i \times n_i)$;

$\boldsymbol{\Gamma}_i(\boldsymbol{\alpha})$ is the matrix describing within-tree correlation of length $(n_i \times n_i)$.

These variance and correlation matrices depend on the variance and correlation parameter vectors $\sigma$, $\boldsymbol{\theta}$, and $\boldsymbol{\alpha}$ as defined in A2.1.1 and A2.1.2. The values of these vectors are common to all individuals.

[4] The subject specific approach discussed here unifies the random parameters (Amateis, R. L. and H. E. Burkhart 1987, amongst others) and random coefficients (Candy, S. G. 1989a) approaches.

Within-tree variation can be described by:

$$\boldsymbol{d}_i = \boldsymbol{f}_i(\boldsymbol{\beta}_i) + \boldsymbol{\varepsilon}_i, \quad \boldsymbol{\varepsilon}_i \mid \boldsymbol{\beta}_i \sim \left(0, \boldsymbol{R}_i(\boldsymbol{\beta}_i, \xi)\right). \tag{AII.22}$$

Between-tree variation can be described by a function $\boldsymbol{c}$ of the random effects:

$$\boldsymbol{\beta}_i = \boldsymbol{c}(\boldsymbol{a}_i, \boldsymbol{\beta}, \boldsymbol{b}_i). \tag{AII.23}$$

Where:

$\boldsymbol{a}_i$ is the covariate vector of length $a \times 1$;

$\boldsymbol{b}_i$ is a vector of random effects of length $k \times 1$. Random effects are independent and identically distributed between trees (usually Normal) by:

$$\boldsymbol{b}_i \sim (\boldsymbol{0}, \boldsymbol{D}).$$

Where:

$\boldsymbol{D}$ is a between-tree covariance matrix of length $k \times k$.

In profile modelling, the population parameters and $\boldsymbol{\beta}$ dimension $\boldsymbol{D}$ are of interest. The tree-level quantities $\boldsymbol{\beta}_i$ and $\boldsymbol{R}_i$ are nuisance parameters.

### *A2.2.1 Inference in subject specific models*

In a linear context, generalised least squares estimating equations can be solved for the fixed effects in the rare cases where variance covariance parameter values are known. Davidian and Giltinan (1995, pgs. 76-79) provide an overview of the GLS approach. When they are unknown, REML or maximum likelihood estimation may be employed by the EM algorithm to estimate them (Dempster, Laird and Rubin 1977; Laird and Ware 1982; Lindstrom and Bates 1990). The ability to formulate a likelihood is restricted by two assumptions. First, the marginal distribution of the response, the random effects and the within-tree errors is normal. Secondly, that the random effects and the within-tree errors enter the model in an additive and linear fashion, and are independent. In the non-linear context more common to profile modelling, these restrictions cannot be met. The common approach to the

problem has been to employ linearisation methods to approximate the likelihood. Numerous methods to achieve linearisation exist (Beal and Sheiner 1982; Sheiner and Beal 1985; Beal and Sheiner 1988; Lindstrom and Bates 1990; Pinheiro and Bates 1995). Splus and R both use the methods described by Lindstrom and Bates (1990).

## AII.3 Comparing nested and non-nested models

Akaike's information criterion (AIC) (Sakamoto, Ishiguro and G. 1986), Schwarz' (1978) Bayesian information criterion (BIC) and likelihood ratio tests (Pinheiro and Bates 2000, pgs. 83-84) may be used to assess the significance of model parameters.

Akaike's information criterion is a modified log likelihood statistic which is penalized according to the number of parameters in the model:

$$AIC = -2l + 2p \qquad \text{(AII.24)}$$

Where:

$l$ is the log likelihood of the model given the data,

$p$ is the number of parameters in the model.

Schwarz' Bayesian information criterion includes a further penalty of the logarithm of the number of observations and so favours more parsimonious models when datasets are small:

$$BIC = -2l + 2p + \log(n) \qquad \text{(AII.25)}$$

Where:

$n$ is the number of observations in the dataset.

Models with smaller values for each information criteria are preferred.

Likelihood ratio tests provide an alternate means to assess model parsimony. The likelihood ratio is calculated by:

$$\lambda = \frac{L_1}{L_0} \text{ and } \chi^2 = -2\lambda \qquad \text{(AII.26)}$$

Where:

$L_0$ is the likelihood of the null model,

$L_1$ is the likelihood of the model with additional $k$ parameters.

The Likelihood ratio test computes $\chi^2$, and rejects the additional parameters as significant if the value of $\chi^2$ is larger than a specified Chi-square percentile with $k$ degrees of freedom where the percentile corresponds with a chosen confidence level.